

Manganese compounds as catalysts for water oxidation and as CO releasing molecules

Dissertation
zur Erlangung des Doktorgrades
der Mathematisch-Naturwissenschaftlichen Fakultät
der Christian-Albrechts-Universität zu Kiel

vorgelegt von

Hans-Martin Berends

Kiel, 2011

Referent: Prof. Dr. Felix Tuzek
Korreferent: Prof. Dr. Wolfgang Bensch
Tag der mündlichen Prüfung: 08.12.2011
Zum Druck genehmigt:

Prof. Dr. L. Kipp, Dekan

Die Rolle des fallenden Wasser aber wird bei der Maschine des Lebens von den Sonnenstrahlen übernommen; ohne die Sonnenstrahlen kann das Rad des Lebens nicht im Gang erhalten werden und wir werden noch genauer erforschen müssen, auf welchen Verhältnissen und Naturgesetzen diese merkwürdige Umwandlung der Sonnenstrahlen in Nahrungsmittel und Wärme beruht.

(Wilhelm Ostwald, Die Mühle des Lebens, 1911)

Abstract

This PhD thesis deals with several aspects of manganese chemistry and is divided into three parts. The first two concern the synthesis and characterization of manganese-based water oxidation catalysts. The four-electron oxidation of water to dioxygen is a key process of oxygenic photosynthesis in which solar energy is captured and stored in the form of carbohydrates. In nature, this reaction is catalyzed by a μ -oxido-Mn₄Ca cluster, the oxygen evolving complex (OEC). Mimicking this reaction with synthetic analogues is of fundamental importance for bioinorganic chemistry. Additionally, manganese based water oxidation catalysts are interesting candidates for the development of so-called artificial photosynthetic devices, i.e. systems for the synthesis of fuels like hydrogen or methanol using the energy of sunlight.

In the first part of this thesis, the synthesis of a new dinuclear manganese complex $[\text{Mn}_2^{\text{III,III}}(\text{tpdm})_2(\mu\text{-O})(\mu\text{-OAc})_2]^{2+}$ (**1**) is presented, in which manganese is coordinated to the unusual, facially-coordinating and oxidation stable ligand tpdm (tris(2-pyridyl)methane). The redox behavior of the compound was studied using both UV/Vis and X-Band EPR spectroelectrochemistry. Electrochemical (+1 200 mV vs. Ag/Ag⁺) and chemical (*t*BuOOH) oxidations transform **1** via a singly oxidized di- μ -oxido Mn₂^{III,IV}-intermediate to a Mn₂^{IV,IV}-form of the complex, and both oxidation reactions show characteristics resembling oxidation steps of the OEC. Furthermore, the ability of complex **1** to evolve O₂ was studied experimentally. Whereas reactions with hydrogen peroxide and peroxomonosulfate yield O₂, homogeneous water-oxidation using Ce^{IV} was not achieved. Thus, despite its favorable coordination geometry and multielectron redox chemistry, complex **1** fails to be a functional catalyst for overall water oxidation.

In the second part, the preparation of functional, manganese-based catalysts for water oxidation could be achieved by the adsorption of different manganese precursors on K10 montmorillonite. The best catalyst hybrid investigated in this study was prepared by the simple adsorption of Mn³⁺ onto montmorillonite clay. Spectroscopic results indicated that the catalytic units on the surfaces most likely consist of more than two manganese centers. Furthermore, a manganese oxidation state of Mn \geq +III seems to be a prerequisite for active catalysts. On the other hand, very different types of manganese(III) precursors can be assembled into active catalysts, so the geometrical arrangement of the manganese precursors seems to be of no importance.

The last part of this thesis deals with an entirely different field of Mn coordination chemistry. Water-soluble complexes containing the fac-[Mn^I(CO)₃]-moiety have been identified as

candidates for photoCORM activity (CORM = CO releasing molecule), which describes the photoactivated release of molecular carbon monoxide, a potential therapeutic agent. For the first time, a combination of spectroscopic methods (UV/Vis, IR and EPR) was employed to reveal details of the processes following CO release for $[\text{Mn}^{\text{I}}(\text{CO})_3]$ -complexes. First, manganese dicarbonyl intermediates are formed after the release of one CO per Mn. The last two carbonyl ligands are then liberated in a reaction accompanied by manganese oxidation to Mn^{II} and beyond, which could be clearly detected by EPR spectroscopy. Ultimately, $\mu\text{-O-Mn}^{\text{III}}$ -compounds appear to be the most likely final reaction products. The additional information gained in this way could be of significant importance for a potential pharmaceutical application of manganese photoCORMs.

Kurzdarstellung

Diese Arbeit beschäftigt sich mit verschiedenen Aspekten der Manganchemie und ist in drei Teile gegliedert. Die ersten beiden behandeln die Synthese und Charakterisierung von manganbasierten Wasseroxidations-Katalysatoren. Die Vierelektronen-Oxidation von Wasser zu Sauerstoff ist ein Schlüsselprozess der oxygenen Photosynthese, bei der Solarenergie in Form von Kohlenhydraten gespeichert wird. In der Natur wird diese Reaktion von einem μ -oxido-Mn₄Ca-Cluster, dem Sauerstoff-entwickelnden Komplex (oxygen evolving complex, OEC), katalysiert. Die Nachbildung dieser Reaktion mit synthetischen Analoga ist von fundamentaler Bedeutung für die bioanorganische Chemie. Des Weiteren sind manganbasierte Wasseroxidations-Katalysatoren interessante Kandidaten für die Entwicklung der sogenannten künstlichen Photosynthese, d.h. Systeme für die Synthese eines Brennstoffes wie Wasserstoff oder Methanol durch die Nutzung von Sonnenenergie.

In dem ersten Teil dieser Arbeit wird die Synthese des neuen zweikernigen Mangankomplexes [Mn₂^{III,III}(tpdm)₂(μ -O)(μ -OAc)₂]²⁺ (**1**) präsentiert. Das Redoxverhalten von **1** wurde durch UV/Vis- und X-Band EPR-Spektroelektrochemie untersucht. Chemische (*t*BuOOH) und elektrochemische (+1 200 mV vs. Ag/Ag⁺) Oxidation überführen **1** über das einfach oxidierte di- μ -oxido Mn₂^{III,IV}-Intermediat in die Mn₂^{IV,IV}-Form des Komplexes, wobei beide Oxidationsreaktionen charakteristische Oxidationsschritte des OEC nachbilden. Des Weiteren wurde die Fähigkeit von Komplex **1** O₂ zu entwickeln untersucht. Während Reaktionen mit Wasserstoffperoxid und Peroxomonosulfat Sauerstoff ergeben, wird keine homogene Wasseroxidation mit Ce^{IV} als Oxidationsmittel erreicht. Folglich ist Komplex **1** trotz Mehrelektronenredoxchemie kein funktionaler Wasseroxidationskatalysator.

Im zweiten Teil wurden funktionale, manganbasierte Katalysatoren für die Wasseroxidation durch die Adsorption verschiedener Manganprecursoren auf K10 Montmorillonit erhalten. Der beste Katalysator, der in dieser Studie untersucht wurde, konnte durch die simple Adsorption von Mn³⁺ auf Montmorillonit-Ton erhalten werden. Spektroskopische Untersuchungen haben gezeigt, dass die katalytischen Einheiten auf den Oberflächen höchstwahrscheinlich aus mehr als zwei Manganzentren bestehen. Darüber hinaus scheint eine Manganoxidationsstufe von Mn_{≥+III} eine Voraussetzung für einen aktiven Katalysator zu sein. Die geometrische Struktur der Manganprecursoren scheint hingegen nicht wichtig zu sein, da aus sehr unterschiedlichen Mangan(III)-Precursoren aktive Katalysatoren erhalten werden können.

Der letzte Teil dieser Arbeit beschäftigt sich mit einem gänzlich anderen Bereich der Mangankoordinationschemie. Für wasserlösliche Komplexe, die die fac-[Mn^I(CO)₃]-Einheit ent-

halten, wurde gezeigt, dass sie photoinduziert Kohlenmonoxid abgeben können, also photo-CORM-Aktivität (CORM = CO releasing molecule, CO freisetzendes Molekül) aufweisen. Erstmals wurde eine Kombination von spektroskopischen Methoden (UV/Vis, IR und EPR) verwendet, um Details der CO-Abspaltungsprozesse zu erhalten. Als erstes entstehen Mangan-dicarbonyl-Intermediate nach der Abgabe von einem Molekül CO pro Mn. Die letzten beiden Carbonylliganden werden nachfolgend in einer Reaktion freigesetzt, die mit einer Manganoxidation zu Mn^{II} und darüber hinaus verbunden ist, wie eindeutig mit Hilfe der EPR-Spektroskopie gezeigt werden konnte. Letztlich scheinen $\mu\text{-O-Mn}^{\text{III}}$ -Verbindungen die Endprodukte der Reaktionen zu sein. Die durch diese Studien gewonnenen Informationen könnten von maßgeblicher Bedeutung für eine potentielle pharmazeutische Anwendung von Mangan-photoCORMs sein.

Contents

1. Introduction	1
2. Water oxidation as part of natural photosynthesis	3
3. Water oxidation as part of artificial photosynthesis	9
4. Manganese catalases	23
5. EPR spectroscopy of manganese complexes	27
6. Is the geometrical arrangement crucial for water oxidation?	33
7. Clay supported manganese catalysts for water oxidation	41
8. Carbon monoxide releasing molecules	49
9. Mn(I) tricarbonyl complexes as photoCORMs	51
10. Outlook	55
References	59
Papers / Manuscripts	
I. A Manganese Oxido Complex Bearing Facially Coordinating Trispyridyl Ligands	71
II. Clay supported manganese catalysts for water oxidation	91
III. Mn(I) tricarbonyl complexes as photoCORMs	101
IV. Water Oxidation Catalysed by Manganese Compounds: From Complexes to “Bio-mimetic Rocks”	125

Papers

This thesis is based on the following publications which are referred to in the text by the Roman numerals.

-
- I** *A Manganese Oxido Complex Bearing Facially Coordinating Trispyridyl Ligands - Is Coordination Geometry Crucial for Water Oxidation Catalysis?*, H.-M. Berends, A.-M. Manke, C. Näther, F. Tuzek and P. Kurz, *in preparation*.
 - II** *K10 Montmorillonite Supported Manganese Catalysts for the Oxidation of Water to Dioxygen*, H.-M. Berends, T. Homburg, I. Kunz and P. Kurz, *Applied Clay Science*, **2011**, *53*, 174-180.
 - III** *Investigation of Light-Triggered Carbon Monoxide Release from Two Manganese PhotoCORMs by IR, UV/Vis and EPR Spectroscopy*, H.-M. Berends and P. Kurz, *Inorganica Chimica Acta*, *in press*, DOI: 10.1016/j.ica.2011.10.047.
 - IV** *Water Oxidation Catalysed by Manganese Compounds: From Complexes to "Biomimetic Rocks"*, M. Wiechen, H.-M. Berends and P. Kurz, *Dalton Transactions*, *in press*.

Manuscript not included in this thesis

-
- V** *MCD and EPR Spectroscopy of Mononuclear Mn(III) Complexes*, A. Westphal, H.-M. Berends, A. Klinkebiel, P. Kurz and F. Tuzek, *in preparation*.

Reprints were made with permission from the publishers.

1. Introduction

With approximately 950 ppm, manganese is the twelfth most abundant element in the Earth's crust and therefore as abundant as carbon or phosphorus.¹ Furthermore, it is the second most abundant transition metal after iron and occurs in seawater with concentrations of 10^{-4} ppm in the form of the $[\text{Mn}(\text{H}_2\text{O})_6]^{2+}$ -ion. The most important minerals are mainly oxides like MnO_2 (pyrolusite), Mn_3O_4 (hausmannite) or $\text{Mn}(\text{O})(\text{OH})$ (manganite).¹ Further deposits are found in depth of sea of 4000 to 6000 m in the form of manganese nodules. Hence, manganese is available on a huge scale as a resource for both industry and biology.²

In nature, manganese is an essential trace element and part of the active sites of several metalloproteins^{3,4} like the mononuclear manganese superoxide dismutase (MnSOD),⁵ the dinuclear manganese catalase (MnCat)⁶ or the Mn_4CaO_x cluster of the oxygen evolving complex (OEC) of photosystem II (PS II).⁷ The latter enzyme catalyzes one of the fundamental reactions on Earth, the oxidation of water during oxygenic photosynthesis. For 2.5 billion years, a wide array of organisms has developed strategies to capture solar energy and store it in the form of carbohydrates.⁸ Imitating this process by producing a so called solar fuel could solve the worlds energy problem, as the annual need of energy on earth is less than the energy from sunlight which strikes the planet in one hour.⁹ The efficient conversion of solar energy to a solar fuel has therefore the capacity to fulfill global energy demands whereas the current use of fossil fuels to satisfy the increasing worldwide hunger for energy is not sustainable. Mimicking nature through the development of low cost systems for efficient capture, conversion and storage of solar energy is one of the greatest challenges of our age.^{10,11} Water oxidation is a key reaction in this area of research because for all substances nowadays considered as solar fuels, water oxidation is the most favorable electron source. On the other hand, several potential reduction reactions yielding hydrogen, methane or other fuels are being discussed. Manganese catalysts are promising compounds for artificial photosynthetic systems as they not only resemble the biological system but are also based on an abundant and low-priced metal.

During the last 30 years, many dimanganese complexes have been synthesized to mimic the OEC. Nevertheless, no manganese complex is currently known which catalyzes water oxidation, whereas several homogeneous water oxidation catalysts containing ruthenium or iridium have been reported.¹² A possible reason for this fact could be that the manganese compounds studied so far did not possess the right coordination geometry for water oxidation catalysis. Thus a dimanganese complex was synthesized in this thesis project which possesses

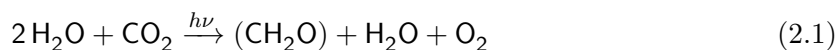
oxidation stable ligands and a geometrical arrangement that would allow reaction scenarios proposed for the critical step of O–O bond formation.¹³ Results concerning the structural and spectroscopic properties, electrochemical investigations and of course the ability to catalyze water oxidation of this complex are presented and discussed extensively in chapter 6 and in paper I.

It had been shown that water oxidation catalysts could be prepared in the form of heterogeneous systems using clays as solid supports for dinuclear manganese complexes.^{14–17} However, it remained unclear how water oxidation is achieved by these clay hybrids and what role the ligand framework of the manganese compounds plays. To answer these questions two dimanganese complexes and two manganese salts were adsorbed on K10 montmorillonite clay. In addition to catalytic experiments, UV/Vis, EPR and XAS spectroscopy were employed to learn more about this class of heterogeneous catalysts. These results are presented in chapter 7 and in paper II.

Furthermore, manganese(I) tricarbonyl complexes seem to be very important in the research of photoactivated carbon monoxide releasing molecules (photoCORMs).¹⁸ Carbon monoxide (CO) is well known nowadays as a small molecule messenger in organisms¹⁹ and, due to many beneficial effects on tissues and organs, it has received much attention regarding its use as therapeutic agent.²⁰ For this application, the release of carbon monoxide must be controlled precisely because of the high cell toxicity of CO in higher concentrations. Studies about the photoactivated CO release of a manganese(I) tricarbonyl complex revealed the high potential of these compounds for CORM activity.^{18,21} Nevertheless, the products and possible intermediates of these reactions remained unknown. As a consequence, a combination of spectroscopic methods were employed in the course of this thesis to reveal details of the processes resulting in CO release for two $\text{Mn}(\text{CO})_3$ model complexes (chapter 9 and paper III).

2. Water oxidation as part of natural photosynthesis

Photosynthesis is one of the most important chemical processes on Earth.¹¹ During oxygenic photosynthesis in green plants, algae and photosynthetic bacteria, water oxidation is achieved through absorption of sunlight and the solar energy is fixed biochemically through the reduction of carbon dioxide. Oxygen is released as a waste product. The enrichment of oxygen in the atmosphere as a consequence of photosynthesis has created the conditions for the development of higher forms of life on our planet as we find them today. An overall “equation” of photosynthesis occurring in plants is given as follows



The process of photosynthesis occurs in plants and algae in the chloroplasts and is divided into light-dependent and light-independent sub-processes.²² The light reactions take place within the thylakoid membrane in two protein complexes, photosystem I (PSI) and photosystem II (PSII) (Fig. 2.1). During the light reactions, reduction equivalents (NADPH) and energy equivalents (ATP) are generated through oxidative water splitting by the conversion of solar energy. These products are later used for carbon dioxide (CO₂) fixation during the light-independent reactions also termed Calvin Cycle. These reactions occur in the stroma, the aqueous fluid inside the chloroplasts.

2.1. Light-dependent reactions of oxygenic photosynthesis

Photosystem I and photosystem II are embedded in the thylakoid membrane (Fig. 2.1).^{7,23} Each photosystem has a light harvesting complex (LHC I/II) which consists of hundreds of chlorophyll *a*, chlorophyll *b*, xanthophyll and carotenoid molecules. Sunlight is absorbed by these LHCs and transported via resonance energy transfer to two chlorophyll *a* molecules in the reaction centers. At PSII these chlorophylls are termed P680 because one of its absorption maxima is found at 680 nm.²⁴ In its excited state, this pigment is able to transfer an electron to a primary acceptor molecule, pheophytin *a*. The oxidized P680 is a strong oxidant and is rereduced by a redoxactive tyrosine Y_Z. With +1.2 V vs. NHE the oxidizing potential of Y_Z^{•+} is one of the highest in nature²⁵ and Y_Z^{•+} can hence be rereduced by the oxygen evolving complex (OEC) with an electron deriving from water oxidation.²⁶

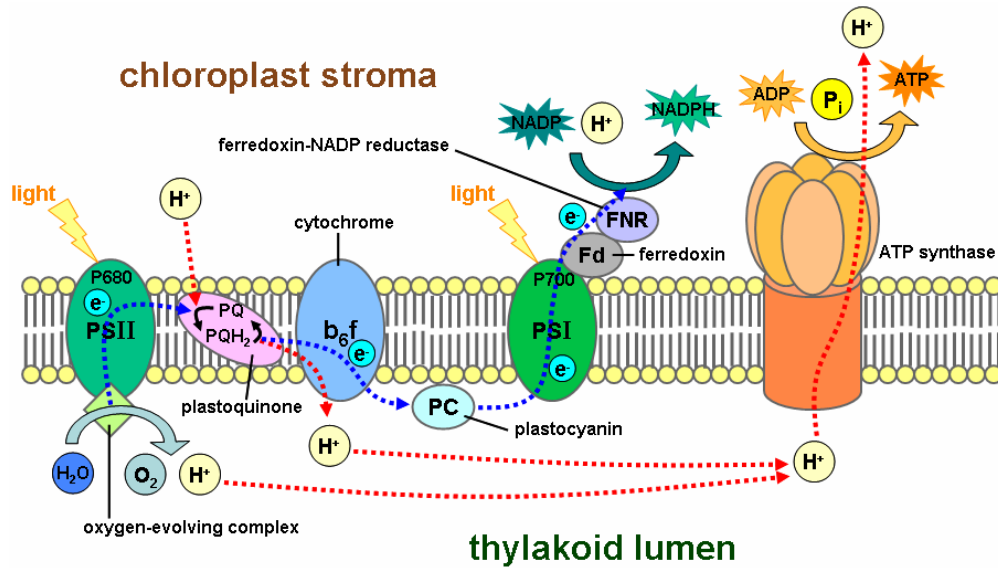


Figure 2.1.: Schematic representation of the light-dependent reactions occurring in the photosystems I and II embedded in the thylakoid membrane.²⁷

The reduced pheophytin transfers the electron via a protein bound plastoquinone Q_a to a reversibly bound plastoquinone (Q_b) which delivers the electron to the mobile plastoquinone pool in the thylakoid membrane. From here the electron can be transferred to a cytochrome b_6f complex. This electron transfer is coupled to proton transfer from the stroma to the lumen. A mobile plastocyanin (PC) collects the electron on the inner site of the thylakoid membrane from the cytochrome b_6f complex and transfers it to PSI.

The P700 in PSI is also oxidized after excitation by solar irradiation whereby charge separation is induced here as well. The mobile plastocyanin then rereduces the $P700^+$. The electron transfer is carried out by the primary electron acceptor of PSI, another chlorophyll a (A_0), via the acceptor A_1 and membrane bound iron sulfur proteins (F_X , F_A , F_B) to a soluble ferredoxin (Fd). At the end of the chain, a flavoprotein (FNR) then reduces $NADP^+$ to NADPH which is used for carbon dioxide reduction in the light independent reactions. The protons from water oxidation and the protons which are transferred via the cytochrome b_6f complex during the electron transfer chain into the lumen provide a proton gradient across the membrane. This gradient is used by the enzyme ATP synthase for the production of ATP from ADP and phosphate.²²

The components which participate in the light reactions are unevenly spread within the thylakoid membrane. PSII is mainly found within the grana thylakoid membranes, while PSI, ATP synthase and cytochrome b_6f complexes are predominantly located within the stroma thylakoid membrane. This uneven arrangement necessitates the presence of mobile electron transmitters like plastocyanin.²²

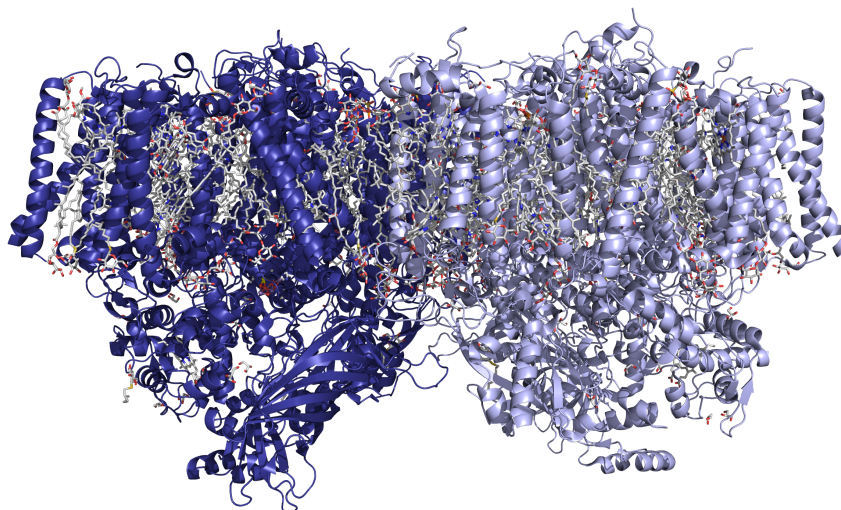


Figure 2.2.: Structure of PSII dimer from *T. vulcanus* at a resolution of 1.9Å.⁷

2.2. Structure of photosystem II

The protein ensemble photosystem II is located in the thylakoid membrane of chloroplasts of oxygenic photosynthetic organisms. The structure of PSII has been solved very recently at a resolution of 1.9 Å for PSII isolated from the cyanobacterium *Thermosynechococcus vulcanus* by Umena et al. (Fig. 2.2).⁷ The protein complex is dimeric and has a total weight of 350 kDa. Each monomer contains 20 subunits. The subunits D1 and D2 form the center of a PSII monomer. In addition to the protein subunits they contain 35 chlorophylls, two pheophytins, more than 20 lipids, 11 β -carotenes, two plastoquinones and a Mn_4CaO_x cluster, the oxygen evolving complex (OEC). Further cofactors are chloride ions and one hydrogen carbonate ion. The geometric arrangement of amino acid side chains, cofactors and, most importantly, of the metal ions of the Mn_4CaO_x cluster could be established from the electron density map.

2.3. Geometric structure of the oxygen evolving complex

For the first time the high resolution structure of Umena et al. (“Osaka structure”) provided a detailed coordination environment of the Mn_4Ca cluster.^{7,28} Five oxygen atoms were detected which serve as oxido bridges between the five metal ions. It was found that an asymmetric cubane-like arrangement is formed in which three manganese and one calcium occupy four corners and four oxygen atoms occupy the other four (Fig. 2.3). The bond lengths between the oxygen and the manganese atoms in the cubane are in the range of 1.8-2.1 Å and between the calcium and the oxygen atoms they are in the range of 2.4-2.5 Å. The fourth manganese atom is connected to two manganese ions by oxido bridges and is located outside the cubane. A cubane-like arrangement had already been proposed by Ferreira and coworkers in 2004, but

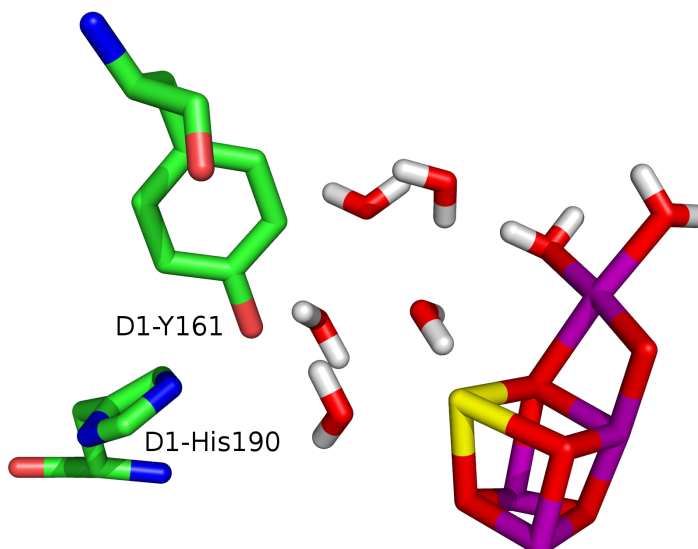


Figure 2.3.: Structure of the Mn_4CaO_5 -cluster determined at 1.9 Å resolution. The metal cluster is held in place by amino acid residues and is linked via a hydrogen-bonding network to Y_{161} ($=\text{Y}_Z$). Color code: manganese, purple; calcium, yellow; oxygen, red; carbon, green; nitrogen, blue; hydrogen, white.²⁸

the exact metal-to-metal distances or the oxido bridges were not resolved in the 3.5 Å crystal structure (“London structure”).²⁹ The determined positions of the metal ions of the London structure do not match the ones of the Osaka structure very well whereas the 2.9 Å structure (“Berlin structure”) of Guskov and coworkers from 2009³⁰ shows only small differences to the recent high resolution Osaka structure. The position of bridging oxygen ligands could not be resolved either in the Berlin structure in which a Y shaped geometrical arrangement of the manganese atoms and the calcium ion as the head of a trigonal pyramid with three manganese atoms as the base was proposed.^{30,31} The whole arrangement of the Mn_4CaO_5 cluster in the Osaka structure was entitled by Umena and coworkers as “distorted chair” with the fourth manganese atom as the back of the chair and the cubane as the seat base (Fig. 2.3). Furthermore, four water molecules were detected in the coordination sphere of the Mn_4CaO_5 cluster, with two water molecules bound to the calcium atom and the other two to the fourth manganese atom outside the cubane. An hydrogen-bonding network was identified in between the electron transfer mediator Y_Z , the Mn_4CaO_5 cluster and the lumen. Therefore, the presence of proton-coupled electron transfer through Y_Z is suggested.²⁸

2.4. Mechanism of photosynthetic water oxidation

In 1969, Joliot and coworkers discovered that upon illumination by short light flashes, isolated chloroplasts or *Chlorella* cells evolve oxygen with a period of four flashes.³² One year later Kok et al. proposed a four step charge accumulation model for water oxidation in which the

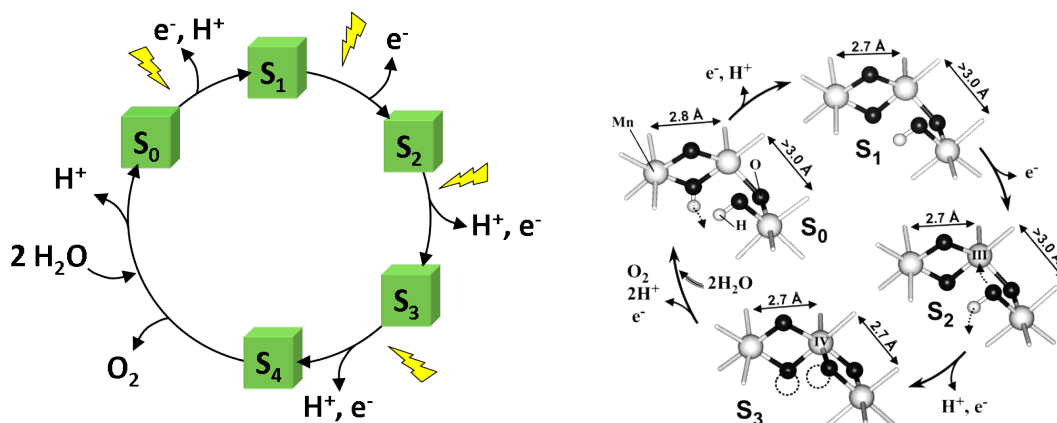


Figure 2.4.: Left: Kok cycle of photosynthetic water oxidation which explains the period-four oscillation in oxygen evolution.³⁵ Oxygen is released and one or two water molecules rebind during the S₄→S₀ transition. Today it is also known that oxidations are accompanied by proton release.³⁶ Right: Model for structural changes of the OEC in the water oxidation cycle derived from EXAFS measurements. Only three manganese ions are shown for clarity. Reprint with permission from reference.³⁷ Copyright 2005, American Chemical Society.

Mn₄CaO₅ cluster cycles through five oxidation states. These were termed S_{*i*} states, where *i* is the number of oxidizing equivalents stored by the OEC. The S₄ state is a transient state, in which oxygen is formed and released, whereby the Mn₄CaO₅ cluster decays into the S₀ state (Fig. 2.4, left). A light reaction is needed for each state transition except for the last one. The oxidation states of the manganese ions are most likely Mn₃^{III}Mn^{IV} in the S₀ state^{12,33,34} and the dark-stable state is S₁.³⁵ It is assumed that each S state transition implicates an oxidation from Mn^{III} to Mn^{IV} up to the S₃ state.^{33,34} The S₃→S₄ transition involves either a Mn^{IV} to Mn^V oxidation or a water-derived ligand oxidation.³⁶

XAS and ⁵⁵Mn-ENDOR spectroscopy indicate that the oxidation steps are accompanied by structural changes of the OEC (Fig. 2.4, right).^{37,38} It is suggested that new oxido bridges form between the manganese centers promoted by deprotonations of terminal water or hydroxido ligands. Four oxidizing equivalents are accumulated and stored by increasing the oxidation states of the manganese ions of the OEC whereas water is not oxidized partly during the oxidation state cycle. This enables the thermodynamically favored concerted four-electron oxidation of water instead of four one-electron oxidation steps. The latter requires an unfavorable step from water to a hydroxyl radical with a potential of 2 V (see the Frost diagram in Fig. 2.5 for further details).^{10,36} This procedure facilitates the coupling between the fast one-electron photochemistry with the several orders of magnitude slower four-electron water oxidation chemistry. The S-state transitions except the S₁→S₂ transition are all supposed to be coupled with proton release of the OEC. These proton-coupled electron transfer steps (PCET) lead to the accumulation of oxidizing equivalents without increasing

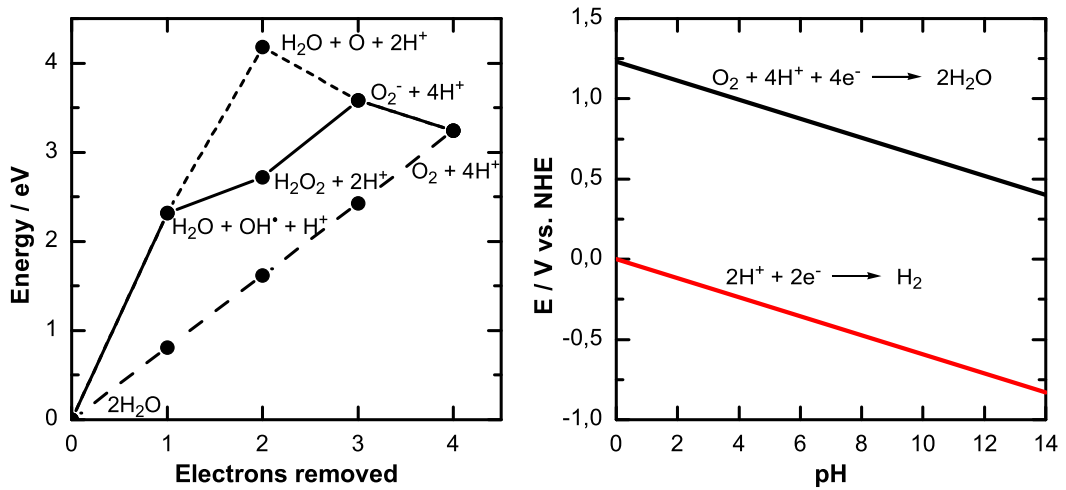


Figure 2.5.: Frost diagram for oxygen electron transfer steps at pH 7 vs. NHE (left). Pourbaix diagrams for the half reactions of hydrogen and oxygen productions (right). Diagrams were plotted according to Moore and Brudvig.¹⁰

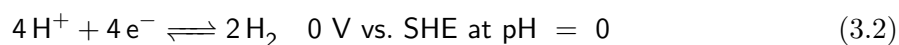
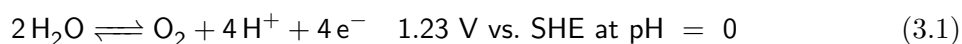
the overall charge of the OEC. Thus the oxidation of the Mn_4CaO_x cluster by Y_Z at constant potentials is facilitated.

3. Water oxidation as part of artificial photosynthesis

In the last 40 years, many approaches concerning artificial photosynthesis have been reported. The ideal low-cost device would be capable of using sunlight to split water into H_2 and O_2 . Effective coupling of light capture, charge separation, and efficient catalysts are required. A theoretical photochemical device for the generation of hydrogen as a solar fuel from the splitting of water has already been described by Lehn and coworkers in 1979 (Fig. 3.1).³⁹ Water oxidation and hydrogen generation occur in spatially divided photo reactions. A relay molecule mediates the two different half reactions for which in each case a photosensitizer and a catalyst are needed. This chapter mainly focuses on recent progress in the development of systems for water oxidation. Reviews on developments in the field of hydrogen generation or other potential solar fuels can be found elsewhere.^{40–44}

As protons are involved in both water oxidation and hydrogen production, the formal potentials of these reactions are pH dependent, as indicated by the Pourbaix diagrams in Figure 2.5 (right). Figure 2.5 (left) illustrates the energy demand of water oxidation depending on the reaction coordinate. The minimum energy path is the concerted water oxidation (long dashed line). Energy demands for pathways via hydrogen peroxide or an oxygen atom vary widely and are generally much higher.

The half reactions and the overall equation of water splitting are given by



In practice a higher electrical potential than the theoretical value of 1.23 V (vs. SHE at $\text{pH} = 0$) is needed. This overpotential is specific to each device due to several contributions such as the ability to stabilize the reaction intermediates. For efficient and low cost water splitting, catalysts based on abundant metals with moderate overpotentials and high persistence are needed. In the following subsections different routes of carrying out water oxidation

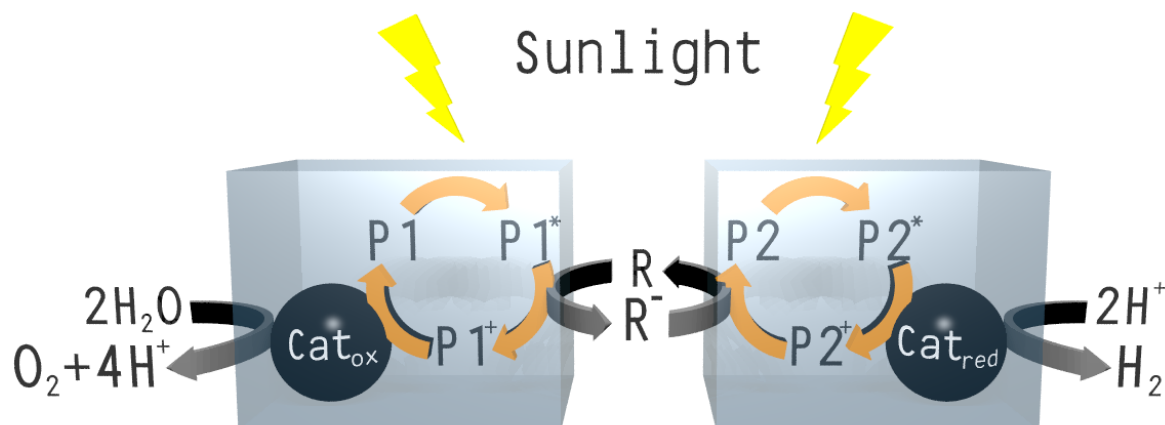


Figure 3.1.: A possible scheme for an artificial photosynthetic device adapted from Lehn et al.³⁹

will be presented.

3.1. Electrochemical water splitting

The electrocatalytic water splitting into oxygen and hydrogen by electricity was already investigated by van Trooswijk and Deiman in 1789, who decomposed water “*by the electric spark into combustible air and vitalized air*”.^{45,46} In 1866 Hofmann identified the developed gases as hydrogen and oxygen in a ratio of 2:1.⁴⁷ At the beginning of the 20th century industrialization of water electrolysis provided pure hydrogen, e.g. for ammonia production through the Haber-Bosch process.^{12,48} Besides the use of precious metals such as Pt, Ru and Ir, several approaches concerning electrochemical water splitting devices have recently been published based on inexpensive first row transition metal oxides. In this section various electrocatalysts are presented which differ e.g. in deposition methods, presence of co-deposits, use of supports or the kind of the electrode used.

The photocatalytic activity of cobalt(II) phosphate solutions was already observed by Sutin and coworkers in 1983.⁴⁹ Nocera et al. have reported a cobalt(II) and phosphate containing catalyst electrodeposited on an indium tin oxide electrode.⁵⁰⁻⁵³ This catalyst showed long time stability and self-healing abilities in phosphate containing solutions.⁵⁴ Similar catalysts could be achieved through sputter-deposition of thin films of cobalt on a glass substrate.⁵⁵ In a following report also borate based catalysts were presented and both borate and phosphate containing cobalt catalysts have shown high water oxidation activities with seawater and river water.⁵⁶ XAS investigations by the group of Dau suggest that the material is composed of interconnected Co(III)-oxido cubanes⁵⁷ whereas XAS experiments performed by Nocera et al. during electrocatalytical water splitting reveal CoO₆ octahedra as structural catalyst motif.⁵⁸

Also spinel type oxides are used for low cost approaches for water oxidation electrocata-

lysts. Nanocrystalline $\text{Co}_x\text{Mn}_{3-x}\text{O}_4$ spinels presented by the group of Chen showed significant electrocatalytic water oxidation activity due to high surfaces and abundant defects.⁵⁹ Furthermore, some active water oxidation catalyst such as the one reported by Bonchio et al. are based on polyoxometalates (POM). This POM with a tetraruthenium center is capable of water oxidation with Ce^{IV} ^{60–62} and can also be immobilized on electrodes.⁶³ The catalyst is codeposited with multiwalled carbon nanotubes (MWCNT) on ITO electrodes improving the electron transfer to the electrode. Electrocatalytic activity with low overpotentials was observed.

Highly active water oxidation catalysts were achieved by Brudvig, Crabtree and coworkers through electrodeposition of amorphous iridium oxides from the molecular precursor $[\text{Cp}^*\text{Ir}(\text{H}_2\text{O})_3]^{2+}$.⁶⁴ In the same work the water-soluble complex $[\text{Cp}^*\text{Ir}(\text{pyrCMe}_2\text{O})\text{X}]$ is presented which deposits homogeneously, as could be proven by an electrochemical crystal nanobalance. Deposition of molecular catalysts on conductive surfaces is another method for the preparation of electrochemical cells that efficiently split water.⁶⁵ However, after several hours of operation, the catalyst detaches from the electrode in most of the systems.⁶⁶ A method to prevent the detachment is the use of a polymer support such as Nafion. A supporting matrix is capable of holding the catalyst at the electrode surface and higher catalyst stabilities are thus achieved.^{65,67}

Manganese oxides are also playing an important role. In a recent communication, Gorlin and Jaramillo presented a nanostructured manganese oxide catalyst electrodeposited onto a glassy carbon substrate.⁶⁸ This electrocatalyst shows activity for both oxygen reduction and water oxidation and these were comparable to that of precious metals and higher than the Co-based catalyst mentioned before. This section has shown that the development of inexpensive water oxidation electrocatalysts has progressed well in recent years. However, these systems are still far away from application and further investigations regarding activity and long-term stability are needed. Furthermore, they are unsuitable for mechanistic studies.

3.1.1. Photoelectrochemical water splitting

Many approaches concerning photoelectrochemical water splitting have been published, and a very recent review by Moore and Brudvig provides an insight into this field.¹⁰ The simplest method to split water photoelectrochemically is the coupling of commercial silicon solar cells which can power a common electrolyzer with an energy storage efficiency of $\sim 11\%$.¹⁰ However, this array is too expensive for global scale applications and cheaper materials are needed. In general, research in this field can be divided into three different approaches: as mentioned, the combination of photovoltaic cells with electrochemical water splitting employing electrodes like the ones presented in the previous section; the use of photoelectrodes mainly based on semiconductors and, in some cases, dye sensitized; or the combination of both techniques in a so called tandem cell. An external bias is needed in most cases for these systems which is

supplied by a tandem cell configuration through the attached photovoltaic cell.

The first device for the coupling of water electrolysis and photovoltaic solar energy conversion was published by Fujishima and Honda in 1972.⁶⁹ In this electrochemical cell, a n-type semiconductor titanium dioxide (rutile) photoanode is connected with a platinum counter electrode. Water photolysis is achieved with an external bias of 0.25 V and irradiation with wavelengths shorter than 415 nm, corresponding to the bandgap of TiO₂ (3.0-3.2 eV). Quantum efficiencies of ~10% and a hydrogen production efficiency of ~1% were estimated. In the last four decades, many n-type metal oxide semiconductors such as α -Fe₂O₃⁷⁰⁻⁷² and WO₃⁷³⁻⁷⁶ have been employed to increase photon-to-electron efficiencies for water oxidation with externally applied potentials. Khaselev and Turner achieved direct water electrolysis with a combined photoelectrochemical-photovoltaic design.⁷⁷ This cell splits water upon irradiation and is voltage biased with an integrated photovoltaic device. A hydrogen production efficiency of 12.4 % is achieved through this tandem cell configuration.

Various approaches concerning photoelectrochemical cells containing molecular catalysts deposited on conductive surfaces have been presented.⁶⁵ Spiccia and coworkers have published several studies concerning a Mn₄O₄⁶⁺ cubane complex deposited on electrode surfaces. Under application of a polarization current of 1.0 V vs. Ag/Ag⁺ and illumination with visible light, turnover numbers of > 1000 were achieved after a reaction period of 65 h.^{67,78,79} In a following study, a photoanode consisting of a TiO₂ layer which is sensitized with a ruthenium dye and coated with the Mn₄O₄⁶⁺ cubane in a Nafion membrane was reported.⁸⁰ Coupled to a platinum cathode, water splitting is achieved without an external bias under irradiation with wavelengths in the UV region. The generated photocurrent was highly increased in comparison to the system of Fujishima and Honda (vide supra). Transmission electron microscopy and in situ XAS measurements revealed that disordered Mn(III/IV)-oxide nanoparticles were formed through reoxidation of Mn(II) species, initially formed from dissociation of the cubane.⁸¹ This results have shown that the Mn₄O₄⁶⁺ cubane complex is just a precursor to the catalytically active manganese oxides.

Another method is the use of dye sensitized solar cells.^{65,82} These devices consist of a photosensitizer (dye) for light absorption attached to a semiconductor (mostly TiO₂). Brudvig et al. achieved enhancement in photoelectrochemical water splitting through codeposition of a zinc porphyrin on titanium dioxide nanoparticles together with a molecular iridium complex.⁸³ The photocurrent is significantly increased through the presence of the porphyrin dye. In comparison to the device of Spiccia⁸⁰ this system operates under irradiation with visible light but under application of an external bias.

The group of Nocera coupled their cobalt catalyst with a silicon solar cell.⁸⁴ A photoanode with high stability and water oxidation activity at neutral pH was achieved under application of an external bias voltage of 0.6 V vs. NHE and illumination with wavelengths between 400 and 1000 nm. In a recent communication, Domen and coworkers have reported, that

fluorine doped tin oxide electrodes coated with strontium niobium oxynitride (SrNbO_2N) can be used as photoelectrodes for water splitting.⁸⁵ Under visible light irradiation and neutral aqueous conditions, water splitting occurs without an externally applied potential. The performance of the SrNbO_2N photoanode has to be further improved as the photon-to-electron conversion efficiencies are very low. The direct use of birnessite-type manganese oxides as a photoanode has been described by Jaramillo and coworkers.⁷⁶ Thin films of sodium birnessite were electrodeposited onto fluorine-doped tin oxide (FTO) substrates. However, only very low external quantum efficiencies ($<1\%$) were reached.

In summary, photoelectrochemical water splitting has a huge potential in solar fuel generation whereas the research is still in its infancy. The different approaches presented here show that there is a large amount of possibly suitable materials to be explored. Many problems on the way to big scale applications like efficiency, stability and scalability have to be solved.

3.2. Homogeneous ruthenium or iridium based catalysts for water oxidation

Molecular water oxidation catalysts have also attracted huge attention in recent years. They show several advantages over heterogeneous catalysts like tunable properties and the ease of characterization. A water oxidation catalyst has to allow the take-out of four electrons at potentials $> +1$ V in one-electron oxidation steps. Only few types of molecular water oxidation catalysts are known. Most of them are based on ruthenium or iridium whereas no manganese complex is currently known which is able to catalyze water oxidation homogeneously. Two test systems for homogeneous water oxidation are nowadays established. One oxidant is cerium(IV) ammonium nitrate (Ce^{IV}) which is reduced to Ce^{III} after electron uptake. This system can only be used at $\text{pH} < 2$ to avoid the precipitation of cerium hydroxides. A further possibility is the use of photogenerated ruthenium(III) tris-bipyridyl ($[\text{Ru}(\text{bpy})_3]^{3+}$). This oxidant originates from $[\text{Ru}(\text{bpy})_3]^{2+}$, which after photoexcitation delivers an electron to a sacrificial electron acceptor like peroxodisulfate.⁸⁶ In both cases, labelling studies using H_2^{18}O clearly showed that both oxygen atoms of the O_2 product originate from labelled water molecules. If oxygen evolves in reactions where either Ce^{IV} or $[\text{Ru}(\text{bpy})_3]^{3+}$ are used as oxidation agents, such reactions can therefore be considered as true water oxidation reactions. In this section, a selection of the most important homogeneous catalysts and the related mechanisms are presented.

The first homogeneous water oxidation catalyst which has been reported was *cis,cis*- $[\text{Ru}_2(\text{O})(\text{H}_2\text{O})_2(\text{bpy})_4]^{4+}$ (bpy = 2,2'-bipyridine, Fig. 3.2, **Ru1**), the so-called "blue dimer" because of its characteristic deep blue color, published by Meyer and coworkers in 1982.⁸⁷⁻⁸⁹ This complex contains two ruthenium centers each coordinated to one water molecule and two bpy ligands and connected via a μ -oxido bridge, which is responsible for the intramolecular

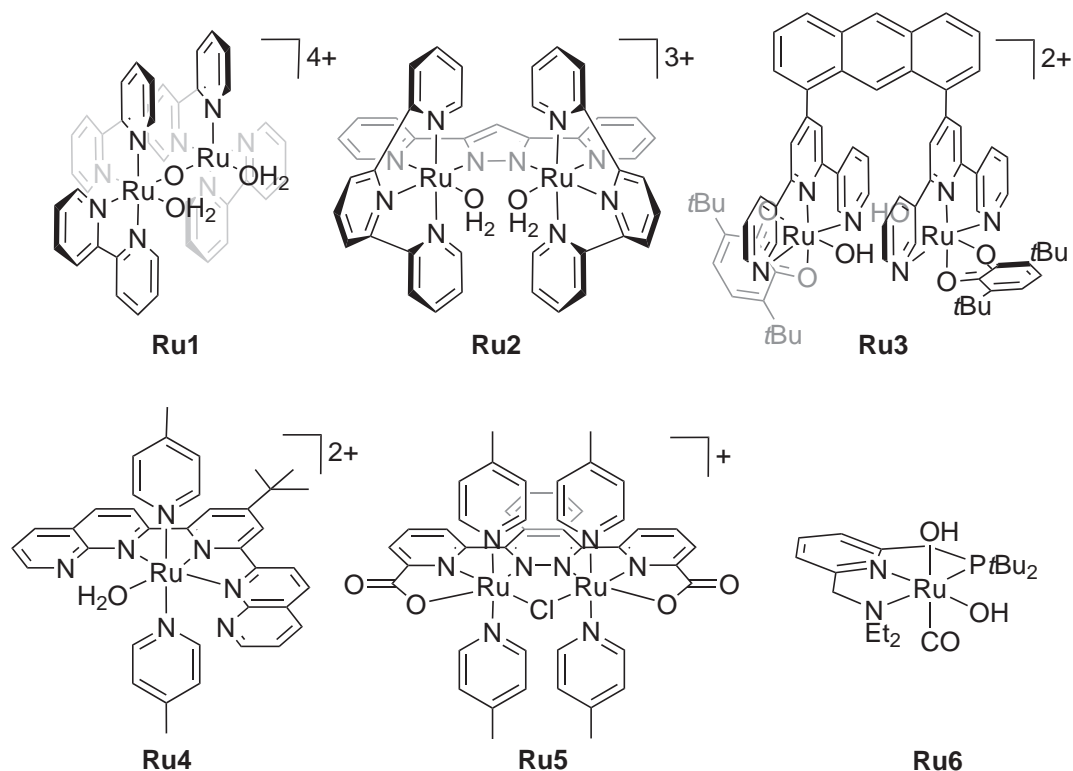


Figure 3.2.: Examples of molecular water oxidation catalysts containing ruthenium. The oxido-bridged blue dimer first published by Meyer and coworkers (**Ru1**),^{87–89} the Ru-hbpp complex of Llobet et al. (**Ru2**),⁹⁰ the dinuclear complex containing redox-active quinones from the group of Tanaka (**Ru3**),⁹¹ the first mononuclear ruthenium catalyst from Zong and Thummel (**Ru4**),⁹² the diruthenium catalyst from Sun and coworkers (**Ru5**)⁹³ and the pincer complex of Milstein et al. (**Ru6**).⁹⁴

electronic and magnetic coupling between the metal centers.

The assumption that at least two metal centers are needed for the oxidative coupling of two water molecules to one dioxygen was disproved.^{92,95,96} In the past ten years, many mononuclear metal complexes have been shown to be able to catalyze the oxidation of water, too (Fig. 3.2). The probably rate-determining step for this might be the process of oxygen–oxygen bond formation. For ruthenium complexes, it seems to occur via different pathways depending on ligands, bridging modes and the number of metal centers.⁹⁷ A recent publication has shown that small alterations of a ruthenium-bound ligand influence reaction kinetics.⁹⁸ The two main pathways involved are either the nucleophilic attack of a solvent water molecule or the direct coupling of two Ru–O units. In a review, Romain, Vígara and Llobet discuss these mechanisms in detail.⁹⁷ A special case are complexes with non-innocent ligands, like redox-active quinones. These ligands can undergo reversible redox processes and mediate electron-transfer between the metal and the ligand.^{91,99}

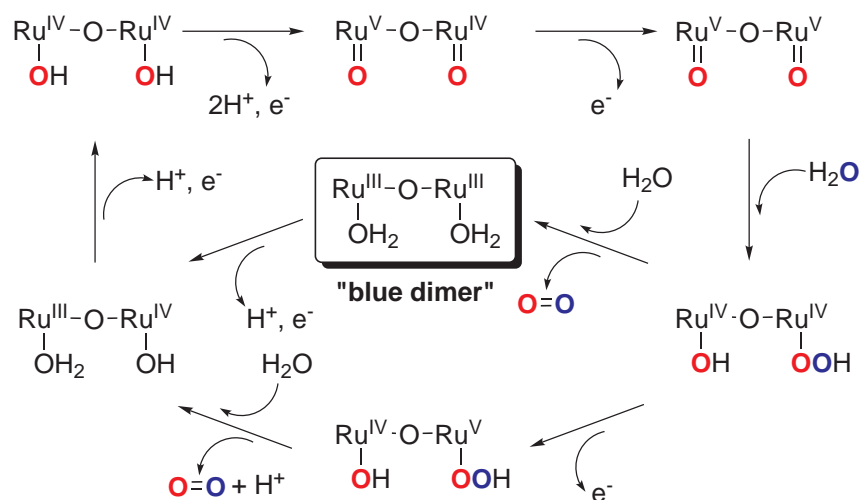


Figure 3.3.: Reaction mechanism proposed for the blue dimer (**Ru1**). Bpy ligands are not shown for clarity.⁹⁷

In general the different mechanisms all involve sequential and simultaneous loss of protons and electrons (proton-coupled electron transfer, PCET). One example for a solvent water nucleophilic attack mechanism is the water oxidation pathway for the blue dimer proposed by Llobet et al., of which a simplified version is presented in Figure 3.3.⁹⁷ The initial $\text{Ru}_2^{\text{III,III}}$ complex is oxidized to $\text{Ru}_2^{\text{V,V}}$ where both ruthenium centers have a terminal oxido ligand. A nucleophilic attack from a water molecule generates a $\text{Ru}_2^{\text{IV,IV}}$ species containing an end-on peroxido and an end-on hydroxido ligand, respectively. This intermediate can then react in two different ways depending on the concentration of the oxidation agent Ce^{IV} . In the absence of excess oxidant, the initial blue dimer is returned under dioxygen release, whereas reaction with an excess of Ce^{IV} involve further oxidations before the release of dioxygen occurs. In this mechanism only one metal ion is directly involved in the O–O bond formation through a nucleophilic attack of solvent water while the other ruthenium primarily acts as a storage for oxidation equivalents.

A recent DFT study of the O–O bond formation step by Bianco and coworkers, shown in Fig. 3.4, includes the surrounding water molecules through an explicit solvent treatment.¹⁰⁰ Two water molecules are bound via hydrogen bridges to the oxido ligands of the $\text{Ru}_2^{\text{V,V}}$ intermediate. The nucleophilic attack on the oxido ligand by a water molecule is coupled to a proton transfer chain mediated by the water molecules and an electron transfer via the Ru–O–Ru bond. While at one terminal oxido ligand the O–O bond is formed, the other one is protonated. Similar results were also found by Yang and Baik with theoretical calculations on a lower level whereas just one water molecule was used and differences exist concerning activation energies and transition states.¹⁰¹

The dinuclear complex $[\text{Ru}_2^{\text{II}}(\text{terpy})_2(\text{H}_2\text{O})_2(\mu\text{-bpp})]^{3+}$ ($\text{bpp}^- = 3,5\text{-bis-(2-pyridyl)pyra-}$

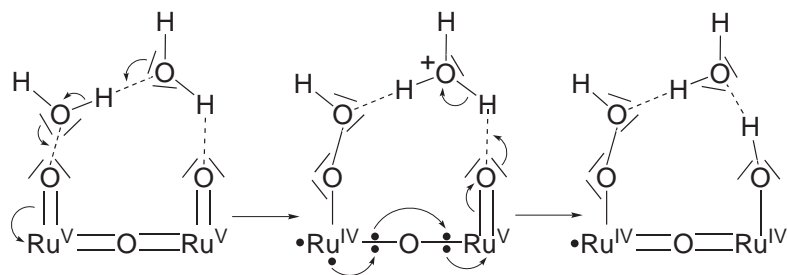


Figure 3.4.: Mechanism for the O–O bond formation step during water oxidation catalyzed by the blue dimer based on a theoretical study from Bianco et al.¹⁰⁰

zolate and terpy = 2,2';6',2''-terpyridine, Fig. 3.2: **Ru2**) of Llobet and coworkers is bridged by the anionic bpp^- ligand. The arrangement of the terpy and bpp^- ligands leads to a very small distance for the oxygen atoms deriving from the water ligands of 2.48 Å. O–O bond formation is supposed to occur via an intramolecular coupling of ruthenium oxido species. This mechanism was supported through ^{18}O labelling experiments⁹⁰ and DFT calculations predicting a μ -1,2-peroxido intermediate before dioxygen is released (Fig. 3.5).¹⁰²

A further water oxidation pathway proceeds via noninnocent ligands. Tanaka et al. have reported the complex $[\text{Ru}_2^{\text{II}}(\text{Q})_2(\text{OH})_2(\mu\text{-btpyan})]^{2+}$ (Fig. 3.2: **Ru3**)⁹¹ where btpyan (1,8-bis(2,2';6',2''-terpyridyl)-anthracene) is a dinucleating ligand based on two terpy molecules bridged by anthracene. Additionally, one hydroxide and one 3,6-di-*tert*-butyl-benzoquinone (Q) are coordinated to each metal center. At an applied potential of 1.7 V (vs. Ag/Ag^+) a high amount of dioxygen is evolved. The dioxygen formation has been assumed to occur via peroxido intermediates which explains the need of this high potential. Theoretical calculations support the assumption that the ruthenium centers are redox inactive during water oxidation and all electron transfer processes are based on the quinone ligands.⁹⁹ However, very recent computational studies by Ghosh and Baik have revealed that only one subunit of the dinuclear complex is redox active and the oxidation state of the quinone ligand shuttles between 0 and –I (semiquinone) while the ruthenium oxidation state changes between +II and +III.¹⁰³

Thummel and coworkers have reported a series of mononuclear ruthenium complexes (Fig. 3.2: **Ru4**) which are capable of oxidizing water upon addition of Ce^{IV} .^{92,95} Water oxidation occurs at mononuclear ruthenium complexes presumably via cycling between Ru^{II} and Ru^{VI} . It has been proposed that the O–O bond formation step involves an additional water molecule which stabilizes higher oxidation states of the metal center. A diruthenium complex with a *cis* geometry (Fig. 3.2: **Ru5**) has been synthesized by the group of Sun.⁹³ This dinuclear compound is one of very few examples with an overpotential low enough to split water by visible light and $[\text{Ru}(\text{bpy})_3]^{3+}$ as photosensitizer. Turnover numbers of 60 ($[\text{Ru}(\text{bpy})_3]^{3+}$) and 10 400 (Ce^{IV}) have been achieved.

As a last example, Milstein et al. have reported the complex $[\text{Ru}^{\text{II}}(\text{OH})_2(\text{PNN})(\text{CO})]$ (Fig.

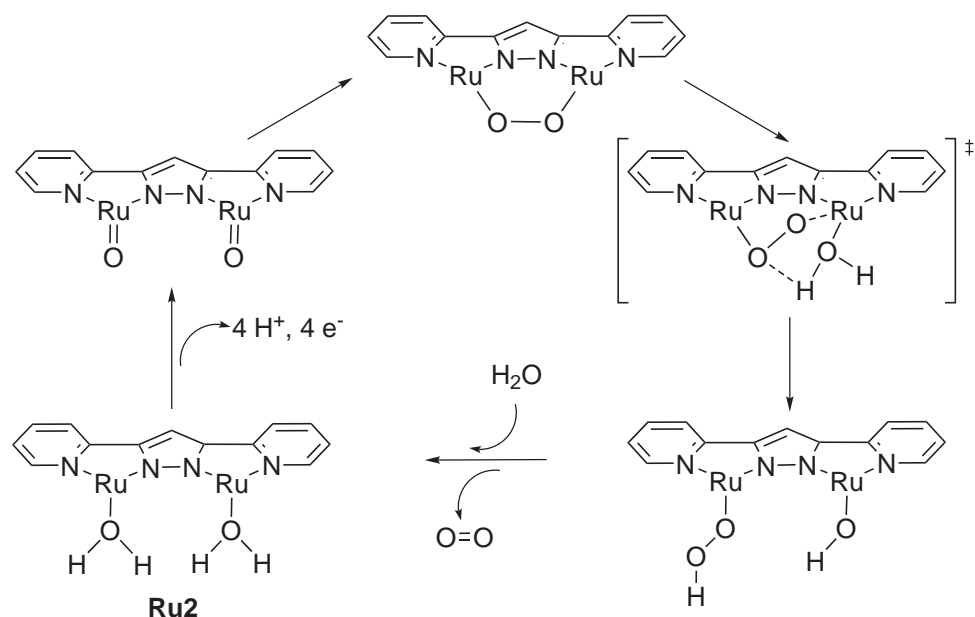


Figure 3.5.: Simplified reaction pathway for dioxygen formation by $[\text{Ru}_2^{\text{II}}(\text{terpy})_2(\text{H}_2\text{O})_2(\mu\text{-bpp})]^{3+}$ (**Ru2**) based on DFT calculations.¹⁰² Terpyridine ligands are not shown for clarity.

3.2: **Ru6**) which contains the meridionally coordinating PNN ligand (PNN = 2-(di-*tert*-butyl-phosphino-methyl)-6-(diethylaminomethyl)pyridine), one carbon monoxide and two *cis* hydroxides.⁹⁴ This system is capable of oxygen and hydrogen production in consecutive thermal- and light-driven steps. Reactions with water at 25°C and subsequently at 100°C have yielded dihydrogen and the following irradiation with wavelength of 320–420 nm range has liberated dioxygen and regenerated the starting complex. Hydrogen peroxide has been assumed to be produced during the last step which quickly disproportionates.

Homogeneous catalysts with similar turnover numbers have been developed in the form of mononuclear iridium complexes. First examples were reported by the group of Bernhard in 2008 where a series of bis(phenylpyridine)-bis(aquo) iridium(III) complexes were synthesized which are efficient water oxidation catalysts upon addition of Ce^{IV} (Fig. 3.6: **Ir1**).¹⁰⁴ In the last two years many other iridium complexes which act as water oxidation catalysts have been published.^{105,106} Most of them contain a pentamethylcyclopentadienyl ligand (Cp^*) like the ones from the groups of Crabtree¹⁰⁷ and Albrecht¹⁰⁸ presented in Figure 3.6. The latter achieves a turnover number of nearly 10 000 for water oxidation driven by Ce^{IV} . Brudvig and coworkers have reported about possible problems which particularly occur for electrochemical water oxidation by iridium complexes. Potential ligand decomposition under highly oxidizing conditions can lead to surface-bound heterogeneous catalysts. An electrochemical quartz crystal balance to conduct piezoelectric gravimetry during water oxidation was used to distinguish between homogeneous and heterogeneous catalysis. While a truly homogeneous

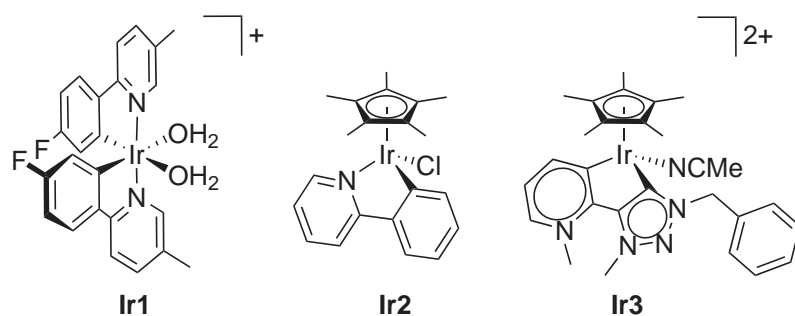


Figure 3.6.: Molecular water oxidation catalysts containing iridium centers. A bis-aquo complex reported by the group of Bernhard (**Ir1**), a Cp* compound of Crabtree et al. (**Ir2**) and the iridium catalyst of Albrecht and coworkers containing a carbene-type donor-ligand (**Ir3**).

catalyst gave no mass change under these conditions, a mass change occurred in the case of deposition of a heterogeneous catalyst on the electrode surface.⁶⁴

Despite the problems associated with the elucidation of the reaction mechanisms, the presented catalysts in this section are good model systems for water oxidation reactions and provide important hints for the water oxidation mechanism in nature via the possible characterization of reaction intermediates. However, the high cost and low bioavailability of both ruthenium and iridium discard these metals as part of water oxidation systems on a large scale for a possible technical application. As mentioned above, the focus has to be on other metals like manganese or cobalt. Nevertheless, the Ru or Ir molecular water oxidation catalysts could be useful as model systems for complexes based on abundant metals.

3.3. Homogeneous manganese model systems

Many manganese complexes have been synthesized and investigated in the context of homogeneous water oxidation. As shown in the previous section, complexes of ruthenium and iridium, elements which are diagonally related in the periodic table to manganese, are able to catalyze water oxidation upon reaction with the one-electron oxidants Ce^{IV} or $[\text{Ru}(\text{bpy})_3]^{3+}$. However, no manganese complex is known today which is able to catalyze the oxidation of water in reactions with these oxidation agents. Nevertheless, there are multiple examples where oxygen has been detected as the product of reactions with oxido-transferring oxidation agents like the peroxides H_2O_2 (for further details, see section 4) and *tert*-butyl hydroperoxide (*t*BuOOH) or the two-electron oxidants hypochlorite (OCl^-) and oxone (HSO_5^-).¹⁰⁹

The complex $[\text{Mn}_2(\text{O})_2(\text{H}_2\text{O})_2(\text{terpy})_2]^{3+}$ of Brudvig et al. (Fig: 3.7: **Mn1**) was the first synthetic homogeneous oxygen evolving catalyst. O_2 formation was detected in reactions with hypochlorite or oxone.^{110,111} Kinetic analyses of these reactions led to the assumption that similar mechanisms in both cases operate (Fig. 3.8). Measurements in the presence

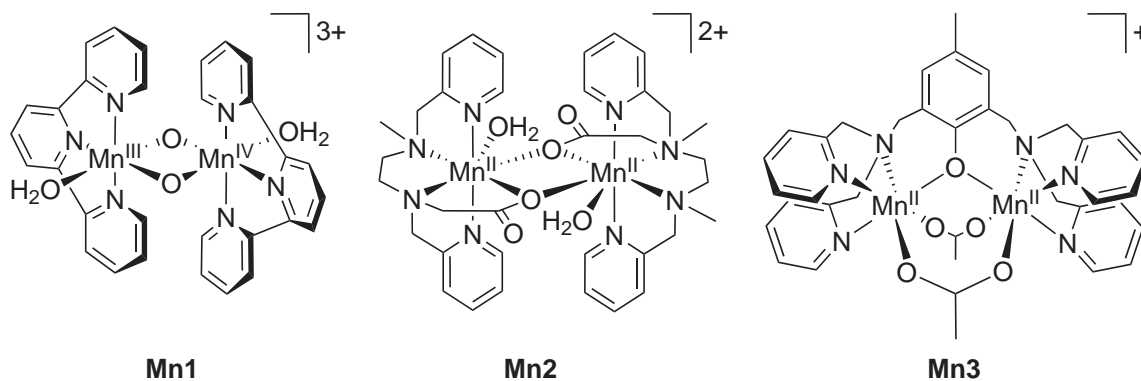


Figure 3.7.: Examples of molecular manganese catalysts that act as oxygen evolving catalysts using oxido-transferring oxidants like hypochlorite (OCl^-), oxone (HSO_5^-) or $t\text{BuOOH}$: $[\text{Mn}_2(\text{O})_2(\text{H}_2\text{O})_2(\text{terpy})_2]^{3+}$ (**Mn1**),^{110–112} $[\text{Mn}_2(\text{H}_2\text{O})_2(\text{mcbpen})]^{2+}$ (**Mn2**)^{113,114} and $[\text{Mn}_2(\text{OAc})_2(\text{bpmp})]^+$ (**Mn3**).^{109,115}

of isotopically enriched water (H_2^{18}O) showed the evolution of $^{18}\text{O}_2$ -enriched dioxygen. Mass spectrometry measurements have shown that this is caused by the reaction of **Mn1** with oxone and water and not by exchange of water-oxygen atoms with other oxygen-containing species in this system.¹¹² Oxygen evolution proceeds via $\text{Mn}^{\text{V}}=\text{O}$ or $\text{Mn}^{\text{IV}}-\text{O}^\bullet$ species and either a subsequent attack of an oxidant molecule (pathway on top) or an attack of a solvent water molecule on the terminal oxido ligand in the proposed mechanism (Fig. 3.8).¹¹¹ However, the detailed mechanism remains unclear.

A further oxygen evolving catalyst is $[\text{Mn}_2(\text{H}_2\text{O})_2(\text{mcbpen})]^{2+}$ ($\text{mcbpen}^- = N\text{-methyl-}N'\text{-carboxymethyl-}N,N'\text{-bis(6-methylpyridin-2-yl)-ethane-1,2-diamine}$) reported by McKenzie and coworkers (Fig. 3.7: **Mn2**).^{113,114} Reactions of this complex and a related analogue with an excess of *tert*-butyl hydroperoxide ($t\text{BuOOH}$) leads to the formation of dioxygen with high turnovers of up to 15 000.

Kurz, Styring and coworkers investigated oxygen evolving reactions of several manganese complexes using six different oxidants.¹⁰⁹ It was shown that oxygen formation was catalyzed by a much larger number of manganese complexes than known so far. In a following isotope-labelling study, the reaction with oxone was analyzed in detail via membrane inlet mass spectrometry (MIMS). During the reaction of $[\text{Mn}_2(\text{OAc})_2(\text{bpmp})]^+$ ($\text{bpmp} = N,N'\text{-bis}((6\text{-methylpyridin-2-yl)methyl})-N\text{-2-pyridylmethylamine}$) (Fig. 3.7: **Mn3**) with oxone or lead acetate as oxidant, the evolution of stoichiometrically labeled dioxygen was observed for a short initial time of the oxidation process.¹¹⁵ This is the first example of a reaction mediated homogeneously by a manganese complex where the formed dioxygen derives completely from water. However, this reaction is not catalytic, because fast degradation of the complex occurs. The main result of this and related studies is that oxidants containing oxygen atoms are non-innocent and should be excluded in true water oxidation experiments, since possible

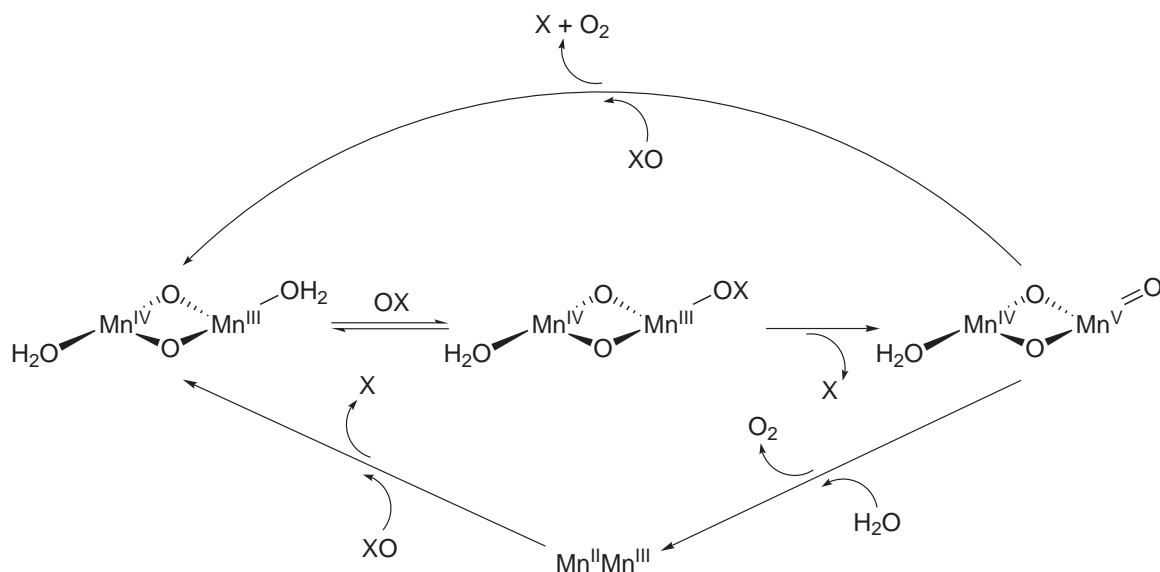


Figure 3.8.: Proposed mechanism by Brudvig and coworkers for the reaction between $[\text{Mn}_2(\text{O})_2(\text{H}_2\text{O})_2(\text{terpy})_2]^{3+}$ and oxido-transferring oxidants XO (XO = OCl^- or HSO_5^-).¹¹¹

disproportionation reactions lead to the formation of dioxygen and through oxygen transfer at least one oxygen of the evolved O₂ derives from the oxidant.¹¹⁶ As mentioned above no manganese complex is currently known which catalyzes water oxidation to dioxygen upon reaction with the oxidants Ce^{IV} or photogenerated $[\text{Ru}(\text{bpy})_3]^{3+}$. The requirements for a metal complex to react with these oxidation agents are discussed in section 6 and in paper I.

3.4. Heterogeneous catalysts

Water oxidation catalysts based on metal oxides have several advantages. Besides their thermodynamic stability, they show high activity and, in some cases, long-term stability. Potential large scale preparations would be comparably easy and for a catalyst based on abundant precursors additionally inexpensive. Oxides of noble metals are the most efficient water oxidation catalysts reported so far.^{117–119} Similar to homogeneous catalysts, especially Ru and Ir compounds are highly active. However, these oxides are no promising catalytic components for artificial photosynthetic devices for large scale solar fuel generation due to the low abundance and high costs of Ru and Ir. Harriman and coworkers compared the water oxidation abilities of several metal oxides under photochemical conditions in 1988.¹¹⁸ Some oxides were found to be efficient catalysts and the highest activity was found for IrO₂, but also inexpensive oxides like the spinel-type Co₃O₄ and Mn₂O₃ showed a high oxygen-evolving capability.

In the last years many metal oxide catalysts mainly based on Co, Ir or Mn have been

reported. Kurz and coworkers have presented calcium manganese oxides which have shown enhanced functional activity upon reaction with Ce^{IV} or $[\text{Ru}(\text{bpy})_3]^{3+}$ which was much higher than that of synthetic or commercial $\alpha\text{-Mn}_2\text{O}_3$.¹²⁰ These findings reproduce the importance of calcium as essential component in natural water oxidation^{121,122} and support the assumption that the reactive center of PSII originates from natural calcium manganese minerals.¹²³ Detailed oxygen evolution studies with these calcium manganese oxides have been performed in ^{18}O -enriched water using membrane inlet mass spectrometry (MIMS).¹¹⁶ The results have clearly shown that different pathways for O–O formation occur depending on the oxidant used indicated by distinct ^{18}O -labelling patterns. In cooperation with the group of Dau, significant similarities with the OEC were found through X-ray absorption spectroscopy (XAS).¹²⁴ The measurements revealed the structure as layered manganese oxides of low order with manganese in an oxidation state close to +4. Calcium is found in the interlayer space where it forms Mn_3CaO_4 cubes or is connected to defects of oxide layer fragments.

An interesting route for the synthesis of photocatalytically active water splitting metal oxide nanoparticles has been presented by Walsh and coworkers.¹²⁵ The low-cost biopolymer xyloglucan (Xyg) was used as stabilizing agent for the synthesis of nanoparticles. Xyg- Co_3O_4 and Xyg- Fe_3O_4 nanoparticles showed highly enhanced water splitting activity with $[\text{Ru}(\text{bpy})_3]^{3+}$ and irradiation compared to commercial unstabilized Co_3O_4 nanoparticles. In a recent communication Styring and coworkers have presented a colloidal catalyst based on cobalt and methylenediphosphonate.¹²⁶ Visible light driven water oxidation is achieved with $[\text{Ru}(\text{bpy})_3]^{3+}$ in aqueous solutions at neutral pH with a comparatively high turnover frequency.

A different approach for water oxidation catalysts has been reported by Jiao and Frei. They have synthesized nanostructured cobalt oxide¹²⁷ and manganese oxide clusters¹²⁸ supported on silica scaffolds. Metal (II) nitrates were adsorbed on silica and calcinated at different temperatures. Dioxygen evolution was achieved with $[\text{Ru}(\text{bpy})_3]^{3+}$ upon irradiation with wavelength between 450 and 500 nm and turnover frequencies of 3450 O_2 molecules s^{-1} ($\text{Co}_3\text{O}_4/\text{SBA-15}$) and 3330 O_2 molecules s^{-1} ($\text{MnO}_x/\text{KIT-6}$) per catalyst cluster. EXAFS and XANES spectroscopy show high structural stability of the catalyst for hours of continuous water oxidation catalysis.

In 1986, Kaneko and coworkers achieved water oxidation using oversaturated, deaerated solutions of $[\text{Mn}_2(\text{O})_2(\text{bpy})_4]^{3+}$ (**Mn4**) or $[\text{Mn}_2(\text{O})_2(\text{phen})_4]^{3+}$ (**Mn5**). After addition of an excess of Ce^{IV} to these oversaturated suspensions, dioxygen evolved non-catalytically.¹²⁹ The adsorption of **Mn4** on kaolin clay performed in a following study enhanced the oxygen evolution, whereas the turnover number was still less than unity.¹⁴ In 2004 Yagi et al. took up this method and prepared different complex@clay hybrids.^{15,16,130} Besides complexes **Mn4** and **Mn5**, which had already been used by Kaneko, the dinuclear manganese complex $[\text{Mn}_2(\text{O})_2(\text{H}_2\text{O})_2(\text{terpy})_2]^{3+}$ (**Mn1**), which does not catalyze water oxidation in solution,

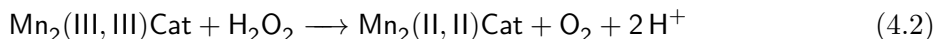
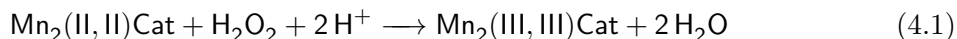
was adsorbed on kaolin, mica and K10 montmorillonite clay. Catalytic water oxidation was achieved using aqueous suspensions of clay hybrids of **Mn1** (**Mn1**@clay) and large excess of Ce^{IV} as oxidant. While the clay hybrids of **Mn4** and **Mn5** do not oxidize water catalytically, turnover numbers of 17 (**Mn1**@kaolin) and 15 (**Mn1**@mica) were achieved after reaction times of four days. Labelling studies clearly identified water as the only source of the O_2 -oxygen atoms. The intercalation of the manganese compounds between the mica interlayer was suggested because of XRD data while the complexes adsorb solely on the surface on kaolin. It is expected that **Mn1** is adsorbed in the interlayer of montmorillonite which is supposed to have a card house structure.¹⁶ For the adsorption of **Mn1** XANES and UV/vis diffuse reflectance data lead to the assumption that the oxidation state of the dimanganese core is still $\text{Mn}_2(\text{III,IV})$, but it is not intact.^{16,130} It was supposed that dioxygen is formed by the cooperation of two molecules of **Mn1**. The terminal water ligands are suggested to be involved in the catalytic mechanism because of the non-catalytical water oxidation of **Mn4**@clay and **Mn5**@clay where **Mn4** and **Mn5** are lacking water ligands. Water oxidation experiments with several other manganese species, including manganese(III) oxide and manganese(IV) oxide as well as Mn^{2+} and Mn^{3+} adsorbed on kaolin or mica clay, did not yield dioxygen.^{15,130} In a recent communication, Yagi and coworkers synthesized a PSII model by the adsorption of $[\text{Ru}(\text{bpy})_3]^{2+}$ and eight equivalents of **Mn1** on mica.¹³¹ XRD data indicate that both complexes are intercalated between mica interlayers. Water oxidation was achieved upon irradiation with wavelength ≥ 420 nm and the turnover number was 3.4 during a reaction time of 17 h.

Several manganese complexes with different coordination geometry and/or oxidation states were adsorbed onto kaolin and montmorillonite K10 clay by Kurz.¹⁷ It was assumed that immobilization of the complexes incorporate changes in the electronic structure due to significant changes in UV/Vis spectra. Performance and stability were distinctly increased in comparison to homogeneous solutions of the complexes for reactions with the oxidants oxone or hydrogen peroxide. Besides the already known **Mn1**@clay hybrids, two other heterogeneous water oxidation systems with Ce^{IV} were found. Tetranuclear manganese units formed by an additional μ -oxido bridge between two complex units have been proposed as the active units for water oxidation with Ce^{IV} , as in this study, water oxidation reactions of complexes containing strongly bound ligands adsorbed on clay did not form dioxygen, either.

This study has shown that water oxidation catalyzed by pyridyl clay hybrids like **Mn1**@clay is not unique as the adsorption of other manganese complexes onto clay also resulted in water oxidation catalysts. However, this study did not reveal information about the catalytically active species and it remains unclear whether the coordination geometries of the adsorbed complexes are important. To solve this questions, we synthesized montmorillonite K10 hybrids of two manganese complexes and two manganese salts. The characterization and water oxidation catalysis of these hybrids are presented and discussed in chapter 7 and in paper II.

4. Manganese catalases

Catalases are a group of enzymes which catalyze the disproportionation of hydrogen peroxide to oxygen and water.¹³² These important antioxidant metalloenzymes are essential for all organisms that are exposed to oxygen. Hydrogen peroxide is formed as side product of respiration, autooxidation of cell components or enzymatically through oxygenases. Catalases prevent organisms from deleterious effects of hydrogen peroxide including DNA damaging or generation of hydroxyl radicals. There are two different protein families of catalases. Heme-containing catalases are found in aerobic organisms¹³³ whereas the nonheme dimanganese containing catalases (MnCat) exist in microorganisms in microaerophilic environments.^{6,134} The active site of MnCat consists of two manganese ions which are linked via two μ -solvent oxygens (Fig. 4.1).⁶ A $\mu_{1,3}$ -carboxylate bridge originating from a glutamate leads to a non-planar $\text{Mn}_2(\text{O}_{\text{solvent}})_2$ core. Furthermore, the coordination sphere consists of histidine and glutamate side chains. One of the manganese ions is six-coordinate whereas the other one is five-coordinate or six-coordinate with a water molecule and the supposed substrate binding site. This has been shown by Barynin and coworkers who synthesized the azide-inhibited complex of the MnCat from *Lactobacillus plantarum*.⁶ Spectroscopic investigations of MnCat by XAS and EPR spectroscopy have shown that the active site cycles between $\text{Mn}_2(\text{II,II})$ and $\text{Mn}_2(\text{III,III})$ states during hydrogen peroxide decomposition.^{135–138} The detailed mechanism is not clear until now, but it can be described by the following net reactions.



Equations 4.1 and 4.2 show that hydrogen peroxide can oxidize the reduced enzyme and it can reduce the oxidized enzyme, too. The turnover number of MnCat has been determined as $2 \times 10^5 \text{ s}^{-1}$.^{139,140} This is just 1% of that for heme-containing catalases which cycle during hydrogen peroxide disproportionation between Fe(III) and Fe(IV).¹⁴¹ It is also possible to reach a so-called superoxidized $\text{Mn}_2(\text{III,IV})$ state of the MnCat active site by oxidizing with potassium periodate¹³⁵ or hydrogen peroxide and hydroxylamine.¹⁴² This state shows no activity concerning hydrogen peroxide disproportionation and does not participate in the reaction mechanism.^{135,136,140} The geometric and electronic structure of this state has many similarities with the Mn_4CaO_x cluster of the OEC like μ -oxido bridged highly valent man-

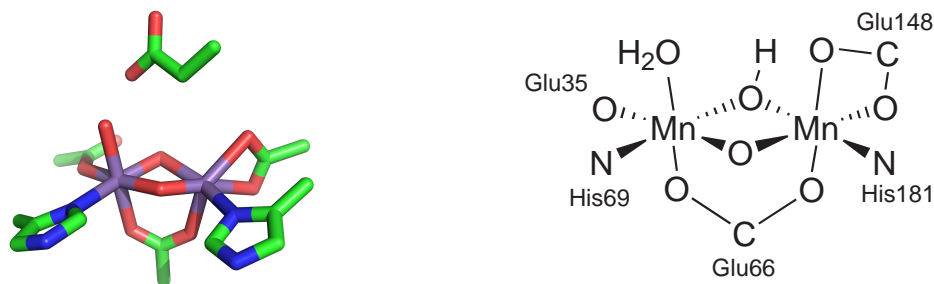


Figure 4.1.: Structure of the MnCat active site in the resting $\text{Mn}_2(\text{III},\text{III})$ state of *Lactobacillus plantarum*. The Mn-Mn distance of 3.03 Å leads to the assumption of a protonation of the oxido bridge trans to the histidine in this oxidation state.⁶

ganese centers or analog protein-derived ligation. That's why it has been studied extensively many times.^{140,142–145} The MnCat active site also shows similarities with Mn ribonucleotide reductases or Mn arginases, which both contain two manganese ions.^{4,140,146}

Two detailed mechanisms for the catalytic hydrogen peroxide disproportionation of MnCat are shown in Figures 4.2 and 4.3. The catalytic mechanism of MnCat has been studied by Siegbahn using quantum chemical methods at the B3LYP level.¹⁴⁷ In this mechanism a hydrogen peroxide replaces a bridging water molecule in the reduced form of MnCat. The O–O bond of hydrogen peroxide is cleaved homolytically after initiation by electron transfer from Mn(II) to hydrogen peroxide. An end-on hydroxyl radical species occurs which reacts with a hydrogen of a bridging hydroxide to form a water molecule. This is loosely bound and replaced by a hydrogen peroxide molecule which protonates the oxido bridge and then binds end-on coordinated. Electron and proton transfer lead to a bridging water molecule and an end-on O_2^- radical ligand which forms a dioxygen molecule after further electron transfer. One-electron redox steps and radical intermediates for the mechanism of hydrogen peroxide decomposition were already proposed by Haber and Weiss in 1934 who suggested a mechanism for the disproportionation of H_2O_2 by iron salts.¹⁴⁸

In the mechanism suggested by Barynin and coworkers (Fig. 4.3), the protein-bound glutamate Glu178 has an important role as proton shuttle in both half reactions.⁶ The proposal involves also a bridging $\mu_{1,1}$ -hydroperoxide complex. Activation toward O–O bond cleavage is achieved through protonation of the nonbridging oxygen by the terminal glutamic acid Glu178 and electron transfer from both manganese centers to the bridging oxygen. In the oxidative half-reaction, the protonation of a bridging hydroxide by an end-on bound hydroperoxide is mediated by the protein-bound Glu178. This mechanism shows similarities to the proposal of Kremer and Stein for the hydrogen peroxide decomposition by ferric perchlorate in 1959 who also suggested two-electron redox chemistry steps.¹⁴⁹

Many dimanganese model complexes have been synthesized and characterized concerning H_2O_2 disproportionation and were mostly shown to be MnCat mimics.^{109,140,150,151} It

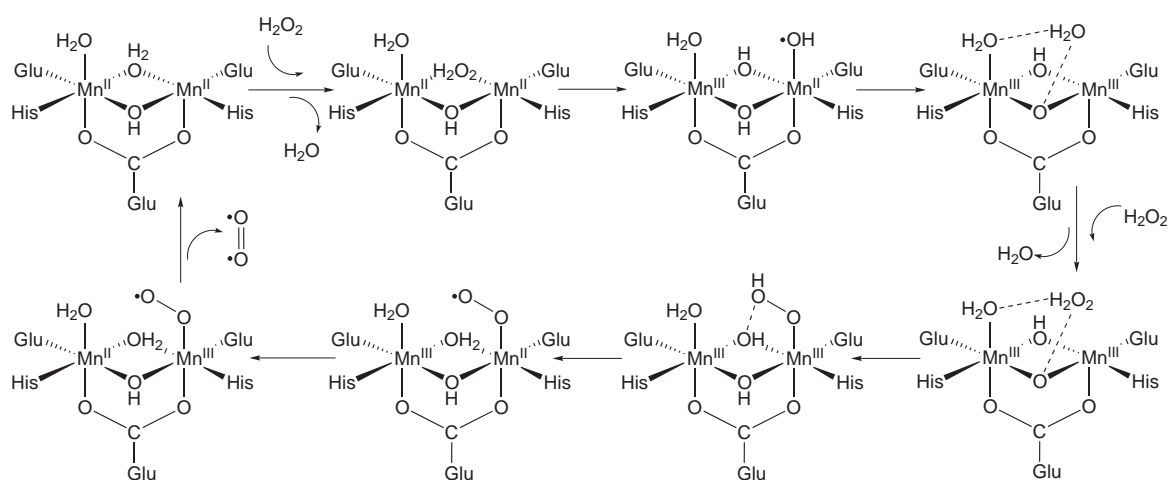


Figure 4.2.: Mechanism of MnCat proposed by Siegbahn based on quantum chemical calculations.¹⁴⁷

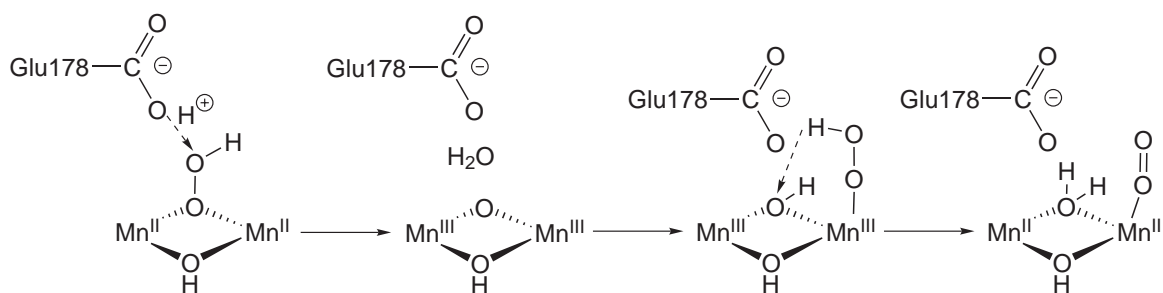


Figure 4.3.: Mechanism of hydrogen peroxide disproportionation proposed by Barynin and coworkers. In the reductive half reaction, a bridging peroxide is protonated by Glu178 and activated toward O–O bond cleavage. In the oxidative half reaction, Glu178 acts as a proton shuttle from a terminal bound peroxide to a bridging hydroxide.⁶

turns out that highly active catalase models need a weakly bound ligand like a carboxylate or solvent molecule or have to be five coordinate at at least one metal center. Catalytic hydrogen peroxide decomposition of the complex $[\text{Mn}_2\text{O}_2\text{cyclam}_2]^{3+}$ (cyclam = 1,4,8,11-tetraazacyclotetradecane) could not be observed in aqueous solutions¹⁷ and only small catalytic activity has been monitored in dimethylformamide.¹⁵² This result is probably due to the strongly binding ligands and the saturated coordination sphere. In a recent study Dubois and coworkers have shown that carboxylate ligands facilitate the oxido exchange in dimanganese(III,IV) complexes drastically and act as internal bases.¹⁵⁰ This indicates that the mechanisms both in MnCat and in MnCat mimics might be much more complicated than proposed in Figure 4.2 and 4.3. The most efficient model known so far is the dimanganese complex $\text{Na}[\text{Mn}_2(3\text{-Me-5-SO}_3\text{-salpentO})(\mu\text{-MeO})(\mu\text{-OAc})(\text{H}_2\text{O})]$ (3-Me-5-SO₃-salpentO = 1,5-bis(salicylidenamino) pentan-3-ol) reported by Signorella and coworkers in 2011. Nevertheless, the catalytic efficiency of this mimic is still 60 times lower than that of MnCat from *L. plantarum* and 2 000 times lower than that of *T. thermophilus*.¹⁵³ The model complexes are also interesting as possible therapeutic agents for the prevention of oxidative stress injuries.¹⁵⁴ Therefore, the development of efficient MnCat mimics is still important and in this thesis the abilities of $[\text{Mn}_2^{\text{III,III}}(\text{tpdm})_2(\mu\text{-O})(\mu\text{-OAc})_2]^{2+}$ (**1**, Fig. 6.3) to catalyze the disproportionation of hydrogen peroxide is therefore discussed in paper I.

5. EPR spectroscopy of manganese complexes

Electron paramagnetic resonance (EPR) spectroscopy is a very powerful analytical tool in manganese chemistry. Within the scope of this thesis, a cw X-band EPR spectrometer was installed and several manganese complexes with different oxidation states and nuclearities were investigated using EPR. Therefore, a short overview of the theoretical background of EPR spectroscopy is given in this chapter. More details can be found in the literature.¹⁵⁵ In general, EPR spectroscopy is used for the investigation of substances in which unpaired electrons exist. These are organic or inorganic radicals, transition metal complexes, metalloproteins or other biomolecules. For instance, dimanganese complexes show characteristic X-Band EPR spectra depending on their metal oxidation states, ligand environment and the type of bridging ligands which influences the exchange interaction between the manganese ions.¹⁴⁵

5.1. Theory

EPR spectroscopy is based on the splitting of the electrons energy levels in an external magnetic field B as a result of the electron Zeeman effect. Electrons with a parallel orientation to the magnetic field possess a lower energy than electrons with an antiparallel orientation. An energy level scheme for the simplest EPR active system (e.g. free electron with $S = 1/2$) as a function of applied magnetic field is shown in Fig. 5.1. The state energy difference is given as a first approximation by

$$\Delta E = g\beta B \quad (5.1)$$

where β is the Bohr magneton and g the electron g -factor, a dimensionless proportionality factor, whose value depends on the electrons environment. An unpaired electron in the $m_S = -1/2$ state can move to the $m_S = +1/2$ state by the absorption of electromagnetic radiation of energy $\epsilon = h\nu = \Delta E$. The interaction of an applied magnetic field B with the magnetic moment of an electron can be described by the spin Hamiltonian

$$\mathcal{H} = \beta \vec{B} g \vec{S} \quad (5.2)$$

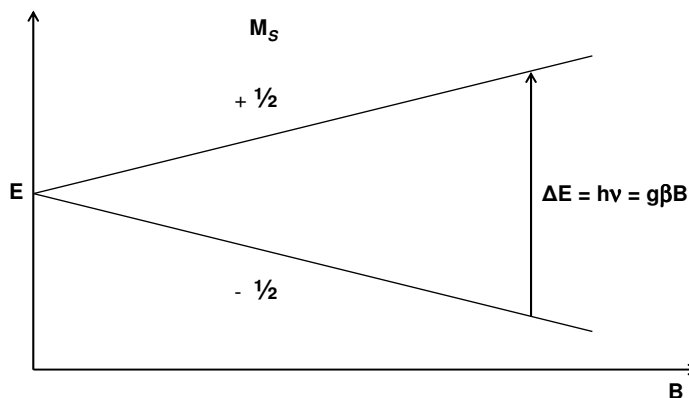


Figure 5.1.: Energy level scheme for the simplest system (e.g. free electron) as a function of applied magnetic field B , showing microwave absorption.

In the majority of cases, further interactions have to be taken into account. The energies of states within the ground state of a mononuclear paramagnetic species with an effective electron spin S and a nuclear spin I can be described by the following spin Hamiltonian

$$\mathcal{H} = \beta \vec{B} g \vec{S} + \vec{S} \mathbf{A} \vec{I} + \vec{S} \mathbf{D} \vec{S} \quad (5.3)$$

The second term in Eq. 5.3 is the hyperfine interaction. This is basically a dipolar coupling between the electron spin S and the nuclear spin I and consists of the anisotropic dipole-dipole interaction and the isotropic Fermi-contact interaction for electrons near to the nucleus. For ^{55}Mn ($I = 5/2$), this interaction leads to a six-fold ($2I + 1$) splitting of each EPR signal (a schematic energy level diagram is shown in Fig. 5.2). The hyperfine interaction can be expressed in terms of the hyperfine coupling tensor \mathbf{A} .

Another relevant important interaction takes place in molecules possessing more than one unpaired electron. The interaction of the individual magnetic moments with the local fields of the other electrons leads to a removal of degeneracy of the spin levels even without an applied magnetic field. This interaction is called zero field splitting (ZFS) and affects the EPR spectra of systems with low symmetry and/or with higher spin states (e.g. Mn^{II} : $S = 5/2$). The final term in equation 5.3 describes this interaction. This can be written by expressing \mathbf{D} as a function of two empirical parameters, the axial ZFS term D and the rhombic ZFS term E

$$\vec{S} \mathbf{D} \vec{S} = D[\hat{S}_z^2 - \frac{1}{3}S(S+1)] + \frac{1}{2}E(\hat{S}_+^2 + \hat{S}_-^2) \quad (5.4)$$

Hydrogen and nitrogen hyperfine and higher order manganese quadrupolar splittings are mostly not resolved in X-band EPR spectra and are therefore insignificant. In $\text{Mn}(\text{II})$ complexes, the $3d^5$ metal ions exist generally in a high spin ($S = 5/2$) ground state electron configuration.¹⁵⁶ ZFS interactions lead to a mixing of the m_I states so that formally for-

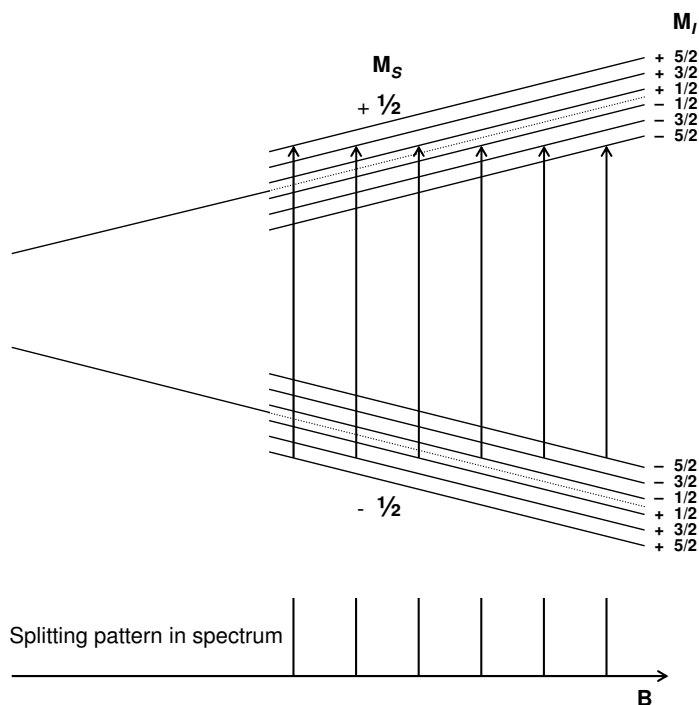


Figure 5.2.: Energy levels of a system with one unpaired electron ($S = 1/2$) and one magnetic nucleus with $I = 5/2$, e.g. ^{55}Mn . The EPR splitting pattern is indicated.

bidden transitions also appear in the EPR spectrum ($\Delta m_S = \pm 1$, $\Delta m_I = \pm 1$). Spectra of Mn(II) complexes can be found in chapter 9 and paper III.

Mononuclear high-spin manganese(III) complexes are in integer spin systems with $S = 2$. The zero field energy gaps between levels separated by $\Delta m_S = \pm 1$ are relatively large. Therefore, the conventional, EPR allowed, $\Delta m_S = \pm 1$ transitions can not be observed at normal X-band microwave frequencies. However, the energy difference between the $m_S = +2$ and the $m_S = -2$ state is relatively small and these states split further with an applied magnetic field. Thus, such transitions can be observed at $g \approx 8$ by parallel-polarization EPR spectroscopy if the zero field splitting parameters are in an appropriate range.¹⁵⁷ These transitions are allowed, because for an oscillating \vec{B}_1 field applied to the static \vec{B}_0 field, the matrix elements connecting the two relevant states are nonzero. In paper III, parallel mode EPR spectroscopy is used to detect mononuclear Mn(III) complexes as products of the CO release by Mn(I) tricarbonyl complexes.

Strongly coupled dimanganese(III,IV) species are of special importance for the work presented here (chapter 6 and paper I). The spin Hamiltonian for such an exchange coupled $\text{Mn}_2^{\text{III,IV}}$ -complex can be written as

$$\mathcal{H} = -2J\vec{S}_1\vec{S}_2 + \beta\vec{B}g_1\vec{S}_1 + \beta\vec{B}g_2\vec{S}_2 + \vec{S}_1\mathbf{a}_1\vec{I}_1 + \vec{S}_2\mathbf{a}_2\vec{I}_2 + \vec{S}_1\mathbf{d}_1\vec{I}_1 + \vec{S}_2\mathbf{d}_2\vec{I}_2 \quad (5.5)$$

The first term describes the exchange coupling. The antiferromagnetic exchange is much larger than other interactions in bis(μ -oxido)-bridged $\text{Mn}_2^{\text{III,IV}}$ -complexes. For this so called strong coupling limit ($J \gg D$), the zero-field dependence is quite small. Therefore, the eigenstates of this Hamiltonian can be grouped according to the total spin S ($S = |S_1 - S_2|, \dots, S_1 + S_2$). At low temperatures, only the $S = 1/2$ state is populated. Thus, the spin Hamiltonian for this coupled system can be approximated as

$$\mathcal{H} = \beta \vec{B} \mathbf{g} \vec{S} + \vec{S} \mathbf{A}_1 \vec{I}_1 + \vec{S} \mathbf{A}_2 \vec{I}_2 \quad (5.6)$$

The coupled g -tensor \mathbf{g} and the hyperfine tensors \mathbf{A}_i are not identical to the tensors of Eq. 5.5. They are referred to as “effective tensors” of the coupled state and also take zero field correction terms into account. In most cases, a ratio of $|2\mathbf{A}_1| \approx |\mathbf{A}_2|$ leads to the characteristic 16-line pattern of a dimanganese(III,IV) complex (chapter 6, Fig. 6.6). More details about this topic can be read elsewhere.^{144,158} Additionally, further manganese complexes containing mononuclear $\text{Mn}^{\text{(IV)}}$,^{159–161} dinuclear $\text{Mn}_2^{\text{(II,II)}}$ ¹⁶² or dinuclear $\text{Mn}_2^{\text{(II,III)}}$ ¹⁶² show distinctly different EPR signals. A list of EPR signals for manganese complexes is found at Huang et al.¹⁶³

In general, the spin Hamiltonian parameters can be determined by simulations of the EPR spectra. Such simulations are mainly based on matrix diagonalization procedures of the corresponding spin Hamiltonian. However, for a precise determination of ZFS parameters, multifrequency EPR spectroscopy has to be applied^{143–145,156,164} and spectra recorded in X-band, as done here, are not sufficient on their own. Nevertheless, a clear identification of manganese redox states is still often possible using X-band EPR, which has therefore been of great value to address analytical questions for this thesis.

5.2. Setup of a cw X-band EPR spectrometer

In Figure 5.3, a picture of the cw X-band EPR spectrometer which was installed and intensively used during this thesis is presented. This EPR spectrometer measures the changes that appear due to spectroscopic transitions in the amount of radiation reflected back from the microwave cavity containing the sample. The main parts of a cw X-band EPR spectrometer are shown in Figure 5.4.

The microwave source is, like in most cases, a Gunn diode. The frequency can be varied between 9.2 and 10 GHz to adjust the microwave source to the resonator. The microwave power can be optimized for every sample and temperature by the use of an attenuator. The circulator is a microwave device which makes it possible to see only the microwave radiation coming back from the cavity. Reflected microwaves are only directed to the detector and not back to the microwave source. The Schottky barrier diode detects the reflected microwaves and converts the microwave power to an electrical current. A detector current



Figure 5.3.: Picture of the cw X-Band EPR spectrometer at the Institute of Inorganic Chemistry, Kiel University.

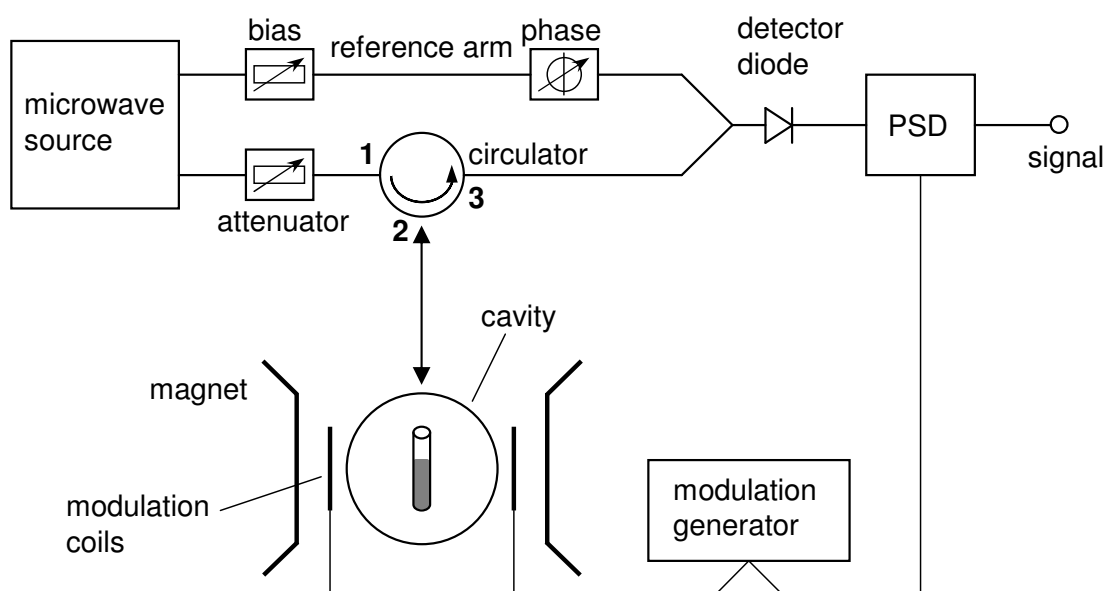


Figure 5.4.: Principle block diagram of a cw X-band EPR spectrometer

of approximately 200 μA is needed, because the diode should operate in the linear region to attain best results. Therefore, the diode is supplied with extra microwave power (which is commonly called a “bias”) by the reference arm. A phase shifter makes sure that the reference arm microwaves are in phase with the reflected signal microwaves at the detector.

The microwave detector diode is sensitive to noise and electrical interference. To suppress these unwanted signals, modulation coils are placed in close vicinity to the sample which apply a field modulation with a typical frequency of 100 kHz. As a consequence of this, the signal is detected as the first derivative of the field-dependent absorption. To measure a spectrum, the magnetic field is varied and from the modulated part of the signal, a phase sensitive detector (PSD) produces a direct current signal which can then be analyzed.

6. Is the geometrical arrangement crucial for water oxidation?

Although many details of the mechanism of water oxidation both in natural and artificial systems are known, the process of O–O bond formation is still unclear. As already mentioned in section 3.2, a large number of partly contradictory mechanisms have been proposed.^{2,13,165} However, in each of these O–O bond formation pathways metal-oxido species play an important role. The reactivity of the oxido ligand is regulated by the electron configuration and the local geometry of the metal. The lack of d-electrons, e.g. in a d^0 metal center such as V^V , leads to an extremely strong metal-oxygen bond and the oxido-ligand cannot be activated. Furthermore, no multiple metal-oxido bonds can be formed between late transition metal ions like Cu^{II} because of the filled d-orbital sets.¹³ Therefore, it is not surprising that nature has chosen iron and manganese as centers for enzymes managing multiple bonded oxidos which are involved in the formation of dioxygen.

Two of the most common mechanisms for O–O bond formation are presented in Figure 6.1.^{36,166,167} One proposal (I) involves the direct interaction of two metal-oxido species. This reaction can be described either as a radical-radical coupling or as reductive elimination depending on the oxidation states of the metal center and the oxygen species. This interaction could be direct or mediated by an additional solvent water molecule. An alternative route for O–O bond formation (II) is the nucleophilic attack of a hydroxide or an activated solvent water molecule.

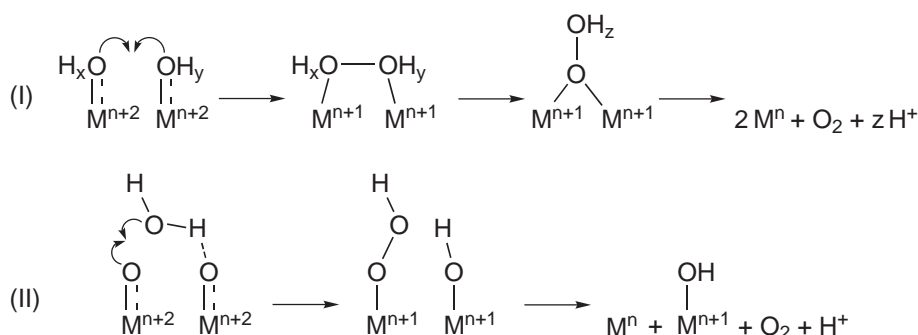


Figure 6.1.: Suggested O–O bond formation pathways adapted from Yang and Baik¹⁶⁶ and Lubitz et al.³⁶

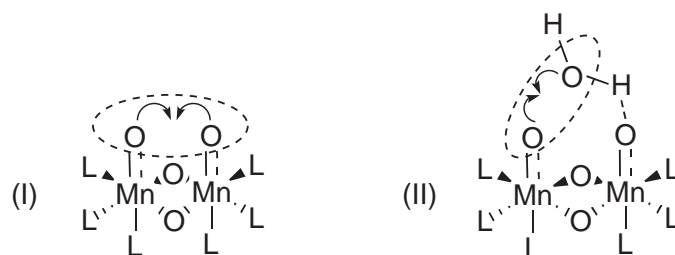
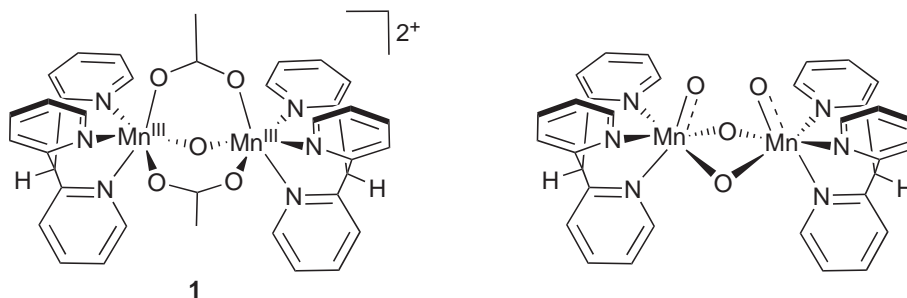


Figure 6.2.: Possible O–O bond formation pathways for a dimanganese complex.

Figure 6.3.: Structure of $[\text{Mn}_2^{\text{III,III}}(\text{tpdm})_2(\mu\text{-O})(\mu\text{-OAc})_2]^{2+}$ (**1**) and a hypothetical intermediate which could be involved in water oxidation catalyzed by **1**.

In Figure 6.2, possible mechanistic pathways of Figure 6.1 are adapted to O–O bond formation by a dinuclear di- μ -oxido-bridged manganese complex. The geometrical arrangement of this complex has to meet the requirements for the discussed pathways. Facial coordinating capping ligands are needed to obtain a dimanganese complex with this geometry. The ligand environment must additionally tolerate the high potentials which are required for water oxidation. However, if one considers the literature, Mn model complexes often contain phenolate-, amine- or carboxylate-ligands. Pyridine-containing ligands were proved to be oxidation stable as shown by the detailed studies of Brudvig et al. on **Mn1** (see section 3.3).^{110–112} But this complex does not fulfill the geometrical requirements for the reaction scenarios shown in Figure 6.2. Based on these considerations, the complex $[\text{Mn}_2^{\text{III,III}}(\text{tpdm})_2(\mu\text{-O})(\mu\text{-OAc})_2]^{2+}$ (**1**, tpdm = tris(2-pyridyl)methane, Fig. 6.3) was synthesized in the context of this thesis. Beside the possible crucial geometrical arrangement, a water oxidation catalyst is required to deal with a four-electron process accompanied with proton transfer. Thus, not only the structural and spectroscopic properties were determined, but also electrochemical investigations were performed. Furthermore, the ability of water oxidation catalysis of **1** was investigated (Paper I).

Following a common route for the synthesis, the perchlorate salt of complex **1** could be obtained by the reaction of the ligand tpdm with manganese(III) acetate in methanol with addition of a small amount of *tert*-butyl hydroperoxide and sodium perchlorate. Red crystals

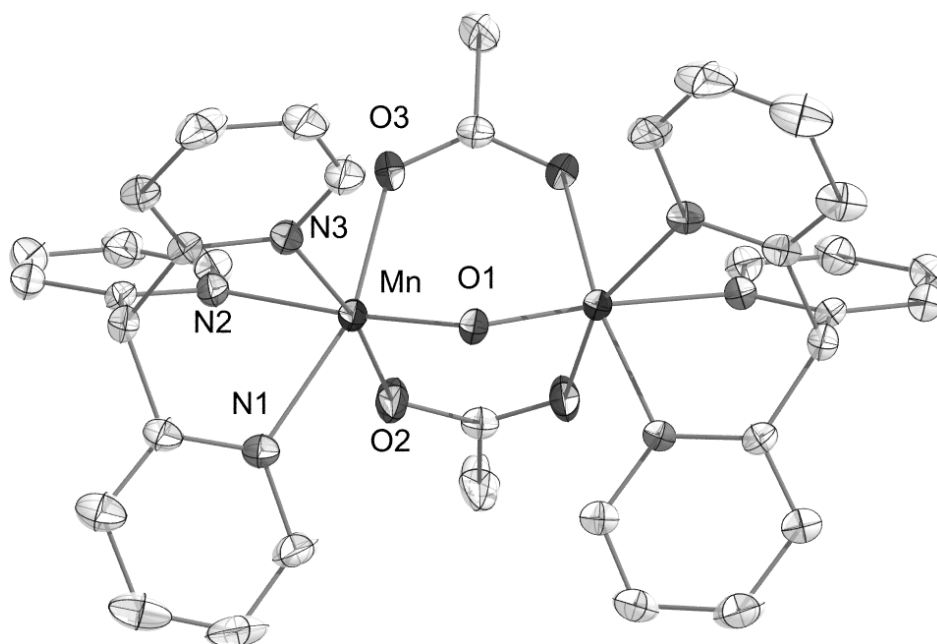


Figure 6.4.: Presentation of the cation $[\text{Mn}_2^{\text{III,III}}(\text{tpdm})_2(\mu\text{-O})(\mu\text{-OAc})_2]^{2+}$ (**1**). Hydrogen atoms and perchlorate ions are omitted for clarity. Thermal ellipsoids are drawn at the 50% level.

of the $\text{Mn}_2^{\text{III,III}}$ **1**(ClO_4)₂ complex were obtained by slow diffusion of methyl tert-butyl ether into a solution of **1**(ClO_4)₂ in acetonitrile. The manganese centers have distorted octahedral coordination geometries and are bridged by two acetate groups and one oxygen atom. On each manganese ion a tpdm ligand is facially coordinated by its three pyridyl nitrogen donor atoms.

The redox behavior of **1** was investigated. The anodic scan of the cyclic voltammogram showed a partially reversible oxidation process at 950 mV with a large peak split of 150 mV and at 1 400 mV a broad irreversible oxidation event (Fig. 6.5). To understand the nature of the formed species during these oxidation processes, UV/Vis and EPR spectroelectrochemical measurements were performed at the potentials marked in Figure 6.5.

The results of the UV/Vis spectroelectrochemical investigations (Paper I) show that complex **1** could be reversibly oxidized to a $\text{Mn}_2^{\text{III,IV}}$ species at a potential of +1 200 mV. To measure EPR spectra of the products obtained by electrochemical oxidation of complex **1**, bulk electrolyses were performed. After different electrolysis times, samples were taken from such solutions, immediately frozen and then analyzed by EPR. Figure 6.6 shows the resulting spectra for the oxidation at +1 200 mV. In the early phase of electrolysis, the typical 16-line EPR signal of a $\text{Mn}_2^{\text{III,IV}}$ -species appears. A simulation of the EPR spectrum yields characteristic g and A values for a bis(μ -oxido)-mono(μ -acetato)bridged $\text{Mn}_2^{\text{III,IV}}$ complex.¹⁴⁵ After further electrolysis, the intensity of this signal decreases again (Fig. 6.6, inset), indicating further electrolysis to a $\text{Mn}_2^{\text{IV,IV}}$ complex for which no EPR signal is expected.^{145,163}

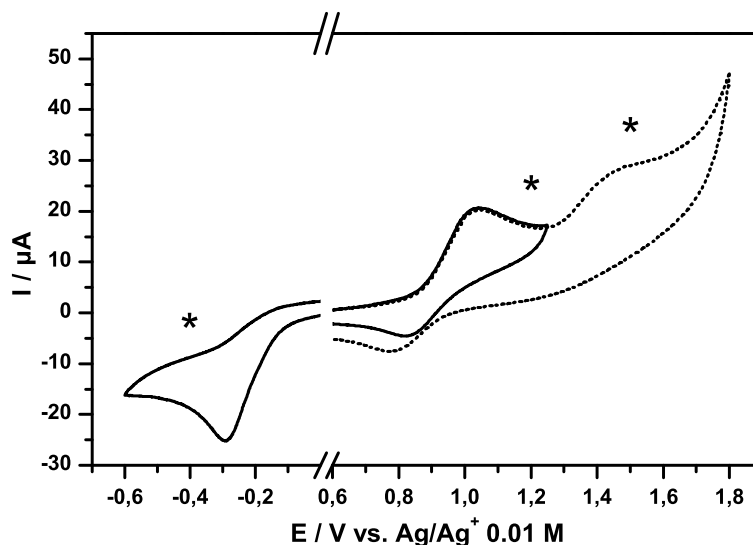


Figure 6.5.: Cyclic voltammogram of **1** at room temperature. Reaction conditions: 1 mM **1** in dry acetonitrile containing 0.1 M TBAClO₄; scan rate: 100 mV/s. Potentials used for UV/Vis and EPR spectroelectrochemistry are marked by asterisks.

On the basis of these and further UV/Vis and EPR measurements (Paper I), insights into the redox processes of complex **1** could be achieved which are summarized in Fig. 6.7. A number of electron-transfer reactions, partly accompanied by ligand exchange (acetate to oxido), occur. Two single-electron oxidation processes take place at $\sim +1$ V and thus at an interesting potential in the context of water oxidation. Therefore, these oxidation events of complex **1** represent a good model system for key events taking place during S-state transition of the oxygen evolving complex (OEC) of natural photosystem II (see section 2.4). Metal centered oxidations from Mn^{III} to Mn^{IV} at potentials $> +0.8$ V, deprotonations of water/hydroxide coordinated to manganese and the formation of additional μ -oxido bridges between manganese centers are proposed here as well.

Compound **1** was not only synthesized as a structural model but also as a potential functional model for manganese metalloenzymes. As a consequence, oxygen evolving reactions with the oxidation agents hydrogen peroxide (H₂O₂), peroxomonosulfate (HSO₅⁻, oxone) and (NH₄)₂[Ce(NO₃)₆] (Ce^{IV}) were performed in a measurement cell of an O₂-sensitive Clark type electrode. Typical traces of oxygen concentrations in solution for reactions of **1** with these oxidants are shown in Fig. 6.8. Complex **1** is an excellent catalyst for H₂O₂ disproportionation generating an O₂-saturated solution within seconds after the addition of small amounts hydrogen peroxide. Therefore, compound **1** is, like many other dimanganese complexes, a good

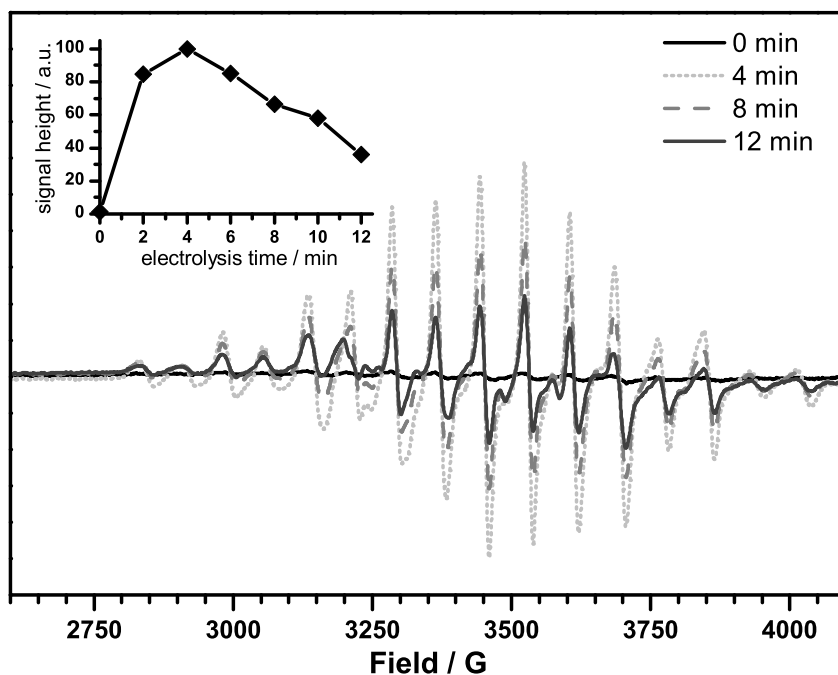


Figure 6.6.: X-band EPR spectra recorded after the electrochemical oxidation of complex **1** at a potential of +1 200 mV vs. Ag/Ag⁺. Recording conditions: microwave frequency: 9.644 GHz, microwave power: 63 μ W; modulation amplitude 4 G, temperature 5 K. The inset shows a quantification of the Mn₂^{III,IV}-signal versus electrolysis time.

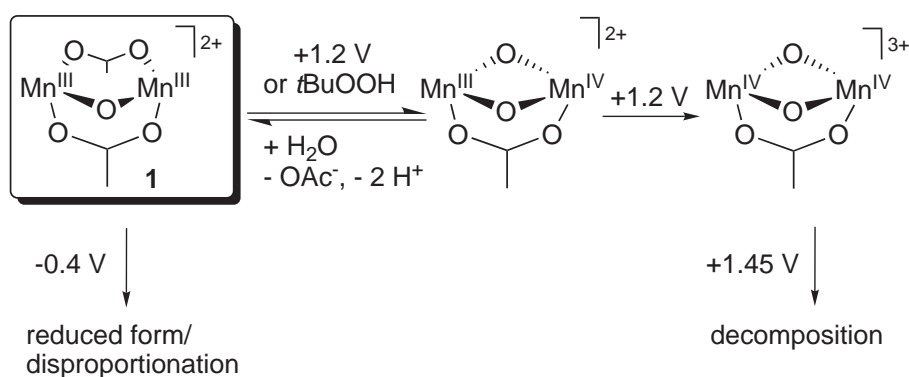


Figure 6.7.: Redox and ligand exchange processes of **1** identified by (spectro)electrochemistry.

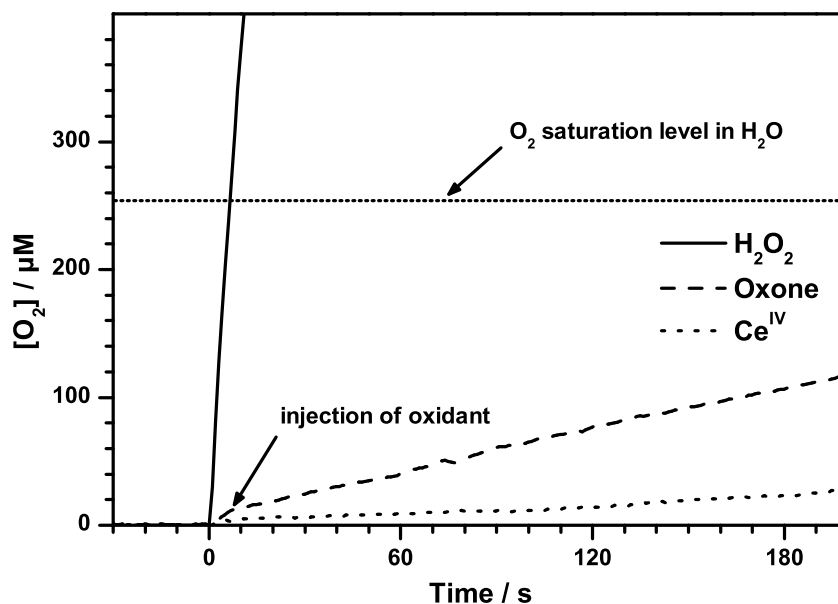


Figure 6.8.: Traces of oxygen evolution for the reactions of complex **1** with hydrogen peroxide, oxone and $(\text{NH}_4)_2[\text{Ce}(\text{NO}_3)_6]$ (Ce^{IV}), respectively.

structural and functional model of manganese catalase (see section 4). Similarly, reactions of **1** with the O-atom donating oxidation agent oxone result in the formation of dioxygen. After the addition of Ce^{IV} to aqueous solutions of **1**, small amounts of formed O_2 were observed. However, the addition of the oxidant was also accompanied by precipitations of brown manganese oxides. As such manganese oxide precipitates are known to catalyze water oxidation (section 3.4),^{118,120} they are most likely responsible for the small amount of dioxygen observed in these reactions.

Unfortunately, this leads to the conclusion that it is at least not primarily the coordination geometry that prohibits manganese catalyzed water oxidation in the case of complex **1** and similar Mn_2 -species. Rather the ability to store four oxidation equivalents at potentials $>+1$ V could be the crucial requirement which complex **1** and all other synthetic manganese coordination compounds prepared so far do not fulfill. On the other hand, catalase-like reactivity only requires that a compound manages $2e^-$ -events at high potentials, which explains why the title compound acts as efficient catalyst for the disproportionation of hydrogen peroxide.

To synthesize manganese complexes which are functional water oxidation catalysts it might be necessary to increase the nuclearity of the compounds at least to Mn_3 to allow the needed $4e^-$ -redox chemistry. First steps in these directions have been made by the synthesis of complexes which contain cubic $[\text{Mn}_4\text{O}_4]^-$ or even $[\text{Mn}_3\text{CaO}_4]^-$ -cores.¹⁶⁸⁻¹⁷⁰ However, these

first examples still lack oxidation- and/or hydrolysis stable ligand sets, so homogeneous water-oxidation catalysis with any of these compounds in reactions with Ce^{IV} or $[\text{Ru}(\text{bipy})_3]^{3+}$ has so far not been reported yet.

6.1. Conclusion

In summary, a new dinuclear manganese complex $[\text{Mn}_2^{\text{III,III}}(\text{tpdm})_2(\mu\text{-O})(\mu\text{-OAc})_2]^{2+}$ (**1**) with Mn coordinated to the unusual, facially-coordinating and oxidation stable ligand tris(2-pyridyl)methane (tpdm) could be synthesized. The molecular and electronic structure were investigated by crystallographic and extensive spectroscopic and electrochemical methods. The redox behavior of the compound was studied by UV/Vis- and X-Band EPR-spectroelectrochemistry. Both electrochemical (+1 200 mV vs. Ag/Ag⁺) and chemical (*t*BuOOH) oxidations transform **1** into the singly oxidized di- μ -oxido species $[\text{Mn}_2^{\text{III,IV}}(\text{tpdm})_2(\mu\text{-O})_2(\mu\text{-OAc})]^{2+}$. Further electrochemical oxidation at the same potential results in the removal of another electron to obtain the complex in a $\text{Mn}_2^{\text{IV,IV}}$ -form. The ability of complex **1** to evolve O₂ was studied using different oxidants. While reactions with hydrogen peroxide and peroxomonosulfate yield O₂, homogeneous water-oxidation using Ce^{IV} was not achieved. Thus, despite its favorable coordination geometry and multielectron redox chemistry, complex **1** fails to be a functional model for natural water oxidation. The oxidation reactions of **1** are nevertheless very interesting as model processes for S-state transitions of the natural manganese water oxidation catalyst in photosynthesis (section 2.4).

7. K10 montmorillonite supported manganese catalysts for the oxidation of water to dioxygen

As shown in the previous chapter, no molecular manganese compound for water oxidation catalysis in homogeneous systems is known. Also, the approach to use facial coordinating ligands in the form of complex **1** did not lead to success. A method for the synthesis of water oxidation catalysts based on Mn₂-complexes has been introduced by Kaneko and co-workers¹⁴ and enhanced by Yagi et al.^{15,16,130,131} and Kurz¹⁷ (for further details, see section 3.4). It was found out that active catalysts are formed by the adsorption of dimanganese complexes on clays as solid supports. Clay materials, e.g. K10 montmorillonite, are very promising supports for water oxidation catalysis because they are widely used as scaffold materials for molecular catalysts in oxidation reactions.^{171,172} Additionally, they are – like the natural Photosystem II – able to immobilize a manganese species in a hydrophilic, highly oxidation stable environment.

However, it is still quite unclear how water oxidation catalysis is achieved by the clay hybrids and what role both the clay support and the ligand framework of the manganese centers play in these reactions. In search for answers to these questions, montmorillonite clay hybrids of complex **1** as well as novel hybrids obtained by the adsorption of Mn²⁺ or Mn³⁺ ions from solutions of simple manganese salts, i.e. manganese(II) sulfate and manganese(III) acetate, were studied. The well known clay hybrids of **Mn1** were prepared as a reference (Fig. 7.2). In addition to catalytic experiments, UV/Vis and EPR spectroscopy were employed to learn more about this interesting class of heterogeneous catalysts (paper II). To reveal the nature of the most active catalyst, XAS measurements were performed by our collaborators Holger Dau and Ivelina Zaharieva (both FU Berlin).

The clay hybrids X@Mt (X = **Mn1**, **1**, Mn²⁺ and Mn³⁺) were synthesized by the addition of montmorillonite to aqueous solutions of the manganese compounds, filtration and following lyophilization. An analysis of the XRD data showed that the manganese species did not displace the Ca²⁺ cations in the interlayer because the interlayer distance was hardly affected by the adsorption reaction. Therefore, it can be assumed that manganese adsorption took place on the silicate and alumina surface groups. The adsorption of the manganese species was accompanied by significant changes of color and subsequently UV/Vis absorption spectra

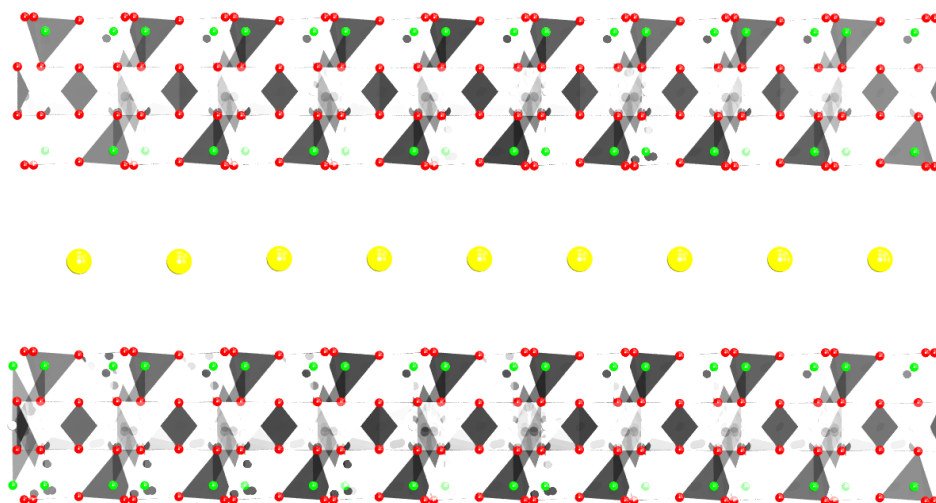


Figure 7.1.: Structure of the 2:1 clay K10 montmorillonite which consists of SiO_4 -tetrahedra and AlO_6 -octahedra and Ca^{2+} interlayer (Al, Mg white; Si green; O red; Ca yellow).¹⁷³

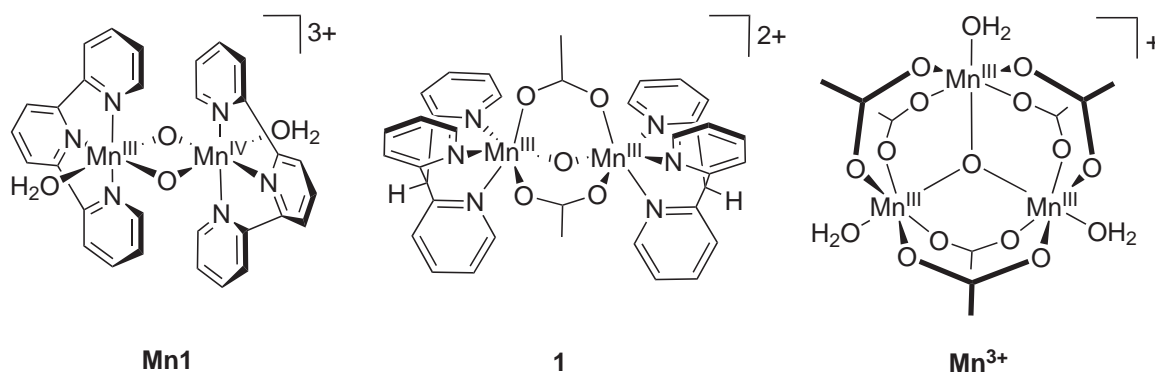


Figure 7.2.: Structure of the dinuclear manganese complexes **Mn1** and **1** used in this study. Additionally, the structure of the trimer $[(\text{Mn}_3^{\text{III}}(\mu_3\text{-O})(\text{OAc})_6(\text{H}_2\text{O})_3)^+]$ which forms in aqueous solutions of manganese(III) acetate is shown.

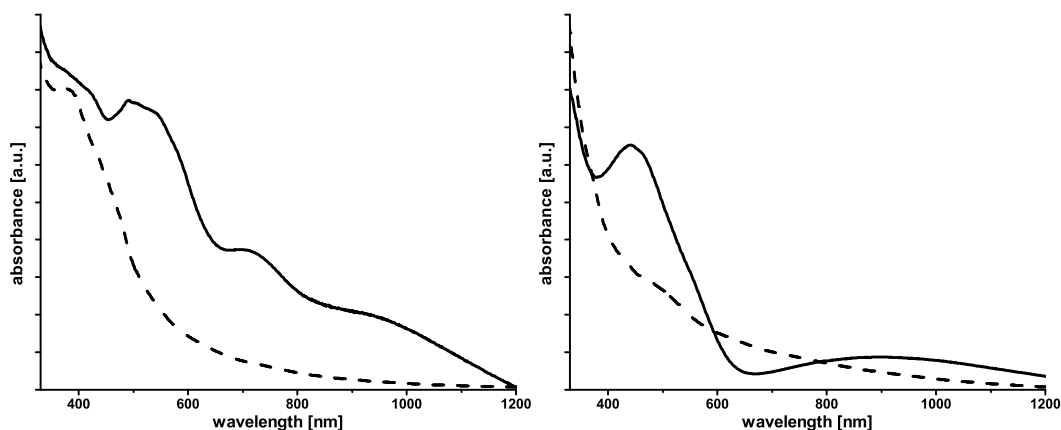


Figure 7.3.: Diffuse reflectance UV/Vis spectra of complex **1** (left) and $\text{Mn}(\text{OAc})_3$ (right) as solids (mixed with BaSO_4 , solid lines) and adsorbed on montmorillonite (dashed lines).

(Fig. 7.3) when comparing the neat manganese compounds with their clay hybrids. The EPR spectra of the clay hybrids also point to significant changes in the electronic structure of the manganese compounds by adsorption, indicating that a strong interaction occurs between the compounds and the clay surfaces.

To study the water oxidation ability, reactions of aqueous suspensions of the clay hybrids with Ce^{IV} were investigated in a measurement cell of a Clark electrode. The oxygen evolving curves in Figure 7.4 show that water oxidation can be clearly detected for all clay hybrids obtained from precursors containing manganese(III) or manganese(IV), but this occurs at significantly different rates. The most active catalyst was $\text{Mn}^{3+}@Mt$, obtained by the adsorption of manganese(III) acetate, followed by $\text{Mn1}@Mt$ and $\mathbf{1}@Mt$, which catalyse the oxidation of water at about half ($\text{Mn1}@Mt$) or a quarter ($\mathbf{1}@Mt$) of the rate of $\text{Mn}^{3+}@Mt$, respectively. Interestingly, the clay hybrid containing manganese(II) ($\text{Mn}^{2+}@Mt$) showed no catalytic activity at all.

Possible mechanistic pathways for the dioxygen formation step during water oxidation catalyzed by manganese clay hybrids are shown in Figure 7.5. All three mechanisms are in agreement with pathways suggested in the literature.^{12,36,174} In mechanism A, the O–O bond formation proceeds between one oxygen species bound end-on to a manganese atom and one bridging oxido atom. In the second pathway B, two end-on oxygen species couple directly to form O_2 . A water or hydroxide attacks nucleophilically on a terminal oxygen species in mechanism C. Both, route B and C are theoretically also possible for di- or even mononuclear manganese complexes. Due to the fact that manganese complexes with terminal oxido ligands exist only with electronically very different porphyrin ligands, these pathways are unlikely to

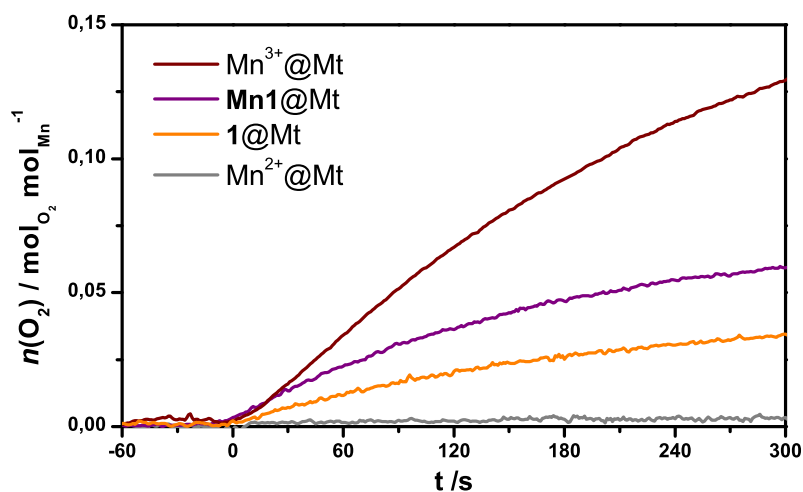


Figure 7.4.: Traces of oxygen evolution for the reactions of different clay hybrids with Ce^{IV} in H_2O . Solutions of the single-electron oxidation agent Ce^{IV} were added at $t = 0$ s.

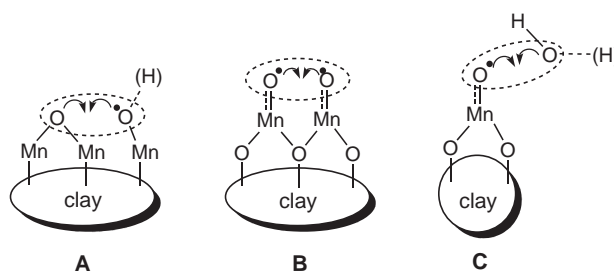


Figure 7.5.: Possible mechanistic pathways of dioxygen formation by manganese clay hybrids in agreement with water oxidation mechanisms suggested in the literature.^{12,36,174}

explain the activity of the manganese adsorbates studied here. The most reasonable route for those appears to be pathway A, in which the coupling oxygen ligands are activated by several manganese centers. Such a route was also suggested for the OEC based on theoretical calculations.¹⁷⁵

7.1. XAS spectroscopy of $\text{Mn}^{3+}@Mt$

X-ray absorption spectroscopy (XAS) is a powerful characterization tool and can reveal many details about a compound due to its sensitivity to the local structure. During XAS measurements, reflections of the transition energy of 1s electrons excited to higher states is observed which depends on the charge and the environment of the metal center. X-ray absorption

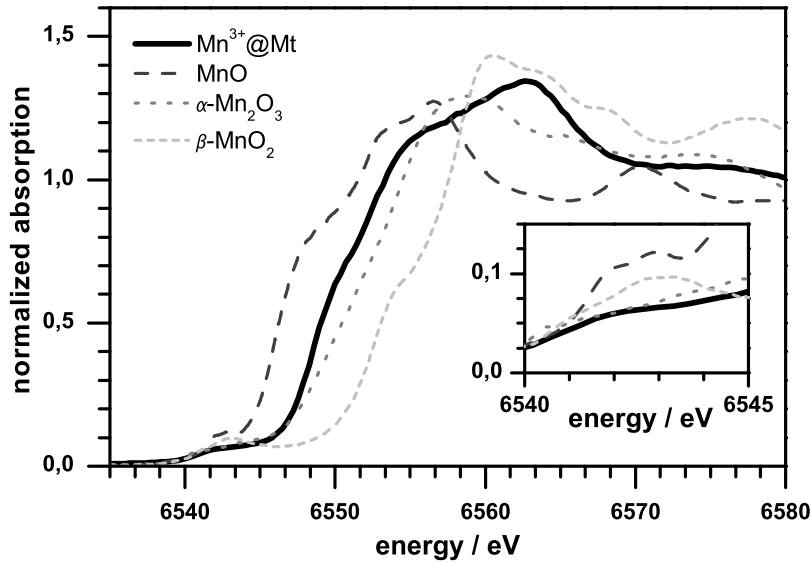


Figure 7.6.: Mn XANES spectra of $\text{Mn}^{3+}@\text{Mt}$ (solid line), $\text{Mn}^{\text{II}}\text{O}$ (dashed line), $\alpha\text{-Mn}^{\text{III}}_2\text{O}_3$ (dotted grey line) and $\beta\text{-Mn}^{\text{IV}}\text{O}_2$ (short dashed light grey line). The inset shows the magnified pre-edge peak area.

near-edge structure (XANES) spectroscopy provides information on the oxidation state while X-ray absorption fine structure (EXAFS) spectroscopy provides geometrical information on the environment of the metal center.^{124,140,176} XAS experiments at the Mn K-edge of the most active catalyst manganese(III) acetate on montmorillonite ($\text{Mn}^{3+}@\text{Mt}$) were performed by Ivelina Zaharieva and Holger Dau at the KMC1 beamline at the BESSY synchrotron (Helmholtz-Zentrum Berlin, Germany)¹⁷⁷ to identify the structural motifs and the oxidation states of the manganese centers.

X-ray absorption near-edge structure (XANES) spectra of $\text{Mn}^{3+}@\text{Mt}$ and manganese oxides with known oxidation states are shown in Figure 7.6. The comparison of the edge-rise energies

	R / Å	N	σ / Å
Mn–O	1.89 ± 0.01	3.7	0.070 ± 0.006
Mn–O	2.18 ± 0.01	2.3 ± 0.2	0.063*
Mn–Mn	2.85 ± 0.01	2.4 ± 0.2	0.063*

Table 7.1.: Parameters obtained from the simulation of the EXAFS spectra of $\text{Mn}^{3+}@\text{Mt}$. The errors represent the 68% confidence intervals of the respective fit parameters. Parameters marked by an asterik were fixed during the least-square fit. The sum of the coordination numbers for the first two shells was fixed to six. The simulation and the measurements were performed by Ivelina Zaharieva and Holger Dau.

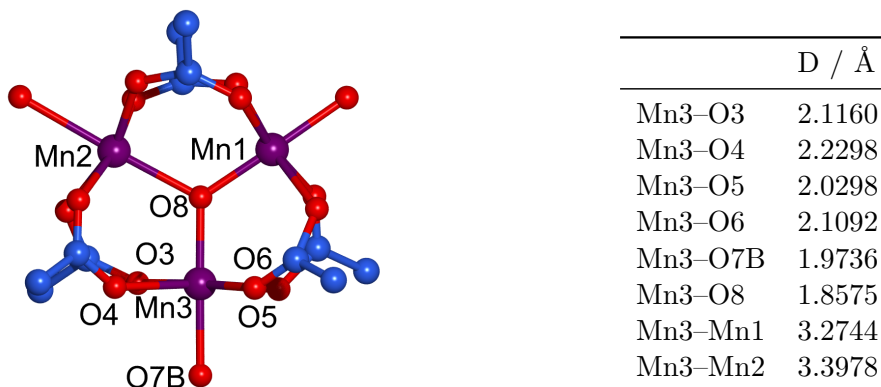


Figure 7.7.: Structure and selected bond distances of manganese(III) acetate which forms an oxido-centered trimer in aqueous solution like the related iron and chromium compounds.¹⁷⁸

reveals that the mean manganese oxidation state in $\text{Mn}^{3+}@Mt$ is very close to +III. The Fourier transformed X-ray absorption fine structure (FT-EXAFS) spectra of $\text{Mn}^{3+}@Mt$, a manganese oxide (G400) and the OEC of Photosystem II in its dark stable S_1 state are shown in Figure 7.8 and the corresponding fit results are given in Table 7.1. The simulation for the first peak of the $\text{Mn}^{3+}@Mt$ spectrum fits to six-coordinated Mn(III)-ions with two different Mn–O distances, four times 1.89 Å and twice 2.18 Å. The Mn–Mn distance is determined as 2.85 Å. The FT-EXAFS spectrum of $\text{Mn}^{3+}@Mt$ shows similarities to the one of Photosystem II, though not to that of the layered manganese oxide G400 which indicates just one Mn–O distance (1.90 Å) and the prevalence of $\text{Mn}^{\text{IV}}\text{O}_6$ octahedra. The precursor of $\text{Mn}^{3+}@Mt$, manganese(III) acetate, forms an oxido centered trimer in aqueous solutions.¹⁷⁸ The structure and selected bond distances of $\text{Mn}^{\text{III}}(\text{OAc})_3$ are given in Figure 7.7. A comparison with the Mn–Mn and Mn–O distances of $\text{Mn}^{3+}@Mt$ obtained by the simulation of the FT-EXAFS illustrates that this trimer structure is lacking in the clay hybrid and presumably there are no acetate bridges between the manganese ions. While the Mn–O distances are similar, the Mn–Mn distances of $\text{Mn}^{3+}@Mt$ are considerably shorter than those in $\text{Mn}^{\text{III}}(\text{OAc})_3$ indicating that the Mn species of $\text{Mn}^{3+}@Mt$ could be purely oxido clusters connected via bis(μ -O) bridges. As the FT-EXAFS data show low order of the subunits, details of the arrangement and the cluster size remain unclear.

7.2. Conclusion

Functional, biomimetic catalysts for water oxidation could be synthesized by the adsorption of different manganese precursors on K10 montmorillonite, although all manganese species are not able to catalyse water oxidation on their own in homogeneous solutions. The best catalyst hybrid investigated in this study was $\text{Mn}^{3+}@Mt$ for which catalytic rates surpass the

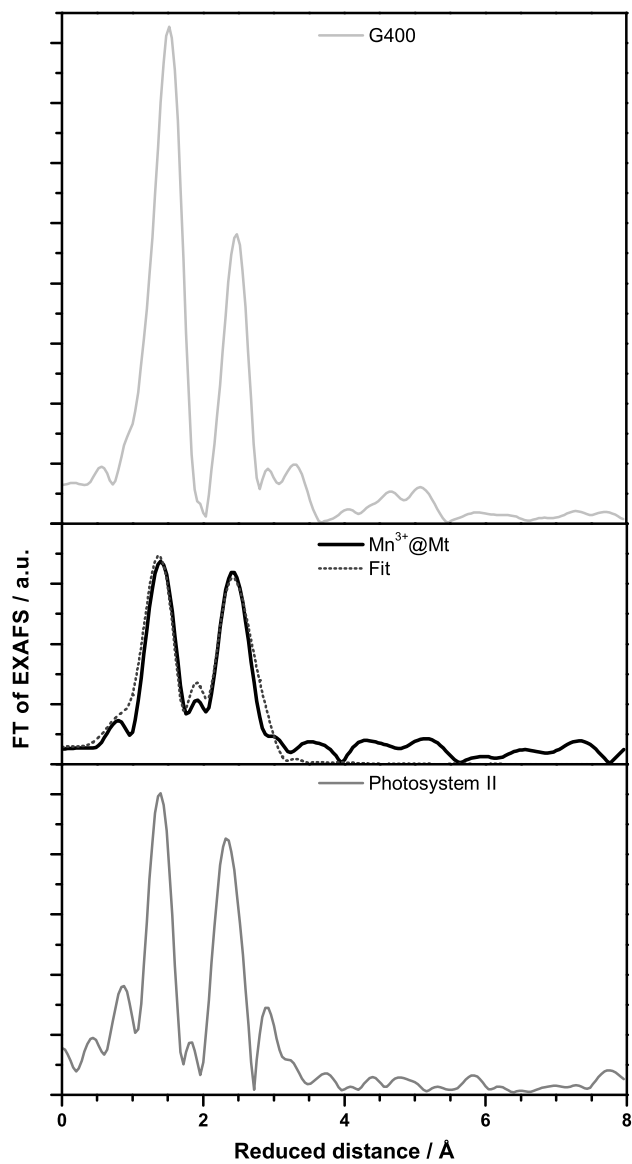


Figure 7.8.: Fourier transformed EXAFS spectra of the layered manganese oxide G400 ($\text{CaMn}^{\text{IV}}_{1.6}\text{Mn}^{\text{III}}_{0.4}(\text{O}_{4.5}(\text{OH})_{0.5})$), $^{124}\text{Mn}^{3+}@\text{Mt}$ and Photosystem II in the S_1 state collected at the Mn K-edge.

best catalyst of this class found so far, which was **Mn1@Mt** discovered by Yagi and Narita in 2004.¹⁵ The results of catalytic studies and spectroscopy indicated that the catalytic units on the surfaces most likely consist of more than two manganese centers. Furthermore, a manganese oxidation state of $\text{Mn} \geq +\text{III}$ seems to be a prerequisite for active catalysts as no activity was found for adsorbed manganese(II) ($\text{Mn}^{2+}@\text{Mt}$).

Additionally, very different types of manganese precursors can be assembled into active catalysts, so the geometrical arrangement of the manganese precursors seems only to be of secondary importance. XAS measurements of the most active catalyst, the $\text{Mn}^{3+}@\text{Mt}$ hybrid, revealed that the original ligand environment of manganese(III) acetate is completely lost. The results indicate that the manganese species of $\text{Mn}^{3+}@\text{Mt}$ consists of disordered manganese(III) oxido clusters. Thus, the adsorption of $\text{Mn}^{\text{III}}(\text{OAc})_3$ did not affect the manganese oxidation state but the ligand environment and therefore the electronic structure. This result is not surprising, as disordered manganese oxides are known to be active water oxidation catalysts in the birnessite form, however with a higher manganese oxidation state of around +3.8.^{120,124} Through the aggregation of manganese centers with sizes of more than two manganese atoms, the aforementioned (see section 3 and 6) requirements for water oxidation were fulfilled.

8. Carbon monoxide releasing molecules

The last part of this thesis is a “spin-off” from my synthetic work and deals with a rather different aspect of chemistry but also with facially coordinated manganese centers. In addition to nitric oxide¹⁷⁹ and hydrogen sulfide,¹⁸⁰ carbon monoxide (CO) acts as an important small molecule messenger in many organisms, including humans.¹⁸¹ Most of the CO is produced endogenously through the enzymatic decomposition of the ring system in heme to ferric iron and biliverdin, which is further reduced to bilirubin by biliverdin reductase (Fig. 8.1).^{182–184} The heme degradation is catalyzed by the enzyme heme oxygenase. This reaction is particularly interesting because heme serves as the cofactor of its own degradation.

It has been shown that low concentrations of CO have many beneficial effects on organs and tissues, mostly protection against oxidative stress.²⁰ Due to these findings CO could be used for therapeutic application. Since a overdose of CO is highly toxic, the release of carbon monoxide must be controlled precisely. A number of carbon monoxide releasing molecules (CORMs) are under investigation to achieve a delivery of CO in beneficial quantities over extend time periods close to the pharmacological target. Most of these CORMs are based on transition metal carbonyls like CORM2¹⁸⁵ and CORM3¹⁸⁶ shown in Figure 8.2. Furthermore, CORMA1 is based on sodium boranocarbonate and decomposes in water to CO and boric acid.¹⁸⁷ These CORMs have already shown high preclinical efficacy in several applications.²⁰ For these and most other CORMS known so far, the release of carbon monoxide starts immediately upon dissolution in water. Another class of CO releasing molecules is known where CO is liberated upon photoactivation.^{18,21,188–190} Such photoCORMs have the

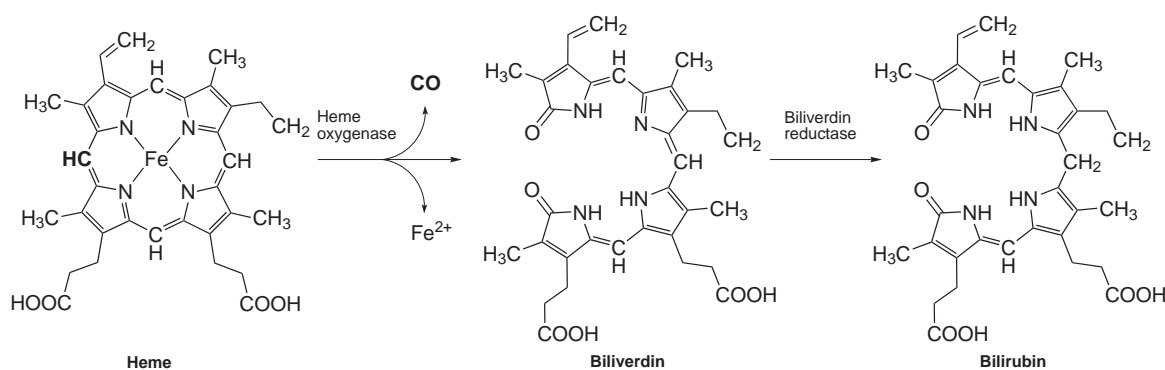


Figure 8.1.: Degradation pathway of heme to carbon monoxide, ferric iron and biliverdin, which is subsequently converted to bilirubin.

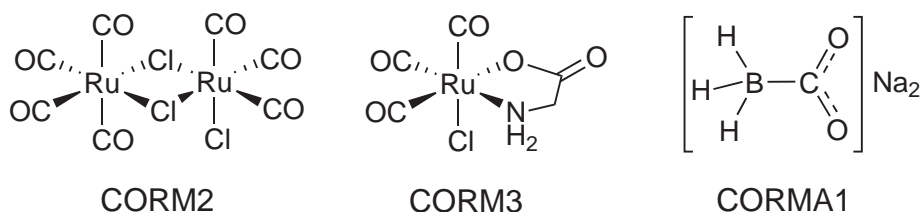


Figure 8.2.: Three carbon monoxide releasing molecules on which preclinical efficacy test were already performed:²⁰ $[\text{Ru}(\text{CO})_3\text{Cl}_2]_2$ (CORM2),¹⁸⁵ $[\text{Ru}(\text{CO})_3\text{Cl-glycinato}]$ (CORM3)¹⁸⁶ and $\text{Na}_2[\text{H}_3\text{BCO}_2]$ (CORMA1).¹⁸⁷

advantage that the release of CO can be initiated through external triggering by irradiation.

The first publication concerning photoactivated release of carbon monoxide was reported by Motterlini et al. in 2002.¹⁸⁵ It was shown that dimanganese decacarbonyl ($\text{Mn}_2(\text{CO})_{10}$) leads to beneficial vascular relaxation effects in mice hearts upon irradiation. In this context Motterlini and coworkers established the deoxy-myoglobin (Mb)/carbonmonoxy-myoglobin (MbCO) UV/Vis assay (Mb assay) as the principal method used for quantifying the rates of CO release from CORMs. The released CO converts Mb to MbCO and this conversion can be followed by UV/Vis spectroscopy by monitoring the change in the Q-bands of the heme group in both Mb and MbCO. Further research concentrated on metal complexes with organic ligands to increase the bioavailability and facilitate possibilities of chemical modification. The group of Schatzschneider performed multiple studies on the light-induced CORM-activity of the manganese(I) *fac*-tricarbonyl complex $[\text{Mn}(\text{CO})_3(\text{tpm})]^+$ (tpm = tris(pyrazolyl)methane, **2**).^{21,191–193} Several *in vitro* studies with complex **2** and derivatives showed beneficial effects, e.g. cytotoxicity upon human colon cancer cells. However, no manganese reaction intermediates or products were identified. It was stated that complex **2** released at least two CO equivalents upon excitation at 365 nm determined using the Mb assay.²¹ If these stoichiometries were correct, the reaction would result in the formation of monocarbonyl manganese complexes. By looking at the literature on manganese carbonyl compounds, it can be assumed that such species could not be stable in aqueous environments for extended time periods. So it seems currently unknown what manganese species are obtained after photoexcitation from manganese tricarbonyls. A better knowledge of the photoreaction products from these photoCORMs is desirable in order to determine the exact amounts of CO that are released from each manganese complex. It is also necessary to characterize the manganese reaction products as this should not cause unwanted side-effects in a possible application. Therefore, spectroscopic investigations on the photoreaction of two Mn(I) tricarbonyl using UV/Vis, IR and EPR spectroscopy were carried out (chapter 9 and paper III).

9. Mn(I) tricarbonyl complexes as photoCORMs

Water-soluble tricarbonyl manganese complexes have been identified as candidates for the photoactivated release of carbon monoxide, a biological effector and potential therapeutic agent. The manganese(I) compound $[\text{Mn}(\text{CO})_3(\text{tpm})]^+$ (tpm = tris(pyrazolyl)methane, **2**) has been studied in detail by the group of Schatzschneider. However, the exact number of released CO equivalents is unclear and no details about manganese reaction intermediates or products are known. These are of particular interest as these should not cause unwanted side-effects in a possible therapeutic application. A combination of spectroscopic methods (UV/Vis, IR and EPR) was employed to reveal details of the processes resulting in carbon monoxide release upon photoexcitation at 366 nm.

Two closely related manganese(I) tricarbonyl complexes were selected for this study on light-triggered carbon monoxide release: the cationic complex **2** and the neutral, structurally related complex $[\text{Mn}(\text{CO})_3(\text{bpzaa})]$ (bpzaa = bis(pyrazolyl) acetic acid, **3**) for which the photoCORM activity has not been studied yet. Both complexes show a broad absorption band in the UV region with a maximum at 349 nm for **2** and 361 nm for **3**, respectively with extinction coefficients of about $2000 \text{ M}^{-1}\text{cm}^{-1}$. Thus both complexes strongly absorbed the light of 366 nm used during the irradiation experiments.

The myoglobin assay was used to detect the released carbon monoxide upon UV irradiation. It is clearly visible in the spectra in Figure 9.2 that CO release takes place as

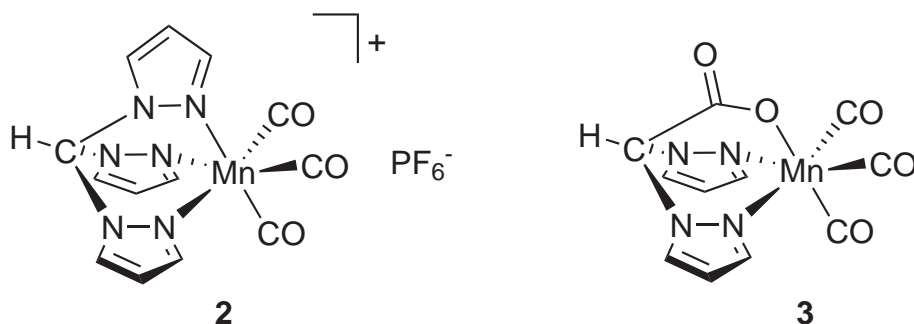


Figure 9.1.: Structures of the manganese(I) tricarbonyl photoCORMs $[\text{Mn}(\text{CO})_3(\text{tpm})]\text{PF}_6$ (**2** PF_6) and $[\text{Mn}(\text{CO})_3(\text{bpzaa})]$ (**3**) investigated in this work.

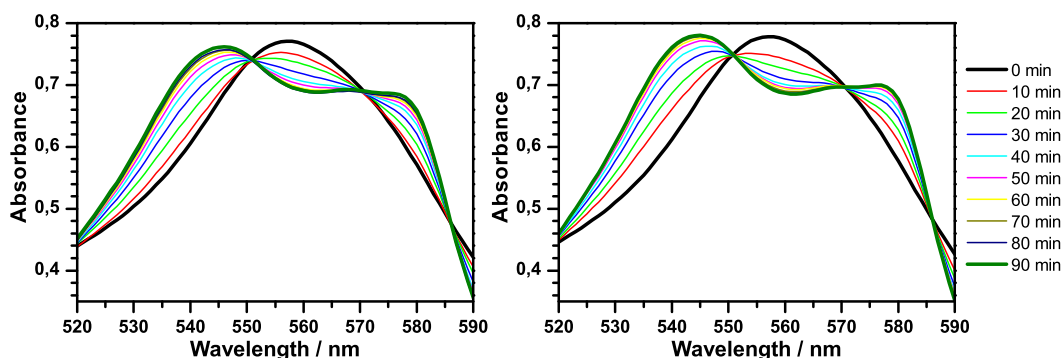


Figure 9.2.: UV/Vis spectra demonstrating the conversion of deoxy-myoglobin (Mb, start spectrum, bold black lines) to carbon monoxide myoglobin (MbCO) caused by the binding of CO released from complexes **2** (left) and **3** (right) to Mb after UV light excitation. See paper III for details.

the characteristic spectral changes known for the conversion of deoxy-myoglobin (Mb) to carbonmonoxy-myoglobin (MbCO) are observed. The neutral carbonyl complex **3** is also an active photoCORM like **2**. Furthermore, it can be seen that CO release from **3** occurs faster than from **2**. Because CO might leave the solution into the head space and additionally CO transfer might be incomplete, further spectroscopic experiments were carried out on irradiated solutions of **2** and **3** in ethanol or ethanol/water = 9:1.

A continuous UV-illumination of **2** or **3** in solution caused the disappearance of the broad absorption band around 350 nm in both cases and resulted in rather featureless spectra within 10-15 min. More information was yielded by IR spectroscopy. Prior to illumination, spectra typical for manganese(I) *fac*-tricarbonyl complexes were observed with one strong IR band found around 2050 cm^{-1} and two additional bands located between 1930 and 1970 cm^{-1} (Fig. 9.3). During UV-irradiation, these strong IR bands of the initial complexes disappeared with half-lives of about 10-15 min indicating that the $[\text{Mn}^{\text{I}}(\text{CO})_3]$ -units of **2** and **3** dissociated. In accordance with the UV/Vis results, the kinetics for this process were faster for complex **3** when compared with **2** and also a slowdown through the addition of water could be observed.

But the most interesting observation is that during the beginning of the photoreactions, small new IR bands emerged in the region between 1850 and 1875 cm^{-1} which completely disappeared again after 30 min of irradiation time. From comparisons with known data on cymantrene ($[\text{Mn}(\text{CO})_3(\text{Cp})]$) and its $[\text{Mn}(\text{CO})_2(\text{Cp})(\text{soln})]$ analogues,¹⁹⁴ these vibrations can be taken as an indication for the formation of manganese(I) *cis*-dicarbonyl intermediates. Such compounds should also show a second IR band at 1950 – 1980 cm^{-1} which cannot be detected here as it would be hidden under the very strong IR absorption of the initial complexes in this region.

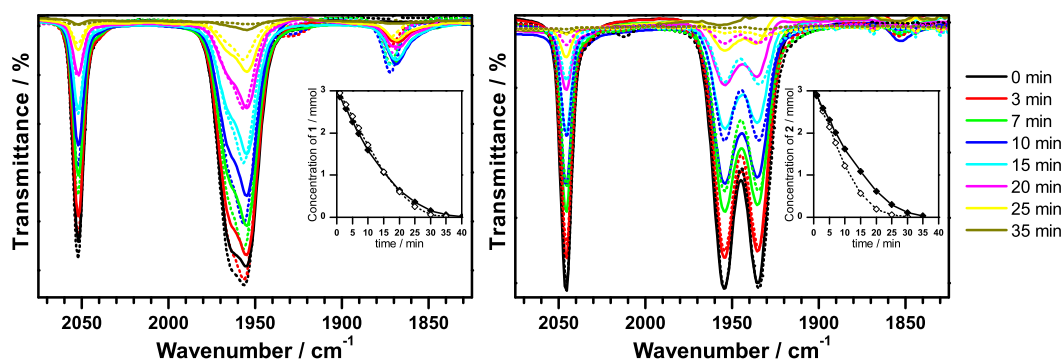


Figure 9.3.: Infrared spectra for 3 mM solutions of **2** (left) or **3** (right) during UV-light-triggered CO release. Solid lines show spectra recorded for solutions in mixtures EtOH:H₂O = 9:1, dotted lines for reactions in pure ethanol. Insets: quantifications for the amounts of remaining tricarbonyl species as a function of illumination time. The sharp IR bands at 2052 or 2045 cm⁻¹ were used to determine the concentrations of **2** or **3**, respectively.

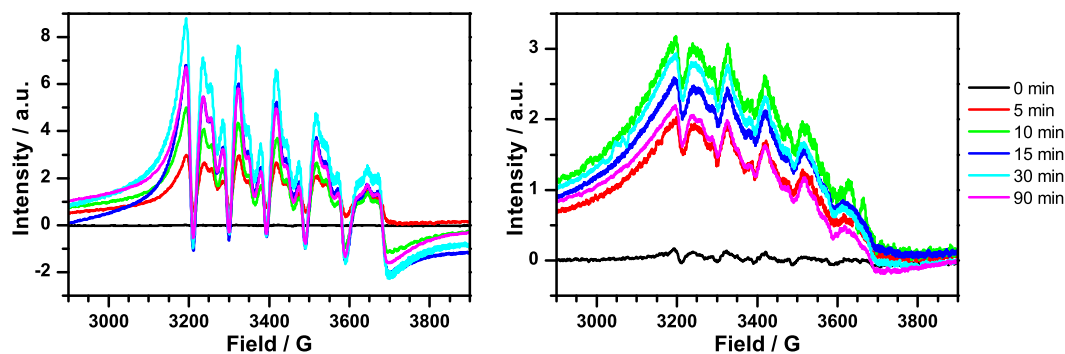


Figure 9.4.: X-band EPR spectra of frozen solutions ($T = 5$ K, 1 mM complex in mixtures EtOH:H₂O = 9:1) of **2** (left) or **3** (right) for the course of UV-light-photolysis. EPR settings: microwave power: 2 mW, modulation amplitude 5 G.

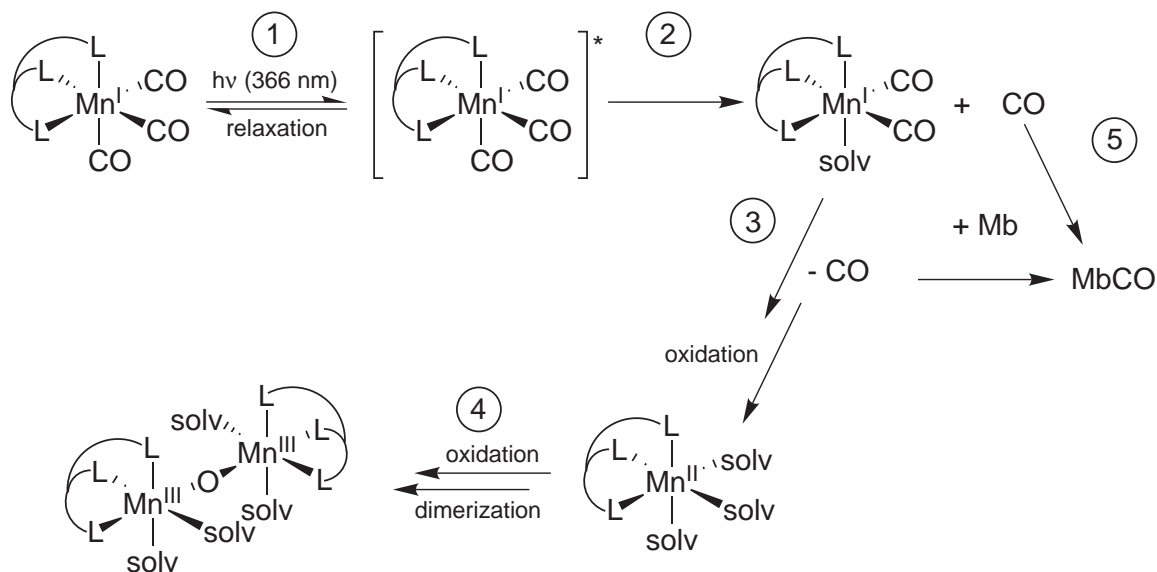


Figure 9.5.: Carbon monoxide release and manganese oxidation reactions following UV excitations of **2** or **3** as identified by UV/Vis, IR and EPR spectroscopy.

EPR spectroscopical investigations of the irradiation reactions revealed information about the oxidation state of manganese intermediates and products. Upon UV irradiation, the emergence of a six-line EPR signal at $g \approx 2$ with a total signal width of about 800 G was observed. This typical spectral signature of mononuclear manganese(II) compounds rises to reach maximum intensities (30 min for **2** and 10 min for **3**, respectively) before the height of the six-line signals decreased again without the appearance of new EPR features.

Combining the results of these spectroscopic investigations, a sequence of possible reactions for **2** and **3** can be proposed (Scheme 9.5). It was found that the manganese complexes lose their carbonyl ligands in a stepwise manner. First, one CO per Mn is released yielding manganese dicarbonyl intermediates, which could be clearly identified by IR spectroscopy (reaction (2)). The last two carbonyl ligands are then liberated in a reaction accompanied by manganese oxidation to Mn^{II} and beyond, as clearly detected by EPR spectroscopy (reaction (3)). Ultimately, μ -O-Mn^{III}-compounds appear to be the most likely final reaction products (reaction (4)). The spectroscopic methodology used here thus enables to present a much more detailed picture of the light-triggered CO releasing reactions of fac-[Mn^I(CO)₃]-complexes than previously accessible by the use of the classical myoglobin assay alone. The additional information on the CO release process gained in this way as well as the fate of the manganese precursors seem essential for a potential pharmaceutical application of manganese photoCORMs.

10. Outlook

The dinuclear manganese complex **1** failed to be a water oxidation catalyst and thereby follows the trend of many other Mn complexes reported so far. A possible manganese water oxidation catalyst will have to allow the take out of four electrons in one-electron steps at high potentials. Furthermore, a flexible and oxidation stable ligand framework is required. Most likely, more than two manganese centers per complex are needed. Just before the completion of this thesis, a molecular manganese water oxidation catalyst has been described by Åkermark and coworkers.¹⁹⁵ The dinuclear complex $[\text{Mn}_2(\text{H}_2\text{L})(\text{OMe})(\text{OAc})]$ ($\text{H}_2\text{L}^{3-} = 2,6$ -bis(4-carboxylato-1*H*-benzimidazol-2-yl)-4-methylphenolate) catalyzes water oxidation upon reactions with $[\text{Ru}(\text{bpy})_3]^{3+}$ directly or with photogenerated $[\text{Ru}(\text{bpy})_3]^{3+}$. This complex seems to be the first manganese-based homogeneous water oxidation catalyst. However, the authors did not investigate the electrochemical properties and the active manganese species have remained completely unclear. A crystal structure of a multiple-bridged tetranuclear species is presented instead. Therefore, future studies should focus on tetranuclear manganese complexes as they seem to be promising candidates for water oxidation catalysis.

Manganese-based water oxidation catalysts could be obtained through the adsorption of manganese precursors onto montmorillonite K10 clay supports. Extensive spectroscopical investigations revealed that the adsorbed Mn species consists of oligonuclear manganese oxido clusters. However, these clay hybrids are not especially efficient or stable. The use of more robust scaffold materials like aluminium oxides or silica alumina oxides, which are industrially used as catalyst support, could increase the long-term stability and may also provide higher water oxidation activities.

Additionally, the work about manganese photoCORMs presented in this thesis clearly demonstrates much more details about the processes leading to light-triggered CO release. Future studies should thus try to identify the nature of the products by mass spectrometry. Furthermore, manganese(I) tricarbonyl complexes have the potential to be used as precursors for the synthesis of multinuclear oxido-bridged manganese complexes.

Abbreviations

ADP	Adenosine diphosphate
ATP	Adenosine triphosphate
bpy	2,2'-Bipyridine
bpzaa	bis(pyrazolyl) acetic acid
CO	Carbon monoxide
CORM	CO releasing molecule
Cp	Cyclopentadienyl
Cp*	1,2,3,4,5-Pentamethylcyclopentadienyl
cw	Continuous wave
DFT	Density functional theory
EDX	Energy-dispersive X-ray spectroscopy
EPR	Electron paramagnetic resonance
et al.	et alii
EXAFS	Extended X-ray absorption fine structure
IR	Infrared
Mb	Myoglobin
MbCO	Carbonmonoxy myoglobin
OEC	Oxygen evolving complex
PSI	Photosystem I
PSII	Photosystem II
SHE	Standard hydrogen electrode
terpy	2,2';6',2"-Terpyridine
TON	Turnover number
TOF	Turnover frequency
tpdm	Tris(2-pyridyl)methane
tpm	Tris(pyrazolyl)methane
UV/Vis	Ultraviolet-visible
XANES	X-ray Absorption Near Edge Structure
XAS	X-ray absorption spectroscopy
XRD	X-ray diffraction
Y _Z	Tyrosine Z (D1-Tyr 161)
ZFS	Zero field splitting

References

- [1] A. F. Holleman, E. Wiberg, *Lehrbuch der Anorganischen Chemie*, de Gruyter, Berlin, **1995**.
- [2] F. A. Armstrong, *Phil. Trans. R. Soc. B* **2008**, *363*(1494), 1263–1270.
- [3] K. Wieghardt, *Angew. Chem. Int. Ed. Engl.* **1989**, *28*(9), 1153–1172.
- [4] G. C. Dismukes, *Chem. Rev.* **1996**, *96*(7), 2909–2926.
- [5] I. A. Abreu, D. E. Cabelli, *Biochim. Biophys. Acta* **2010**, *1804*(2), 263–274.
- [6] V. V. Barynin, M. M. Whittaker, S. V. Antonyuk, V. S. Lamzin, P. M. Harrison, P. J. Artymiuk, J. W. Whittaker, *Structure* **2001**, *9*(8), 725–738.
- [7] Y. Umena, K. Kawakami, J.-R. Shen, N. Kamiya, *Nature* **2011**, *473*(7345), 55–60.
- [8] J. Raymond, R. E. Blankenship, *Coord. Chem. Rev.* **2008**, *252*(3-4), 377–383.
- [9] N. S. Lewis, D. G. Nocera, *Proc. Natl. Acad. Sci. U.S.A.* **2006**, *103*(43), 15729–15735.
- [10] G. F. Moore, G. W. Brudvig, *Annu. Rev. Condens. Matter Phys.* **2011**, *2*(1), 303–327.
- [11] R. E. Blankenship, D. M. Tiede, J. Barber, G. W. Brudvig, G. Fleming, M. Ghirardi, M. R. Gunner, W. Junge, D. M. Kramer, A. Melis, T. A. Moore, C. C. Moser, D. G. Nocera, A. J. Nozik, D. R. Ort, W. W. Parson, R. C. Prince, R. T. Sayre, *Science* **2011**, *332*(6031), 805–809.
- [12] H. Dau, C. Limberg, T. Reier, M. Risch, S. Roggan, P. Strasser, *ChemCatChem* **2010**, *2*(7), 724–761.
- [13] T. A. Betley, Q. Wu, T. Van Voorhis, D. G. Nocera, *Inorg. Chem.* **2008**, *47*(6), 1849–1861.
- [14] R. Ramaraj, A. Kira, M. Kaneko, *Chem. Lett.* **1987**, *16*(2), 261–264.
- [15] M. Yagi, K. Narita, *J. Am. Chem. Soc.* **2004**, *126*(26), 8084–8085.
- [16] M. Yagi, K. Narita, S. Maruyama, K. Sone, T. Kuwabara, K. Shimizu, *Biochim. Biophys. Acta* **2007**, *1767*(6), 660–665.

- [17] P. Kurz, *Dalton Trans.* **2009**, 6103–6108.
- [18] U. Schatzschneider, *Inorg. Chim. Acta* **2011**, *374*(1), 19–23.
- [19] S. W. Ryter, J. Alam, A. M. Choi, *Physiol. Rev.* **2006**, *86*(2), 583–650.
- [20] R. Motterlini, L. E. Otterbein, *Nat. Rev. Drug Discov.* **2010**, *9*(9), 728–743.
- [21] J. Niesel, A. Pinto, H. W. P. N’Dongo, K. Merz, I. Ott, R. Gust, U. Schatzschneider, *Chem. Commun.* **2008**, (15), 1798–1800.
- [22] L. Taiz, E. Zeiger, *Plant Physiology*, Sinauer Associates, **2010**.
- [23] A. Ben-Shem, F. Frolov, N. Nelson, *Nature* **2003**, *426*(6967), 630–635.
- [24] G. Renger, T. Renger, *Photosynth. Res.* **2008**, *98*, 53–80.
- [25] F. Rappaport, M. Guergova-Kuras, P. J. Nixon, B. A. Diner, J. Lavergne, *Biochemistry* **2002**, *41*(26), 8518–8527.
- [26] H. Dau, I. Zaharieva, *Acc. Chem. Res.* **2009**, *42*(12), 1861–1870.
- [27] Wikipedia, Light-dependent reactions — Wikipedia, The Free Encyclopedia, **2011**, online; accessed 10-October-2011.
- [28] K. Kawakami, Y. Umena, N. Kamiya, J.-R. Shen, *J. Photochem. Photobiol. B: Biol.* **2011**, *104*(1-2), 9–18.
- [29] K. N. Ferreira, T. M. Iverson, K. Maghlaoui, J. Barber, S. Iwata, *Science* **2004**, *303*, 1831–1838.
- [30] A. Guskov, J. Kern, A. Gabdulkhakov, M. Broser, A. Zouni, W. Saenger, *Nat. Struct. Mol. Biol.* **2009**, *16*(3), 334–342.
- [31] B. Loll, J. Kern, W. Saenger, A. Zouni, J. Biesiadka, *Nature* **2005**, *438*(7070), 1040–1044.
- [32] P. Joliot, G. Barbieri, R. Chabaud, *Photochem. Photobio.* **1969**, *10*, 309–329.
- [33] L. V. Kulik, B. Epel, W. Lubitz, J. Messinger, *J. Am. Chem. Soc.* **2005**, *127*(8), 2392–2393.
- [34] L. V. Kulik, B. Epel, W. Lubitz, J. Messinger, *J. Am. Chem. Soc.* **2007**, *129*(44), 13421–13435.
- [35] B. Kok, B. Forbush, M. McGloin, *Photochem. Photobio.* **1970**, *11*, 457.
- [36] W. Lubitz, E. J. Reijerse, J. Messinger, *Energy Environ. Sci.* **2008**, *1*, 15–31.

- [37] M. Haumann, C. Müller, P. Liebisch, L. Iuzzolino, J. Dittmer, M. Grabolle, T. Neisius, W. Meyer-Klaucke, H. Dau, *Biochemistry* **2005**, *44*(6), 1894–1908.
- [38] J. H. Robblee, J. Messinger, R. M. Cinco, K. L. McFarlane, C. Fernandez, S. A. Pizarro, K. Sauer, V. K. Yachandra, *J. Am. Chem. Soc.* **2002**, *124*(25), 7459–7471.
- [39] M. Kirch, J. M. Lehn, J. P. Sauvage, *Helv. Chim. Acta* **1979**, *62*(4), 1345–84.
- [40] S. Fukuzumi, Y. Yamada, T. Suenobu, K. Ohkubo, H. Kotani, *Energy Environ. Sci.* **2011**, *4*(8), 2754–2766.
- [41] A. J. Morris, G. J. Meyer, E. Fujita, *Acc. Chem. Res.* **2009**, *42*(12), 1983–1994.
- [42] M. Rakowski Dubois, D. L. Dubois, *Acc. Chem. Res.* **2009**, *42*(12), 1974–1982.
- [43] S. C. Roy, O. K. Varghese, M. Paulose, C. A. Grimes, *ACS Nano* **2010**, *4*(3), 1259–1278.
- [44] R. H. Crabtree (Ed.), *Energy Production and Storage: Inorganic Chemical Strategies for a Warming World*, John Wiley & Sons Ltd, New York, **2010**.
- [45] A. P. van Troostwijk, J. R. Deiman, *J. Phys. Chim. Hist. Nat.* **1789**, *35*(35), 369–378.
- [46] V. Engelhardt, *The electrolysis of water*, Vol. I of *Monographs on applied electrochemistry*, The chemical publishing company, **1904**.
- [47] A. Hofmann, *Introduction to modern chemistry: experimental and theoretic; embodying twelve lectures delivered in the Royal College of Chemistry, London*, Walton and Maberly, **1866**.
- [48] R. LeRoy, *Int. J. Hydrogen Energy* **1983**, *8*(6), 401–417.
- [49] B. S. Brunshwig, M. H. Chou, C. Creutz, P. Ghosh, N. Sutin, *J. Am. Chem. Soc.* **1983**, *105*(14), 4832–4833.
- [50] M. W. Kanan, D. G. Nocera, *Science* **2008**, *321*(5892), 1072–1075.
- [51] M. W. Kanan, Y. Surendranath, D. G. Nocera, *Chem. Soc. Rev.* **2009**, *38*(1), 109–114.
- [52] Y. Surendranath, M. Dinca, D. G. Nocera, *J. Am. Chem. Soc.* **2009**, *131*(7), 2615–2620.
- [53] Y. Surendranath, M. W. Kanan, D. G. Nocera, *J. Am. Chem. Soc.* **2010**, *132*(46), 16501–16509.
- [54] D. A. Lutterman, Y. Surendranath, D. G. Nocera, *J. Am. Chem. Soc.* **2009**, *131*(11), 3838–3839.
- [55] E. R. Young, D. G. Nocera, V. Bulovic, *Energy Environ. Sci.* **2010**, *3*(11), 1726–1728.

- [56] A. J. Esswein, Y. Surendranath, S. Y. Reece, D. G. Nocera, *Energy Environ. Sci.* **2011**, *4*(2), 499–504.
- [57] M. Risch, V. Khare, I. Zaharieva, L. Gerencser, P. Chernev, H. Dau, *J. Am. Chem. Soc.* **2009**, *131*(20), 6936–6937.
- [58] M. W. Kanan, J. Yano, Y. Surendranath, M. Dinca, V. K. Yachandra, D. G. Nocera, *J. Am. Chem. Soc.* **2010**, *132*(39), 13692–13701.
- [59] F. Cheng, J. Shen, B. Peng, Y. Pan, Z. Tao, J. Chen, *Nature Chem.* **2011**, *3*(1), 79–84.
- [60] Y. V. Geletii, B. Botar, P. Kögerler, D. A. Hillesheim, D. G. Musaev, C. L. Hill, *Angew. Chem. Int. Ed.* **2008**, *47*(21), 3896–3899.
- [61] A. Sartorel, M. Carraro, G. Scorrano, R. D. Zorzi, S. Geremia, N. D. McDaniel, S. Bernhard, M. Bonchio, *J. Am. Chem. Soc.* **2008**, *130*(15), 5006–5007.
- [62] A. Sartorel, P. Miró, E. Salvadori, S. Romain, M. Carraro, G. Scorrano, M. D. Valentin, A. Llobet, C. Bo, M. Bonchio, *J. Am. Chem. Soc.* **2009**, *131*(44), 16051–16053.
- [63] F. M. Toma, A. Sartorel, M. Iurlo, M. Carraro, P. Parisse, C. Maccato, S. Rapino, B. R. Gonzalez, H. Amenitsch, T. D. Ros, L. Casalis, A. Goldoni, M. Marcaccio, G. Scorrano, G. Scoles, F. Paolucci, M. Prato, M. Bonchio, *Nature Chem.* **2010**, *2*(10), 826–831.
- [64] N. D. Schley, J. D. Blakemore, N. K. Subbaiyan, C. D. Incarvito, F. D’Souza, R. H. Crabtree, G. W. Brudvig, *J. Am. Chem. Soc.* **2011**, *133*(27), 10473–10481.
- [65] R. Brimblecombe, G. C. Dismukes, G. F. Swiegers, L. Spiccia, *Dalton Trans.* **2009**, (43), 9374–9384.
- [66] T. Wada, J. T. Muckerman, E. Fujita, K. Tanaka, *Dalton Trans.* **2011**, *40*(10), 2225–2233.
- [67] R. Brimblecombe, D. R. J. Kolling, A. M. Bond, G. C. Dismukes, G. F. Swiegers, L. Spiccia, *Inorg. Chem.* **2009**, *48*(15), 7269–7279.
- [68] Y. Gorlin, T. F. Jaramillo, *J. Am. Chem. Soc.* **2010**, *132*(39), 13612–13614.
- [69] A. Fujishima, K. Honda, *Nature* **1972**, *238*(5358), 37–38.
- [70] K. L. Hardee, A. J. Bard, *J. Electrochem. Soc.* **1976**, *123*(7), 1024–1026.
- [71] Y.-S. Hu, A. Kleiman-Shwarstein, G. D. Stucky, E. W. McFarland, *Chem. Commun.* **2009**, (19), 2652–2654.
- [72] S. D. Tilley, M. Cornuz, K. Sivula, M. Grätzel, *Angew. Chem. Int. Ed.* **2010**, *49*(36), 6405–6408.

- [73] G. Hodes, D. Cahen, J. Manassen, *Nature* **1976**, *260*(5549), 312–313.
- [74] F. Amano, D. Li, B. Ohtani, *Chem. Commun.* **2010**, *46*(16), 2769–2771.
- [75] R. Liu, Y. Lin, L.-Y. Chou, S. W. Sheehan, W. He, F. Zhang, H. J. M. Hou, D. Wang, *Angew. Chem. Int. Ed.* **2011**, *50*(2), 499–502.
- [76] B. A. Pinaud, Z. Chen, D. N. Abram, T. F. Jaramillo, *J. Phys. Chem. C* **2011**, *115*(23), 11830–11838.
- [77] O. Khaselev, J. A. Turner, *Science* **1998**, *280*(5362), 425–427.
- [78] R. Brimblecombe, G. F. Swiegers, G. C. Dismukes, L. Spiccia, *Angew. Chem. Int. Ed.* **2008**, *47*(38), 7335–7338.
- [79] R. Brimblecombe, A. M. Bond, G. C. Dismukes, G. F. Swiegers, L. Spiccia, *Phys. Chem. Chem. Phys.* **2009**, *11*(30), 6441–6449.
- [80] R. Brimblecombe, A. Koo, G. C. Dismukes, G. F. Swiegers, L. Spiccia, *J. Am. Chem. Soc.* **2010**, *132*(9), 2892–2894.
- [81] R. K. Hocking, R. Brimblecombe, L.-Y. Chang, A. Singh, M. H. Cheah, C. Glover, W. H. Casey, L. Spiccia, *Nature Chem.* **2011**, *3*(6), 461–466.
- [82] M. Grätzel, *Inorg. Chem.* **2005**, *44*(20), 6841–6851.
- [83] G. F. Moore, J. D. Blakemore, R. L. Milot, J. F. Hull, H.-e. Song, L. Cai, C. A. Schmuttenmaer, R. H. Crabtree, G. W. Brudvig, *Energy Environ. Sci.* **2011**, *4*(7), 2389–2392.
- [84] J. J. H. Pijpers, M. T. Winkler, Y. Surendranath, T. Buonassisi, D. G. Nocera, *Proc. Natl. Acad. Sci. U.S.A.* **2011**.
- [85] K. Maeda, M. Higashi, B. Siritanaratkul, R. Abe, K. Domen, *J. Am. Chem. Soc.* **2011**.
- [86] M. Hara, C. C. Waraksa, J. T. Lean, B. A. Lewis, T. E. Mallouk, *J. Phys. Chem. A* **2000**, *104*(22), 5275–5280.
- [87] S. W. Gersten, G. J. Samuels, T. J. Meyer, *J. Am. Chem. Soc.* **1982**, *104*(14), 4029–4030.
- [88] J. A. Gilbert, D. S. Eggleston, W. R. Murphy, D. A. Geselowitz, S. W. Gersten, D. J. Hodgson, T. J. Meyer, *J. Am. Chem. Soc.* **1985**, *107*(13), 3855–3864.
- [89] J. J. Concepcion, J. W. Jurss, J. L. Templeton, T. J. Meyer, *Proc. Natl. Acad. Sci. U.S.A.* **2008**, *105*(46), 17632–17635.

- [90] S. Romain, F. Bozoglian, X. Sala, A. Llobet, *J. Am. Chem. Soc.* **2009**, *131*(8), 2768–2769.
- [91] T. Wada, K. Tsuge, K. Tanaka, *Angew. Chem. Int. Ed.* **2000**, *39*(8), 1479–1482.
- [92] R. Zong, R. P. Thummel, *J. Am. Chem. Soc.* **2005**, *127*(37), 12802–12803.
- [93] Y. Xu, A. Fischer, L. Duan, L. Tong, E. Gabrielsson, B. Åkermark, L. Sun, *Angew. Chem. Int. Ed.* **2010**, *49*(47), 8934–8937.
- [94] S. W. Kohl, L. Weiner, L. Schwartsburd, L. Konstantinovski, L. J. W. Shimon, Y. Ben-David, M. A. Iron, D. Milstein, *Science* **2009**, *324*(5923), 74–77.
- [95] H.-W. Tseng, R. Zong, J. T. Muckerman, R. Thummel, *Inorg. Chem.* **2008**, *47*(24), 11763–11773.
- [96] J. J. Concepcion, M. K. Tsai, J. T. Muckerman, T. J. Meyer, *J. Am. Chem. Soc.* **2010**, *132*(5), 1545–1557.
- [97] S. Romain, L. Vigara, A. Llobet, *Acc. Chem. Res.* **2009**, *42*(12), 1944–1953.
- [98] L. Tong, L. Duan, Y. Xu, T. Privalov, L. Sun, *Angew. Chem. Int. Ed.* **2011**, *50*(2), 445–449.
- [99] J. T. Muckerman, D. E. Polyansky, T. Wada, K. Tanaka, E. Fujita, *Inorg. Chem.* **2008**, *47*(6), 1787–1802.
- [100] R. Bianco, P. J. Hay, J. T. Hynes, *J. Phys. Chem. A* **2011**, *115*(27), 8003–8016.
- [101] X. Yang, M.-H. Baik, *J. Am. Chem. Soc.* **2006**, *128*(23), 7476–7485.
- [102] F. Bozoglian, S. Romain, M. Z. Ertem, T. K. Todorova, C. Sens, J. Mola, M. Rodriguez, I. Romero, J. Benet-Buchholz, X. Fontrodona, C. J. Cramer, L. Gagliardi, A. Llobet, *J. Am. Chem. Soc.* **2009**, *131*(42), 15176–15187.
- [103] S. Ghosh, M.-H. Baik, *Inorg. Chem.* **2011**, *50*(13), 5946–5957.
- [104] N. D. McDaniel, F. J. Coughlin, L. L. Tinker, S. Bernhard, *J. Am. Chem. Soc.* **2008**, *130*(1), 210–217.
- [105] J. F. Hull, D. Balcells, J. D. Blakemore, C. D. Incarvito, O. Eisenstein, G. W. Brudvig, R. H. Crabtree, *J. Am. Chem. Soc.* **2009**, *131*(25), 8730–8731.
- [106] D. G. H. Hetterscheid, J. N. H. Reek, *Chem. Commun.* **2011**, *47*(9), 2712–2714.

- [107] J. D. Blakemore, N. D. Schley, D. Balcells, J. F. Hull, G. W. Olack, C. D. Incarvito, O. Eisenstein, G. W. Brudvig, R. H. Crabtree, *J. Am. Chem. Soc.* **2010**, *132*(45), 16017–16029.
- [108] R. Lalrempuia, N. D. McDaniel, H. Müller-Bunz, S. Bernhard, M. Albrecht, *Angew. Chem. Int. Ed.* **2010**, *49*(50), 9765–9768.
- [109] P. Kurz, G. Berggren, M. F. Anderlund, S. Styring, *Dalton Trans.* **2007**, (38), 4258–4261.
- [110] J. Limburg, J. Vrettos, L. Liable-Sands, A. Rheingold, R. Crabtree, G. Brudvig, *Science* **1999**, *283*, 1524–1527.
- [111] J. Limburg, J. S. Vrettos, H. Y. Chen, J. C. de Paula, R. H. Crabtree, G. W. Brudvig, *J. Am. Chem. Soc.* **2001**, *123*(3), 423–430.
- [112] H. Y. Chen, R. Tagore, G. Olack, J. S. Vrettos, T. C. Weng, J. Penner-Hahn, R. H. Crabtree, G. W. Brudvig, *Inorg. Chem.* **2007**, *46*(1), 34–43.
- [113] A. K. Poulsen, A. Rompel, C. J. McKenzie, *Angew. Chem. Int. Ed.* **2005**, *44*(42), 6916–6920.
- [114] R. K. Seidler-Egdal, A. Nielsen, A. D. Bond, M. J. Bjerrum, C. J. McKenzie, *Dalton Trans.* **2011**, *40*(15), 3849–3858.
- [115] K. Beckmann, H. Uchtenhagen, G. Berggren, M. F. Anderlund, A. Thapper, J. Messinger, S. Styring, P. Kurz, *Energy Environ. Sci.* **2008**, *1*, 668–676.
- [116] D. Shevela, S. Koroidov, M. M. Najafpour, J. Messinger, P. Kurz, *Chem. Eur. J.* **2011**, *17*(19), 5415–5423.
- [117] J. Kiwi, M. Grätzel, *Nature* **1979**, *281*, 657–658.
- [118] A. Harriman, I. J. Pickering, J. M. Thomas, P. A. Christensen, *J. Chem. Soc., Faraday Trans. 1* **1988**, *84*(8), 2795–2806.
- [119] W. J. Youngblood, S.-H. A. Lee, K. Maeda, T. E. Mallouk, *Acc. Chem. Res.* **2009**, *42*(12), 1966–1973.
- [120] M. M. Najafpour, T. Ehrenberg, M. Wiechen, P. Kurz, *Angew. Chem. Int. Ed.* **2010**, *49*(12), 2233–2237.
- [121] D. F. Ghanotakis, G. T. Babcock, C. F. Yocum, *FEBS Lett.* **1984**, *167*(1), 127–130.
- [122] M. Miyao, N. Murata, *FEBS Lett.* **1984**, *168*(1), 118–120.

- [123] K. Sauer, V. K. Yachandra, *Proc. Natl. Acad. Sci. U.S.A.* **2002**, *99*(13), 8631–8636.
- [124] I. Zaharieva, M. M. Najafpour, M. Wiechen, M. Haumann, P. Kurz, H. Dau, *Energy Environ. Sci.* **2011**, *4*(7), 2400–2408.
- [125] C. Neudeck, Y.-Y. Kim, W. Ogasawara, Y. Shida, F. Meldrum, D. Walsh, *Small* **2011**, *7*(7), 869–873.
- [126] D. Shevchenko, M. F. Anderlund, A. Thapper, S. Styring, *Energy Environ. Sci.* **2011**, *4*(4), 1284–1287.
- [127] F. Jiao, H. Frei, *Angew. Chem. Int. Ed.* **2009**, *48*(10), 1841–1844.
- [128] F. Jiao, H. Frei, *Chem. Commun.* **2010**, *46*(17), 2920–2922.
- [129] R. Ramaraj, A. Kira, M. Kaneko, *Angew. Chem. Int. Ed. Engl.* **1986**, *25*(9), 825–827.
- [130] K. Narita, T. Kuwabara, K. Sone, K.-i. Shimizu, M. Yagi, *J. Phys. Chem. B* **2006**, *110*(46), 23107–23114.
- [131] M. Yagi, M. Toda, S. Yamada, H. Yamazaki, *Chem. Commun.* **2010**, *46*(45), 8594–8596.
- [132] M. Zamocky, P. G. Furtmüller, C. Obinger, *Antioxid. Redox Signal.* **2008**, *10*(9), 1527–1548.
- [133] J. Bravo, M. J. Mate, T. Schneider, J. Switala, K. Wilson, P. C. Loewen, I. Fita, *Proteins* **1999**, *34*(2), 155–166.
- [134] Y. Kono, I. Fridovich, *J. Biol. Chem.* **1983**, *258*(10), 6015–6019.
- [135] S. V. Khangulov, V. V. Barynin, N. V. Voevodskaya, A. I. Grebenko, *Biochim. Biophys. Acta, Bioenerg.* **1990**, *1020*(3), 305–310.
- [136] G. S. Waldo, R. M. Fronko, J. E. Penner-Hahn, *Biochemistry* **1991**, *30*(43), 10486–10490.
- [137] G. S. Waldo, S. Yu, J. E. Penner-Hahn, *J. Am. Chem. Soc.* **1992**, *114*(14), 5869–5870.
- [138] G. S. Waldo, J. E. Penner-Hahn, *Biochemistry* **1995**, *34*(5), 1507–1512.
- [139] V. Barynin, A. Grebenko, *Dokl. Akad. Nauk S.S.S.R.* **1986**, *286*, 461–464.
- [140] A. J. Wu, J. E. Penner-Hahn, V. L. Pecoraro, *Chem. Rev.* **2004**, *104*(2), 903–938.
- [141] I. Fita, M. G. Rossmann, *J. Mol. Biol.* **1985**, *185*(1), 21–37.

- [142] T. A. Stich, J. W. Whittaker, R. D. Britt, *J. Phys. Chem. B* **2010**, *114*(45), 14178–14188.
- [143] K.-O. Schäfer, R. Bittl, W. Zweggart, F. Lenzian, G. Haselhorst, T. Weyhermüller, K. Wieghardt, W. Lubitz, *J. Am. Chem. Soc.* **1998**, *120*(50), 13104–13120.
- [144] K.-O. Schäfer, Ph.D. Thesis, Technische Universität Berlin, Berlin, **2002**.
- [145] K.-O. Schäfer, R. Bittl, F. Lenzian, V. Barynin, T. Weyhermüller, K. Wieghardt, W. Lubitz, *J. Phys. Chem. B* **2003**, *107*(5), 1242–1250.
- [146] T. L. Stemmler, T. M. Sossong, J. I. Goldstein, D. E. Ash, T. E. Elgren, D. M. Kurtz, J. E. Penner-Hahn, *Biochemistry* **1997**, *36*(32), 9847–9858.
- [147] P. E. M. Siegbahn, *Theor. Chem. Acc.* **2001**, *105*, 197–206.
- [148] F. Haber, J. Weiss, *Proc. Roy. Soc. A* **1934**, *147*, 332–351.
- [149] M. L. Kremer, G. Stein, *Trans. Faraday Soc.* **1959**, *55*(6), 959–973.
- [150] L. Dubois, J. Pecaut, M. F. Charlot, C. Baffert, M. N. Collomb, A. Deronzier, J. M. Latour, *Chem. Eur. J.* **2008**, *14*(10), 3013–3025.
- [151] G. Berggren, P. Huang, L. Eriksson, S. Styring, M. F. Anderlund, A. Thapper, *Dalton Trans.* **2010**, *39*(45), 11035–11044.
- [152] Y. Nishida, T. Akamatsu, K. Tsuchiya, M. Sakamoto, *Polyhedron* **1994**, *13*(15-16), 2251–2254.
- [153] C. Palopoli, N. Bruzzo, C. Hureau, S. Ladeira, D. Murgida, S. Signorella, *Inorg. Chem.* **2011**, *50*(18), 8973–8983.
- [154] B. J. Day, *Biochem. Pharmacol.* **2009**, *77*(3), 285–296.
- [155] J. Weil, J. Bolton, *Electron Paramagnetic Resonance, Elementary Theory and Practical Application*, John Wiley & Sons Ltd, New York, **2007**.
- [156] T. Stich, S. Lahiri, G. Yeagle, M. Dicus, M. Brynda, A. Gunn, C. Aznar, V. DeRose, R. Britt, *Appl. Magn. Reson.* **2007**, *31*(1), 321–341.
- [157] K. A. Campbell, E. Yikilmaz, C. V. Grant, W. Gregor, A.-F. Miller, R. D. Britt, *J. Am. Chem. Soc.* **1999**, *121*(19), 4714–4715.
- [158] M. Zheng, S. V. Khangulov, G. C. Dismukes, V. V. Barynin, *Inorg. Chem.* **1994**, *33*(2), 382–387.

- [159] T. Weyhermüller, T. K. Paine, E. Bothe, E. Bill, P. Chaudhuri, *Inorg. Chim. Acta* **2002**, *337*, 344–356.
- [160] C. Duboc, M.-N. Collomb, *Chem. Commun.* **2009**, (19), 2715–2717.
- [161] C. Herrero, J. L. Hughes, A. Quaranta, N. Cox, A. W. Rutherford, W. Leibl, A. Aukauloo, *Chem. Commun.* **2010**, *46*(40), 7605–7607.
- [162] M. F. Anderlund, J. Höglblom, W. Shi, P. Huang, L. Eriksson, H. Weihe, S. Styring, B. Åkermark, R. Lomoth, A. Magnuson, *Eur. J. Inorg. Chem.* **2006**, *24*, 5033–5047.
- [163] P. Huang, P. Kurz, S. Styring, *Appl. Magn. Reson.* **2007**, *31*(1), 301–320.
- [164] C. Duboc, M.-N. Collomb, J. Pécaut, A. Deronzier, F. Neese, *Chem. Eur. J.* **2008**, *14*(21), 6498–6509.
- [165] J. P. McEvoy, G. W. Brudvig, *Chem. Rev.* **2006**, *11*(11), 4455–4483.
- [166] X. F. Yang, M. H. Baik, *J. Am. Chem. Soc.* **2008**, *130*(48), 16231–16240.
- [167] X. Li, G. Chen, S. Schinzel, P. E. M. Siegbahn, *Dalton Trans.* **2011**, *40*(42), 11296–11307.
- [168] G. C. Dismukes, R. Brimblecombe, G. A. N. Felton, R. S. Pryadun, J. E. Sheats, L. Spiccia, G. F. Swiegers, *Acc. Chem. Res.* **2009**, *42*(12), 1935–1943.
- [169] S. Nayak, H. P. Nayek, S. Dehnen, A. K. Powell, J. Reedijk, *Dalton Trans.* **2011**, *40*(12), 2699–2702.
- [170] J. S. Kanady, E. Y. Tsui, M. W. Day, T. Agapie, *Science* **2011**, *333*(6043), 733–736.
- [171] F. Bergaya, B. Thend, G. Lagaly, *Handbook of Clay Science I*, Elsevier, Oxford, Amsterdam, **2006**.
- [172] D.-F. Zhou, Q.-Y. Chen, Y. Qi, H.-J. Fu, Z. Li, K.-D. Zhao, J. Gao, *Inorg. Chem.* **2011**.
- [173] A. Viani, A. Gualtieri, G. Artioli, *Am. Mineral.* **2002**, *87*, 966–975.
- [174] C. W. Cady, R. H. Crabtree, G. W. Brudvig, *Coord. Chem. Rev.* **2008**, *252*(3-4), 444–455.
- [175] P. E. M. Siegbahn, *Acc. Chem. Res.* **2009**, *42*(12), 1871–1880.
- [176] H. Dau, P. Liebisch, M. Haumann, *Anal. Bioanal. Chem.* **2003**, *376*, 562–583.
- [177] M. Barra, M. Haumann, P. Loja, R. Krivanek, A. Grundmeier, H. Dau, *Biochemistry* **2006**, *45*(48), 14523–14532.

- [178] L. Hessel, C. Romers, *Recl. Trav. Chim. Pays-Bas* **1969**, 88(5), 545–552.
- [179] P. G. Wang, M. Xian, X. Tang, X. Wu, Z. Wen, T. Cai, A. J. Janczuk, *Chem. Rev.* **2002**, 102(4), 1091–1134.
- [180] C. Szabo, *Nat. Rev. Drug. Discov.* **2007**, 6(11), 917–935.
- [181] L. Wu, R. Wang, *Pharmacol. Rev.* **2005**, 57(4), 585–630.
- [182] P. R. Ortiz de Montellano, *Curr. Opin. Chem. Biol.* **2000**, 4(2), 221–227.
- [183] T. Matsui, M. Unno, M. Ikeda-Saito, *Acc. Chem. Res.* **2010**, 43(2), 240–7.
- [184] T. Matsui, M. Iwasaki, R. Sugiyama, M. Unno, M. Ikeda-Saito, *Inorg. Chem.* **2010**, 49(8), 3602–9.
- [185] R. Motterlini, J. E. Clark, R. Foresti, P. Sarathchandra, B. E. Mann, C. J. Green, *Circ. Res.* **2002**, 90(2), E17–24.
- [186] J. E. Clark, P. Naughton, S. Shurey, C. J. Green, T. R. Johnson, B. E. Mann, R. Foresti, R. Motterlini, *Circ. Res.* **2003**, 93(2), e2–8.
- [187] R. Motterlini, P. Sawle, J. Hammad, S. Bains, R. Alberto, R. Foresti, C. J. Green, *FASEB J.* **2005**, 19(2), 284–6.
- [188] C. R. Child, S. Kealey, H. Jones, P. W. Miller, A. J. P. White, A. D. Gee, N. J. Long, *Dalton Trans.* **2011**, 40(23), 6210–6215.
- [189] R. D. Rimmer, H. Richter, P. C. Ford, *Inorg. Chem.* **2010**, 49(3), 1180–1185.
- [190] C. S. Jackson, S. Schmitt, Q. P. Dou, J. J. Kodanko, *Inorg. Chem.* **2011**, 50(12), 5336–8.
- [191] P. C. Kunz, W. Huber, A. Rojas, U. Schatzschneider, B. Spingler, *Eur. J. Inorg. Chem.* **2009**, (35), 5358–5366.
- [192] H. Pfeiffer, A. Rojas, J. Niesel, U. Schatzschneider, *Dalton Trans.* **2009**, (22), 4292–4298.
- [193] K. Meister, J. Niesel, U. Schatzschneider, N. Metzler-Nolte, D. A. Schmidt, M. Havenith, *Angew. Chem. Int. Ed.* **2010**, 49(19), 3310–3312.
- [194] J. A. Calladine, S. B. Duckett, M. W. George, S. L. Matthews, R. N. Perutz, O. Torres, K. Q. Vuong, *J. Am. Chem. Soc.* **2011**, 133(7), 2303–10.
- [195] E. A. Karlsson, B.-L. Lee, T. Åkermark, E. V. Johnston, M. D. Kärkäs, J. Sun, O. Hansson, J.-E. Bäckvall, B. Åkermark, *Angew. Chem. Int. Ed.* **2011**, doi: 10.1002/anie.201104355.

Paper I.

A Manganese Oxido Complex
Bearing Facially Coordinating
Trispyridyl Ligands – Is
Coordination Geometry Crucial for
Water Oxidation Catalysis?

Cite this: DOI: 10.1039/c0xx00000x

www.rsc.org/xxxxxx

ARTICLE TYPE

A Manganese Oxido Complex Bearing Facially Coordinating Trispyridyl Ligands – Is Coordination Geometry Crucial for Water Oxidation Catalysis?

Hans-Martin Berends,^a Anne-Marie Manke,^a Christian Näther,^a Felix Tuczek^{*a} and Philipp Kurz^{*a}

⁵ Received (in XXX, XXX) Xth XXXXXXXXX 20XX, Accepted Xth XXXXXXXXX 20XX

DOI: 10.1039/b000000x

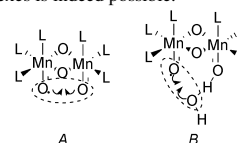
In this work the synthesis of the novel manganese complex $[\text{Mn}_2^{\text{III,III}}(\text{tpdm})_2(\mu\text{-O})(\mu\text{-OAc})_2]^{2+}$ (**1**) is reported containing two manganese centres ligated to the unusual, facially coordinating, all-pyridine ligand tpdm (tris(2-pyridyl)methane). The geometric and electronic properties of complex **1** were characterised by X-ray crystallography, vibrational (IR and Raman) and optical spectroscopy (UV/Vis and MCD). Cyclic voltammograms of **1** showed a quasireversible oxidation event at 950 mV and an irreversible reduction wave at -250 mV vs. Ag/Ag⁺. The redox behaviour of the compound was investigated in detail by UV/Vis- and X-band EPR- spectroelectrochemistry. Both electrochemical (+1 200 mV) and chemical (*t*BuOOH) oxidations transform **1** into the singly oxidized di- μ -oxido species $[\text{Mn}_2^{\text{III,IV}}(\text{tpdm})_2(\mu\text{-O})_2(\mu\text{-OAc})_2]^{2+}$. Further electrochemical oxidation at the same potential results in the removal of another electron to obtain the $\text{Mn}_2^{\text{IV,IV}}$ -form. The ability of compound **1** to evolve O₂ was studied using different oxidants. While reactions with hydrogen peroxide and peroxomonosulfate yield O₂, homogeneous water-oxidation using Ce^{IV} was not achieved. The oxidation reactions of **1** are nevertheless very interesting model processes for oxidation state (S-state) transitions of the natural manganese water-oxidation catalyst in photosynthesis. However, despite its favourable coordination geometry and multielectron redox chemistry, complex **1** fails to be a functional model for natural water-oxidation catalysis.

Introduction

A large number of dinuclear manganese complexes has been synthesised¹⁻⁶ to mimic the active sites of manganese containing redox enzymes like arginase⁷, manganese catalase⁸ or the oxygen-evolving-complex (OEC) of photosystem II.^{3, 9-14} Models for the latter two enzymes – both involved in the formation of molecular oxygen – have also been investigated in detail concerning their catalytic properties. These studies showed that it is possible to develop a variety of functional molecular Mn₂-mimics for the catalase reaction, *i.e.* dinuclear manganese complexes which are able to catalyse the disproportionation of H₂O₂ into O₂ and H₂O both at impressive rates and with high catalyst stability.^{2, 15, 16} There are also multiple examples where oxygen has been detected as the product of reactions of the oxido transferring, two-electron oxidation agents oxone (HSO₅⁻) and hypochlorite (OCl⁻) with manganese compounds, most prominent amongst them the very well-studied “Yale dimer” $[\text{Mn}_2^{\text{III,IV}}(\text{terpy})_2(\mu\text{-O})(\text{H}_2\text{O}_2)]^{3+}$ (**2**, *terpy* = 2,2':6',2''-terpyridine).¹⁷⁻²⁰

In contrast, no dimanganese complex is currently known which is able to catalyse water oxidation in a fashion similar to the OEC in reactions with one-electron oxidants like cerium(IV) or ruthenium(III) tris-bipyridyl. This is in marked contrast especially to coordination compounds of ruthenium, a metal diagonally

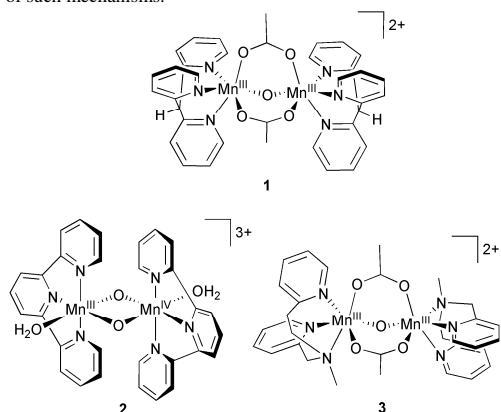
related to Mn within the periodic table. Here, a large number of recently discovered catalytically active di- and even mononuclear complexes indicate that, given the right ligand arrangement and metal centres, water oxidation catalysis in homogeneous solution by metal complexes is indeed possible.²¹⁻²⁶



Scheme 1 Possible mechanistic pathways of dioxygen formation by a dinuclear di- μ -oxido-metal complex. Both routes involve two parallel orientated, axial oxygen ligands to form the O–O bond. The manganese coordination sphere therefore would have to be completed by facial, oxidation stable ligands L.

It has been suggested that the geometrical arrangement of the metal centres might be of critical importance for water oxidation catalysis.²⁷ A number of scenarios see two neighbouring axial oxido- or oxyl ligands involved in the critical step of O–O bond formation. These oxygen-ligands are supposed to be coordinated to two μ -oxido-interconnected metal centres in high oxidation states.^{23, 27, 28} Two examples of such pathways are shown in Scheme 1 and involve either a direct coupling of the oxygen ligands or the nucleophilic attack by an activated aquo-species on

one of them to yield the O₂ product. There is evidence that both routes might indeed be important for oxygen formation catalysed by ruthenium complexes.^{23, 28} Additionally, theoretical calculations on water oxidation pathways support the feasibility of such mechanisms.²⁹⁻³²



Scheme 2 Schematic drawings of compounds **1**, **2** and **3**.

A great number of studies on the synthesis of manganese complexes has shown that dinuclear μ -oxido-manganese compounds readily form in the presence of water and in an oxidizing environment. Commonly, such complexes contain [Mn₂(μ -O)_n]-cores (n = 1 or 2) with manganese in its +III or +IV oxidation states.¹ If one aims to combine this very robust Mn₂-arrangement with the potentially catalytically active geometry outlined in Scheme 1, a facially coordinating, tridentate ligand has to be chosen. In this way it would be possible to complete the ligand sphere of the manganese centres without blocking the axial sites – and these sites might be crucial for water / oxido coordination and subsequent oxidation (Scheme 1).

With this coordination geometry in mind, we synthesized the novel dimanganese complex [Mn₂^{III,III}(tpdm)₂(μ -O)(μ -OAc)₂]²⁺ (**1**, Scheme 2), in which two manganese centres are coordinated to facially coordinating tris(2-pyridyl)methane (tpdm) ligands. An all-pyridine environment was chosen for two reasons: a) the detailed studies by Brudvig *et al.* of complex **2** proved that a pyridine environment provided high stability in water at the strongly oxidising conditions necessary for O₂ formation;³³ b) histidine ligands are coordinated to the manganese centres in both Mn-catalase⁸ and the OEC¹², so an aromatic N-donor system appeared to be a good choice for a biomimetic approach to Mn-catalysed dioxygen formation. Interestingly, none of the nearly 100 dinuclear manganese complexes recently reviewed in the context of OEC model chemistry¹ possesses such an all-pyridine, facial coordination environment. Instead, related ligands used in this context so far all contain aliphatic amine and / or alkoxy functionalities which are most likely not the best option considering oxidation stability.

An example for such a compound and closely related to **1** is the complex [Mn₂^{III,III}(pepmma)₂(μ -O)(μ -OAc)₂]²⁺ (**3**),³⁴ also shown in Scheme 2. Detailed electrochemical investigations on manganese compounds like **3** have been reported and clearly

showed that such species – like the OEC – are able to store multiple oxidation equivalents at high oxidation potentials (two electrons at ~+1 V vs. SCE in the case of **3**). Oxidation events are accompanied by ligand-exchange and deprotonation reactions to stabilize higher oxidation states.⁶ However, studies on the ability of these complexes to catalyse O₂ formation or eventually water-oxidation are very rare and for example unknown for complex **3**.

In the following, we first present the synthesis and detailed spectroscopic characterisation of the complex **1**, which might be considered as a facial analogue of the Yale dimer **2**. We then focus on the behaviour of **1** at oxidising conditions where we studied redox potentials, spectroscopic properties, ligand exchange phenomena and ultimately the ability of **1** to act as a catalyst for O₂ formation and water oxidation.

Experimental

General

Reagents and solvents were purchased commercially and used as received, except the following solvents which were distilled under argon over calcium hydride (acetonitrile), sodium (toluene) and lithium aluminium hydride (diethyl ether), respectively.

Caution: Perchlorate salts of metal complexes with organic ligands are potentially explosive! Therefore only small quantities of these compounds should be prepared and handled with caution.

Synthesis

The ligand tris(2-pyridyl)methane (tpdm) and its precursor bis(2-pyridyl)methane (Scheme 3) were prepared according to literature procedures starting from commercially available bis(2-pyridyl)ketone.^{35, 36}

Synthesis of **1**(ClO₄)₂

A solution of tpdm (0.22 mmol, 54 mg) in methanol (1 mL) was combined with a suspension of manganese(III)acetate monohydrate (0.20 mmol, 54 mg) in methanol (2 mL) under a nitrogen atmosphere at 0 °C and the resulting mixture was stirred for 1 h. After the dropwise addition of a solution of aqueous *tert*-butyl hydroperoxide (0.10 mmol, 12 μ L) in methanol (200 μ L) the solution was stirred for another 30 min. Solid sodium perchlorate hydrate (1.0 mmol, 140 mg) was then added and after 20 min the precipitate was filtered off, washed with a small amount of methanol and dried to give **1** as a reddish brown powder (57 mg, 60% yield). Crystals suitable for X-ray crystallography were obtained by slow diffusion of methyl *tert*-butyl ether into a solution of **1** in acetonitrile. IR (KBr) ν /cm⁻¹: 1604 (vs), 1573 (vs) (tpdm), 1563 (sh, μ -OAc), 1473 (s), 1442 (vs) (tpdm), 1416 (s, μ -OAc), 1092 (vs), 623 (s) (ClO₄). Analysis calcd (%) for C₃₆H₃₂Cl₂Mn₂N₆O₁₃: C 46.1, H 3.4, Mn 11.7, N 9.0. Found: C 45.6, H 3.0, Mn 12.3, N 8.9.

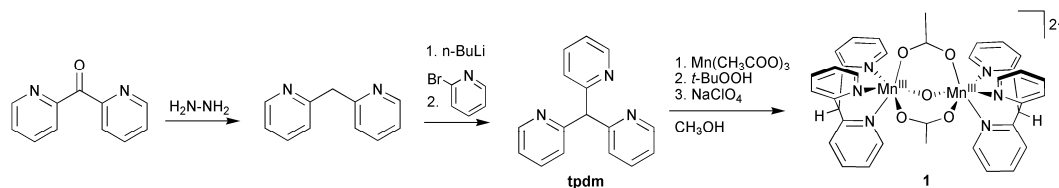
Crystallographic data collection and refinement of the structure of **1**(ClO₄)₂

A dark red crystal with approximate dimensions of 0.3 x 0.2 x 0.2 mm³ was selected. Intensity data was collected using a STOE imaging plate diffraction system (IPDS-1) with Mo K α radiation (Table 1). The structure was solved with direct methods using SHELXS-97, and refinement was performed against F₂ using SHELXL-97.³⁷ All non-hydrogen atoms were refined

anisotropically. The hydrogen atoms were positioned with idealized geometry and refined isotropic with $U_{\text{iso}}(\text{H}) = 1.2 \cdot U_{\text{eq}}(\text{C})$ (1.5 for methyl H atoms) using a riding model. This compound contains a small amount of solvent in cavities of the structure for which no reasonable structure model can be found. Therefore, the data were corrected using the SQUEEZE option in

Platon.³⁸

CCDC-????? contain the supplementary crystallographic data for this paper. These data can be obtained free of charge from the Cambridge Crystallographic Data Centre via <http://www.ccdc.cam.ac.uk/>.



Scheme 3 Synthesis of the ligand tpdm^{35,36} and compound **1**.

Table 1 Selected crystallographic data

Empirical formula	$\text{C}_{36}\text{H}_{32}\text{Cl}_2\text{Mn}_2\text{N}_6\text{O}_{13}$
Formula weight	937.46
Temperature	170(2) K
Wavelength	0.71073 Å
Crystal system	monoclinic
Space group	C2/c
a	21.315(2) Å
b	12.446(1) Å
c	20.061(2) Å
α	90°
β	121.76(1)°
γ	90°
Volume	4525.0(6) Å ³
Z	4
Density (calculated)	1.376 Mg/m ³
Absorption coefficient	0.740 mm ⁻¹
F(000)	1912
Crystal size	0.3 x 0.2 x 0.2 mm ³
Theta range for data collection	1.98 to 25.03°
Index ranges	-16<=h<=25, -14<=k<=14, -23<=l<=23
Reflections collected	10190
Independent reflections	3875 [R(int) = 0.0701]
Reflections with I>2σ(I)	2608
Completeness to theta = 25.03°	97.0 %
Refinement method	Full-matrix least-squares on F ²
Data / restraints / parameters	3875 / 0 / 269
Goodness-of-fit on F ²	0.944
Final R indices [I>2σ(I)]	R1 = 0.0533, wR2 = 0.1304
R indices (all data)	R1 = 0.0815, wR2 = 0.1411
Extinction coefficient	0.0036(4)
Largest diff. peak and hole	0.431 and -0.536 e.Å ⁻³

Physical measurements

Elemental analyses were performed with a Heraeus CHNS Elemental Analyzer. The manganese percentage was determined by atomic absorption measurements using an Analyst spectrometer system by Perkin Elmer. Prior to analysis, the sample was digested by dissolving it in concentrated nitric acid. FT-IR spectra were recorded in KBr pellets with a Mattson Genesis Type I spectrometer from 4000–40 cm⁻¹ with a resolution of 2 cm⁻¹. Resonance Raman spectra were recorded with a DILOR XY-multichannel Raman spectrometer with a triple monochromator and a CCD detector. Excitation wavelengths between 454.5 and 647.1 nm were generated by an

Ar⁺/Kr⁺ laser. The resolution was between 2.5 and 0.8 cm⁻¹ depending on the excitation wavelength. Raman intensities were calibrated relative to the 932 cm⁻¹ peak of ClO₄⁻. The direct-current magnetic susceptibilities of a powder sample of about 32 mg compound **1** were measured on a Quantum Design Magnetic Properties Measurement System (MPMS; Quantum Design). MCD spectra have been obtained in a propionitrile / butyronitrile glass which was placed between two quartz plates (Suprasil 1). MCD spectra were recorded using a setup³⁹ that consists of an Oxford SM4000 cryostat and a Jasco J810 CD spectropolarimeter. UV/Vis spectra were recorded with a Varian Cary 5000 spectrometer. UV/Vis spectroelectrochemical measurements were performed using an OTTE cell⁴⁰ with 1 mm path length and measured with an Analytik Jena Specord S100 spectrometer.

Cyclic voltammetry and bulk electrolysis

Cyclic voltammetry and chronoamperometry measurements were recorded with an EG&G PAR 273A galvanostat/potentiostat at room temperature. Sample solutions were prepared from dry acetonitrile containing 0.1 M tetrabutylammonium perchlorate (Fluka, electrochemical grade) as supporting electrolyte. The cell for cyclic voltammetry experiments consisted of a platinum button working electrode, a platinum rod counter electrode and a Ag/Ag⁺ reference (a silver wire immersed in 0.01 M AgNO₃ in acetonitrile, -87 mV vs. Fc/Fc⁺)⁴¹. For bulk electrolyses a platinum gauze served as working electrode and for UV/Vis spectroelectrochemical measurements a platinum net as working electrode was used. The counter electrode was in a compartment separated from the bulk solution by fritted disks. Before all measurements, oxygen was removed by bubbling solvent-saturated nitrogen through the stirred solutions. Samples were kept under nitrogen during measurements. To obtain EPR spectra of **1** in different oxidation states, solutions were subjected to bulk electrolyses at controlled potentials. After time intervals of two minutes, samples of 200 μL were taken from the electrolysis solution with an air-tight, nitrogen-filled syringe, transferred to nitrogen-flushed quartz EPR tubes, frozen and stored in liquid nitrogen prior to EPR measurements.

EPR spectroscopy

X-band (9 GHz) electron paramagnetic resonance spectra were collected using a Bruker EMXplus spectrometer equipped with a PremiumX microwave bridge and a dual mode cavity (Bruker ER-4116DM). For measurements at liquid helium temperatures an Oxford Instrument ESR 900 cryostat and ITC-4 temperature controller were installed. EPR spectra were analyzed with the Bruker Xenon 1.0 software package. Computer simulation of the EPR spectrum was performed using the XSophe computer simulation software suite (v 1.1.4)⁴² with the following expression for the spin Hamiltonian:

$$\hat{H} = \mu_B \hat{B} \tilde{g} \hat{S} + \hat{S} \tilde{A}_{Mn(III)} \hat{I}_{Mn(III)} + \hat{S} \tilde{A}_{Mn(IV)} \hat{I}_{Mn(IV)}$$

Chemical oxidation reactions

For chemical redox reactions, nitrogen-purged solutions of **1** in acetonitrile and *t*BuOOH were mixed at room temperature and after a reaction time of 4 min UV/Vis spectra were measured and samples of 200 μ L were filled into EPR tubes, frozen and stored in liquid nitrogen prior to EPR measurements.

Oxygen detection and oxygen evolution experiments

The polarographic signal of a standard Clark electrode (Rank Brothers Ltd.), separated from the sample solution by a 12.7 μ m thick teflon membrane, was recorded for the entire duration of the experiments at 1 s intervals using the SoftFox software package by Skantronnic. Air saturated water ($[O_2] = 253 \mu$ M,⁴³) was used for the calibration of the electrode. The volume of the solution at the beginning of each experiment was 900 μ L, thermostated inside the double walled measurement cell at 20 °C. The gas volume (ca. 200 μ L) above the sample solution was sealed from the atmosphere using a rubber septum. The cell was placed on top of a magnetic stirrer to continuously stir the solution using a teflon-coated stir bar.

For oxygen evolution experiments 0.94 mg (1 μ mol) of complex **1** were dissolved in 900 μ L water to reach a final concentration of 1 mM complex. These solutions were then transferred into the Clark cell and dissolved oxygen was removed by argon purging to reach residual oxygen concentrations of $[O_2] \leq 10 \mu$ M. After an equilibration time of 1 min, 100 μ L of degassed, freshly prepared oxidant (5 equivalents H_2O_2 , 7.5 equivalents oxone or 25 equivalents $(NH_4)_2[Ce(NO_3)_6]$, respectively) were injected into the cell. Oxygen evolution was followed for 10 min after injection and measured at least twice for each oxidant.

Results and discussion

Synthesis

The ligand tpdm was synthesised from bis(2-pyridyl)keton by a combination of published procedures via the intermediate bis(2-pyridyl)methane.^{35, 36} Compound **1** was then obtained by the reaction of the tpdm ligand with manganese(III) acetate in methanol (Scheme 3) and isolated as the perchlorate salt **1**(ClO₄)₂. It was interesting to note that the synthesis of **1** could not be achieved via an analogous route starting from Mn^{II}(OAc)₂ in the presence of excesses of different tested oxidation agents (*tert*-butyl hydroperoxide (*t*BuOOH), OCl⁻, H₂O₂ and HSO₅⁻ (oxone) were investigated as possibilities). One would expect that ligand exchange - and thus the coordination of the tpdm ligand - is much faster for the manganese(II) state in comparison to

manganese(III).⁴⁴ However, it has been reported that the trinuclear species $[Mn_3(\mu_3-O)(OAc)_6]^+$ is formed in solutions containing manganese(III) acetate and water (the Mn salt is dissolved as a hydrate).⁴⁵ Under our reaction conditions $[Mn_3(\mu_3-O)(OAc)_6]^+$ might thus serve as a precursor for the $(Mn_2(\mu-O)(OAc)_2)$ - core later found as part of complex **1**, making manganese(III) acetate the superior Mn starting material for this synthesis. Additionally, we found that the substoichiometric addition of the mild oxidant *t*BuOOH (0.5 equiv. per Mn) greatly enhanced both purity and yield of the obtained product. As Mn^{III} is quite a strong oxidation agent in solution, we suspect that after complexation by tpdm a part of the Mn^{III} is reduced to Mn^{II} in the presence of methanol at the early stages of the synthesis. The *t*BuOOH would then act as oxidation agent to bring these intermediately formed Mn^{II} species back to the Mn^{III} state found in complex **1**.

X-ray crystal structure

Red crystals of the Mn₂^{III,III} complex **1**(ClO₄)₂ were obtained by slow diffusion of methyl *tert*-butyl ether into a solution of compound **1**(ClO₄)₂ in acetonitrile. A view of the complex cation, which is located on a twofold rotation axis, is presented in Figure 1. The manganese centres have distorted octahedral coordination geometries and are bridged by two acetate groups and one oxygen atom. On each manganese ion a tpdm ligand is facially coordinated by its three pyridyl nitrogen donor atoms. A Mn-Mn distance of 3.172 Å and the Mn-O_{oxido}-Mn angle of 123.2 ° are both typical for mono(μ -oxido)-bis($\mu_{1,3}$ -acetato)bridged Mn₂^{III,III} complexes¹ (for further details see Table 1).

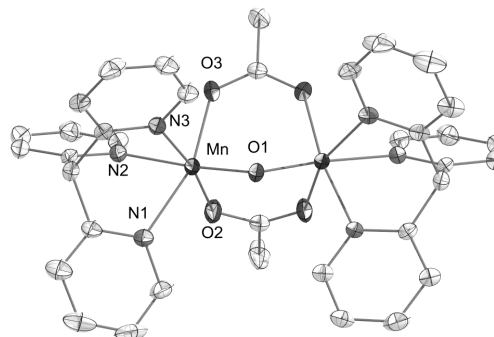


Fig 1. ORTEP presentation of the cation $[Mn_2^{III,III}(tpdm)_2(\mu-O)(\mu-OAc)_2]^{2+}$ (**1**). Hydrogen atoms and perchlorate counter ions are omitted for clarity. Thermal ellipsoids are drawn at the 50% level.

Table 1 Selected distances [Å] and angles [°] obtained from the crystal structure analysis for **1**.

Mn–O1	1.803(2)	Mn–N1	2.280(3)
Mn–O2	1.988(3)	Mn–N2	2.082(3)
Mn–O3	2.116(3)	Mn–N3	2.182(3)
Mn–Mn'	3.172(1)		
Mn–O1–Mn'	123.2(2)	O1–Mn–N3	90.3(2)
O1–Mn–N2	175.3(1)	N1–Mn–N2	80.8(2)
O2–Mn–N3	170.4(2)	O2–Mn–O3	95.8(2)

Vibrational spectroscopy

Compound **1**(ClO₄)₂ was studied by solid state IR and Raman spectroscopy (Fig. 2). The IR spectrum is dominated by strong signals from the tpdm (1604, 1573, 1473 and 1442 cm⁻¹) and acetate ligands (1563 and 1416 cm⁻¹) as well as the perchlorate counterions (1092 and 623 cm⁻¹). No bond vibration involving manganese could be assigned in the infrared. On the other hand, characteristic bands for Mn-O_{oxido} moieties can often be observed by Raman spectroscopy.⁴⁶ This is also the case here where a strong Raman peak found at 555 cm⁻¹ in the spectrum of **1** is found at a very typical frequency for the symmetric stretch vibration of bent dimanganese mono-μ-O cores.⁴⁷

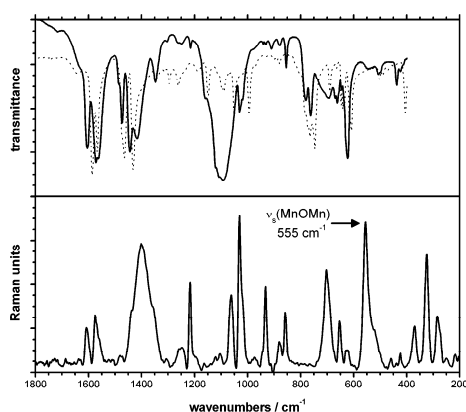


Fig. 2 Top: IR spectra of the free tpdm ligand (dotted line) and **1**(ClO₄)₂ (KBr pellets, room temperature). Bottom: Resonance Raman spectrum of compound **1**(ClO₄)₂. Experimental conditions: KCl pellets, excitation wavelength: 488 nm, T= 20 K (see ESI, Fig. SI 1, for resonance Raman spectra using other excitation wavelengths).

UV/Vis / MCD spectroscopy

A solution of **1** in acetonitrile is reddish brown. The corresponding UV/Vis absorption spectrum shows a band of small intensity at 13 500 cm⁻¹, a broad band between 16 000 and 22 000 cm⁻¹ and a rising slope to the UV region containing a shoulder ranging from about 23 000 to 28 000 cm⁻¹ (Figure 3, top).⁴⁸ A better resolution of the optical absorption bands can be reached if the technique of magnetic circular dichroism (MCD) spectroscopy is employed.⁴⁹⁻⁵¹ In MCD spectroscopy, the difference in absorption between left and right polarized light is measured for a sample placed in a magnetic field at cryogenic temperatures (see experimental section for details). The MCD spectrum of **1** in a propionitrile / butyronitrile glass at T = 2 K shows that the broad, featureless absorption band around 20 000 cm⁻¹ can be resolved into at least three MCD bands (Figure 3, bottom).

MCD spectra have been reported by Brunold *et al.* in 1998 for related complexes containing two Mn^{III} centres linked by a μ-oxido and two μ-acetato ligands, and also for manganese catalase in its oxidized Mn₂^{III,III}-state.⁴⁸ While the MCD spectra for the synthetic dimers with bpea, HB(pz)³⁻ and tppn ligands¹ are very similar to the MCD spectrum of **1**, the spectrum of the μ-oxido bis(μ-carboxylato) Mn(III) dimer with the Me₃tacn ligand¹ is somewhat different. For the latter system, however, detailed band assignments were presented on the basis of selection rules and

DFT calculations.⁵² Specifically, the optical absorption band at 13 500 cm⁻¹ (band I) was assigned to the ⁹A₁(z²) → ⁹B₂(yz) transition and the band at 20 000 cm⁻¹ (band II) to the ⁹A₁(z²) → ⁹A₁(xz) transition of the electronically coupled Mn(III)-Mn(III) system. While compound **1** does not exhibit ferro-, but antiferromagnetic coupling of the two Mn(III) centers (see ESI, Fig. SI 2-3 for further details), the orbital characters of the Me₃tacn electronic transitions certainly can be adapted to the former complex, meaning that the low-intensity band at 13500 (band I) can also be assigned to the z² → yz transition and the more intense band between 16000 and 22000 cm⁻¹ (band II) to the z² → xz transition of the coupled system. Assignment of these two lowest-energy bands to ligand field transition is supported by the fact that the resonance Raman excitation profile for the symmetric Mn—O—Mn stretching mode shows only minor enhancement below 20 000 cm⁻¹, but strongly increases in intensity at an excitation wavelength of 454.5 nm (22 000 cm⁻¹).

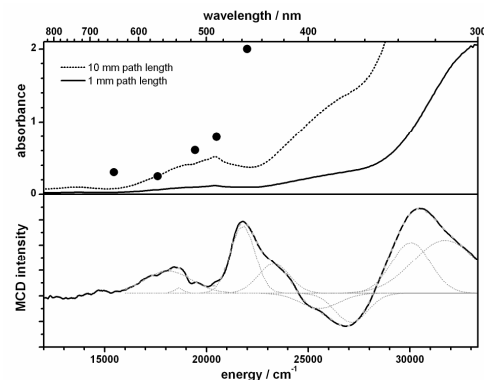


Fig. 3 Absorption and magnetic circular dichroism spectra of **1**. Top: UV/Vis absorption spectrum of **1** (2.5 mM) in acetonitrile at room temperature. The 20 K resonance Raman excitation profile for the symmetric Mn—O—Mn stretching mode (●) is superimposed. Bottom: MCD spectrum of **1** in a frozen propionitrile / butyronitrile glass at T = 2 K and a magnetic field of 2 T. Dotted lines show Gaussian fits for the absorption bands.

Electrochemistry

The redox behaviour of **1** in acetonitrile was investigated. The cyclic voltammogram (CV) of the complex (Fig. 4) showed a partially reversible oxidation process at 950 mV with a large peak split of 150 mV. At an even more positive potential of about 1 400 mV, a broad irreversible oxidation wave is observed. This process is not merely the oxidation of the ligand as tpdm oxidation does not occur at least up to a potential of 1 800 mV (see ESI Fig. SI 4). In the cathodic scan an irreversible reduction at -250 mV is found. The Mn compounds generated by reduction seem to be prone to reoxidation up to potentials of at least +750 mV, as no oxidation current was observed during the reverse sweep. The redox potentials of both the first oxidation and the first reduction processes observed here are within the typical range for [Mn₂^{III,III}(μ-O)(μ-OAc)₂] complexes.⁶ No significant changes on neither of the processes at -250 mV or 950 mV were observed when the scan rate was varied to up to 500 mV s⁻¹ (see ESI, Fig. SI 5).

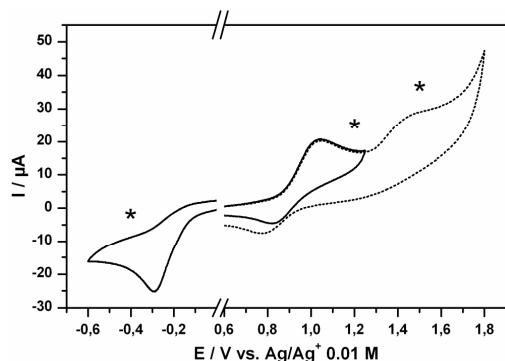


Fig. 4 Cyclic voltammogram of **1** in acetonitrile at room temperature. Reaction conditions: 1 mM **1** in acetonitrile containing 0.1 M TBAClO₄; scan rate: 100 mV s⁻¹. Potentials used for UV/Vis and EPR spectroelectrochemistry are marked by asterisks.

UV/Vis spectroelectrochemistry

To study changes in the absorption spectrum of the complex during oxidation and reduction processes, a 2.5 mM solution of **1** in acetonitrile was filled into an optically transparent thin layer electrochemical (OTTLE) cell.⁴⁰

As shown in Figure 5, the oxidation of the complex at a potential of +1 200 mV vs. Ag/Ag⁺ causes the decrease of the absorption band around 490 nm (20 400 cm⁻¹) and the appearance of a broad peak at 625 nm (16 000 cm⁻¹). The feature at 16 000 cm⁻¹ is characteristic for the μ-O → Mn^{IV} charge transfer band of a bis(μ-oxido)-bridged Mn₂^{III,IV} core.⁵³ An electrochemical re-reduction of this electrochemically generated species at a potential of ±0V resulted in the regeneration of the initial spectrum of **1** (see ESI, Fig. SI 6). This indicates that, despite the incomplete reversibility found in the CV, an oxidation-reduction cycle within the OTTLE cell, which takes much longer (several minutes), allows the re-generation of **1** from its oxidized form. Interestingly, the development of the μ-O → Mn^{IV} charge transfer band at 16 000 cm⁻¹ could also be observed for the chemical oxidation of **1** by 10 equiv. of *tert*-butyl hydroperoxide (*t*BuOOH) in acetonitrile (ESI, Fig. SI 7). The same oxidation product therefore seems to be accessible by both electrochemical and chemical oxidation.

The electrochemical reduction of **1** in the OTTLE cell resulted in a slow and small decrease in absorbance in the entire visible section of the spectrum, thus not yielding any information on the formed species (ESI, Fig. SI 8). As in the case of the oxidation of the complex, a re-oxidation at +500 mV over an extended time period re-generated the spectrum of **1**, despite the fact that a completely irreversible reduction event had been detected by CV.

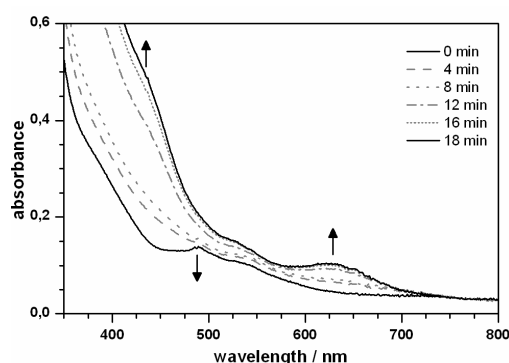


Fig. 5 Changes observed for absorption spectra of **1** (2.5 mM in acetonitrile / 0.1 M TBAClO₄) in an OTTLE cell (1mm path length) recorded during the electrochemical oxidation of the complex at a potential of +1 200 mV vs. Ag/Ag⁺.

EPR spectroscopy

Electron paramagnetic resonance (EPR) spectroscopy is a very powerful analytical method in manganese chemistry. It allows the qualitative and quantitative analysis of Mn oxidation states, nuclearity and in some cases even geometry of manganese complexes.^{16, 54-56} No EPR signal is detected for a frozen solution of complex **1** in acetonitrile at 5 K (Figure 6, solid line). This is expected for antiferromagnetically coupled Mn₂^{III,III} systems, which are often EPR silent, but this depends on the anisotropies of their zero field splittings.⁵⁵

To measure EPR spectra of the products obtained by oxidation of complex **1**, we carried out bulk electrolyses of **1** in acetonitrile at the same potentials as probed before by UV/Vis-spectroelectrochemistry. After different electrolysis times samples were taken from such solutions, immediately frozen and then analysed by EPR.

For the oxidation at +1 200 mV, a 16-line EPR signal, centred at $g = 2$, appears in the early phase of the electrolysis and reaches its maximum after about 4 min of electrolysis time (Figure 6, dotted line). This signal has a total signal width of 1 210 G, which clearly identifies the electrolysis product as a Mn₂^{III,IV} species.⁵⁷ A simulation of the EPR spectrum yields typical g and A values for a bis(μ-oxido)-mono(μ-acetato)bridged Mn₂^{III,IV} complex,⁵⁴ which are listed in Table 2 (see ESI, Table SI 1, for simulation details). If the oxidative electrolysis is carried out longer, the Mn₂^{III,IV}- signal decreases again as shown in Figure 6 for reaction times of 8 min (dashed dark grey line) and 12 min (grey line). An oxidation at +1 450 mV (and thus at a potential of the second oxidation event identified by CV, Figure 4) for 8 min produces species which give rise to a small Mn₂^{III,IV} EPR signal accompanied by a six-line spectrum characteristic for mononuclear Mn^{II} (ESI, Fig. SI 9).

Similar to the UV/Vis results, EPR also identifies the same reaction product for both electrochemical and chemical oxidations of **1**. If *t*BuOOH is added stepwise to a solution of **1** in acetonitrile, the same 16-line Mn₂^{III,IV}- EPR- signal is observed as had been found during electrochemical experiments (ESI, Fig. SI 10 and Table SI 2 for simulation parameters). Quantifications of the 16-line- signal allowed us to compare the amount of

[Mn₂^{III,IV}(μ-O)₂]- species formed for each reaction conditions. We find that in comparison to the concentration determined for the electrochemical oxidation, the chemical oxidation of **1** with 100 equiv. of *t*BuOOH yields only 80 % Mn₂^{III,IV} species after a reaction time of 4 min. But in contrast to the electrochemical oxidation no decrease of the signal in size is observed for *t*BuOOH-oxidations carried out over longer reaction times with a large excess of oxidation agent.

Interestingly, for EPR samples obtained after an electrochemical reduction of **1** at -400 mV a small 16-line signal was detected as well, with a slightly larger peak split in comparison to the one detected after electrochemical oxidation (total signal width 1230 G) and of a relative size corresponding to a Mn₂^{III,IV}- concentration of 15 % (ESI Figure SI 11). Such spectra also showed a marginal underlying six-line signal. The fact that an oxidized form of **1** is detected at reducing conditions indicates that the reduction of the complex apparently causes a complicated series of events. It does not only involve the reduction and decomposition of **1** to mononuclear Mn^{II}- species but also disproportionation steps generating significant amounts of the single-electron oxidized form of the compound. Attempts to identify mononuclear Mn^{III}-species by parallel-mode EPR spectroscopy⁵⁸ failed in all cases.

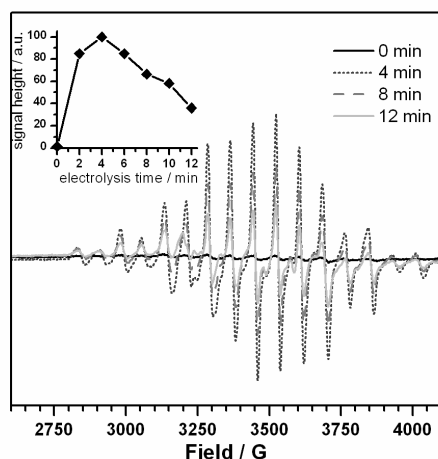


Fig. 6 X-band EPR spectra recorded after the electrochemical oxidation of complex **1** at a potential of +1200 mV vs. Ag/Ag⁺. Recording conditions: Microwave frequency: 9.644 GHz, microwave power: 63 μW; modulation amplitude 4 G, temperature 5 K.

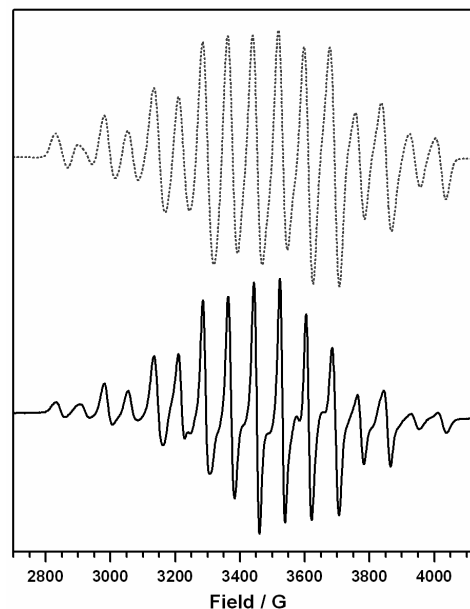


Fig. 7 Experimental (solid line) and simulated (dotted line) X-band EPR spectra for **1** oxidized electrochemically at 1200 mV vs. Ag/Ag⁺ for 4 min.

Table 2 EPR parameters for the Mn₂^{III,IV} form of **1** obtained by electrochemical oxidation as determined by a simulation of the signal using the X Sophe software suite. Hyperfine coupling constants A are given in gauss.

	g	A _{Mn(III)}	A _{Mn(IV)}
x	2.004	-169	72
y	1.998	-150	83
z	1.985	-108	80

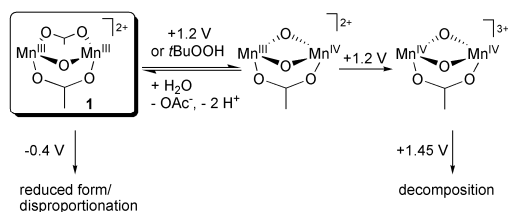
Redox reaction pathways of complex **1**

Taking together the electrochemical and spectroscopic results on redox events of complex **1** presented so far, we propose that a number of electron-transfer and ligand exchange reactions occur, as summarized in Scheme 4. Under reducing conditions, no stable reduced reaction product retaining a Mn₂-core could be identified. We thus conclude that potentially formed Mn₂^{II,III}- or Mn₂^{II,II}- intermediates are unstable (both would show characteristic EPR-signals⁵⁵) and immediately react further to yield mononuclear Mn^{II}- decomposition and/or Mn₂^{III,IV}-disproportionation products.

On the - for our purposes much more important - oxidative side, we detect that two single-electron oxidation processes for complex **1** occur, both at ~+1V and thus at an interesting potential in the context of water-oxidation. Following the first oxidation, a [Mn₂^{III,IV}(μ-O)₂]- complex is formed first by ligand-exchange, as an acetate is replaced by a bridging oxido-ligand. In this way charge compensation occurs and it is possible to oxidize the [Mn₂^{III,IV}(μ-O)₂]- compound once more at ~+1V to its

$\text{Mn}_2^{\text{IV,IV}}$ -form.

Preceding the actual water-oxidation step, the Mn_4Ca -cluster of the natural photosystem accumulates oxidation equivalents as it reaches different oxidized forms commonly known as S-states. Current mechanistic proposals for the individual S-state transitions still differ in many details but it seems clear that the following essential events occur:⁵⁹⁻⁶¹ i) metal centred oxidations from Mn^{III} to Mn^{IV} at potentials $>+0.8\text{ V}$; ii) deprotonations of water / hydroxide coordinated to manganese and iii) the formation of additional μ -oxido bridges between manganese centres (as a consequence of i) and ii)). All these three types of processes are observed here for the oxidation of **1** as it undergoes the two single-electron oxidation steps towards the $\text{Mn}_2^{\text{IV,IV}}$ form of the complex. The two proton- and ligand-exchange-coupled oxidation processes linking the $\text{Mn}_2^{\text{III,III}}$ and $\text{Mn}_2^{\text{IV,IV}}$ states of **1** thus represent a good model system for key events taking place during S-state transitions of the OEC.



Scheme 4 Redox and ligand exchange processes of **1** identified by (spectro)electrochemistry.

Oxygen evolving reactions

As stated in the introduction, we synthesised compound **1** not only with the intent of preparing a *structural* but also a potentially *functional* model for manganese metalloenzymes, especially hoping to reach OEC-like water-oxidation reactivity due to the unusual manganese coordination geometry imposed by the facial tris-pyridyl environment of the tpdm ligand. In order to investigate at which conditions **1** is able to catalyse the formation of dioxygen, anaerobic aqueous solutions of the complex were filled into the measurement cell of an O_2 -sensitive Clark type electrode and small volumes of degassed solutions of either hydrogen peroxide (H_2O_2), peroxomonosulfate (HSO_5^- , oxone) or $(\text{NH}_4)_2[\text{Ce}(\text{NO}_3)_6]$ (Ce^{IV}) were added. The concentration of dioxygen in the solution was then monitored for the duration of up to 10 min after oxidant addition. Hydrogen peroxide and oxone were chosen as strong oxygen-donating oxidants. In contrast, Ce^{IV} is a non-oxygen-donating, single-electron oxidant and its reactions with potential catalysts are commonly used as test systems for water oxidation catalysis.²¹

Typical traces of O_2 concentrations in solution for reactions of **1** with the three different oxidation agents are shown in Figure 7. Oxygen evolution was observed for reactions with all three oxidants, but the rates of evolved oxygen are very different depending on the oxidant used. Complex **1** is an excellent catalyst for the catalase reaction generating an O_2 -saturated solution within seconds after the addition of H_2O_2 . Such behaviour has already been found for many dinuclear μ -oxido manganese complexes and did thus not come as a surprise.¹⁹ Similarly, a number of Mn_2 -complexes are known to be able to generate

dioxygen in reactions with oxone⁶² and **1** is clearly another example for this type of oxygen evolving catalysts. The rates of O_2 -formation detected here for H_2O_2 - or oxone-reactions are well within the range found during recent screenings of various other Mn_2 -compounds.^{19, 63}

The formation of a small amount of O_2 was also observed after the addition of Ce^{IV} to solutions of **1**. However, we cannot take this as proof that **1** is able to catalyse the oxidation of water as a molecular catalyst. The rate of O_2 -formation is very slow and additionally a precipitate of brown manganese oxide formed immediately after the oxidant was added (unlike in the cases of H_2O_2 or oxone). As such manganese oxide precipitates are known to catalyse water-oxidation^{64, 65} they are most likely responsible for the small catalytic activity observed here for reactions with Ce^{IV} .

We thus unfortunately have to conclude that despite the altered coordination geometry, the catalytic performance of **1** in oxygen-evolving reactions follows a by now quite established pattern: many dinuclear, μ -oxido manganese complexes with stable oxidation states of $\geq \text{Mn}_2^{\text{III,III}}$ are able to act as efficient catalase mimics and yield O_2 in reactions with oxone, but homogeneous water-oxidation catalysis cannot be achieved. Work by us and others using ^{18}O -isotope labelling¹⁷ clearly showed that these three types of reactions occur via completely different reaction routes, presented in detail in a recent publication.⁶⁶ It is therefore understandable how the same complex (like **1** here) showing good O_2 -formation performance with peroxides might be completely inactive when used for water-oxidation catalysis.

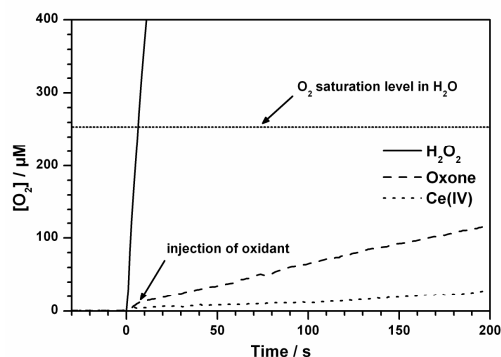


Fig. 7 Traces of oxygen evolution for the reactions of complex **1** with hydrogen peroxide, oxone and $(\text{NH}_4)_2[\text{Ce}(\text{NO}_3)_6]$ (Ce^{IV}), respectively.

Conclusions

We were able to synthesise a new dinuclear manganese complex $[\text{Mn}_2^{\text{III,III}}(\text{tpdm})_2(\mu\text{-O})(\mu\text{-OAc})_2]^{2+}$ (**1**) with Mn coordinated to the unusual, facially-coordinating and oxidation stable ligand tris(2-pyridyl)methane (tpdm). The molecular and electronic structure of the compound were investigated by crystallographic and extensive spectroscopic methods and establish **1** as a typical representative of the $[\text{Mn}_2(\mu\text{-O})(\mu\text{-OAc})_2]$ -family of manganese complexes.¹

A bis- μ -oxido $\text{Mn}_2^{\text{III,IV}}$ form of the compound could then be obtained at oxidising conditions via ligand exchange. A second

electron can be removed from this $\text{Mn}_2^{\text{III,IV}}$ species at an oxidation potential of +1.2 V vs. Ag/Ag^+ to reach a $\text{Mn}_2^{\text{IV,IV}}$ oxidation state. Thus, **1** shows charge-compensated, proton-coupled two-electron oxidation chemistry at potentials high enough to make even water-oxidation thermodynamically feasible. Additionally, the facially coordinating tpdm-ligands together with the $[\text{Mn}_2(\mu\text{-O})_2]$ -core allow for a reaction geometry identified as favourable for water-oxidation by mechanistic considerations (Scheme 1). Nevertheless, we find that the complex is no homogeneous water-oxidation catalyst. On the other hand, reactions of **1** with the strong peroxo oxidation agents H_2O_2 or oxone yield O_2 , demonstrating that $[\text{Mn}_2^{\text{III,III}}(\text{tpdm})_2(\mu\text{-O})(\mu\text{-OAc})_2]^{2+}$ is able to act as a functional mimic for the enzyme catalase.

Thus, to address the question raised in the title of this article, we take the results as strong indication that it is at least not primarily the coordination geometry that prohibits manganese catalysed water-oxidation in the case of complex **1** and similar Mn_2 -species. Rather, the ability to store four oxidation equivalents at potentials $>+1\text{V}$ seems to be the crucial requirement which complex **1** and all other synthetic manganese coordination compounds prepared so far do not meet. On the other hand, catalase-like reactivity only requires that a compound manages $2e^-$ -events at high potentials,⁶⁶ which explains why the title compound acts as efficient catalyst for the disproportionation of H_2O_2 .

A possible strategy to make four-electron chemistry possible is the formation of tetranuclear manganese species from the combination of two Mn_2 -complexes like **1** – **3**. Solid supports, especially clay minerals, have emerged as suitable platforms for the formation and stabilization of Mn-aggregates of higher manganese nuclearity.^{63, 67-69} We recently studied the adsorption of complex **1** on montmorillonite clay and detected that $\text{Mn}_{>2}$ -units form on the clay's surface.⁶⁹ Most importantly, our results showed that such clay hybrids of **1** are indeed active catalysts for water oxidation. We also found that very different multinuclear complexes with manganese oxidation states $\geq +\text{III}$ could be adsorbed to obtain catalytically active hybrids. Therefore the approach to increase the number of interacting manganese centres to ≥ 3 seems to be the strategy to follow in manganese-catalysed water oxidation.

Returning to the title question we would thus offer this modified answer: if one aims to develop a molecular, manganese-based water-oxidation catalyst, we think that the central requirement of four-electron redox chemistry has to be mastered first - only then an advantageous molecular geometry might come into play.

Acknowledgements

The authors thank Anne Westphal, Ursula Cornelissen, Stefanie Pehlke and Monika Schneeweiß (all CAU Kiel) for experimental support. This work was generously funded by the federal state of Schleswig-Holstein and the Fonds der Chemischen Industrie (Liebig fellowship of Ph.K.).

Notes and references

^a Institut für Anorganische Chemie, Christian-Albrechts-Universität zu Kiel, Max-Eyth-Str. 2, 24118 Kiel, Germany. E-mail: ftuczek@ac.uni-kiel.de, phkurz@ac.uni-kiel.de; Fax: (+49) 431 880 1520; Tel: (+49) 431 880 1410, (+49) 431 880 5817

[†] Electronic Supplementary Information (ESI) available: Resonance raman spectra with different excitation wavelength, cyclic voltammogram of **1** at different scan rates, UV/Vis OTTL spectra of electrochemical reduction at 500 mV after oxidation at 1 200 mV, UV/Vis spectra after oxidation with *t*BuOOH, UV/Vis OTTL spectra of electrochemical reduction at -500 mV, X-Sophe EPR simulation output file, EPR parameters for the simulation of the chemical oxidation of **1** with *t*BuOOH, EPR spectra after bulk electrolysis at 1 450 mV, EPR spectra of the chemical oxidation of **1** with *t*BuOOH, EPR spectra after bulk electrolysis at -400 mV, cyclic voltammogram of the ligand tpdm, magnetic data of **1**. See DOI: 10.1039/b000000x/

1. S. Mukhopadhyay, S. K. Mandal, S. Bhaduri and W. H. Armstrong, *Chem. Rev.*, 2004, **104**, 3981-4026.
2. A. J. Wu, J. E. Penner-Hahn and V. L. Pecoraro, *Chem. Rev.*, 2004, **104**, 903-938.
3. C. W. Cady, R. H. Crabtree and G. W. Brudvig, *Coord. Chem. Rev.*, 2008, **252**, 444-455.
4. C. Herrero, B. Lassalle-Kaiser, W. Leibl, A. W. Rutherford and A. Aukauloo, *Coord. Chem. Rev.*, 2008, **252**, 456-468.
5. C. S. Mullins and V. L. Pecoraro, *Coord. Chem. Rev.*, 2008, **252**, 416-443.
6. M. N. Collomb and A. Deronzier, *Eur. J. Inorg. Chem.*, 2009, 2025-2046.
7. D. W. Christianson, *Acc. Chem. Res.*, 2005, **38**, 191-201.
8. V. V. Barynin, M. M. Whittaker, S. V. Antonyuk, V. S. Lamzin, P. M. Harrison, P. J. Artymiuk and J. W. Whittaker, *Structure*, 2001, **9**, 725-738.
9. B. Loll, J. Kern, W. Saenger, A. Zouni and J. Biesiadka, *Nature*, 2005, **438**, 1040-1044.
10. J. Yano, J. Kern, K. Sauer, M. J. Latimer, Y. Pushkar, J. Biesiadka, B. Loll, W. Saenger, J. Messinger, A. Zouni and V. K. Yachandra, *Science*, 2006, **314**, 821-825.
11. W. Lubitz, E. J. Reijerse and J. Messinger, *Energy Environ. Sci.*, 2008, **1**, 15-31.
12. J. Barber, *Chem. Soc. Rev.*, 2009, **38**, 185-196.
13. K. Kawakami, Y. Umena, N. Kamiya and J.-R. Shen, *J. Photochem. Photobiol. B: Biol.*, 2011, **104**, 9-18.
14. Y. Umena, K. Kawakami, J.-R. Shen and N. Kamiya, *Nature*, 2011, **473**, 55-60.
15. A. E. M. Boelrijk and G. C. Dismukes, *Inorg. Chem.*, 2000, **39**, 3020-3028.
16. L. Dubois, J. Pecaot, M. F. Charlot, C. Baffert, M. N. Collomb, A. Deronzier and J. M. Latour, *Chem. Eur. J.*, 2008, **14**, 3013-3025.
17. J. Limburg, J. S. Vrettos, H. Y. Chen, J. C. de Paula, R. H. Crabtree and G. W. Brudvig, *J. Am. Chem. Soc.*, 2001, **123**, 423-430.
18. H. Y. Chen, R. Tagore, S. Das, C. Incarvito, J. W. Faller, R. H. Crabtree and G. W. Brudvig, *Inorg. Chem.*, 2005, **44**, 7661-7670.
19. P. Kurz, G. Berggren, M. F. Anderlund and S. Styring, *Dalton Trans.*, 2007, 4258-4261.
20. G. Berggren, A. Thapper, P. Huang, P. Kurz, L. Eriksson, S. Styring and M. F. Anderlund, *Dalton Trans.*, 2009, 10044-10054.
21. J. K. Hurst, *Coord. Chem. Rev.*, 2005, **249**, 313-328.

22. J. D. Blakemore, N. D. Schley, D. Balcells, J. F. Hull, G. W. Olack, C. D. Incarvito, O. Eisenstein, G. W. Brudvig and R. H. Crabtree, *J. Am. Chem. Soc.*, 2010, **132**, 16017-16029.
23. J. J. Concepcion, M. K. Tsai, J. T. Muckerman and T. J. Meyer, *J. Am. Chem. Soc.*, 2010, **132**, 1545-1557.
24. W. C. Ellis, N. D. McDaniel, S. Bernhard and T. J. Collins, *J. Am. Chem. Soc.*, 2010, **132**, 10990-10991.
25. D. G. H. Hetterscheid and J. N. H. Reek, *Chem. Commun.*, 2011, **47**, 2712-2714.
26. S. Roeser, P. Farràs, F. Bozoglian, M. Martínez-Belmonte, J. Benet-Buchholz and A. Llobet, *ChemSuschem*, 2011, **4**, 197-207.
27. T. A. Betley, Q. Wu, T. Van Voorhis and D. G. Nocera, *Inorg. Chem.*, 2008, **47**, 1849-1861.
28. S. Romain, L. Vigara and A. Llobet, *Acc. Chem. Res.*, 2009, **42**, 1944-1953.
29. X. Yang and M.-H. Baik, *J. Am. Chem. Soc.*, 2006, **128**, 7476-7485.
30. X. F. Yang and M. H. Baik, *J. Am. Chem. Soc.*, 2008, **130**, 16231-16240.
31. L.-P. Wang, Q. Wu and T. Van Voorhis, *Inorg. Chem.*, 2010, **49**, 4543-4553.
32. R. Bianco, P. J. Hay and J. T. Hynes, *J. Phys. Chem. A*, 2011, **115**, 8003-8016.
33. H. Y. Chen, R. Tagore, G. Olack, J. S. Vrettos, T. C. Weng, J. Penner-Hahn, R. H. Crabtree and G. W. Brudvig, *Inorg. Chem.*, 2007, **46**, 34-43.
34. T. K. Lal and R. Mukherjee, *Inorg. Chem.*, 1998, **37**, 2373-2382.
35. A. J. Canty and N. J. Minchin, *Aust. J. Chem.*, 1986, **39**, 1063-1069.
36. F. R. Keene, M. R. Snow, P. J. Stephenson and E. R. T. Tiekink, *Inorg. Chem.*, 1988, **27**, 2040-2045.
37. G. M. Sheldrick, *Acta Cryst. A*, 2008, **64**, 112-122.
38. A. L. Spek, *J. Appl. Cryst.*, 2003, **36**, 7-13.
39. F. Paulat and N. Lehnert, *Inorg. Chem.*, 2008, **47**, 4963-4976.
40. W. Kaim and A. Klein, *Spectroelectrochemistry*, Royal Society of Chemistry, London, 2008.
41. A. W. Addison and V. V. Pavlishchuk, *Inorg. Chim. Acta*, 2000, **298**, 97-102.
42. G. R. Hanson, K. E. Gates, C. J. Noble, M. Griffin, A. Mitchell and S. Benson, *J. Inorg. Biochem.*, 2004, **98**, 903-916.
43. G. A. Truesdale and A. L. Downing, *Nature*, 1954, **173**, 1236.
44. L. Helm and A. E. Merbach, *Chem. Rev.*, 2005, **105**, 1923-1960.
45. L. W. Hessel and C. Romers, *Recl. Trav. Chim. Pays-Bas*, 1969, **88**, 545-552.
46. A. Cua, J. S. Vrettos, J. C. De Paula, G. W. Brudvig and D. F. Bocian, *J. Biol. Inorg. Chem.*, 2003, **8**, 439-451.
47. B. C. Dave and R. S. Czernuszewicz, *Inorg. Chim. Acta*, 1998, **281**, 25-35.
48. T. C. Brunold, D. R. Gamelin, T. L. Stemmler, S. K. Mandal, W. H. Armstrong, J. E. Penner-Hahn and E. I. Solomon, *J. Am. Chem. Soc.*, 1998, **120**, 8724-8738.
49. J. A. Larrabee, S.-A. Chyun and A. S. Volwiler, *Inorg. Chem.*, 2008, **47**, 10499-10508.
50. S. Piligkos, L. D. Slep, T. Weyhermüller, P. Chaudhuri, E. Bill and F. Neese, *Coord. Chem. Rev.*, 2009, **253**, 2352-2362.
51. R. A. Geiger, S. Chattopadhyay, V. W. Day and T. A. Jackson, *J. Am. Chem. Soc.*, 2010, **132**, 2821-2831.
52. T. C. Brunold, D. R. Gamelin and E. I. Solomon, *J. Am. Chem. Soc.*, 2000, **122**, 8511-8523.
53. D. R. Gamelin, M. L. Kirk, T. L. Stemmler, S. Pal, W. H. Armstrong, J. E. Pennerhahn and E. I. Solomon, *J. Am. Chem. Soc.*, 1994, **116**, 2392-2399.
54. K. O. Schäfer, R. Bittl, F. Lendzian, V. Barynin, T. Weyhermüller, K. Wieghardt and W. Lubitz, *J. Phys. Chem. B*, 2003, **107**, 1242-1250.
55. P. Huang, P. Kurz and S. Styring, *Appl. Magn. Reson.*, 2007, **31**, 301-320.
56. T. A. Stich, J. W. Whittaker and R. D. Britt, *J. Phys. Chem. B*, 2010, **114**, 14178-14188.
57. C. Hureau, L. Sabater, E. Anxolabehere-Mallart, M. Nierlich, M. F. Charlot, F. Gonnet, E. Riviere and G. Blondin, *Chem. Eur. J.*, 2004, **10**, 1998-2010.
58. K. A. Campbell, E. Yikilmaz, C. V. Grant, W. Gregor, A.-F. Miller and R. D. Britt, *J. Am. Chem. Soc.*, 1999, **121**, 4714-4715.
59. J. P. McEvoy and G. W. Brudvig, *Chem. Rev.*, 2006, **106**, 4455-4483.
60. P. E. M. Siegbahn, *Acc. Chem. Res.*, 2009, **42**, 1871-1880.
61. H. Dau, C. Limberg, T. Reier, M. Risch, S. Roggan and P. Strasser, *ChemCatChem*, 2010, **2**, 724-761.
62. K. Beckmann, H. Uchtenhagen, G. Berggren, M. F. Anderlund, A. Thapper, J. Messinger, S. Styring and P. Kurz, *Energy Environ. Sci.*, 2008, **1**, 668-676.
63. P. Kurz, *Dalton Trans.*, 2009, 6103-6108.
64. A. Harriman, I. J. Pickering, J. M. Thomas and P. A. Christensen, *J. Chem. Soc. Faraday Trans. 1*, 1988, **84**, 2795-2806.
65. M. M. Najafpour, T. Ehrenberg, M. Wiechen and P. Kurz, *Angew. Chem. Int. Ed.*, 2010, **49**, 2233-2237.
66. D. Shevela, S. Koroidov, M. M. Najafpour, J. Messinger and P. Kurz, *Chem. Eur. J.*, 2011, **17**, 5415-5423.
67. M. Yagi, K. Narita, S. Maruyama, K. Sone, T. Kuwabara and K. Shimizu, *Bba-Bioenergetics*, 2007, **1767**, 660-665.
68. M. Yagi and K. Narita, *J. Am. Chem. Soc.*, 2004, **126**, 8084-8085.
69. H.-M. Berends, T. Homburg, I. Kunz and P. Kurz, *Appl. Clay Sci.*, 2011, **53**, 174-180.

Electronic Supplementary Information

A Manganese Oxido Complex Bearing Facially Coordinating Trispyridyl Ligands – Is
Coordination Geometry Crucial for Water Oxidation Catalysis?

Hans-Martin Berends,^a Anne-Marie Manke,^a Christian Näther,^a Felix Tucek^{*a} and Philipp
Kurz^{*a}

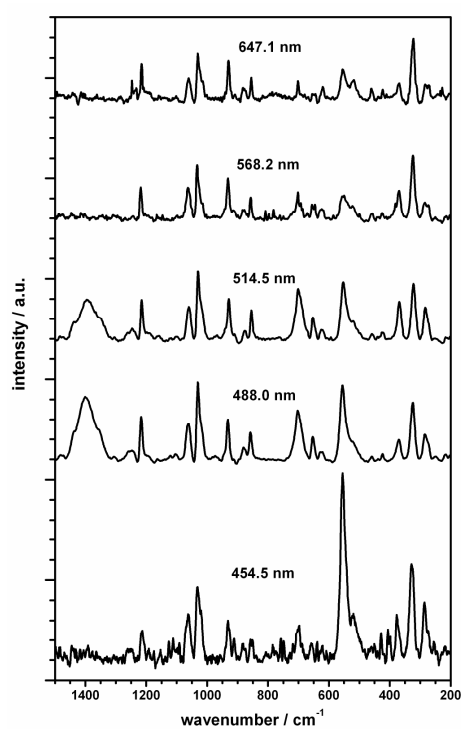


Fig. SI 1 Resonance Raman spectra recorded with different excitation wavelengths.

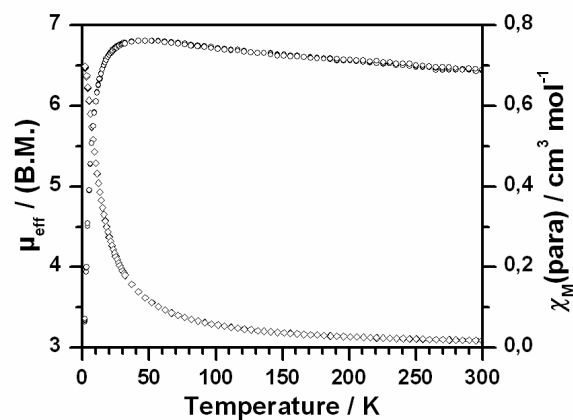


Fig. SI 2 Plots of magnetic susceptibility and effective magnetic moment per dinuclear complex versus temperature at $H = 3$ T for a polycrystalline sample of complex **1**.

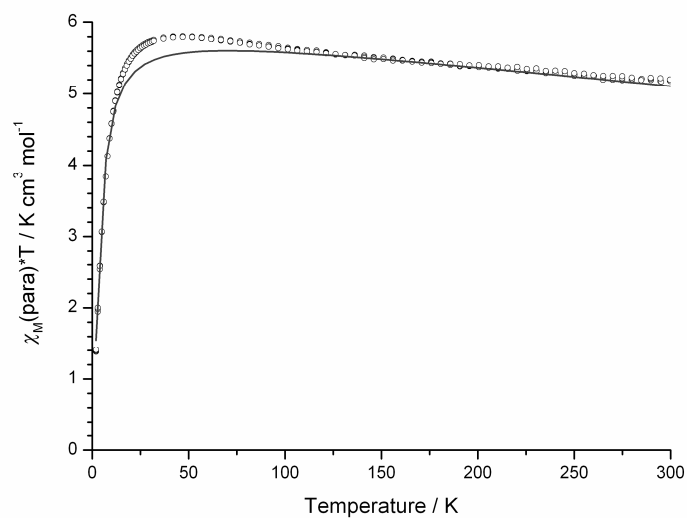


Fig. SI 3 Plot of $\chi_M T$ vs. T at $H = 3$ T for a polycrystalline sample of complex **1**. The solid line shows a least square fit to the Bleaney-Bowers equation for a $S_1 = S_2 = 2$ dimer resulting in weak antiferromagnetically coupling ($J = -0.4$ cm $^{-1}$, $H = -2S_1S_2$).¹

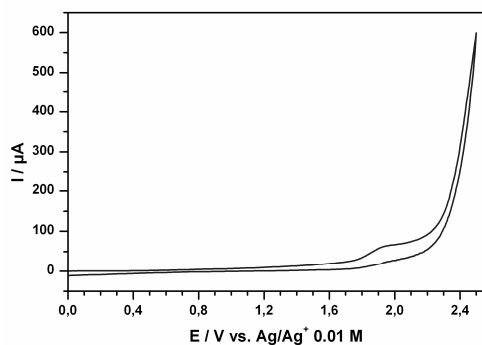


Fig. SI 4 Cyclic voltammogram of the ligand tpdm measured in acetonitrile.

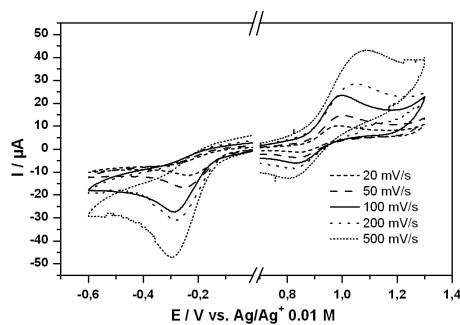


Fig. SI 5 Cyclic voltammogram of **1** measured with different scan rates.

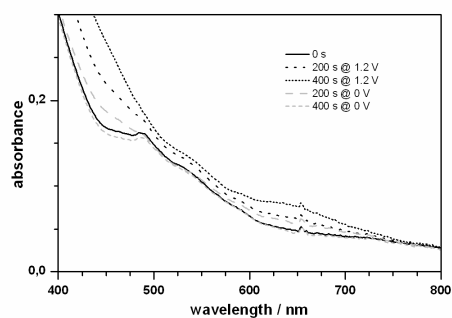


Fig. SI 6 Changes observed for absorption spectra of **1** (2.5 mM in acetonitrile / 0.1 M TBAClO₄) in an OTTE cell (1mm path length) recorded during the electrochemical oxidation of the complex at a potential of +1 200 mV vs. Ag/Ag⁺ and following re-reduction at 0 mV.

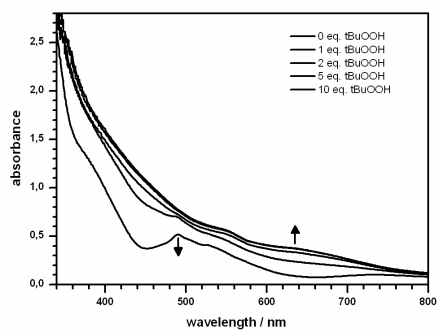


Fig. SI 7 UV/Vis spectra of **1** recorded after oxidation with *t*BuOOH.

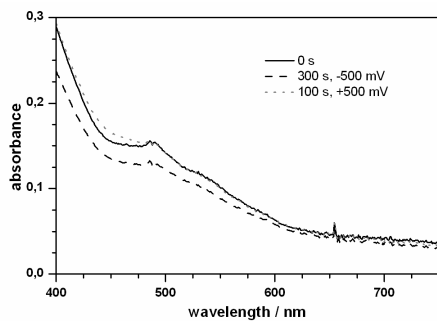


Fig. SI 8 Changes observed for absorption spectra of **1** (2.5 mM in acetonitrile / 0.1 M TBAClO₄) in an OTTE cell (1mm path length) recorded during the electrochemical reduction of the complex at a potential of -500 mV vs. Ag/Ag⁺ and following re-oxidation at +500 mV.

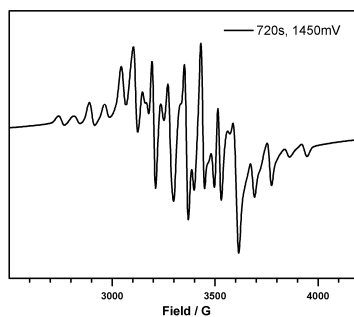


Fig. SI 9 EPR spectrum of **1** recorded after electrochemical oxidation at a potential of 1450 mV vs. Ag/Ag⁺.

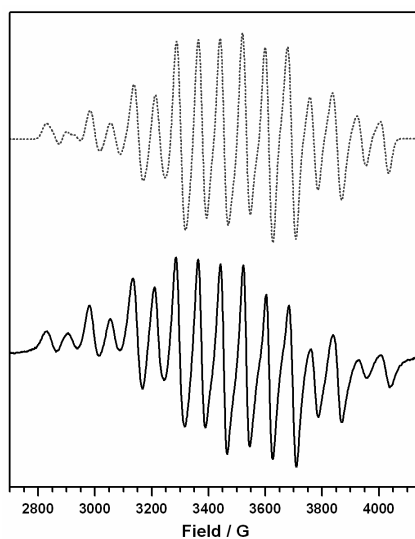


Fig. SI 10 Experimental (solid line) and simulated (dotted line) X-band EPR spectra for **1** oxidized chemically with five equivalents of *t*BuOOH.

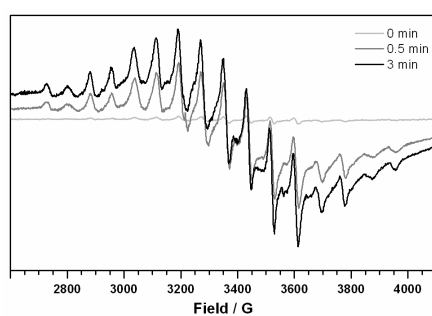


Fig. SI 11 X-band EPR spectra for **1** reduced electrochemically at -400 mV vs. Ag/Ag⁺.

Table SI 1 X-Sophe parameters for the Mn₂^{III,IV} form of **1** obtained by electrochemical oxidation.

Experiment Title	G4b_5K_2mW_DM*1000 esp
Operator	xuser
Spin Hamiltonian =	(Mn : beta B.g.S + S.A.I[Mn] + S.A.I[Mn1]). ;
Experiment Type	Continuous Wave
Spectrum Type	Randomly Oriented Spectrum
Method	Matrix Diagonalisation
Superhyperfine Method	Matrix Diagonalisation
<hr/>	
Spin System	
Number of Paramagnetic Centres	1
<hr/>	
Atomic Element for Electron Spin	Mn
Electron Spin	0.5
Number of Nuclei	2
<hr/>	
Atomic Element for Nuclear Spin	Mn
Number of Equivalent Nuclei	1
Number of Isotopes	1
Nuclear Spin - Mn-55	2.5
Nuclear g value - Mn-55	1.3874800
Natural Abundance - Mn-55	100.0000%
<hr/>	
Atomic Element for Nuclear Spin	Mn1
Number of Equivalent Nuclei	1
Number of Isotopes	1
Nuclear Spin - Mn1-55	2.5
Nuclear g value - Mn1-55	1.3874800
Natural Abundance - Mn1-55	100.0000%
<hr/>	
Instrument Parameters	
Abscissa - 1	Magnetic Field
Center Field [G]	3500.000200
Sweep Width [G]	2000.000000
Number of Points	5000
Abscissa - 2	None
Temperature [K]	0.000000
Microwave Frequency [GHz]	9.644088
Harmonic	First
Phase	Normal
Units	Gauss
Cavity Mode	Perpendicular
Magnetic Field - 1 Theta [deg]	0.000000
Magnetic Field - 1 Phi [deg]	90.000000
Magnetic Field - 2 Theta [deg]	90.000000
Magnetic Field - 2 Phi [deg]	90.000000
<hr/>	
File/Execution Information	
Sophe Input File Version	1.0.1
Sophe Output File Version	1.0.1
Rewrite Input File [y/n]	n
Input Spectrum Directory	/home/xuser/.../echem
Input Spectrum Filename	G4b_5K_2mW.par
Output Spectrum To	Xepr
Output Spectrum Directory	/home/xuser/.../echem
Output Spectrum Filename	echem_d
Input Format	Bruker ESP
Output Format	Bruker ESP

Hostname	ESP									
Execution Mode	Single Interactive									
Batch File Name	File									
<hr/>										
Sophe Parameters										
Number of Theta Orientations	25									
Number of Field Segments	10									
Interpolation Step [G]	1.000000									
Symmetry	Orthorhombic									
<hr/>										
Line Shape Parameters										
Line Shape Model	Angular Dependence of g									
Electron Spin / Nucleus	Mn Mn									
Line Shape	Gaussian									
Line Shape Cutoff [No. Std. Dev.]	6.000000									
Linewidth Units	Gauss									
<hr/>										
Transition Probabilities										
Transition Threshold	0.010000									
Number of Transitions	0									
<hr/>										
Optimisation Parameters										
Method	Simplex									
Error Function	Raw Data									
Error	6.000000e-03									
Normalisation Method	Peak Extrema									
Total Number of Iterations	1000									
Output Results Every N Iterations	25									
Output Parameters To	Disk									
Output Spectra To	Disk									
<hr/>										
Matrix/ Tensor	Values			Deviation			Parameter Space Half Width			Means of Varying Par.
Mn-g	1.99811	0.00000	0.00000	0.500000	0.00000	0.00000	0.500000	0.00000	0.00000	1 0 0
	0.00000	2.00369	0.00000	0.00000	0.500000	0.00000	0.00000	0.500000	0.00000	0 2 0
	0.00000	0.00000	1.98482	0.00000	0.00000	0.500000	0.00000	0.00000	0.500000	0 0 3
Mn-A	-149.992	0.00000	0.00000	2.00000	0.00000	0.00000	20.0000	0.00000	0.00000	4 0 0
	0.00000	-168.994	0.00000	0.00000	0.00000	2.00000	0.00000	0.00000	20.0000	0 5 0
	0.00000	0.00000	-107.989	0.00000	0.00000	2.00000	0.00000	0.00000	20.0000	0 0 6
Mn1-A	82.9967	0.00000	0.00000	1.00000	0.00000	0.00000	20.0000	0.00000	0.00000	7 0 0
	0.00000	72.0060	0.00000	0.00000	1.00000	0.00000	0.00000	0.00000	20.0000	0 8 0
	0.00000	0.00000	79.9954	0.00000	0.00000	1.00000	0.00000	0.00000	20.0000	0 0 9
Linewidth x	15.5031			1.00000			20.0000			10
Linewidth y	15.5031			1.00000			20.0000			10
Linewidth z	15.5031			1.00000			20.0000			10

Table SI 2 EPR parameters for the $Mn_2^{III,IV}$ form of **1** obtained by chemical oxidation as determined by a simulation of the signal using the X Sophe software suite. Hyperfine coupling constants A are given in gauss.

	<i>g</i>	A^{III}	A^{IV}
<i>x</i>	2.005	-168	72
<i>y</i>	1.996	-149	83
<i>z</i>	1.985	-107	79

1. C. J. O'Connor, *Prog. Inorg. Chem.*, 1982, **29**, 203-283.

Paper II.

K10 montmorillonite supported manganese catalysts for the oxidation of water to dioxygen



Research Paper

K10 montmorillonite supported manganese catalysts for the oxidation of water to dioxygen

Hans-Martin Berends, Thomas Homburg, Igor Kunz, Philipp Kurz*

Institute for Inorganic Chemistry, Christian-Albrechts-University Kiel, Max-Eyth-Straße 2, 24118 Kiel, Germany

ARTICLE INFO

Article history:

Received 15 June 2010

Received in revised form 7 December 2010

Accepted 7 December 2010

Available online 15 December 2010

Keywords:

Montmorillonite

Manganese

Heterogeneous catalysis

Water oxidation

EPR spectroscopy

ABSTRACT

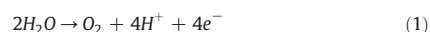
Two dimanganese complexes and two manganese salts were adsorbed on K10 montmorillonite clay to prepare water oxidation catalysts inspired by the manganese-containing active site of Photosystem II, the enzyme where water oxidation occurs *in vivo*. The montmorillonite hybrids of the dinuclear manganese(III,III) complex $[\text{Mn}_2^{\text{III,III}}(\mu\text{-O})(\text{tpdm})_2(\mu\text{-OAc})_2]^{2+}$ (2@Mt, $\text{tpdm} = \text{tris}(2\text{-pyridyl})\text{methane}$), manganese(II) sulphate (Mn^{2+} @Mt) and manganese(III) acetate (Mn^{3+} @Mt) are presented as an addition to the well studied clay hybrid system of $[\text{Mn}_2^{\text{III,IV}}(\mu\text{-O})_2(\text{terpy})_2(\text{H}_2\text{O})_2]^{3+}$ (1@Mt, $\text{terpy} = 2,2':6',2''\text{-terpyridine}$). As indicated by UVVis and EPR spectroscopy, the immobilization of the manganese compounds on the clay surfaces was associated with changes of their structure and their electronic properties (with the exception of Mn^{2+} @Mt). No remarkable changes in clay interlayer distance could be observed suggesting that the manganese compounds do not intercalate between the montmorillonite layers but adsorb only on the surface of the clay mineral. Three of the four heterogeneous systems were found to be able to catalyse water oxidation with the single-electron oxidation agent Ce^{IV} . The manganese(III) acetate clay hybrid Mn^{3+} @Mt showed the highest activity, nearly three times higher than the best catalytic system of this class found so far, the montmorillonite hybrid 1@Mt. Because there are only very few examples of functional, manganese-based catalysts for water oxidation, these new materials represent interesting additions to the original hybrid systems. The spectroscopic results additionally indicate that the formation of manganese oligomers on the clay surface seems to be the most likely explanation for the fact that catalytically active materials are generated.

© 2010 Elsevier B.V. All rights reserved.

1. Introduction

In nature, the oxygen evolving complex (OEC) of Photosystem II, a cluster containing four μ -oxido-bridged manganese atoms, catalyses the four-electron oxidation of water to molecular oxygen (Eq. (1)). The OEC is embedded in the very complex structure of Photosystem II's membrane protein ensemble, which ensures (among other functions) the controlled access of the water substrate, the release of the dioxygen and proton products as well as the directed transport of the generated reducing equivalents along a chain of acceptor molecules (Ferreira et al., 2004; Guskov et al., 2009; Loll et al., 2005; Yano et al., 2006). It has been the aim of a number of research groups, including us, to develop water oxidation catalysts inspired by the architecture of the OEC (Cady et al., 2008; Lubitz et al., 2008; Mukhopadhyay et al., 2004; Mullins and Pecoraro, 2008). From the development of such model systems one hopes to gain additional insights on how the natural enzyme achieves the complicated redox catalysis of light-driven water oxidation. Additionally, recent years have seen fast growing research on synthetic water oxidation catalysts based on abundant metals like manganese, as these are

essential components for the development of systems for light-driven water splitting into hydrogen and oxygen to generate H_2 as a "solar fuel".



For several decades, μ -oxido-bridged, dinuclear manganese complexes bearing oxidation stable supporting ligands have been prepared as potential models of the OEC. But despite numerous reports concerning the syntheses and careful characterizations of such compounds, studies about their interaction with water under oxidative conditions – and especially their ability to indeed catalyse the water oxidation reaction – are rare (Kurz et al., 2007; Limburg et al., 1999; Poulsen et al., 2005). In the few cases where catalytic experiments were reported, true water oxidation could not be observed, because all manganese compounds tested so far require the use of oxygen-transferring and/or two-electron oxidising agents like hydrogen peroxide (H_2O_2), hypochlorite (OCl^-) or hydrogen peroxosulphate (HSO_5^-) to catalyse the formation of oxygen in homogeneous solutions. Such reactions, however, do not represent real water oxidation, as demonstrated by ^{18}O isotope labelling of the O_2 product (Beckmann et al., 2008).

It was demonstrated in 2004 that manganese-catalysed water oxidation could be observed for a heterogeneous system using clay minerals as solid supports for molecular manganese compounds (Yagi

* Corresponding author. Fax: +49 431 880 1520.

E-mail address: phkurz@ac.uni-kiel.de (P. Kurz).

and Narita, 2004; Yagi et al., 2007). Yagi et al. adsorbed the dinuclear Mn₂-complex 1 (Fig. 1) and the closely related compound [(bpy)₂Mn^{III}(μ-O)₂Mn^{IV}(bpy)₂]³⁺ (bpy = 2,2'-bipyridine) on kaolinite or montmorillonite clays. The reaction of such manganese clay hybrids with the single-electron oxidation agent (NH₄)₂[Ce^{IV}(NO₃)₆] (Ce^{IV}) in aqueous suspensions yielded O₂. Experiments in H₂¹⁸O labelled water confirmed the bulk water as exclusive source of the produced oxygen. Since then, it has also been shown that similar reactivity can be observed for 1 adsorbed on TiO₂ (Li et al., 2009). Additionally, work by our group proved that functional water oxidation catalysts can also be synthesized by adsorbing other manganese complexes than the polypyridyl species used by Yagi et al. (Kurz, 2009). Very recent work by Yagi et al. showed that 1 adsorbed on mica is able to produce O₂ derived by visible light and [Ru(bpy)₃]³⁺ as photosensitizer (Yagi et al., 2010).

Clay materials, e.g. the K10 montmorillonite used in this study, are very promising supports for water oxidation catalysis, because they are widely used as scaffold materials for molecular catalysts in oxidation reactions (Jiang et al., 2009; Salavati-Niasari et al., 2007; Zhou, 2010). Additionally, they are – like the natural Photosystem II – able to immobilize a manganese species in a hydrophilic, highly oxidation stable environment. The manganese clay hybrids have therefore been considered as promising inorganic models for the OEC's manganese cluster embedded within the PSII enzyme (Yagi et al., 2007).

However, it is still quite unclear how water oxidation catalysis is achieved by the clay hybrids and what role both the clay support and the ligand framework of the manganese centres play in these reactions. In search for answers to these questions we here present a study of a new montmorillonite clay hybrid of a dinuclear manganese(III,III) complex with an unusual, facially coordinating trispyridyl ligand (Berends et al., 2009) as well as novel hybrids obtained by the adsorption of Mn²⁺ or Mn³⁺ ions from solutions of simple manganese salts, i.e. manganese(II) sulphate and manganese(III) acetate. In addition to catalytic experiments and UVVis measurements, we employed EPR spectroscopy, a powerful method in manganese chemistry, to learn more about this interesting class of heterogeneous catalysts.

2. Materials and methods

2.1. Materials

(NH₄)₂[Ce(NO₃)₆], Mn(OAc)₃·2H₂O (both Aldrich Chemical Co. Inc), 2,2':6',2''-terpyridine (terpy, ABCR), K10 montmorillonite (Fluka, product no. 69866) and MnSO₄·4H₂O (Merck) were used without further purification. [Mn^{III,IV}(μ-O)₂(terpy)₂(H₂O)₂]³⁺ (1) and [Mn^{III,III}(μ-O)(tpdm)₂(μ-OAc)₂]²⁺ (2) (tpdm = tris(2-pyridyl)methane) were prepared according to established procedures (Berends et al., 2009; Yagi and Narita, 2004). Deionised water (>10 MΩ cm) was used for all experiments.

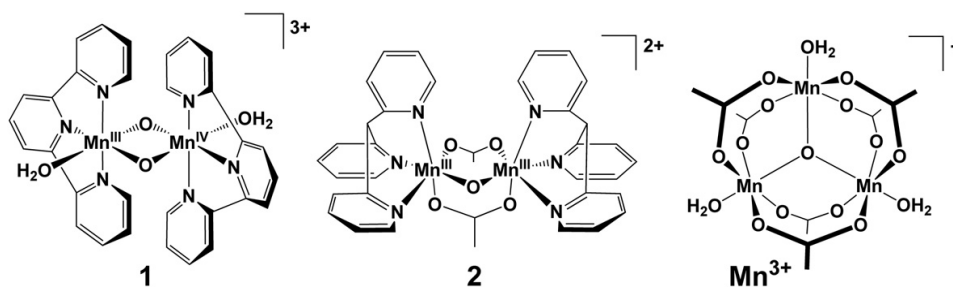


Fig. 1. Structures of the dinuclear manganese complexes [Mn^{III,IV}(O)₂(terpy)₂(H₂O)₂]³⁺ (1) and [Mn^{III,III}(O)(tpdm)₂(OAc)₂]²⁺ (2) used in this study. Additionally, the structure of the trimer [(Mn^{III}(μ₃-O)(OAc)₆(H₂O)₃]⁺, which forms in aqueous solutions of manganese(III) acetate is shown.

2.2. Adsorption of manganese species on montmorillonite

Manganese salts or complexes were dissolved in 25 mL of water to reach total manganese concentrations of 1 mM. A sample (1 mL) of these solutions was taken to analyse the total manganese concentration by atomic absorption spectroscopy (AAS, see below). Now 200 mg of montmorillonite clay were added and the suspensions were stirred gently. After 30 min the suspensions were centrifuged for 5 min at 4000 rpm, after which a 1 mL sample of the supernatant was taken for AAS analysis, while the rest was removed. The material was then resuspended in about 10 mL of water, frozen in a PE bottle to 77 K and lyophilised using an Alpha 1 freeze dryer by Martin Christ Gefriertrocknungsanlagen. In this way four different montmorillonite hybrids, namely 1@Mt, 2@Mt, Mn²⁺@Mt and Mn³⁺@Mt were synthesized. Catalyst loadings in μmol_{Mn} g⁻¹ were calculated from the concentration differences in solution obtained from AAS results.

2.3. Analytical methods

X-ray powder diffractometry (XRD). Samples were homogenised before reflection patterns were recorded in reflection geometry on a PANalytical X'Pert Pro equipped with a PiCCel using Cu Kα radiation. Typical measurement parameters were: 2θ step size: 0.007°; step time: 49.5 s, 2θ range: 2–60°.

N₂ physisorption isotherms were measured with a BEL Sorpmax instrument and analyzed according to BET theory to establish surface areas.

AAS measurements. Manganese atomic absorption spectroscopy was performed on an AAnalyst spectrometer system by Perkin Elmer. Prior to analysis, AAS sample solutions (1 mL) were added to 1 mL of concentrated nitric acid, left at room temperature for at least 24 h to ensure complete destruction of the complexes and then diluted to 25 mL.

Scanning electron microscopy (SEM) was carried out with a Philips ESEM XL30.

Diffuse reflectance UVVis spectroscopy. UVVis spectra of powders were recorded using a Varian Cary 5000 spectrometer equipped with an Ulbricht sphere to record spectra in reflectance mode. If necessary, compounds were diluted with analytical grade barium sulphate. The signals were baseline corrected against the spectrum of PTFE powder using the Kubelka–Munk function.

EPR spectroscopy. X-band (9 GHz) electron paramagnetic resonance spectra were collected using a Bruker EMXplus spectrometer equipped with an Oxford Instrument ESR 900 cryostat and a dual mode cavity (Bruker ER-4116DM) at 5 K. Spectra were recorded in both parallel and perpendicular mode detection on the same sample tube. An EPR spectrum of pure montmorillonite was subtracted from the data to remove the signals of paramagnetic impurities in the clay (most likely iron).

2.4. Oxygen detection

The polarographic signal of a standard Clark electrode (Rank Brothers Ltd.), separated from the sample solution by a 12.7 mm thick teflon membrane, was recorded for the entire duration of the experiments at 1 s intervals using the SoftFox software package by Skanntronic. Air saturated water ($[O_2] = 253 \mu\text{M}$, (Truesdale and Downing, 1954)) was used for the calibration of the electrode. The volume of the solution at the beginning of each experiment was 900 μL , thermostated inside the double walled measurement cell at 20 °C. The gas volume (ca. 100 μL) above the sample solution was sealed from the atmosphere using a rubber septum. The cell was placed on top of a magnetic stirrer to continuously stir the solution using a teflon-coated stir bar.

2.5. Oxygen evolution experiments

The manganese hybrids were suspended in water using 12 mg of hybrid in 900 μL of water. These suspensions were then transferred into the Clark cell and made anaerobic by argon purging to reach residual oxygen concentrations of $[O_2] \leq 10 \mu\text{M}$. After an equilibration time of 1 min, 100 μL of degassed, freshly prepared Ce^{IV} -stock solution (2.5 M $(\text{NH}_4)_2[\text{Ce}(\text{NO}_3)_6]$) were injected into the cell. Oxygen evolution was followed for 10 min after injection and measured at least twice for each adsorbed species. Control experiments showed that neither the pure clay material nor solutions of the manganese complexes or manganese salts on their own catalysed the formation of detectable amounts of O_2 . Oxygen concentration traces for control experiments as well as details on the interaction of the Ce^{IV} oxidant with montmorillonite can be found in our previous report on this topic (Kurz, 2009). For experiments concerning the reusability of the catalysts, 100 mg of $\text{Mn}^{3+}@Mt$ was suspended in 0.25 M $(\text{NH}_4)_2[\text{Ce}(\text{NO}_3)_6]$, stirred for 2 h and then filtered off. The supernatant solution was analysed by AAS for dissolved manganese, while the clay hybrid was washed, dried and again used in catalytic experiments.

3. Results and discussion

3.1. Synthesis

Four different manganese species were used for the synthesis of the clay hybrids. Two dinuclear manganese complexes were prepared, namely $[\text{Mn}_2^{\text{III,IV}}(\mu\text{-O})_2(\text{terpy})_2(\text{H}_2\text{O})_2]^{3+}$ (1, originally used by Yagi et al.), and $[\text{Mn}_2^{\text{III,III}}(\mu\text{-O})(\text{tpdm})_2(\mu\text{-OAc})_2]^{2+}$ (2), a complex with manganese centres bearing facially coordinating trispyridine ligands (Fig. 1). Additionally, a simple manganese(II) salt (MnSO_4) as well as a manganese(III) precursor ($\text{Mn}(\text{OAc})_3$) formed parts of this study. The addition of commercial montmorillonite clay to aqueous solutions of these manganese species resulted in the removal of >90% of the total dissolved manganese as indicated by atomic absorption spectroscopy. In this way four different hybrids $X@Mt$ (with $X = 1, 2, \text{Mn}^{2+}$ and Mn^{3+}) were prepared. For these materials manganese loadings of up to 94 μmol manganese per gram of montmorillonite were determined, values which are within the range of the cation-exchange-capacity (CEC) reported for montmorillonite (70–120 $\mu\text{mol g}^{-1}$) (Bergaya et al., 2006).

As montmorillonite is a 2:1 clay containing interlayer $\text{Na}^+/\text{Ca}^{2+}$ cations, intercalation reactions are possible which would result in the exchange of the interlayer ions for the positively charged complexes and an increase in layer-to-layer distance. But an analysis of the powder diffractometry data (Fig. 2) showed that the interlayer distance was hardly affected by the adsorption reaction, remaining at the value of the untreated montmorillonite ($\sim 0.8 \text{ nm}$, Table 1). This seems to indicate that manganese adsorption took place on the silicate and aluminate surface groups of the montmorillonite and that intercalation was of no importance here. The surface of the clay, determined by N_2 adsorption experiments to be 170–190 $\text{m}^2 \text{g}^{-1}$ in

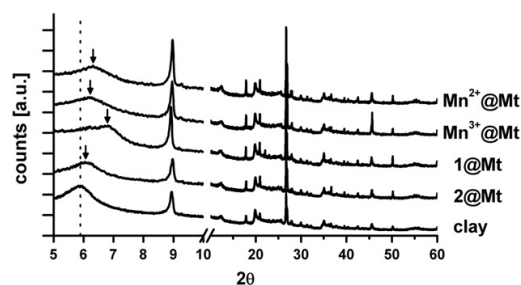


Fig. 2. Powder XRD of the synthesized manganese clay hybrids.

size and unaffected by manganese adsorption (Table 1), surely offers a large enough area for surface adsorption reactions to occur. Scanning electron microscopy revealed that the K10 montmorillonite used here consisted of particles with sizes of between a few to 50 μm , both for the untreated clay and the clay hybrids (Fig. 3).

3.2. Spectroscopy

The adsorption of the manganese species was accompanied by significant colour changes when comparing the neat manganese compounds with their clay hybrids. For example, complex 2 was reddish brown as a solid and red in aqueous solution while 2@Mt hybrids were ochre. Diffuse reflectance UVVis spectra of neat 2 showed absorption bands at 490 and 740 nm and a shoulder at 550 nm. For 2@Mt an absorption band at 380 nm and a weak shoulder at 460 nm was visible (Fig. 4, left). $\text{Mn}(\text{OAc})_3$ was light reddish brown as a solid, but here $\text{Mn}^{3+}@Mt$ was grey. A broad absorption band could be found for the neat solid compound at 440 nm in the UVVis spectrum while the clay hybrid $\text{Mn}^{3+}@Mt$ showed only a very small shoulder in this region and a new shoulder at 500 nm (Fig. 4, right). Similar effects were observed earlier for 1 adsorbed on both montmorillonite and kaolinite (Yagi and Narita, 2004). Only the adsorption of Mn^{2+} had no influence on the UVVis spectra and $\text{Mn}^{2+}@Mt$ was an off-white powder like the untreated clay itself.

EPR spectroscopy is a key method to characterize oxidation states and nuclearity of manganese species. Therefore, low temperature EPR spectra of the clay hybrids as frozen aqueous suspensions were recorded. After subtraction of the signals from iron impurities of the used montmorillonite, characteristic six-line signals of mononuclear Mn^{II} -species (Fig. 5, top) with hyperfine splittings varying from 85 to 93 G were found in all cases (Groni et al., 2008). However, these signals differed clearly in intensity. As expected, the signal of $\text{Mn}^{2+}@Mt$ had the highest intensity followed by the signal of $\text{Mn}^{3+}@Mt$ ($\sim 60\%$ signal size

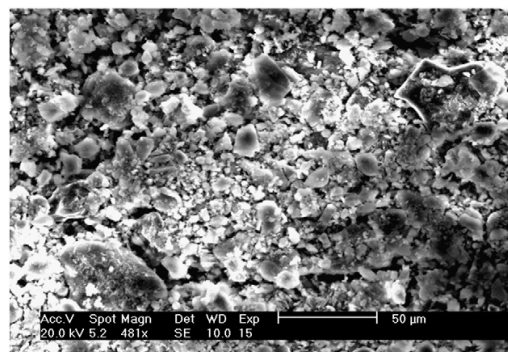


Fig. 3. SEM image of $\text{Mn}^{3+}@Mt$.

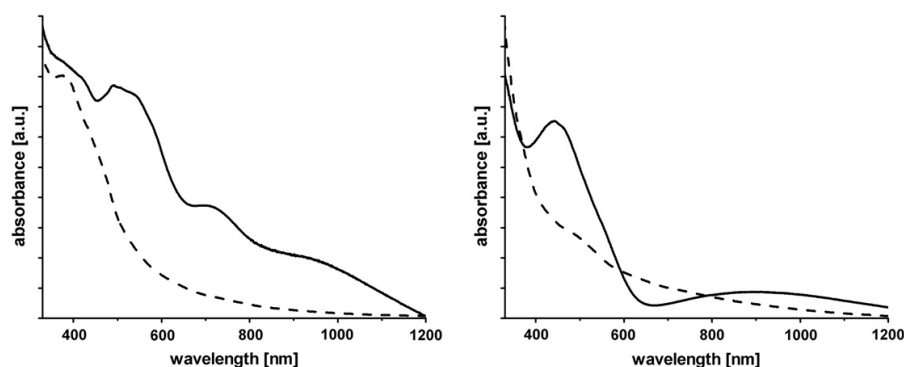


Fig. 4. Diffuse reflectance UVVis spectra of complex 2 (left) and $\text{Mn}(\text{OAc})_3$ (right) as solids (mixed with BaSO_4 , solid lines) and adsorbed on montmorillonite (dashed lines).

when compared to $\text{Mn}^{2+}@\text{Mt}$, Table 1). EPR spectra of 1@Mt and 2@Mt showed only very small signals. Interestingly, the typical sixteen-line signal of dimanganese(III,IV) complexes, which is also known for 1 in solution (Collomb et al., 1999), could not be observed for the clay hybrid 1@Mt. These results showed that the original complex did clearly undergo chemical changes during the adsorption process. EPR spectra measured in parallel detection mode (used to detect mononuclear Mn^{III} -species at $\sim 500\text{--}1500$ G) (Campbell et al., 1999) also contained small signals of Mn^{III} -species for all hybrids (Fig. 5, bottom). Again large size differences existed: signals for the clay hybrids of the manganese salts had roughly the same intensity, but only very weak manganese(III)-signals could be observed for the adsorbed complexes.

The results of the UVVis and EPR spectra showed that the manganese species are not only immobilised on the clay supports. The shifts and (dis)appearances of absorption bands in the visible region indicated that the compounds' electronic structures changed during the adsorption process. The EPR spectra displayed that the adsorbed manganese was not present in the form of dimeric manganese(III,IV) species and only a small part as monomeric manganese(II or III), except for $\text{Mn}^{2+}@\text{Mt}$. Common disproportionation reactions of Mn^{III} into Mn^{II} and Mn^{IV} could be the reason for the Mn^{II} -signals of $\text{Mn}^{3+}@\text{Mt}$, 1@Mt and 2@Mt. Additionally, oligo- or polymeric μ -oxido-manganese-clusters containing Mn^{III} and/or Mn^{IV} might accumulate on the surface of the montmorillonite. The formation of such species is well documented e.g. for the adsorption of manganese(II) precursors on silicates (Jiao and Frei, 2010) or the oxidation of complex 1. The latter yields the tetrameric all- Mn^{IV} -species $[(\text{Mn}_2^{\text{IV}}(\mu\text{-O})_2(\text{terpy})_2(\text{H}_2\text{O})_2)_2(\text{O})]^{6+}$ in aqueous solution (Baffert et al., 2005). One also has to bear in mind that the trimeric manganese species $[(\text{Mn}_3^{\text{III}}(\mu_3\text{-O})(\text{OAc})_6(\text{H}_2\text{O})_3)]^+$ (Fig. 1) is formed spontaneously in aqueous solutions of $\text{Mn}(\text{OAc})_3$ (Holleman and Wiberg, 1995). Based on these facts and the presented UVVis-/EPR-analyses, a model how manganese might be adsorbed on the montmorillonite clay is proposed here. It is suggested that this takes

place both as mononuclear Mn^{II} -species and as larger μ -oxido-manganese clusters (Fig. 6). The formation of such manganese aggregates was already proposed by Yagi et al. (2007) for 1@Mt and our results support this suggestion.

3.3. Water oxidation catalysis

The catalytic properties of the clay hybrids were studied in a standardised reaction procedure already employed earlier by us in oxygen formation experiments (Kurz, 2009; Kurz et al., 2007). Aqueous suspensions of the different manganese clay hybrids were filled into the measurement cell of a Clark type oxygen selective electrode. Dissolved oxygen was removed by argon purging and after an equilibration time small volumes of concentrated Ce^{IV} solutions were added to the suspensions. Cerium(IV) has been routinely used in water oxidation catalysis as it acts as a strong, single-electron oxidation agent in water ($\sim +1.4$ V vs. NHE, (Holleman and Wiberg, 1995)). Most importantly, isotope labelling using H_2^{18}O as substrate showed that the oxygen formed in reactions of both manganese and ruthenium compounds with Ce^{IV} originates exclusively from the bulk water (Hurst, 2005). Thus, such reactions represent "true" water oxidation catalysis. However, the use of Ce^{IV} is accompanied by the

Table 1
Properties of the different montmorillonite clay hybrids prepared for this study.

Adsorbed species	$2\theta^a$ [°]	d [nm]	Loading [$\mu\text{mol}_{\text{Mn}} \text{g}_{\text{clay}}^{-1}$]	S_{BET} [$\text{m}^2 \text{g}^{-1}$]	Size of the Mn^{II} EPR signal ^b
None	5.90	0.8	–	190	–
$\text{Mn}^{2+}@\text{Mt}^c$	6.32	0.7	78	170	1
$\text{Mn}^{3+}@\text{Mt}^d$	6.21	0.7	94	180	0.6
1@Mt	6.82	0.7	79	170	0.1
2@Mt	6.04	0.7	87	170	0.2

^a Of the reflection with the lowest 2θ value (characteristic for the clay interlayer distance d).

^b Relative to the size of the Mn^{II} perpendicular mode six-line signal for $\text{Mn}^{2+}@\text{Mt}$.

^c From solutions of manganese(II) sulphate.

^d From solutions of manganese(III) acetate.

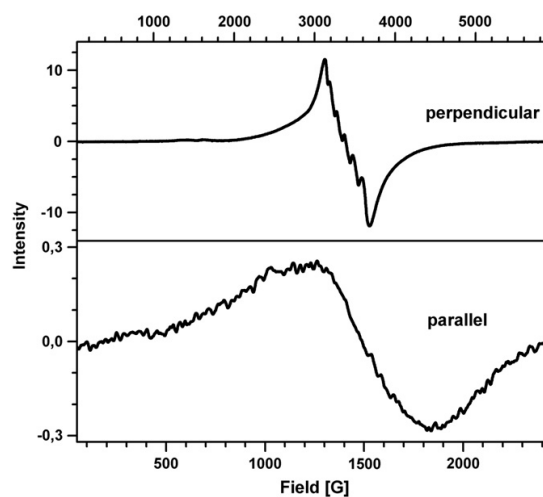


Fig. 5. EPR spectrum of $\text{Mn}^{3+}@\text{Mt}$ as a frozen aqueous suspension (EPR settings: microwave power perpendicular mode: 6.3 mW, parallel mode: 31.7 mW; $T = 5$ K, modulation amplitude 10 G). The total manganese concentration is 1 mM. Signals obtained for suspensions of the neat montmorillonite clay were subtracted.

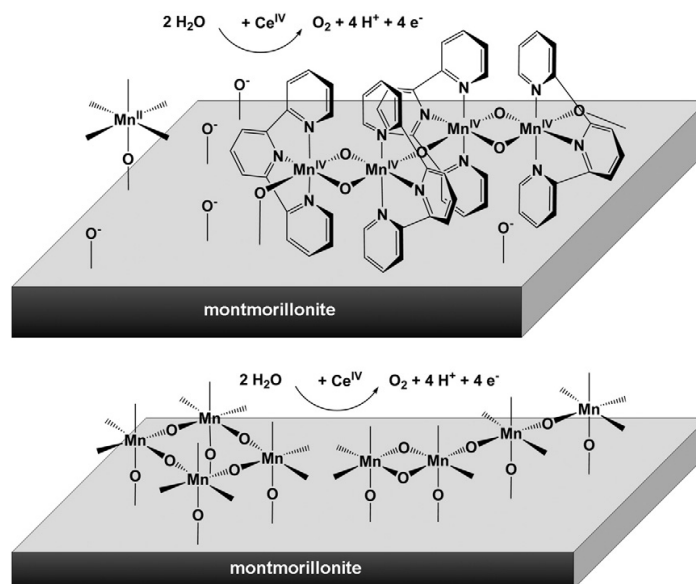


Fig. 6. Suggestion for possible modes of adsorption for manganese species in accordance with UVVis/EPR data of the presented study. Suggestions for the adsorption of dinuclear manganese complexes (top) and simple manganese salts (bottom) are shown.

drawback that a low pH regime (pH~2) has to be used as less acidic conditions result in the precipitation of cerium hydroxides. It therefore has to be noted that oxidation by cerium(IV) represents a valid, though far from ideal, test system for water oxidation. Additionally, it should be mentioned that in the entire report the term “catalyst” is used only to indicate that the clay hybrids open reaction pathways for water oxidation which are otherwise not accessible. Due to the upper detection limit of the Clark electrode, the experimental setup does not allow the establishment of catalytic turnover numbers (TON) and it is therefore not possible to differentiate between oxygen evolution reactions which are “truly catalytic” (TON > 1) and those that are not. For a more thorough discussion of this see the previous work (Kurz, 2009).

Oxygen evolution curves for reactions with Ce^{IV} with the different hybrids prepared for this study are shown in Fig. 7. Oxygen concentrations were normalized relative to the amount of total suspended manganese to allow for a comparison of the detected $[\text{O}_2]$ values. All hybrids obtained here from precursors containing manganese as Mn^{III} and/or Mn^{IV} did clearly catalyse oxygen formation from water, though at markedly different rates (Table 2). The most active catalyst was $\text{Mn}^{\text{3+}}@\text{Mt}$, obtained

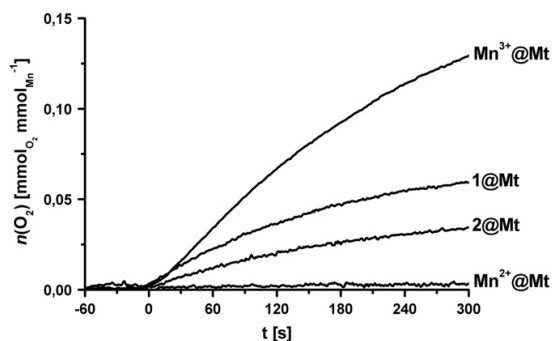


Fig. 7. Traces of oxygen evolution for the reactions of different clay hybrids with Ce^{IV} in H_2O . Solutions of the single-electron oxidation agent Ce^{IV} were added at $t = 0$ s.

by the adsorption of manganese(III) acetate, followed by 1@Mt and 2@Mt, which catalyse reaction (1) at a about half (1@Mt) or a quarter (2@Mt) of the rate of $\text{Mn}^{\text{3+}}@\text{Mt}$, respectively. Interestingly, montmorillonite bearing adsorbed manganese(II) ($\text{Mn}^{\text{2+}}@\text{Mt}$) was not an active catalyst. Also, no activity was observed for the neat montmorillonite clay, proving that transition metal impurities of the clay (especially Fe is clearly detectable by EPR), did not contribute to water oxidation catalysis.

As reactions involving Ce^{IV} take place at very acidic conditions, catalyst stability is of course an issue. To estimate catalyst degradation, leaching experiments were carried out where $\text{Mn}^{\text{3+}}@\text{Mt}$ was stirred in a Ce^{IV} solution under reaction conditions for two hours. Despite the fact that we found that about 60% of the adsorbed manganese was dissolved by this rather extreme treatment, catalyst activity was retained at a level of 70% of the rate found for the untreated hybrids.

A comparison of the catalytic rates for the different manganese hybrids in Table 2 reveals neither a correlation of the rate with the total manganese loading nor with the amount of Mn^{II} present. Instead, our data suggests that the catalytic performance appears to depend on two main factors:

- a) the manganese oxidation state: $\text{Mn}^{\text{2+}}@\text{Mt}$ is inactive and active materials all contain Mn^{III} or Mn^{IV} and only lower amounts of monomeric Mn^{II} as detected by EPR.

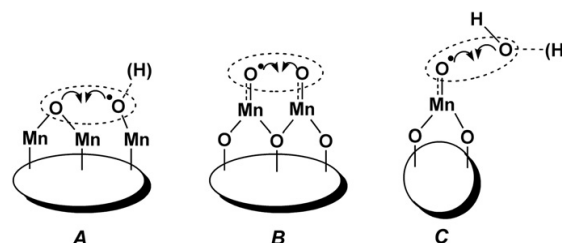


Fig. 8. Possible mechanistic pathways of dioxygen formation by manganese clay hybrids in agreement with water oxidation mechanisms suggested in the literature (Cady et al., 2008; Dau et al., 2010; Lubitz et al., 2008).

Table 2
Catalytic rates of the different montmorillonite clay hybrids prepared for this study.

Adsorbed species	Catalytic rate [mmol _{O₂} ·mol _{Mn} ⁻¹ ·min ⁻¹]
None	n.d.
Mn ²⁺ @Mt	n.d.
Mn ³⁺ @Mt	32
1@Mt	13
2@Mt	6

n.d.: no oxygen evolution detected above the lower detection limit of $-0.5 \text{ mmol}_{\text{O}_2} \text{ min}^{-1} \text{ mol}_{\text{Mn}}^{-1}$.

b) the *preorganization* of the manganese precursor as a multinuclear entity: the trinuclear species $[(\text{Mn}^{\text{III}}(\mu_3\text{-O})(\text{OAc})_6(\text{H}_2\text{O})_3)]^+$ formed in solutions of $\text{Mn}(\text{OAc})_3$ is apparently a very good precursor for catalytically active Mn-sites on the clay. Our results also indicate that 1 and 2 act as preorganized dinuclear catalyst precursors which then undergo significant changes during adsorption according to our results from UVVis- and EPR spectroscopy.

Many different mechanisms for the water oxidation reaction have been proposed (Cady et al., 2008; Dau et al., 2010; Lubitz et al., 2008) and three of the currently discussed models are shown in Fig. 8. All can well be imagined to occur for a manganese cluster adsorbed on a clay mineral surface. In mechanism A the O–O bond formation proceeds between one oxygen species bound end-on to a manganese atom and one bridging oxido atom. Two end-on oxygen species are coupling directly in mechanism B to form dioxygen. In the third pathway C a water or hydroxide oxygen atom attacks nucleophilically on a terminal oxygen species.

4. Conclusions

Functional, biomimetic catalysts for water oxidation could be synthesized by the adsorption of different manganese species on K10 montmorillonite clay, with all manganese species not able to catalyse water oxidation in homogeneous solution (Kurz, 2009; Kurz et al., 2007). The best catalytic performance was observed for hybrids of manganese(III) acetate (Mn^{3+} @Mt) for which catalytic rates surpass the best catalytic system of this class found so far, the material 1@Mt discovered by Yagi and Narita in 2004. A manganese oxidation state $\geq +\text{III}$ seems to be a prerequisite for active catalysts, as no activity was found for adsorbed manganese(II). Our results are in agreement with previous results showing that active catalysts for water oxidation can be generated by a variety of very different $\text{Mn}^{\text{II/IV}}$ -precursors (Kurz, 2009), so that manganese coordination geometry appears to be only of secondary importance. Lacking convincing alternatives, the present study was limited to the use of the very acidic cerium(IV) oxidation agent. Serious degradation of the catalysts was detected over a period of hours in this reaction medium, resulting in markedly reduced catalytic rates. This should, however, not be seen as general disadvantage of the presented catalyst design as the acidic Ce^{IV} oxidant serves here as a first and easy to handle test reaction for possible – and much more biomimetic – light-driven water oxidation at neutral pH in the future.

The formation of manganese oligomers on the clay surface seems to be the most likely explanation for the fact that catalytically active materials are generated by the surface adsorption of species which are on their own inactive for water oxidation in homogeneous solution. The clay mineral with its large surface area, multiple binding sites and hydrophilic character represents an ideal platform for the formation and stabilisation of such manganese clusters. Further investigations, e.g. by X-ray spectroscopy, might be able to identify the nature of these manganese aggregates in greater detail. The OEC, the active site for water oxidation in nature, with its four oxido-bridged manganese centres, will be an inspiration for models of how such catalytically active manganese oligomers might be organized.

Acknowledgements

The authors thank Ursula Cornelissen, Jannes Ophey, Helge Reinsch, Monika Schneeweiß, Malte Snoyek, Christian Stoltenberg and Mathias Wiechen (all Inorganic Chemistry, CAU Kiel) for experimental support. Klaus Beneke and Norbert Stock offered valuable advice concerning the properties and handling of clay compounds. This work was financially supported by the Fonds der Chemischen Industrie (Liebig fellowship of PhK) and the Christian-Albrechts-University Kiel.

References

- Baffert, C., Romain, S., Richardot, A., Lepretre, J.C., Lefebvre, B., Deronzier, A., Collomb, M.N., 2005. Electrochemical and chemical formation of $[\text{Mn}_4\text{IVO}_5(\text{terpy})_4(\text{H}_2\text{O})_2]^{6+}$, in relation with the photosystem II oxygen-evolving center model $[\text{Mn}_2\text{III}, \text{IVO}_2(\text{terpy})_2(\text{H}_2\text{O})_2]^{3+}$. *J. Am. Chem. Soc.* 127, 13694–13704.
- Beckmann, K., Uchtenhagen, H., Berggren, G., Anderlund, M.F., Thapper, A., Messinger, J., Styring, S., Kurz, P., 2008. Formation of stoichiometrically ^{18}O -labelled oxygen from the oxidation of ^{18}O -enriched water mediated by a dinuclear manganese complex – a mass spectrometry and EPR study. *Energy Environ. Sci.* 1, 668–676.
- Berends, H.-M., Manke, A.-M., Näther, C., Tuzcek, F., Kurz, P., 2009. A dimanganese(III/IV) oxido complex with unusual ligand geometry. *Molecular Science for Solar Fuel*, Sigtuna.
- Bergaya, F., Theng, B.K.G., Lagaly, G., 2006. *Handbook of Clay Science 1*. Elsevier, Oxford, Amsterdam.
- Cady, C.W., Crabtree, R.H., Brudvig, G.W., 2008. Functional models for the oxygen-evolving complex of photosystem II. *Coord. Chem. Rev.* 252, 444–455.
- Campbell, K.A., Yikilmaz, E., Grant, C.V., Gregor, W., Miller, A.F., Britt, R.D., 1999. Parallel polarization EPR characterization of the Mn(III) center of oxidized manganese superoxide dismutase. *J. Am. Chem. Soc.* 121, 4714–4715.
- Collomb, M.N., Deronzier, A., Richardot, A., Pecaut, J., 1999. Synthesis and characterization of a new kind of Mn(III), IV μ -oxo complex: $[\text{Mn}_2\text{O}_2(\text{terpy})_2(\text{H}_2\text{O})_2(\text{NO}_3)_2] \cdot 6 \text{H}_2\text{O}$, $\text{terpy} = 2, 2': 6', 2''$ -terpyridine. *New J. Chem.* 23, 351–353.
- Dau, H., Limberg, C., Reier, T., Risch, M., Roggan, S., Strasser, P., 2010. The mechanism of water oxidation: from electrolysis via homogeneous to biological catalysis. *ChemCatChem* 2, 724–761.
- Ferreira, K.N., Iverson, T.M., Maghlaoui, K., Barber, J., Iwata, S., 2004. Architecture of the photosynthetic oxygen-evolving center. *Science* 303, 1831–1838.
- Gromi, S., Dorlet, P., Blain, G., Bourcier, S., Guillot, R., Anxolabehere-Mallart, E., 2008. Reactivity of an aminopyridine $[\text{LMn}^{\text{II}}]^{2+}$ complex with H_2O_2 . Detection of intermediates at low temperature. *Inorg. Chem.* 47, 3166–3172.
- Guskov, A., Kern, J., Gabdulkhakov, A., Broser, M., Zouni, A., Saenger, W., 2009. Cyanobacterial photosystem II at 2.9 Å resolution and the role of quinones, lipids, channels and chloride. *Nat. Struct. Mol. Biol.* 16, 334–342.
- Holleman, A.F., Wiberg, E., 1995. *Lehrbuch der Anorganischen Chemie*. de Gruyter, Berlin.
- Hurst, J.K., 2005. Water oxidation catalyzed by dimeric μ -oxo bridged ruthenium diimine complexes. *Coord. Chem. Rev.* 249, 313–328.
- Jiang, J., Ma, K., Zheng, Y.F., Cai, S.L., Li, R., Ma, J.T., 2009. Cobalt salophen complex immobilized into montmorillonite as catalyst for the epoxidation of cyclohexene by air. *Appl. Clay Sci.* 45, 117–122.
- Jiao, F., Frei, H., 2010. Nanostructured manganese oxide clusters supported on mesoporous silica as efficient oxygen-evolving catalysts. *Chem. Commun.* 46, 2920–2922.
- Kurz, P., 2009. Oxygen evolving reactions catalysed by manganese-oxo-complexes adsorbed on clays. *Dalton Trans.* 6103–6108.
- Kurz, P., Berggren, G., Anderlund, M.F., Styring, S., 2007. Oxygen evolving reactions catalysed by synthetic manganese complexes: a systematic screening. *Dalton Trans.* 4258–4261.
- Li, G., Sproviero, E.M., Snoeberger III, R.C., Iguchi, N., Blakemore, J.D., Crabtree, R., Brudvig, G., Batista, V.S., 2009. Deposition of an oxomanganese water oxidation catalyst on TiO₂ nanoparticles: computational modeling, assembly and characterization. *Energy Environ. Sci.* 2, 230–238.
- Limburg, J., Vrettos, J.S., Liable-Sands, L.M., Rheingold, A.L., Crabtree, R.H., Brudvig, G.W., 1999. A functional model for O–O bond formation by the O₂-evolving complex in photosystem II. *Science* 283, 1524–1527.
- Loll, B., Kern, J., Saenger, W., Zouni, A., Biesiadka, J., 2005. Towards complete cofactor arrangement in the 3.0 Å resolution structure of photosystem II. *Nature* 438, 1040–1044.
- Lubitz, W., Reijerse, E.J., Messinger, J., 2008. Solar water-splitting into H₂ and O₂: design principles of photosystem II and hydrogenases. *Energy Environ. Sci.* 1, 15–31.
- Mukhopadhyay, S., Mandal, S.K., Bhaduri, S., Armstrong, W.H., 2004. Manganese clusters with relevance to photosystem II. *Chem. Rev.* 104, 3981–4026.
- Mullins, C.S., Pecoraro, V.L., 2008. Reflections on small molecule manganese models that seek to mimic photosynthetic water oxidation chemistry. *Coord. Chem. Rev.* 252, 416–443.
- Poulsen, A.K., Rompel, A., McKenzie, C.J., 2005. Water oxidation catalyzed by a dinuclear Mn complex: a functional model for the oxygen-evolving center of photosystem II. *Angew. Chem. Int. Ed.* 44, 6916–6920.
- Salavati-Niasari, M., Zamani, E., Bazarganipour, M., 2007. Epoxidation of cyclohexene with K10-montmorillonite and Schiff-base macrocyclic copper complexes. *Appl. Clay Sci.* 38, 9–16.
- Truesdale, G.A., Downing, A.L., 1954. Solubility of oxygen in water. *Nature* 173, 1236.

- Yagi, M., Narita, K., 2004. Catalytic O₂ evolution from water induced by adsorption of [(OH₂)(terpy)Mn(μ-O)₂Mn(terpy)(OH₂)]³⁺ complex onto clay compounds. *J. Am. Chem. Soc.* 126, 8084–8085.
- Yagi, M., Narita, K., Maruyama, S., Sone, K., Kuwabara, T., Shimizu, K., 2007. Artificial model of photosynthetic oxygen evolving complex: catalytic O₂ production from water by di-μ-oxo manganese dimers supported by clay compounds. *Biochim. Biophys. Acta* 1767, 660–665.
- Yagi, M., Toda, M., Yamada, S., Yamazaki, H., 2010. An artificial model of photosynthetic photosystem II: visible-light-derived O₂ production from water by a di-μ-oxo-bridged manganese dimer as an oxygen evolving center. *Chem. Commun.* 46, 8594–8596.
- Yano, J., Kern, J., Sauer, K., Latimer, M.J., Pushkar, Y., Biesiadka, J., Loll, B., Saenger, W., Messinger, J., Zouni, A., Yachandra, V.K., 2006. Where water is oxidized to dioxygen: structure of the photosynthetic Mn₄Ca cluster. *Science* 314, 821–825.
- Zhou, C.H., 2010. Emerging trends and challenges in synthetic clay-based materials and layered double hydroxides. *Appl. Clay Sci.* 48, 1–4.

Paper III.

Investigation of Light-Triggered Carbon Monoxide Release from Two Manganese PhotoCORMs by IR, UV/Vis and EPR Spectroscopy

Investigation of Light-Triggered Carbon Monoxide Release from Two Manganese PhotoCORMs by IR, UV/Vis and EPR Spectroscopy

Hans-Martin Berends and Philipp Kurz*

Institute for Inorganic Chemistry, Christian-Albrechts-University Kiel, Max-Eyth-Straße 2,

24118 Kiel, Germany

Fax: (+49) 431-880-1520

E-mail: phkurz@ac.uni-kiel.de

Abstract

Water-soluble complexes containing the *fac*-[Mn^I(CO)₃]-moiety have been identified as candidates for the photoactivated release of molecular carbon monoxide, a potential therapeutic agent. Here, we employed a combination of spectroscopic methods (UV/Vis, IR and EPR) to reveal details of the processes following CO release. Studying the two manganese(I) complexes [Mn(CO)₃(tpm)](PF₆) (**1**, tpm = *tris*(pyrazolyl)methane) and [Mn(CO)₃(bpzaa)] (**2**, bpzaa = *bis*(pyrazolyl)acetic acid), we find that the manganese centres lose their carbonyl ligands in a stepwise manner. First, manganese dicarbonyl intermediates are formed after the release of one CO per Mn. The last two carbonyl ligands are then liberated in a reaction accompanied by manganese oxidation to Mn^{II} and beyond, as clearly detected by EPR spectroscopy. Ultimately, μ-O-Mn^{III}-compounds appear to be the most likely final reaction products. The spectroscopic methodology used here thus enables us to present a much more detailed picture of the light-triggered CO releasing reactions of *fac*-[Mn^I(CO)₃]-complexes than previously accessible by the use of the classical myoglobin assay alone. The additional information gained in this way on the CO release

process as well as the fate of the manganese precursors seems essential to us for a potential pharmaceutical application of manganese photoCORMs.

Keywords: carbon monoxide, manganese, CORMs, photoCORMs, IR spectroscopy, EPR spectroscopy

1. Introduction

Research in recent years has clearly identified carbon monoxide (CO) as a potential therapeutic agent.[1-5] In order to reach an optimal effect and also to overcome the molecule's known toxicity at higher concentrations, the generation of a constant, low concentration of CO in the medium close to the pharmacological target is desirable. With this aim in mind, a number of carbon monoxide releasing molecules (CORMs) are under investigation to achieve an *in vivo* delivery of CO in beneficial quantities over extended time periods. Most studies have focused on the possibility to use metal carbonyl complexes as CORMs.[6-12] A well-examined example of these is CORM-3 ([RuCl(glycinato)(CO)₃]), known to release CO ligands when dissolved in water.[13] CORM-3 showed multiple beneficial properties in test systems when evaluated for example for antimicrobial,[14] anti-inflammatory[15] or organ preservation effects.[13] While the release of CO from a compound like CORM-3 starts immediately when the complex is dissolved in water, other carbonyl complexes are known where CORM-action is only observed upon irradiation of the molecules with light of an appropriate wavelength.[10, 16-22] Such photoCORMs thus have the potential advantage that CO release can be externally triggered to make a more controlled release of CO possible.

Manganese(I) *fac*-tricarbonyl complexes are a prominent class of photoCORMs and multiple studies on their light-induced CORM-activity have been carried out.[17-19, 23] Interestingly, we found no report where any manganese reaction intermediates or products of the CO release reaction were identified. The amount of produced carbon monoxide has routinely been determined using the myoglobin assay and this method provided lower limits for the number of produced CO molecules per manganese centre, with

reported numbers ranging between 1 to 2 CO per Mn.[24, 25] If these stoichiometries were correct, the reactions would result in the formation of di- or monocarbonyl complexes of manganese, respectively. Looking at the literature on $[\text{Mn}(\text{CO})_x]$ -compounds, such species should not be stable in an aqueous environment for extended time periods.[26] So it seems currently to be unknown what manganese containing reaction products are obtained following light-excitation of the $[\text{Mn}(\text{CO})_3]$ -compounds. Nevertheless, a better knowledge of the photoreaction products originating from manganese(I) tricarbonyl photoCORMs seems highly desirable in order to *a*) determine the exact number of CO released from each manganese complex and *b*) characterize the manganese reaction product (as this should not cause unwanted side-effects in a possible application).

Inspired by a recent investigation of CO release reactions of the tungsten(0) photoCORM $[\text{W}(\text{CO})_5(\text{tris}(\text{sulphonatophenyl})\text{phosphine})]^{3-}$ by Rimmer *et al.*,[20] we thus carried out a spectroscopic investigation on the photoreactions of two manganese(I) tricarbonyl complexes using UV/Vis and IR spectroscopy to identify possible reaction products. Additionally, we recorded EPR spectra of reaction mixtures for the course of light-triggered CO release. EPR spectroscopy is a very useful technique in manganese chemistry to characterize both Mn oxidation states and complex nuclearity [27]. As we suspected that a loss of the strongly π -accepting CO ligands could be accompanied by manganese oxidation,[26] paramagnetic species could form from the diamagnetic Mn^{I} precursor.

2. Materials and Methods

All reagents and solvents were purchased from commercial sources and used without further purification. The ligands tpm (*tris*(pyrazolyl)methane) and bpzaa (*bis*(pyrazolyl)acetic acid) as well as their manganese(I) carbonyl complexes $[\text{Mn}(\text{CO})_3(\text{tpm})](\text{PF}_6)$ (**1**) and $[\text{Mn}(\text{CO})_3(\text{bpzaa})]$ (**2**) were synthesized according to literature procedures.[17, 28] The solutions for irradiation experiments were prepared using analytical grade ethanol (Carl Roth GmbH) and deionized water ($>10\text{M}\Omega$ cm), respectively. Lyophilized myoglobin isolated from equine skeletal muscle was obtained from Sigma-Aldrich.

UV irradiation experiments to trigger CO release were in all cases carried out in 10 mm UV cuvettes (total volume 4 mL). A UV hand lamp (CAMAG, Switzerland, equipped with a Philips TUV G8 T5 fluorescent tube with 8W irradiation power), positioned at a distance of 10 cm from the solution, served as source for UV irradiation centred at $\lambda = 366$ nm. At defined intervals the irradiations were interrupted either for UV/Vis spectroscopic measurements or for the removal of parts of the solutions for IR or EPR spectroscopy.

Spectroscopy. UV/Vis spectra in solution were measured using a Varian Cary 5000 spectrometer. For IR analysis, 100 μ L of the reaction mixtures were filled into a 0.1 mm path length liquid-IR cell (Specac Omni cell) equipped with calcium fluoride windows (Korth Kristalle GmbH, transmittance >50% for the range of 1000 cm^{-1} - 65000 cm^{-1}). FT-IR spectra were then recorded on a Bruker VERTEX 70 spectrometer. X-band (9 GHz) electron paramagnetic resonance spectra were collected using a Bruker EMXplus spectrometer equipped with an Oxford Instrument ESR 900 cryostat and a dual mode cavity (Bruker ER-4116DM) at 5 K. EPR data were recorded in both parallel and perpendicular mode detection on the same sample tube containing 200 μ L of frozen solution removed from the illumination reaction at the indicated time intervals.

Deoxy-myoglobin/carbonmonoxy-myoglobin assay.[25] A stock solution of myoglobin (75 μ M final concentration) was freshly prepared by dissolving the protein in 0.1 M phosphate buffer (pH = 7.4). The solution was degassed by nitrogen purging and an excess of sodium dithionite was then added to remove dissolved O_2 and to completely convert the myoglobin to its deoxy-form. Dimethylsulfoxide solutions of either complex **1** or **2**, respectively, were now added to the 75 μ M deoxy-myoglobin solutions in UV cuvettes (pathlength 10 mm) to obtain final concentrations of the manganese compounds of 20 μ M in a total volume of 3 mL. The cuvettes were sealed with a Teflon stopper to prevent CO escape and the exposure to air. Solutions were then irradiated at 366 nm with the UV hand lamp (see above) positioned at a distance of 10 cm from the cuvette and UV/Vis spectra were recorded every five minutes. As introduced by Fairlamb *et al.*,[25] additional solutions of **1** or **2** were prepared exactly as described above

without added Mb and illuminated in parallel. These cuvettes served as reference samples in the dual-beam UV/Vis spectrometer to correct for the spectral changes caused by the illuminated manganese species on their own.

3. Results and Discussion

Two closely related manganese(I) tricarbonyl complexes were selected for this study on light-triggered carbon monoxide release. The first, $[\text{Mn}(\text{CO})_3(\text{tpm})](\text{PF}_6)$ (**1**), has already been studied in detail by the Schatzschneider group as isolated complex molecule,[17] in the form of bioconjugates (where **1** was successfully connected to oligopeptides)[19] and also adsorbed on SiO_2 nanoparticles to achieve improved drug delivery.[29] The neutral, structurally closely related complex $[\text{Mn}(\text{CO})_3(\text{bpzaa})]$ (**2**), is closely related to **1** in structure but has so far not been studied for photoCORM activity. By studying its photoCORM activity we wanted to see to which extent small variations of the overall charge or the manganese ligand sphere influence CO release reactivity.

Scheme 1 here

Previous studies on **1** had shown that the irradiation of the complex with UV light ($\lambda = 365 \text{ nm}$) causes the release of at least 1.96 CO molecules per complex within 100 min, as indicated by the analyses of myoglobin assays.[17] To make a correlation of our results with these previous reports possible, we employed very similar conditions for the light reactions here as reported before, thus also illuminating our sample solutions of **1** and **2** in quartz cuvettes using (as in the previous study [17]) a standard laboratory UV lamp with a $\lambda = 366 \text{ nm}$ emission maximum as light source. Such an irradiation procedure is of course rather ill defined and it thus not possible to obtain photochemical data like quantum yields from our experimental results.

The solubility of **1** or **2** in aqueous buffer is sufficient to detect CO release using the myoglobin assay, as CO concentrations of the order of $10 \mu\text{M}$ can be detected using this methodology. For spectroscopic

investigations of the products of CO release from **1** or **2** we changed the solvent system to ethanol or 9:1 ethanol:water mixtures. This enabled us able to dissolve the complexes in millimolar concentrations in a protic and also water-containing environment which we considered to be important for a possible transfer of our results to processes in cell media.

3.1 Detection of released carbon monoxide by deoxy-myoglobin assays

Spectra recorded for the detection of liberated CO by the “classical” deoxy-myoglobin assay[24] are shown in Figure 1. It is clearly visible that CO release takes place during UV irradiations of solutions of both **1** and **2**, as the characteristic spectral changes known for the conversion of deoxy-myoglobin (Mb) to carbonmonoxy-myoglobin (MbCO) are observed. This reactivity was known for complex **1** and we observed the reaction here as well. We also find similar kinetics as previously reported[17] and also detect that the reaction needs about ~90 min to reach it final state.

Fig. 1 here

It is a new - but due to its similar structure not unexpected - result that the neutral carbonyl complex **2** is also an active photoCORM like **1**. It is clearly visible from the right spectrum of Figure 1 that CO release from **2** occurs faster then from **1**. For example, the Mb absorbance at 557nm after 30 min. is already distinctly lower for the experiment with **2** and the spectrum reaches its final appearance already after about 45 min. Additionally, the MbCO absorption bands at 540 and 576 nm reach higher maxima after 90 min of irradiation time for **2** in comparison to **1**.

As already mentioned, the lower estimate for the number of released CO molecules for **1** from myoglobin assays has been given as close to 2 CO per Mn.[17] For a quantitative analysis, the absorbance at the position of the bands for the MbCO product of the reaction is usually determined and [MbCO] is then calculated using the absorption coefficient for MbCO at 540 nm ($\epsilon_{540}(\text{MbCO})=15400 \text{ M}^{-1} \text{ cm}^{-1}$).[17, 24, 25] An analysis of the UVVis spectra shown in Figure 1 reveals that over 90 min, **1** and **2** release 2.4 and 2.5 equivalents of CO per complex, respectively. However, a recent, very careful analysis of the

various ways of calculating CO equivalents from the data of myoglobin assays indicates that this method contains various possibilities for analytical errors and that it is also not well suited for detailed kinetic investigations.[25] For example, the analysis of the traces measured for **1** by us yield a higher value than the 1.96 equivalents reported previously [17], even though identical reaction conditions were employed.

In consequence, even though a very valuable tool, the myoglobin assay seemed to us insufficient as single method to analyse the photoCORM reactivities of **1** and **2**. To gain further insights, we therefore carried out spectroscopic experiments on irradiated solutions of **1** and **2** using UV/Vis, IR and EPR spectroscopy which are described in the following.

3.2 UV/Vis monitoring of the photoCORM reaction

Solutions of complexes **1** and **2** in ethanol or EtOH:H₂O = 9:1 show very similar absorption spectra (Fig. 2, see traces for 0 min), dominated by a broad absorption band between 300 and 450 nm. The absorption maximum is found at slightly lower wavelength for **1** (349 nm) than for **2** (361 nm), but for both maxima similar extinction coefficients are found ($\epsilon_{349}(\mathbf{1})=2150 \text{ M}^{-1} \text{ cm}^{-1}$; $\epsilon_{361}(\mathbf{2})=1790 \text{ M}^{-1} \text{ cm}^{-1}$) that also correspond well with literature values.[22] Thus both complexes strongly absorb the light of 366 nm used during our illumination experiments. For **1** this absorption has been assigned to originate from a mixed MM/MLCT excitation. The excited state of the complex is thought to feature additional electron density in molecular orbitals of antibonding metal–carbonyl character and therefore CO release from the excited complex is facilitated.[22]

Fig. 2 here

As Figure 2 shows, a continuous UV-illumination ($\lambda=366 \text{ nm}$) of **1** or **2** in solution causes the disappearance of these broad absorption bands in both cases. Rather featureless spectra with weak absorptions over the entire 350-650 nm region are reached within 10 to 15 min and thus much faster than expected from the kinetics of the deoxy-myoglobin assay shown above, where 90 min of reaction time were required to reach the end spectrum. However, this could be an effect of the solvent system as we find

for both complexes that reactions in pure ethanol are faster than for EtOH/H₂O mixtures (Fig. 2, dotted vs. solid lines). Alternatively, the presence of oxygen as an oxidation agent for Mn^I (see section 3.4 below) could explain the faster reaction rates found here. While we carried out all experiments in the presence of air (which seemed appropriate in the context of a possible transfer of our results to photoCORM behaviour in a cell environment), the myoglobin assays had to be performed in anaerobic media as the protein has to be present in its deoxy-form. The CO release reaction in the Mb-assay could thus be significantly slower than observed here by UVVis spectroscopy in ethanol either due to the influence of the solvent or the influence of oxygen.

A comparison of the series of spectra recorded for complexes **1** and **2** (Fig. 2) reveals two interesting differences. Firstly, the transformation from the start to the end spectra is again proceeding faster for complex **2** in comparison to **1**, in agreement with the trend observed in the myoglobin assays. Additionally, an isosbestic point at 429 nm is observed for the spectral changes accompanying the reactions of complex **2** both in the presence and absence of water, indicating direct reactions of **2** into its photoproduct(s). For **1**, the situation in the spectral region between 375 and 450 nm is more complex, so that intermediate species might be formed as reaction intermediates.

3.3 Characterization of manganese carbonyl compounds by IR spectroscopy

IR spectroscopy is the “textbook tool” to investigate metal carbonyl compounds[30] and it was therefore a surprise to us that IR had so far not been used to study CO release from manganese(I) tricarbonyl photoCORMs. Recent publications concerning the CORM reactivities of [W⁰(CO)₅][20] and [Mn^I(CO)₄][7] moieties indicated that IR spectroscopy can yield important information in this context. We therefore recorded solution IR spectra during the course of photoreactions using the identical irradiation setup as described in the previous section for the UV/Vis studies. Again, solutions of **1** and **2** in EtOH or EtOH:H₂O = 9:1 were prepared and illuminated in quartz cuvettes using 366 nm light. At certain time intervals, solution samples of the reaction mixtures were filled into a liquid IR cell to record IR spectra. The results for both complexes are shown in Figure 3.

Fig. 3 here

Prior to illumination, spectra typical for manganese(I) *fac*-tricarbonyl complexes are observed.[30] These show one sharp IR band is found around 2050 cm^{-1} and two additional bands are located between 1930 and 1970 cm^{-1} which are - as expected - more resolved for compound **2** or than for **1**, as the latter bears a ligand of higher symmetry and thus comes closer to an ideal C_{3v} case. In general, the carbonyl vibrations of **2** are detected at lower wavenumbers than the corresponding bands of **1**. This indicates stronger backbonding into the CO ligands for **2**, possibly a result of the difference in overall charge between **1** (a positively charged complex) and **2** (neutral).

During UV-illumination, these strong IR bands of the initial complexes disappear with half-lives of about 10-15 min. (Fig. 3, see also insets), indicating that the $[Mn^I(CO)_3]$ -units of **1** and **2** dissociate. Again, the kinetics for this process are faster for complex **2** when compared to **1**. In accordance with the UV/Vis results, we also detect here that the addition of water slows down the reaction of compound **2**, while this effect is not observed for the IR kinetics of **1**.

However, the most interesting result of the IR experiments is the detection of small new IR bands emerge in the region between 1850 and 1875 cm^{-1} observed at the beginning of the photoreactions. These signals completely disappear again after 30 min of UV-irradiation time. From comparisons with known data on cymantrene ($[Mn(CO)_3Cp]$) and its $[Mn(CO)_2Cp(solvent)]$ analogue,[31] we tentatively take these vibrations as an indication for the formation of manganese(I) *cis*-dicarbonyl intermediates. Such compounds should also show a second IR band at 1950 - 1980 cm^{-1} which we are unfortunately unable to detect as they would be hidden under to the very strong IR-absorption of the initial complexes **1** and **2** in this region. Also, we do not detect any free CO at no time during the entire course of the photolysis. Its signal would be expected at $\sim 2140\text{ cm}^{-1}$ but as the signal of the uncoordinated molecule is very weak in the IR,[30] it escapes detection here (see ESI, Fig. S1).

Nevertheless, we can conclude from the IR data that UV-irradiations of both complexes **1** and **2** initially result in the intermediate formation of *cis*- $[Mn^I(CO)_2]$ -species which reach a greater maximum

concentration for **1** than for **2** (Fig. 3). This difference nicely matches the observation of an isosbestic point only for compound **2**, which indicated already in the the UV/Vis results discussed above that the photoreaction of **2** proceeds to its final products without the build-up of significant concentrations of intermediates.

After photolyses of 30 min or longer, no manganese carbonyl vibration can be observed by IR any more in the spectroscopically accessible solvent window between 1800 and 2500 cm^{-1} for neither complex, indicating that most likely all metal bound CO molecules have been released into the medium at this time.

3.4 Detection of manganese decarbonylation products by EPR spectroscopy

EPR spectroscopy is a powerful method to identify both manganese oxidation states and the nuclearity of Mn-compounds.[27, 32-34] Due to the coupling of the complexes' unpaired electrons with the $I = 5/2$ spin of the ^{55}Mn nucleus, characteristic six-line EPR signals can be observed for mononuclear Mn^{II} , Mn^{III} or Mn^{IV} coordination compounds. Because manganese moieties additionally have a strong tendency to form dinuclear species for oxidation states of $\text{Mn}^{\geq\text{II}}$ in the presence of water or alcohols, characteristic multiline EPR signals are also known for dinuclear $\text{Mn}_2^{\text{II,II}}$, $\text{Mn}_2^{\text{II,III}}$, and $\text{Mn}_2^{\text{III,IV}}$ units where the Mn centres couple via bridging oxygen ligands.

Fig. 4 here

As shown in Figure 4, both Mn^{I} complexes **1** and **2** are EPR silent (see spectra for 0 min.) – as expected for d^6 low-spin systems. But already after an UV-irradiation time of 5 min. clearly visible six-line EPR signals are observed for frozen EtOH/ H_2O solution samples at a measurement temperature of 5 K. These signals are centred at $g \approx 2$ and have a total signal width of about 800 G which is the typical spectral signature of mononuclear Mn^{II} coordination compounds. The six lines which dominate the spectrum originate from the hyperfine interaction of the ^{55}Mn nucleus ($I = 5/2$) with the unpaired electrons. Additionally, a number of forbidden transitions can be observed for the $S = 5/2$ spin system of the Mn^{II} (d^5), which have been described in detail elsewhere.[35] A theoretical calculation of a spectrum using

typical values for g-factor, hyperfine interaction **A** and zero-field splitting parameters **D** and **E** yielded a simulation which reproduces the key features of the observed EPR signal rather well (see ESI, Fig. S1). However, a deeper understanding of the electron spin interactions would require much more elaborate EPR spectroscopy than the CW X-band EPR data presented here as has been demonstrated by Stich *et al.*[35]

During the photoreactions the Mn^{II} six-line signals initially rise to reach maximum intensities after irradiation times of 30 (for **1**) or 10 min (for **2**). After this, the height of the six-line signals decrease again without the appearance of new EPR features. This effect is also observed for complexes dissolved in pure ethanol where the spectra are less well resolved (see ESI, Fig. S3). Judging from the size of the six-line signals, the amounts of generated intermediate mononuclear Mn^{II} species are about twice as high for photoreactions of **1** in comparison to **2** (Fig. 4). In both cases the EPR signals decrease again for extended illumination times, reaching in both cases only about 70% of their highest values for samples which have been irradiated for 60 min.

Mononuclear Mn^{III} compounds can also be identified by EPR, but for this the parallel detection mode has to be employed. We thus recorded parallel mode EPR spectra for all samples as well but did not find major Mn^{III} signals at any time for the photoreactions. Very small parallel mode signals can be detected (see ESI, Fig. S4 and S5), some also showing the expected six-line interactions with the Mn nucleus, but from their small size we conclude that mononuclear Mn^{III} species play no important role in the CO release reactions of neither **1** nor **2**. The same seems to be true for potential Mn₂^{II,II} or Mn₂^{II,III} intermediates: as none of the multiline EPR signals characteristic for these species[27] were found, they apparently do not represent major reaction products. However, the EPR results for example do not exclude the formation of electronically strongly μ -oxido coupled dinuclear Mn₂^{III,III} or Mn₂^{IV,IV} products,[36, 37] as these species are known to be EPR silent [27] and can thus not be detected by X-band EPR.

3.5 Possible reaction products following the photoCORM reactions

Based on the results of the spectroscopic investigations presented in the previous sections, we propose a sequence of possible reactions for **1** and **2** following light-induced CO loss as depicted in Scheme 2. After excitation by UV-light (Scheme 2, reaction ①) one carbon monoxide ligand is labilized and released in reaction ②. This yields the intermediate manganese(I) dicarbonyl species detected by IR spectroscopy. At the illumination conditions of this study, the time-scale for the combined reactions ① and ② is 15 to 20 min during which both the broad UV charge transfer band and the tricarbonyl IR signals disappear (Figs. 2 and 3). The removal of the first carbonyl ligand is then quickly followed by the loss of the other two COs and manganese oxidation to Mn^{II} and beyond (reaction ③). These steps are clearly indicated by the complete disappearance of the intermediate [Mn(CO)₂]-signal in the IR after 40 min photolysis time (Fig. 3) as well as the evolving characteristic Mn^{II} EPR spectra, which reach their maximum intensities after 30 min (**1**) and 10 min (**2**), respectively (Fig. 4). Whether oxygen is the oxidation agent for manganese oxidation has to be elucidated in more detailed experiments in the future. However, we can conclude that the presence of O₂ is not essential for the actual CO releasing processes ① and ②, as the results from the (oxygen free) myoglobin assays proved that the release of more than two CO per complex also occurs in oxygen-free solutions.

Scheme 2 here

Finally, reaction times of an hour and beyond yield species for which we neither find CO signals in the IR nor new EPR signals involving manganese. At this point the solutions have a reddish colour but do not show any signs of manganese oxide precipitates. Looking at typical reactions for manganese moieties bearing multidentate ligands like tpm or bpzaa,[36, 37] we think it most likely that dinuclear Mn^{III}₂-complexes are formed in a final process ④. Our data does not provide information on the exact composition of these products. However, the reaction conditions and the fact that the final product is EPR-

silent in both the parallel and the perpendicular detection mode can be taken as a good indication that the final species could very well be composed of di- or even tetranuclear μ -oxido or μ -alkoxy Mn^{III} -cores.

The reaction sequence presented in Scheme 2 might also explain the different reaction kinetics observed by the individual spectroscopic methods. The fast disappearance of the UV and IR bands of the original complexes **1** and **2** would be the result of reactions ① and ②. The oxidation reactions yielding EPR active Mn^{II} products are slower, as they are formed by reactions ① - ③. Finally, the build-up of a maximum carbonmonoxy-myoglobin concentration (Fig. 1) takes longer still, as the route to MbCO formation involves reactions ① - ③ and additionally the subsequent binding of the released CO to Mb (reaction ⑤).

In general, it should also be noted that our reaction Scheme 2 for the manganese complexes **1** and **2** resembles the one recently presented for the processes involved in light-triggered CO release from the tungsten carbonyl complex $[W(CO)_5(tris(sulphonatophenyl)phosphine)]^3$.^[20] The authors of that investigation also observed that UV irradiation of the complex first triggered the release of only one of the CO ligands which was then followed by the oxidation of the tungsten centre and the release of further carbon monoxide molecules. The series of processes shown in Scheme 2 could therefore be considered as an example of a more general photoCORM reaction sequence.

4. Conclusions

The results of this study clearly demonstrate that the combination of different spectroscopic techniques (UV/Vis, IR, EPR) offers a much more complete picture of the processes leading to light-triggered CO release than the use of the classical myoglobin assay on its own. The photolysis of the $[Mn(CO)_3]$ -photoCORMs **1** and **2** is for both complexes a stepwise process involving at least two CO releasing steps which are additionally accompanied by the oxidation of the manganese centre to Mn^{II} and beyond. Manganese dicarbonyl species are involved as reaction intermediates but such complexes are not the final product of the photoCORM reactions. From our myoglobin assay data, the IR evidence and also from the

fact that water- and air-stable manganese *monocarbonyl* complexes are to the best of our knowledge unknown, we conclude that each complex **1** or **2** eventually yields three equivalents of CO after longer reaction times. This is more CO than previously estimated by photoCORM activity tests using the myoglobin assay. To us the most likely manganese products which are eventually formed are μ -O-Mn^{III}-complexes, for which we can provide so far only indirect evidence.

Future studies on photoCORMs like **1** or **2** should thus try to identify the nature of the generated manganese products e.g. by HPLC and / or ESI-MS. They represent the by-product of a potential photoCORM therapy and therefore have to be non-toxic to be tolerated *in vivo*. As stated above, it is also necessary to carry out more detailed experiments to clarify the possible role of O₂ in the manganese oxidation processes. Finally, we would like to note from a synthetic point of view that the reaction sequence of Scheme 2, if correct, could be very useful as an entirely new approach to synthesize dinuclear manganese(\geq +III) complexes from manganese(I) carbonyl precursors. For all these reasons investigations on this potential synthetic route as well as a more detailed characterization of the μ -O-Mn^{III}₂- products of the process are the topic of current investigations in our laboratory.

Acknowledgements

The authors thank Ursula Cornelissen, Stefanie Pehlke and Hanne Jacob (all Institute for Inorganic Chemistry, CAU Kiel) for experimental support and Nele Hermer, Friederike Schulz, Jessica Hamann and Svenja Harm for their help as part of advanced inorganic chemistry lab projects. Henning Broda (also from our institute) carried out simulations of the EPR spectra. This work was financially supported by the Fonds der Chemischen Industrie (Liebig fellowship of PhK) and the Christian-Albrechts-University Kiel.

Appendix A. Supplementary material

References

- [1] R.E. Bigler, G. Sgouros, *J. Nucl. Med.*, 24 (1983) 431-437.
- [2] L. Wu, R. Wang, *Pharmacol. Rev.*, 57 (2005) 585-630.
- [3] R.A. Dercho, K. Nakatsu, R.J. Wong, D.K. Stevenson, H.J. Vreman, *J. Pharmacol. Toxicol. Methods*, 54 (2006) 288-295.
- [4] S.W. Ryter, J. Alam, A.M. Choi, *Physiol. Rev.*, 86 (2006) 583-650.
- [5] R. Motterlini, L.E. Otterbein, *Nat. Rev. Drug Discov.*, 9 (2010) 728-743.
- [6] D.E. Bikiel, E.G. Solveyra, F. Di Salvo, H.M.S. Milagre, M.N. Eberlin, R.S. Correa, J. Ellena, D.A. Estrin, F. Doctorovich, *Inorg. Chem.*, 50 (2011) 2334-2345.
- [7] S.H. Crook, B.E. Mann, A.J.H.M. Meijer, H. Adams, P. Sawle, D. Scapens, R. Motterlini, *Dalton Trans.*, 40 (2011) 4230-4235.
- [8] R.P. Doyle, M.D. Bartholoma, A.R. Vortherms, S. Hillier, J. Joyal, J. Babich, J. Zubieta, *Dalton Trans.*, 40 (2011) 6216-6225.
- [9] M.A. Gonzalez, N.L. Fry, R. Burt, R. Davda, A. Hobbs, P.K. Mascharak, *Inorg. Chem.*, 50 (2011) 3127-3134.
- [10] C.R. Child, S. Kealey, H. Jones, P.W. Miller, A.J.P. White, A.D. Gee, N.J. Long, *Dalton Trans.*, 40 (2011) 6210-6215.
- [11] S. Romanski, B. Kraus, U. Schatzschneider, J.M. Neudorfl, S. Amslinger, H.G. Schmalz, *Angew. Chem. Int. Ed.*, 50 (2011) 2392-2396.
- [12] F. Zobi, O. Blacque, *Dalton Trans.*, 40 (2011) 4994-5001.
- [13] J.E. Clark, P. Naughton, S. Shurey, C.J. Green, T.R. Johnson, B.E. Mann, R. Foresti, R. Motterlini, *Circ. Res.*, 93 (2003) e2-e8.
- [14] M. Desnard, K.S. Davidge, O. Bouvet, D. Morin, D. Roux, R. Foresti, J.D. Ricard, E. Denamur, R.K. Poole, P. Montravers, R. Motterlini, J. Boczkowski, *FASEB J.*, 23 (2009) 1023-1031.
- [15] P. Urquhart, G. Rosignoli, D. Cooper, R. Motterlini, M. Perretti, *J. Pharmacol. Exp. Ther.*, 321 (2007) 656-662.
- [16] I. de Aguiar, S.D. Inglez, F.C.A. Lima, J.F.S. Daniel, B.R. McGarvey, A.C. Tedesco, R.M. Carlos, *Inorg. Chem.*, 47 (2008) 11519-11526.
- [17] J. Niesel, A. Pinto, H.W. Peindy N'Dongo, K. Merz, I. Ott, R. Gust, U. Schatzschneider, *Chem. Commun.*, (2008) 1798-1800.
- [18] P.C. Kunz, W. Huber, A. Rojas, U. Schatzschneider, B. Spingler, *Eur. J. Inorg. Chem.*, (2009) 5358-5366.
- [19] H. Pfeiffer, A. Rojas, J. Niesel, U. Schatzschneider, *Dalton Trans.*, (2009) 4292-4298.
- [20] R.D. Rimmer, H. Richter, P.C. Ford, *Inorg. Chem.*, 49 (2010) 1180-1185.
- [21] C.S. Jackson, S. Schmitt, Q.P. Dou, J.J. Kodanko, *Inorg. Chem.*, 50 (2011) 5336-5338.
- [22] U. Schatzschneider, *Inorg. Chim. Acta*, 374 (2011) 19-23.
- [23] K. Meister, J. Niesel, U. Schatzschneider, N. Metzler-Nolte, D.A. Schmidt, M. Havenith, *Angew. Chem. Int. Ed.*, 49 (2010) 3310-3312.
- [24] R. Motterlini, J.E. Clark, R. Foresti, P. Sarathchandra, B.E. Mann, C.J. Green, *Circ. Res.*, 90 (2002) e17-e24.
- [25] A.J. Atkin, J.M. Lynam, B.E. Moulton, P. Sawle, R. Motterlini, N.M. Boyle, M.T. Pryce, I.J.S. Fairlamb, *Dalton Trans.*, 40 (2011) 5755-5761.
- [26] N.N. Greenwood, A. Earnshaw, *Chemistry of the Elements*, Butterworth-Heinemann, Oxford, Woburn, 1998.
- [27] P. Huang, P. Kurz, S. Styring, *Appl. Magn. Reson.*, 31 (2007) 301-320.
- [28] N. Burzlaff, I. Hegelmann, B. Weibert, *J. Organomet. Chem.*, 626 (2001) 16-23.
- [29] G. Dördelmann, H. Pfeiffer, A. Birkner, U. Schatzschneider, *Inorg. Chem.*, 50 (2011) 4362-4367.

- [30] K. Nakamoto, *Infrared and Raman Spectra of Inorganic and Coordination Compounds*, John Wiley & Sons, Hoboken, 2009.
- [31] J.A. Calladine, S.B. Duckett, M.W. George, S.L. Matthews, R.N. Perutz, O. Torres, K.Q. Vuong, *J. Am. Chem. Soc.*, 133 (2011) 2303-2310.
- [32] K.O. Schäfer, R. Bittl, F. Lenzian, V. Barynin, T. Weyhermüller, K. Wieghardt, W. Lubitz, *J. Phys. Chem. B*, 107 (2003) 1242-1250.
- [33] L. Dubois, J. Pecaut, M.F. Charlot, C. Baffert, M.N. Collomb, A. Deronzier, J.M. Latour, *Chem. Eur. J.*, 14 (2008) 3013-3025.
- [34] T.A. Stich, J.W. Whittaker, R.D. Britt, *J. Phys. Chem. B*, 114 (2010) 14178-14188.
- [35] T.A. Stich, S. Lahiri, G. Yeagle, M. Dicus, M. Brynda, A. Gunn, C. Aznar, V.J. DeRose, R.D. Britt, *Appl. Magn. Reson.*, 31 (2007) 321-341.
- [36] M.N. Collomb, A. Deronzier, *Eur. J. Inorg. Chem.*, (2009) 2025-2046.
- [37] S. Mukhopadhyay, S.K. Mandal, S. Bhaduri, W.H. Armstrong, *Chem. Rev.*, 104 (2004) 3981-4026.

Figures and Schemes

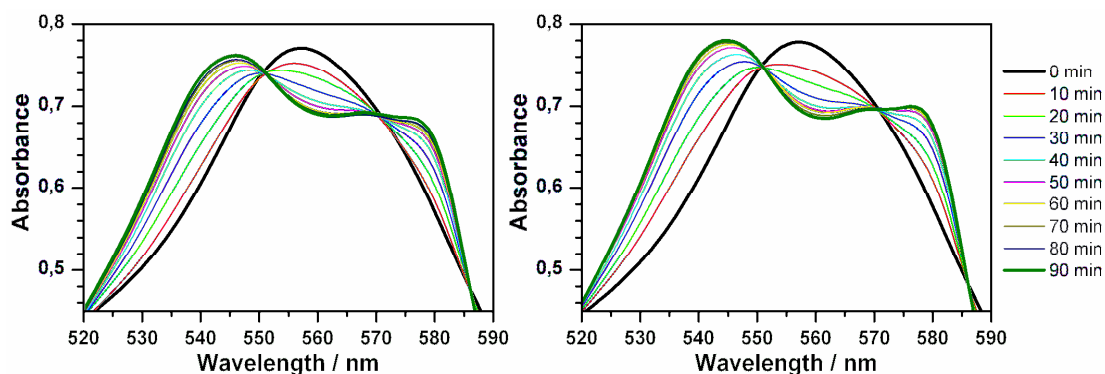


Figure 1. UV/Vis spectra demonstrating the conversion of deoxy-myoglobin (Mb, start spectrum, bold black lines) to carbon monoxide myoglobin (MbCO) caused by the binding of CO released from complexes **1** (left) and **2** (right) to Mb after UV light excitation. See materials and methods for details.

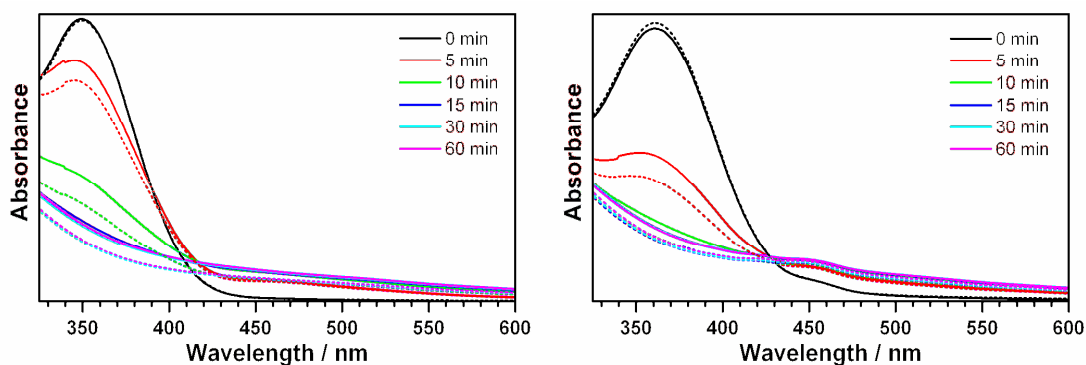


Figure 2. Changes of the UV/Vis spectra for 1 mM solutions of **1** (left) or **2** (right) during the course of continuous UV illuminations ($\lambda=366$ nm, as indicated by vertical dashed line). Solid lines show spectra recorded for solutions in EtOH:H₂O = 9:1 mixtures, dotted lines for reactions in pure ethanol.

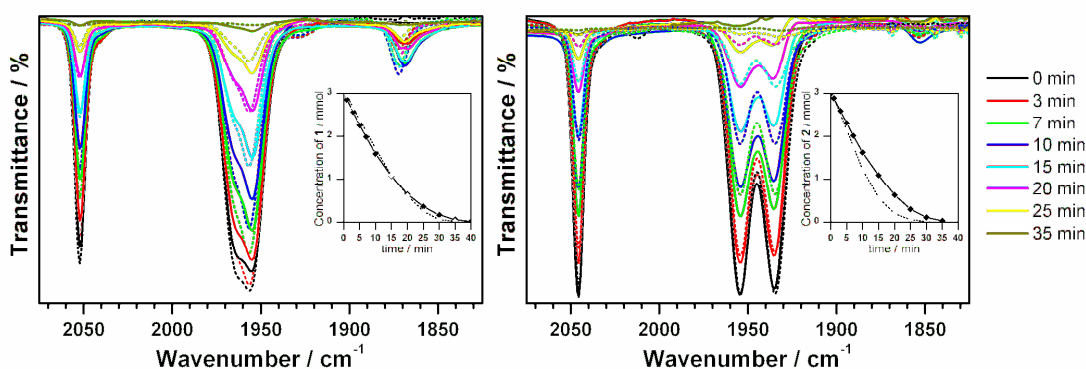


Figure 3. Infrared spectra for 3 mM solutions of **1** (left) or **2** (right) during UV-light-triggered CO release. Solid lines show spectra recorded for solutions in mixtures EtOH:H₂O = 9:1, dotted lines for reactions in pure ethanol. *Insets:* quantifications for the amounts of remaining tricarbonyl species as a function of illumination time. The sharp IR bands at 2052 or 2045 cm⁻¹ were used to determine the concentrations of **1** or **2**, respectively.

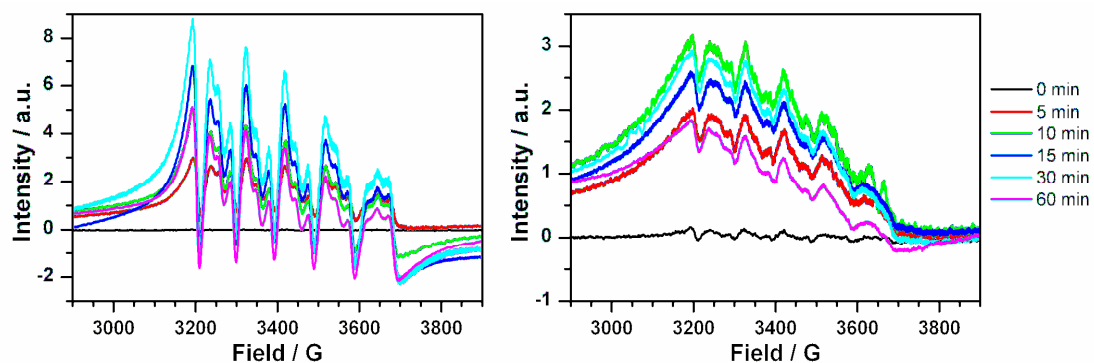
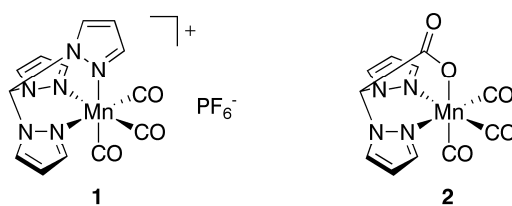


Figure 4. X-band EPR spectra of frozen solutions (1 mM complex in mixtures EtOH:H₂O = 9:1, T = 5 K) of **1** (left) or **2** (right) for the course of UV-light-photolysis. EPR settings: microwave power: 2 mW, modulation amplitude 5 G.



Scheme 1. Structures of the manganese(I) tricarbonyl photoCORMs [Mn(CO)₃(tpm)](PF₆) (**1**) and [Mn(CO)₃(bpzaa)] (**2**) investigated in this study.

Supplementary Information

Investigation of Light-Triggered Carbon Monoxide Release from Two Manganese PhotoCORMs by IR, UV/Vis and EPR Spectroscopy

Hans-Martin Berends and Philipp Kurz*

Institute for Inorganic Chemistry, Christian-Albrechts-University Kiel, Max-Eyth-Straße 2,
24118 Kiel, Germany

Fax: (+49) 431-880-1520

E-mail: *phkurz@ac.uni-kiel.de*

Figure S1. Infrared spectra for 3 mM solutions of **1** (left) or **2** (right) during UV-light-triggered CO release. Solid lines show spectra recorded for solutions in mixtures EtOH:H₂O = 9:1, dotted lines for reactions in pure ethanol. In neither case a signal indicative of unbound CO (~2140 cm⁻¹) can be detected. The signals between 2300 and 2400 cm⁻¹ originate from CO₂ in the laboratory atmosphere.

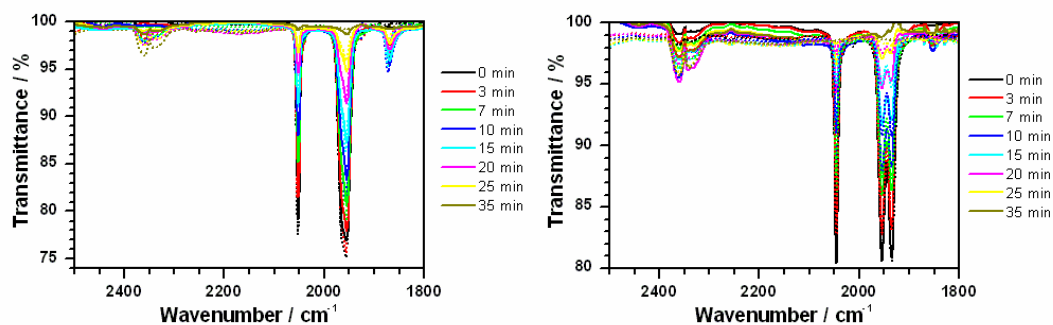
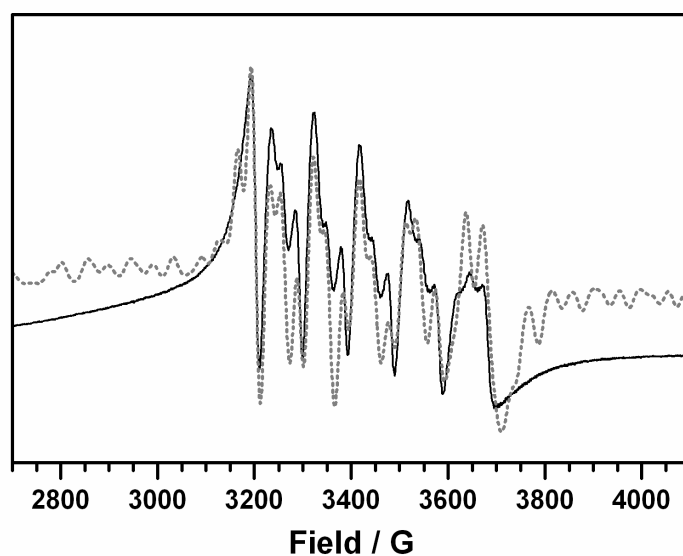


Figure S2. Experimental (solid line) and simulated (dotted line) X-band EPR spectra for **1** after irradiation time of 30 min in EtOH:H₂O = 9:1. Simulation parameters obtained using the “pepper” fitting function of the *EasySpin* simulation software [1] are: $g = [2.001, 1.997, 1.996]$; $A = 266$ MHz; $D = 566$ MHz; $E = 151$ MHz; linewidth = 22 G.



[1] S. Stoll, A. Schweiger, *J. Magn. Reson.*, 178 (2006) 42-55.

Figure S3. Perpendicular X-band EPR spectra of frozen solutions (1 mM complex in pure ethanol, T = 5 K) of **1** (left) or **2** (right) for the course of UV-light-photolysis. EPR settings: microwave power: 2 mW, modulation amplitude 5 G.

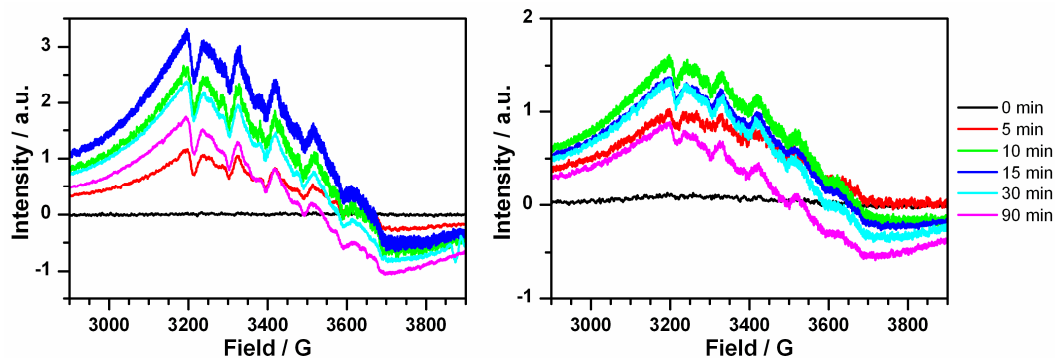


Figure S4. Parallel X-band EPR spectra of frozen solutions (1 mM complex in pure ethanol, T = 5 K) of **1** (left) or **2** (right) for the course of UV-light-photolysis. EPR settings: microwave power: 20 mW, modulation amplitude 5 G.

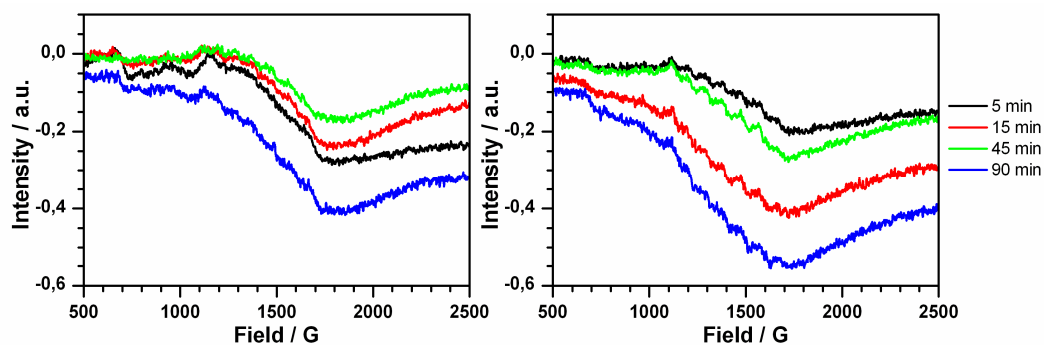
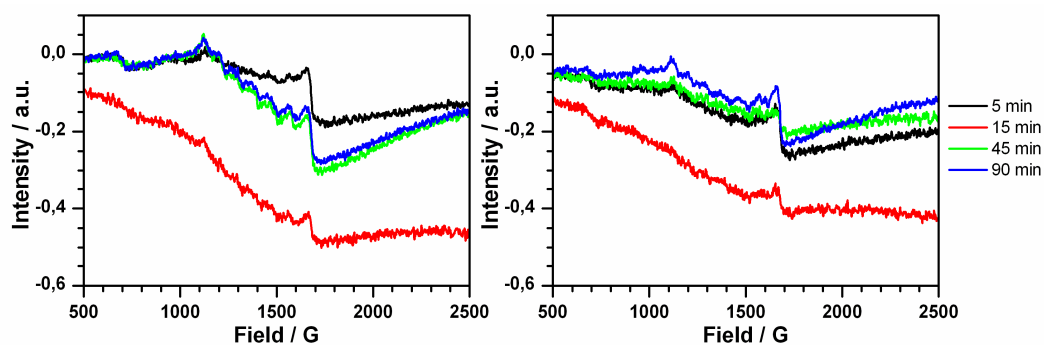


Figure S5. Parallel X-band EPR spectra of frozen solutions (1 mM complex in pure ethanol, T = 5 K) of **1** (left) or **2** (right) for the course of UV-light-photolysis. EPR settings: microwave power: 20 mW, modulation amplitude 5 G.



Paper IV.

Water Oxidation Catalysed by
Manganese Compounds: From
Complexes to “Biomimetic Rocks”

Water oxidation catalysed by manganese compounds: from complexes to 'biomimetic rocks'[†]

Mathias Wiechen, Hans-Martin Berends and Philipp Kurz*

Received 16th August 2011, Accepted 29th September 2011

DOI: 10.1039/c1dt11537e

One of the most fundamental processes of the natural photosynthetic reaction sequence is the light-driven oxidation of water to molecular oxygen. *In vivo*, this reaction takes place in the large protein ensemble Photosystem II, where a μ -oxido-Mn₄Ca- cluster, the oxygen-evolving-complex (OEC), has been identified as the catalytic site for the four-electron/four-proton redox reaction of water oxidation. This Perspective presents recent progress for three strategies which have been followed to prepare functional synthetic analogues of the OEC: (1) the synthesis of dinuclear manganese complexes designed to act as water-oxidation catalysts in homogeneous solution, (2) heterogeneous catalysts in the form of clay hybrids of such Mn₂-complexes and (3) the preparation of manganese oxide particles of different compositions and morphologies. We discuss the key observations from the studies of such synthetic manganese systems in order to shed light upon the catalytic mechanism of natural water oxidation. Additionally, it is shown how research in this field has recently been motivated more and more by the prospect of finding efficient, robust and affordable catalysts for light-driven water oxidation, a key reaction of artificial photosynthesis. As manganese is an abundant and non-toxic element, manganese compounds are very promising candidates for the extraction of reduction equivalents from water. These electrons could consecutively be fed into the synthesis of "solar fuels" such as hydrogen or methanol.

Introduction

We live on a planet dominated by the presence of water, H₂O. Large parts of the Earth are covered by oceans, lakes or sea ice, continental landscapes are shaped by rivers or glaciers, and rain, snowfall, clouds (or the lack of them!) influence our everyday lives.

Most importantly, due to its abundance on Earth, water has emerged during evolution as the "solvent of life": all living organisms require water to survive because fundamental biochemical reactions take place in aqueous solution.¹ For many enzymes such as hydrolases or carbonic anhydrase, water molecules even constitute the substrates of their catalysed reactions and are thus more than just a reaction medium. However, for the vast majority of such water-involving processes *in vivo*, the H₂O molecules themselves are not involved in redox reactions, meaning that hydrogen and oxygen ions derived from water retain their H⁺ and O^{-II} oxidation states in the course of the transformations. In fact, the potential range where water is redox stable at pH = 7

(−0.4 to +0.8 V) defines the span where most of redox processes in organisms occur, the 'redox spectrum of life'.²

This Perspective will focus on a unique reaction in nature where water is the substrate of an oxidation reaction: the oxidation of H₂O to O₂ which is part of the complex sequence of reactions constituting photosynthesis.^{1,3} Nature has developed just one, strictly conserved catalyst for this process as all cyanobacteria, algae and higher plants capable of water oxidation use an identical manganese-containing oxido-cluster as catalyst, the oxygen-evolving-complex (OEC) or water-oxidising-complex (WOC) of the multi-domain membrane enzyme Photosystem II.^{1,3}

After an introduction to key features of the enzymatic catalytic site, we will describe three different approaches followed by bioinorganic chemists (including us) over the last 40 years with the aim to synthesise manganese model compounds as functional water-oxidation catalysts. In addition to the fundamental interest in this reaction, we will also describe how the focus of studies in this field has somewhat shifted in recent years. Water-oxidation catalysis is a key reaction of artificial photosynthesis schemes and these have gained more and more attention in times when the global community becomes increasingly aware of the problems associated with climate-change and energy insecurity.^{4,5}

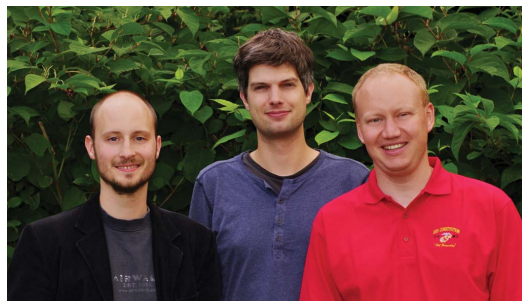
Institute for Inorganic Chemistry, Christian-Albrechts-University Kiel, Max-Eyth-Straße 2, 24118, Kiel, Germany. E-mail: phkurz@ac.uni-kiel.de; Fax: (+49) 431-880-1520; Tel: (+49) 431-880-5803

[†] Dedicated to Stenbjörn Styring, professor at Uppsala University (Sweden) and pioneer of artificial photosynthesis on the occasion of his 60th birthday.

Mathias Wiechen (left) studied chemistry in Dortmund, where he completed his diploma degree in 2008 with a thesis on self assembled DNA-nanostructures at solid surfaces under the mentoring of Barbara Saccà and Christof M. Niemeyer. In 2009 he started his PhD thesis on the investigation of manganese oxides for biomimetic water-oxidation catalysis at the Institute for Inorganic Chemistry at the Christian-Albrecht-University Kiel as a member of the Kurz group.

Hans-Martin Berends (middle) moved to Kiel in 2002 for chemistry studies at the Christian-Albrechts-University. In 2007 he obtained his diploma degree after completing a thesis dealing with dinuclear manganese complexes under the supervision of Felix Tuczek. He continued research in this field and investigates manganese complexes using a variety of electrochemical, spectroscopic and catalytic methods.

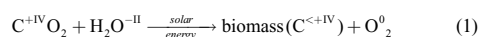
Philipp Kurz (right) received his chemistry education in Leipzig and Zurich. His interest in photosynthesis started already as a diploma student, when he investigated picoplankton from Lake Lucerne in Switzerland. Since then, the synthesis and investigation of inorganic compounds for artificial photosynthesis has been the central topic of his research, both as a PhD student of Roger Alberto in Zurich and as a postdoc in the group of Stenbjörn Styring in Uppsala. Since 2007 he is a junior research group leader at the Institute for Inorganic Chemistry in Kiel.



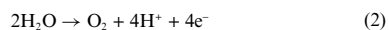
Mathias Wiechen, Hans-Martin Berends and Philipp Kurz

Photosynthetic water oxidation catalysed by Photosystem II

A very simplistic, stoichiometrically non-correct equation for the extremely complex processes of natural photosynthesis may be written as:



Without going into any detail and looking at eqn (1) purely as inorganic chemists, the process is thus a light-driven redox reaction where carbon dioxide is reduced to a variety of chemicals making up biomass (and therefore almost all life) around us. In the second “half-reaction”, which is the topic of this Perspective, the reducing equivalents for CO₂ reduction are obtained from the four-electron oxidation of water to molecular oxygen (eqn (2)):



Even as it was known for a long time that the OEC contained four Mn and one Ca ion interconnected by oxido ligands ($\mu\text{-O}^{2-}$), details of the connectivity between these centres were the topic of intense debates for decades. This is hardly surprising, as the task was to elucidate the structure of an unsymmetrical domain containing five metal centres, located within a very large membrane protein and additionally existing in five different redox states (*vide infra*). Until quite recently, various significantly differing Mn₄Ca-arrangements were therefore discussed as possible geometries for the OEC. However, very elaborate experiments of recent years employing especially EPR⁶ and X-ray absorption spectroscopy,^{7,8} X-ray diffraction^{9–11} and theoretical calculations^{12–14} resulted

in breakthroughs concerning our knowledge about OEC’s structure.

As a result, the general features of the three-dimensional arrangement of the metal ions and connectivity at the catalytic centre of PSII is rather clear today. Fig. 1 shows one of several rather similar structural models for the OEC, this one derived from the 1.9 Å crystal structure published this year¹¹ and showing the enzyme in a reduced form. At the centre one can see the central unit of the OEC as a very distorted Mn₃CaO₄-cube connected to the fourth manganese *via* additional $\mu\text{-O}$ ligands. The whole metal cluster is bound to the PSII protein by oxidation-stable imidazole or carboxylate amino acid side chains. The pocket containing the catalytic site also provides room for water molecules, the substrate of the reaction catalysed by the OEC. Thus the overall cluster composition at this reduced, S₂₀-like redox state can be given as Mn₄CaO₅(H₂O)₄.

A large number of studies have been carried out concerning the catalytic mechanism by which the OEC achieves water oxidation. Many details still need to be clarified and the reader is referred to several excellent reviews on this topic.^{13,15–17} However, important features of the OEC’s catalytic cycle for water oxidation seem to be agreed upon by now, such as the fact that during catalysis of the four-electron reaction (2), the OEC cycles through five different oxidation states. These states are separated from each other by single-electron oxidations and are commonly denoted S₀ from the most reduced to S₄ as the most oxidised state. Most of these oxidations are Mn-centred with manganese being oxidized from its Mn^{III} to the Mn^{IV} oxidation state and the

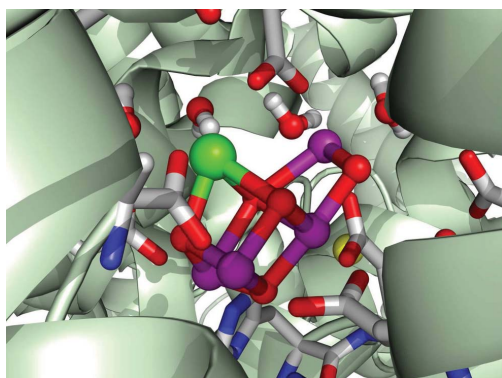


Fig. 1 Structure of the OEC determined by X-ray diffraction (plotted using PDB dataset 3ARC).¹¹ Manganese (purple) and calcium (green) centres are interconnected by oxido-ligands (red). The whole metal cluster is bound to the protein environment *via* histidine (nitrogen atoms in blue) and carboxylic acid ligands. Several water molecules and a chloride ion (yellow) are also located in the vicinity of the OEC.

average manganese oxidation state during the entire S-state cycle has been determined to stay between $Mn^{3.0}$ and $Mn^{4.0}$. Only the fourth oxidation to generate the water-oxidizing state S_4 could very likely be an oxygen-centred process to generate a reactive oxyl ($O^{\cdot-}$) radical intermediate with an oxygen oxidation state O^{-1} . Otherwise oxygen-centred oxidation steps, for example to generate peroxido-intermediates, are avoided by PSII as they would be very energy demanding. Multiple studies have also demonstrated that the removal of four electrons from the OEC at $\sim +1$ V is energetically only possible if the oxidation steps are accompanied by proton release from the aquo/hydroxido ligands. This results in a higher number of μ -O ligands for higher S-states and, most importantly, charge compensation *via* proton coupled electron transfer (PCET) steps. And finally, Mn-centred oxidations and the formation of additional oxido-bridges cause significant decreases of the Mn–Mn-distances as higher S-states are reached. In consequence, the OEC and its environment need to possess a high degree of flexibility to make such geometry changes possible.

The structural and mechanistic knowledge concerning the OEC is thus quite advanced, but of course far from complete. However, and most important for our goal, the key properties of photosystem II's catalytic site are today known in sufficient detail to serve as a guidance for bioinorganic chemists to design synthetic models for manganese-based water-oxidation catalysis.

At the beginning, the preparation of manganese containing compounds in this field was mainly motivated by the classical bioinorganic approach of modelling the reactivity of natural metalloenzymes by synthetic complexes. In this way it was hoped that one could learn more about both the structure and the catalytic mechanism of the OEC from synthetic mimics. In recent years, a second motivation in this field beyond pure modelling chemistry has emerged: the idea to use bio-inspired water-oxidation catalysts for the production of solar fuels, as will be described in the following section.

Water oxidation as part of artificial photosynthesis

Already at the end of the 1970s (and probably under the impression of the first oil crisis), the Lehn group in Strasbourg proposed a concept for the conversion of solar into chemical energy based on the blueprint of natural photosynthesis.¹⁸ Solar energy represents by far the most abundant possible source of renewable energy on the surface of the earth. Therefore concepts for solar energy conversion have recently again come into the focus of research, as alternatives to the use of fossil fuels are much looked for today.^{4,5,17,19–21}

The general outline of the artificial photosynthetic system of the Strasbourg team is shown in Fig. 2 (top). Two separate photoreactions using suitable dyes P_1 and P_2 are envisioned to drive water oxidation and proton reduction as redox half-reactions. The two processes are linked by a relay molecule R to shuttle reduction equivalents. Possibly a membrane might also be used to physically separate the two reactions from each other.

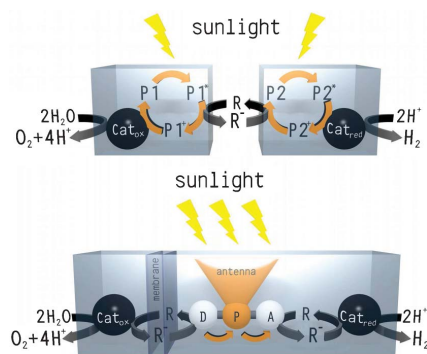


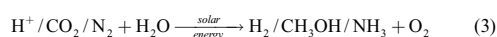
Fig. 2 Strasbourg¹⁸ (top) and Bologna²² (bottom) designs for the conversion of solar energy into H_2 as a solar fuel. Components: catalytic sites for water oxidation/proton reduction (Cat_{ox}/Cat_{red}), photosensitizers (P), redox relays (R) and (in the case of Bologna) primary donor/acceptor moieties (D/A) for the initial light reaction.

This “Strasbourg design” is still very much considered today as an attractive system for solar energy conversion. It conceptually copies the electron flow of natural photosynthesis where reduction equivalents, which have been photochemically obtained from water oxidation by PSII, are transferred *via* multiple carriers to photosystem I.¹⁷ They are then used by PSI in a second photoreaction to generate “nature’s solar fuel” NADPH from $NADP^+$.

Alternatively, the Bologna team of Balzani and co-workers has designed a related and also much-cited scheme for solar fuel production where a single photoreaction is responsible for initial charge separation between a donor moiety D and an acceptor A (Fig. 2, bottom).²² Electrons and holes generated this way are then used for subsequent redox processes taking place on different sides of a membrane, again using relay molecules to transport charges.

In both schemes, there seems to be no alternative to water oxidation as the apparently only feasible source for reduction equivalents. For the other half-reaction, different possible reduction processes are discussed to generate a variety of energy carrier molecules such as H_2 , CH_3OH , NH_3 , $HCOOH$ *etc.*,^{4,5,17,23} so that a

more generalised equation for the production of solar fuels might be written as shown in eqn (3) below. The possible success of any device for the production of solar fuels thus critically depends on the development of efficient, robust and affordable catalysts Cat_{ox} for water oxidation which then have to be linked to photochemical reaction chains as shown in Fig. 2.



As light-driven, biomimetic water oxidation is a $4 \times 1\text{e}^-$ - process (eqn (2)), transition metal catalysts are needed to couple the single-electron charge accumulation steps with multi-electron redox catalysis. Platinum metal might be considered as the archetypical man-made water-oxidation catalyst, already used by Hofmann 150 years ago in his famous apparatus for water electrolysis.²⁴ Today we know that catalysis on platinum proceeds *via* the initial formation of oxido-platinum-species on the electrode surface.²⁵ Indeed water oxidation catalysts are generally of an “oxide-like” nature at the water-oxidizing stage of their catalytic cycles as all of them belong either to the compound classes of metal-oxido complexes,^{26–28} polyoxometallates^{29,30} or transition metal oxides.^{31–37}

Of the latter, a screening by the Harriman group in 1988 revealed that from the investigated oxides of 16 different metals, only six showed significant catalytic activity for reaction (2).³² Those found to be active belonged to either (a) platinum-metal oxides, with IrO_2 and RuO_2 as most active species or (b) metal oxides from the middle of the first row of transition metals, notably Co_3O_4 and Mn_2O_3 .

Looking at reports of water-oxidation catalysts today, the identification of interesting metal centres for the catalysis of reaction (2) from 1988 seems to be still valid, because well-performing synthetic catalysts all contain either Ir, Ru, Co or Mn.^{26–37}

In general two approaches have been successful for the synthesis of water-oxidation catalysts. First, there is a large number of coordination compounds (especially of Ru and Ir)^{26–28,38} with oxidation stable ligand systems which are able to catalyse reaction (2) in homogeneous solution as molecular species. Secondly, synthetic chemists have prepared efficient heterogeneous catalysts through modifications of the compositions and morphologies of Ir-, Ru-, Co- and Mn-oxides.^{31–37}

In the following, we will focus only on manganese-containing compounds studied in the context of water oxidation because it has always been central for us to study species that are both potential OEC models *and* possible catalysts for artificial photosynthesis. The very successful work concerning water oxidation catalysis using other metals than manganese can be studied by the reader in a number of other publications.^{26–36,39}

The discussion will take us from investigations on molecular manganese coordination compounds in solution *via* their immobilisation on surfaces to water-oxidation catalysis by manganese oxides. In the tradition of a Perspective article, we neither try to offer a comprehensive review nor a complete list of references on these themes. Rather we in a way follow the topics of the scientific work of the corresponding author from his introduction to manganese coordination chemistry in the Uppsala team within the Swedish Consortium for Artificial Photosynthesis to current research activities in Kiel.

Manganese based catalysts for oxygen evolution and water oxidation

Dinuclear μ -oxido manganese complexes as OEC mimics

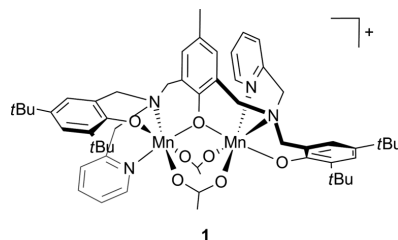
It is a common approach in bioinorganic chemistry to model the active sites of metalloenzymes by transition-metal complexes containing the metal centre of interest in a ligand environment similar to that found in the enzyme.⁴⁰ Such a transfer is comparably easy in some cases. For example, key features concerning the structure and reactivity of the iron sites in haem iron containing enzymes can be modelled by Fe-porphyrin complexes.⁴⁰ In our case however, a synthetic ligand system would have to imitate the highly asymmetric topology of the pentanuclear Mn_4Ca -oxido-cluster of OEC and its ligand surroundings (Fig. 1) and bind to it in five different oxidation states. Due to this difficulty, such a manganese complex has so far not been developed.

Instead, the common strategy for the synthesis of OEC-mimics has been to simplify the model even more and use dinuclear manganese compounds as model systems.^{15,41–44} Fortunately, complexes containing a $[\text{Mn}_2(\mu\text{-O})_x]$ core ($x = 1$ and 2 are most common) are often very stable and can be prepared using a large variety of chelating ligand systems.^{42,45} As a result, more than 100 coordination compounds of this type are known, containing manganese in different combinations of Mn^{II} , Mn^{III} and Mn^{IV} .

Over the last 30 years, such species have been extensively studied, especially concerning their spectroscopic, electrochemical and also catalytic properties. Additionally, another oxygen-evolving manganese enzyme, manganese catalase, contains a $[\text{Mn}_2(\mu\text{-O})(\mu\text{-OH})]$ -active site for the catalytic disproportionation of hydrogen peroxide (H_2O_2) into H_2O and O_2 .⁴⁶ Many of the model complexes were therefore investigated as mimics for the catalase enzyme as well.

As a typical example for this research approach, key results concerning the chemistry of a dinuclear manganese(III,III) model complex studied extensively by the Uppsala team^{47–49} will be presented in the following section.

Scheme 1 shows the structure of this Mn_2 -compound, the complex, $[\text{Mn}_2^{\text{III,III}}\text{L}(\mu\text{-OAc})_2]^+$, where the ligand L is the anion of the heptadentate ligand 2,6-bis[*N*-(3,5-di-*tert*-butyl-2-hydroxybenzyl) - *N*'-(2-pyridylmethyl)amino]methyl]-4-methylphenol. The centre of the compound is made up by two manganese(III) ions in a typical distorted octahedral ligand environment. The two Mn^{III} centres strongly interact electronically *via* two μ -acetato and one μ -phenolato ligand.



Scheme 1 Structure of the dinuclear manganese(III) complex $[\text{Mn}_2^{\text{III,III}}\text{L}(\mu\text{-OAc})_2]^+$ (1). Geometry adapted from ref.

To characterize the redox properties of such a model complex in the presence of water, it is common to carry out extensive electrochemical investigations,⁴¹ as was also done for **1**.⁴⁹ In order to assign redox states and to learn more about the reversibility of the redox events, it has additionally been very fruitful to employ spectroelectrochemical methods, where bulk electrolyses of solutions containing complexes such as **1** are carried out in combination with UV-Vis, IR, ESI-MS or EPR analyses.^{41,50–52} Especially EPR is a powerful technique in manganese chemistry, as the strong coupling of the ⁵⁵Mn nuclei ($I = 5/2$) with unpaired electrons of the complex results in EPR signal patterns which are characteristic for distinct manganese redox states and complex nuclearities.⁵³

For example, the electrochemical oxidation of **1** (an EPR silent compound) at +0.69 V vs. Fc/Fc⁺ in acetonitrile containing 0.5 M water leads to the formation of a species for which the 16-line X-band EPR spectrum shown in Fig. 3 is detected.⁴⁹ By comparison with the abundant reference data on manganese EPR, it is known that such a signal can only arise from the formation of a complex containing a [Mn₂^{III,IV}(μ-O)₂]-core.^{54,55} EPR thus provided evidence that the oxidation of **1** in the presence of water does result in an increase of the oxidation state for one of the manganese centres from Mn^{III} to Mn^{IV}. Furthermore, ligand exchange of acetate for water apparently occurs followed by the deprotonation of Mn-bound water to introduce at least one new μ-O ligand in addition to the existing μ-phenolato linkage between the manganese centres.⁵³

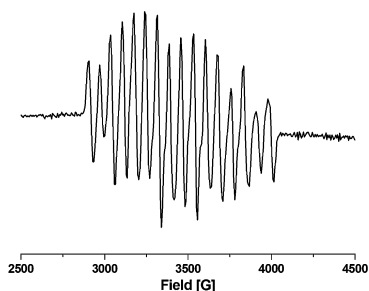
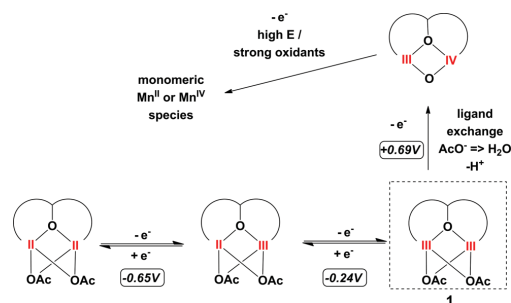


Fig. 3 Characteristic [Mn^{III,IV}₂(μ-O)₂] EPR spectrum measured for a solution of **1** (1 mM) in MeCN–0.5 M H₂O after bulk electrolysis at +0.69 V vs. Fc/Fc⁺. For details see ref. 49.

If such combinations of electrolyses and spectroscopic measurements are carried out for different potentials, it is possible to develop “maps” of redox- and ligand-exchange-events.^{41,49,51,56} Scheme 2 below shows such a graph for the reactions of complex **1**, which is a typical example of an analysis of this type.

A look at the scheme clearly shows that important processes in the context of water oxidation (see above) can be studied with a model compound such as **1**:

- multi-electron redox chemistry involving electronically coupled Mn^{III} and Mn^{IV} centres is observed.
- the coordination and deprotonation of water occurs as new μ-O ligands are introduced.
- the oxidation to the Mn₂^{III,IV} state occurs at a potential which is relevant for H₂O-oxidation.



Scheme 2 “Map” of important redox and ligand exchange reactions for **1** in MeCN–0.5 M H₂O. Potentials are given vs. Fc/Fc⁺. Simplified from ref. 49.

One can thus conclude that reactions as shown in Scheme 2 for complex **1** serve as interesting study cases for the processes associated with the S-state transitions of the OEC, because the accumulation of oxidation equivalents and the accompanying ligand exchange reactions are nicely modelled. Additionally, the fundamentally important topics of PCET, Mn-oxido/hydroxido/oxyl species and manganese water interactions can be studied in detail by manganese model chemistry using mono- or dinuclear complexes.^{41,57} However, a look at Scheme 2 also shows two common drawbacks of complexes such as **1** for actual water oxidation: first, the ligand system is not ideal, because an oxidation beyond the Mn₂^{III,IV} state is not possible without the decomposition of the complex (in the case of **L** most likely the phenolate moieties are oxidised). Additionally, even though three one-electron redox processes are observed, only one of them occurs at a high enough potential for water oxidation (eqn (2) requires the generation of four holes at high E).

While a large number of fundamental studies on the redox properties for Mn₂-compounds such as **1** can be found in the literature, reports concerning their catalytic properties for water oxidation are rare.^{58–62} To us, the investigation of catalysis has always been of central importance and thus some systematic screenings have been carried out in which we used the formation of the O₂ product as a measure for catalytic activity.^{58,60,61} In these studies, we treated a variety of dinuclear manganese complexes with different strong oxidation agents in argon-purged water or water–acetonitrile mixtures. The concentration of dissolved dioxygen [O₂] was then followed for the course of the reaction. Three typical oxygen evolution traces recorded in such experiments are depicted in Fig. 4, showing the example of O₂-formation catalysed by the dinuclear complex **6** (see Scheme 3).⁶³

Looking at the solid [O₂]-trace in Fig. 4, it is obvious that complex **6** is a very efficient catalase-mimic: treatment with H₂O₂ results in the immediate formation of large amounts of O₂ with the sensor’s detection limit being reached within seconds after the H₂O₂-addition. Oxygen is also formed in reactions with the inorganic peroxide oxone (HSO₅⁻, Fig. 4, dashed line) or the organic peroxide ^tBuOOH (not shown). On the other hand, the treatment of **6** with the very strong oxidation agent Ce^{IV} yields virtually no dioxygen product.

As mentioned above, we (and others) have carried out such experiments for a number of Mn₂-complexes (see Scheme 3 for

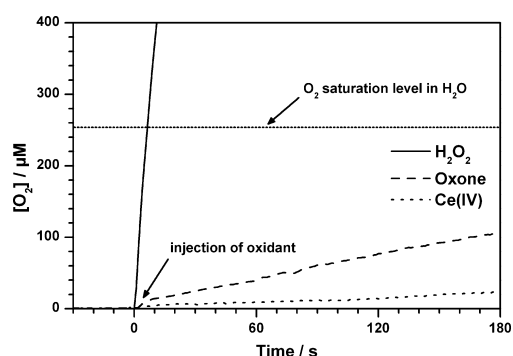
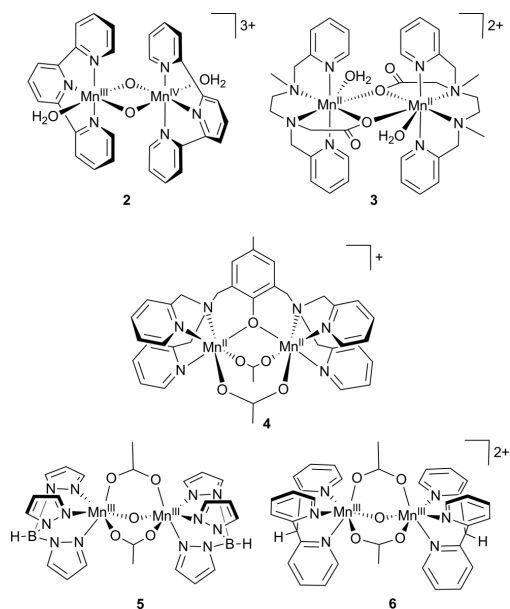


Fig. 4 Traces of oxygen evolution for the reactions of complex **6** with hydrogen peroxide (H_2O_2), oxone (HSO_5^-) or Ce^{IV} ($(\text{NH}_4)_2[\text{Ce}(\text{NO}_3)_6]$) in aqueous solution. $[\text{O}_2]$ was monitored using an oxygen-sensitive Clark electrode.⁶³



Scheme 3 Examples of dinuclear manganese complexes of various oxidation states and geometries, which have been investigated for their ability to catalyse O_2 -evolution.^{58–62}

prominent examples) and observed a general reactivity pattern: one finds that nearly all dinuclear manganese systems act as catalase mimics, *i.e.* catalyse the reaction $2\text{H}_2\text{O}_2 \rightarrow 2\text{H}_2\text{O} + \text{O}_2$. Additionally, the treatment of dinuclear manganese systems with oxone or $^t\text{BuOOH}$ also results in oxygen-evolution in many cases. But on the contrary and to much disappointment, reactions of Mn_2 -systems with the non-oxygen-containing oxidants Ce^{IV} or $[\text{Ru}(\text{bipy})_3]^{3+}$ generally do not yield O_2 , even though these are very powerful oxidation agents.

The results of ^{18}O -isotope labelling experiments provided likely explanations for these trends in reactivity.^{64,65} In these studies,

oxygen-evolution experiments as shown in Fig. 4 were carried out in aqueous solutions enriched in H_2^{18}O and the generated dioxygen isotopologues were detected by mass spectrometry. It was found that the ^{18}O -isotope label is not at all (H_2O_2 , $^t\text{BuOOH}$) or only to a degree of 50% (HSO_5^-) incorporated into the O_2 -product for reactions with peroxides. These processes therefore follow different mechanisms rather than the water-oxidation reaction because the O_2 product is formed at least partially from other sources than the two water molecules as required by eqn (2). Potential pathways of dioxygen-formation for these reactions were suggested and all involve the transfer of at least one oxygen atom from the peroxide oxidation agents to a manganese centre.^{64,65} As the oxidants do not bear the ^{18}O -label, the O_2 -product is in consequence not stoichiometrically ^{18}O -labelled. It seems that the majority of dinuclear manganese complexes are able to catalyse the formation of oxygen along these oxygen-transfer routes. This could explain the first two general reactivity trends mentioned above.

On the other hand, the catalysis of real water oxidation requires that the manganese unit is able to form O_2 directly from two H_2O substrate molecules after four oxidizing equivalents have been stepwise accumulated by the Mn complex. Additionally, $2e^-$ -oxidation steps or oxygen transfer to Mn from any other source than water should not be involved. These are not part of any currently discussed mechanism for water oxidation by the OEC whereas both are key features of the catalytic routes to obtain O_2 product in H_2O_2 , $^t\text{BuOOH}$ or HSO_5^- reactions.

To the best of our knowledge there are only two non-oxygen transferring, single-electron oxidation agents which can be used in experiments to screen for real water oxidation, which are Ce^{IV} or $[\text{Ru}(\text{bipy})_3]^{3+}$. Oxygen formation has been observed using these oxidants in homogeneous solution especially in combination with ruthenium complexes. If analysed, the oxygen formed in such reactions is stoichiometrically labelled and the single-electron oxidation chemistry of Ce^{IV} or $[\text{Ru}(\text{bipy})_3]^{3+}$ ensures that a OEC-like accumulation of oxidation equivalents has to precede O–O bond formation.^{27,28,66}

However, no dinuclear manganese complex has shown significant catalytic water-oxidation activity in reactions with Ce^{IV} or $[\text{Ru}(\text{bipy})_3]^{3+}$. We are aware of the fact that there are claims in the literature stating that manganese complexes which are able to catalyse the formation of O_2 in reactions with $^t\text{BuOOH}$ or HSO_5^- are water-oxidation catalysts.^{62,67–69} From the results known to us this has never been convincingly proven by either ^{18}O -labelling or by the isolation of reaction intermediates. In summary, we thus take the results on O_2 -evolution catalysis as strong indication that homogeneous, biomimetic catalysis of the water-oxidation reaction using manganese complexes has so far not been achieved – much in contrast to homogeneous catalysis involving ruthenium, iridium or even iron.^{28,39,70}

Furthermore, on the basis of the available data the strategy of using Mn_2 -compounds looks unlikely to succeed, because none of the complexes prepared so far meets all of the following five requirements which to us seem mandatory for the catalysis of reaction (2). A successful manganese water-oxidation catalyst will have to:

- possess an *oxidation stable*, multinuclear manganese-oxido-core

- allow the take-out of *four electrons* at potentials $>+1$ V in $1e^-$ -oxidation steps
- be able to level the potentials of the different oxidation steps through *ligand exchange* and/or *proton-coupled electron-transfer* processes
- be held together by a rather *flexible ligand framework* in order to react to the necessary oxidation- and ligand-exchange-events by changes in geometry
- have coordination sites of the H_2O substrate

To synthesise manganese complexes which are functional water-oxidation catalysts we in consequence think it necessary to increase the Mn-nuclearity of the compounds to Mn_{2-2} -species. This seems to be especially important if the second requirement ($4e^-$ -redox chemistry) is to be met. First steps in this directions have been made by the synthesis of complexes which contain cubic $[Mn_4O_4]$ - or even $[Mn_3CaO_4]$ -cores.^{68,71,72} However, these first examples still lack oxidation- and/or hydrolysis- stable ligand sets, so homogeneous water-oxidation catalysis with any of these compounds in reactions with Ce^{IV} or $[Ru(bipy)_3]^{3+}$ has so far not been reported.

Mn_2 -complexes adsorbed on clay surfaces catalyse water oxidation

Already in 1987 a different strategy for the preparation of manganese-based water-oxidation catalysts was introduced by Kaneko and co-workers. It was found that the adsorption of the dinuclear complex $[(bpy)_2Mn(\mu-O)_2Mn(bpy)]^{2+}$ (with bpy = 2,2'-bipyridyl) on the surface of kaolin clay resulted in the formation of an active catalyst.⁷³ Improved versions of this system were then prepared and investigated by the Yagi group which immobilised complex **2** on montmorillonite clay or mica.⁷⁴⁻⁷⁶

The use of clays as a solid support for water-oxidation catalysts seems to be an excellent choice. These layered aluminium silicates are known to strongly bind metal complexes (especially cations) to their surfaces.⁷⁷ Furthermore, clay minerals are oxidation- and hydrolysis- stable and very hydrophilic, all important parameters for biomimetic oxidation chemistry in general and water oxidation in particular.

Concerning the case of $2@clay$, it was known from other studies that complex **2** is a very good O_2 -evolution catalyst in reactions with oxone in solution. Due to this activity a wealth of data on **2** is available from detailed work by the groups of Brudvig, Crabtree and others.^{59,67,78,79} However, **2** is not a homogeneous water-oxidation catalyst in Ce^{IV} -experiments and it is thus remarkable that active catalysts could be obtained when the bpy or tpy complexes were adsorbed on surfaces.

In consecutive work the research groups of Yagi, Brudvig and also us therefore tried to find the reason for the catalytic activity of clay hybrids such as $2@montmorillonite$. Though many details are lacking, a crude picture has emerged how reaction (2) is catalysed on the clay surfaces.

First, we could show that the method developed by Kaneko and Yagi is not limited to manganese complexes containing pyridine ligands but also yields active catalysts if other complexes are adsorbed on kaolin or montmorillonite. For example, the immobilization of complexes **5**, **6** or even species such as manganese(III) acetate all resulted in the formation of heterogeneous water-oxidation catalysts.^{58,60} Secondly, UV-Vis and EPR spectroscopy

clearly demonstrated that the electronic structures of the compounds are greatly influenced by their adsorption, indicating that a strong interaction occurs between the complexes and the clay-surfaces.⁵⁸

Most importantly, the results of catalytic studies⁷⁵ and EPR spectroscopy^{58,80} indicated that the catalytic units on the surfaces most likely consist of more than two manganese centres. These Mn_{2-2} -aggregates seem to be built up from oxido-linked manganese centres with Mn centres in an oxidation state of +III or higher. In contrast, the adsorption of Mn^{II} ions on montmorillonite did not result in catalytically active materials.⁵⁸

A possible arrangement of such a Mn_4 -cluster which could result from the adsorption of complex **6** is shown in Fig. 5. For complex **2** it has been shown that a dimerisation of two Mn_2 -units *via* μ -oxido ligands can occur and even precise structures for the resulting Mn_4 -species could be obtained using X-ray crystallography.^{78,79,81} We take these results as indication that an aggregation of the manganese centres could thus take place *via* the formation of oxido-bridges between Mn centres adsorbed on the clay and have drawn the tentative model shown in Fig. 5 accordingly. However, it has to be noted that the exact nuclearity or geometry of such clay-supported manganese clusters is currently not known.

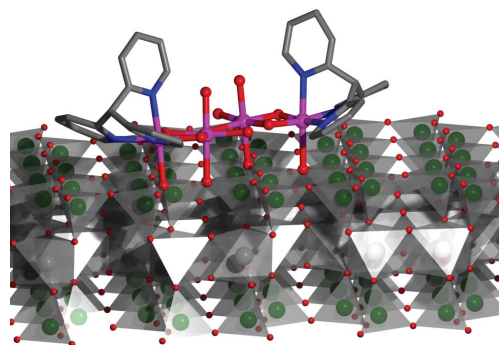


Fig. 5 Model of a catalytically active Mn_4 -cluster which might form following the adsorption of complex **6** on the surface of montmorillonite clay. As in Fig. 1, Mn atoms are in purple and O in red. Stick models of the tpdm ligands show nitrogen in blue and carbon in grey. The montmorillonite structure consists of SiO_4 tetrahedra and AlO_6 octahedra⁷⁷ and is shown as idealized 2 : 1-layer. No geometry optimisation of the Mn_4 -unit or the clay surface was carried out.

Looking at Fig. 5 and its potential manganese arrangement for the clay hybrids, one can imagine how such a cluster could indeed meet the five requirements for water-oxidation catalysis listed at the end of the previous section. Additionally, it might explain why the clay hybrids are superior to their dinuclear precursors: the clay surfaces strongly bind metal centres and will thus stabilise adsorbed manganese moieties and provide an excellent platform for the formation of robust ensembles of more than two manganese centres. The latter might be crucial for the four-electron redox chemistry of water oxidation.

It should be noted that the water oxidation catalysts obtained by clay-adsorption are not especially efficient. Nevertheless, we think that the syntheses and investigations of these hybrids have been quite important for the field of OEC model chemistry. First, they

proved that artificial Mn-based water-oxidation catalysts can be prepared at all. Secondly, they indicated that a special manganese coordination geometry does not seem to be of critical importance for catalytic activity. On the contrary, very different types of manganese precursors can be assembled into active catalysts as long as the product contains more than three μ -oxido linked Mn^{III} or Mn^{IV} centres in a non-rigid ligand environment.

Manganese oxides as catalytically highly active solid state models of the OEC

The results of the clay systems described in the previous section indicated that catalytic activity for reaction (2) seems to depend on choosing the right manganese oxidation state (Mn^{III}/Mn^{IV}), high Mn-nuclearity and flexible μ -oxido linkages between the Mn-centres. In a rather simplistic approach, one could argue that all these criteria might also be met by manganese oxides (MnO_x) without the use of elaborate Mn-ligand systems. Thus, it should be possible to model the functionality of the OEC by considering the OEC as “a MnO_x-particle embedded in a protein matrix”. Looking again at Fig. 1 from this angle, we hope that the reader agrees that this is not an entirely remote approach.

Additionally, a study of the literature on manganese oxides provided a number of reasons why this class of materials might be a good choice for heterogeneous water-oxidation catalysis. First, a look at the Pourbaix diagram for manganese (Fig. 6) shows that thermodynamically manganese(IV) oxides are able to oxidise water over a large pH-range.^{82,83} Furthermore, MnO_x electrodes were already successfully used in the 1970s as anode materials for electrochemical water oxidation^{84–86} and the Shilov group identified manganese oxides as possible OEC model compounds as early as 1981.⁸⁷ Additionally, the oxide screening by the Harriman group mentioned above showed that Mn₂O₃ belonged to the most active catalysts in water-oxidation experiments using photochemically generated [Ru(bipy)₃]³⁺ as oxidant.³² And finally, extensive studies by the Nocera team on cobalt oxides^{84,88} (the other “cheap oxide catalyst” identified by Harriman *et al.*) recently demonstrated that first-row transition metal oxides can be efficient and robust electrocatalysts for water oxidation.

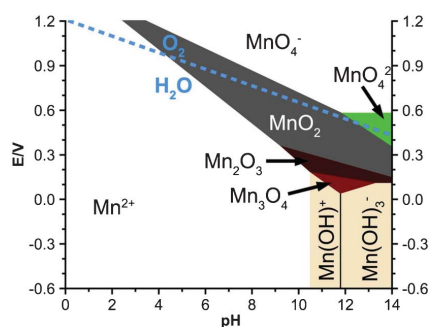


Fig. 6 Simplified Pourbaix diagram for manganese showing the dependence of stable manganese species (and their approximate colours) as function of pH and E . For a large pH-range the thermodynamic potential for water oxidation (blue dashed line) is located in the stability region of manganese(IV) oxides (MnO_x). Modified from refs. 82 and 83.

However, when we used commercially available α -MnO₂ or α -Mn₂O₃ in initial experiments with Ce^{IV} or [Ru(bipy)₃]³⁺ as oxidants, no or only very modest catalytic activities were found for these materials.³⁷ Thus it is clearly not possible to use just any kind of manganese oxide as an efficient heterogeneous catalyst for reaction (2). Fortunately, the chemistry of manganese oxides is very rich and a large variety of MnO_x materials can be synthesised following facile established routes.^{89–91} Additionally, many of these oxides contain alkali or alkali-earth metal cations and are thus mixed water-containing oxides/hydroxides of a general formula M_nMnO_x(OH)_y·zH₂O. The existence of these mixed-metal materials inspired us to prepare “biomimetic oxides” which should include Ca²⁺ in addition to manganese with the aim to model the composition of the OEC more closely.

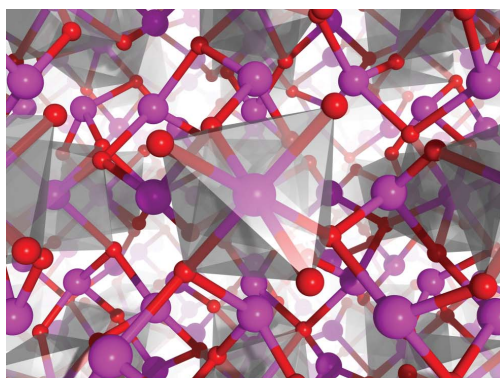
Analysing the phase diagram for the system Ca–Mn–air,⁹² we identified CaMn₂O₄, the naturally occurring mineral marokite,⁹³ as an accessible calcium containing Mn oxide with manganese in its +III oxidation state. Microcrystalline marokite could be successfully prepared *via* a comproportionation reaction of Mn²⁺ and MnO₄⁻ in Ca²⁺-containing aqueous solution followed by the heating of the precipitate to 1000 °C. However, the catalytic rates measured for marokite showed no improvement in comparison to α -Mn₂O₃.³⁷ Fig. 7 shows the structures of the manganese oxides α -Mn₂O₃ and marokite, both consisting of three-dimensional networks of μ -oxido linked metal ions.

Interestingly, highly active water-oxidation catalysts were obtained if the Ca–Mn-oxide precipitates from the comproportionation reactions are heated to much lower temperatures (60 or 400 °C) than necessary for the synthesis of marokite. The catalytic rates for water-oxidation of these mixed oxides were found to be improved more than tenfold in comparison to α -Mn₂O₃ (Fig. 8).³⁷

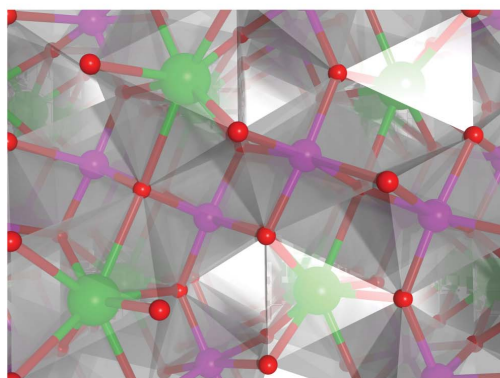
The efficient Ca–Mn-catalysts were found to be amorphous oxide powders, and it was therefore not possible to analyse their structures by X-ray diffraction. Vibrational spectroscopy and thermogravimetric analyses indicated the presence of aquo- or hydroxido- moieties,³⁷ but only the use of X-ray absorption spectroscopy (XAS) revealed more detailed structural information.

Using a combined analysis of Ca- and Mn-XAS-data⁹⁴ the catalysts were identified as layered manganese oxides of the birnessite mineral family^{90,91} with an average Mn^{+3.8} oxidation state. The composition of the Ca-birnessite heated to 400 °C is thus much more complex than that of a “hydrated marokite” and best described as CaMn^V_{1.6}Mn^{III}_{0.4}O_{4.5}(OH)_{0.5}·zH₂O.⁹⁴ A model for a section of one oxide layer of this Ca-birnessite structure is shown in Fig. 9. In contrast to the atomic arrangements for the hardly catalytically active manganese oxides α -Mn₂O₃ and CaMn₂O₄ (Fig. 7), birnessites consist of highly disordered sheets of MnO₆-octahedra with an interlayer distance of 7–10 Å. Ca and Mn ions are positioned in between the layers resulting in the formation of distorted [Mn₃CaO₄]- or [Mn₄O₄]-cube like structures. Additionally, water molecules occupy parts of the interlayer space (not shown).

It is known from numerous mineralogical studies that such layered birnessite oxides are rather abundant on Earth as they form spontaneously when Mn²⁺ is oxidised in an aqueous environment.^{90,91} Therefore a structure such as the one depicted in Fig. 9 might look very complicated but is not at all exotic for manganese oxides formed in water.



(a)



(b)

Fig. 7 Sections of the rather complex arrangements of the three-dimensionally μ -oxido linked metal centres in α - Mn_2O_3 (top) and marokite (CaMn_2O_4 , bottom). Colour code of the atoms as in Fig. 1.

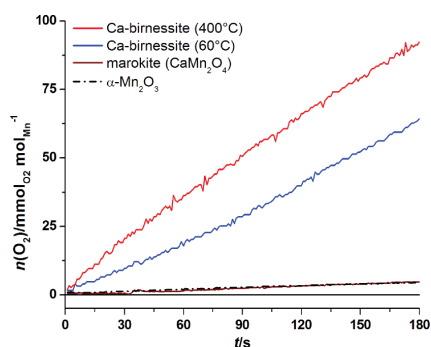


Fig. 8 Oxygen evolution traces for water-oxidation catalysis by different (calcium) manganese oxides in reactions with Ce^{IV} ($(\text{NH}_4)_2[\text{Ce}(\text{NO}_3)_6]$). Figure modified from ref. 37.

Most importantly, a comparison of Fig. 1 and 9 shows that birnessites have a number of properties that are closely related to

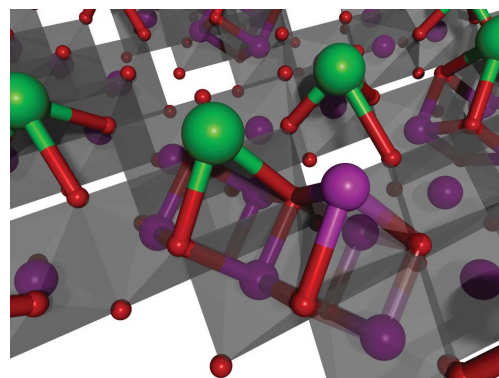


Fig. 9 Model for the structure of one sheet of the catalytically active layered Ca-Mn-oxides belonging to the birnessite family of Mn-minerals. The manganese layer is build up of edge-sharing $[\text{MnO}_6]$ octahedra (grey) and contains a large number of defects in the form of Mn vacancies. Colour code of the atoms as in Fig. 1.

the OEC, which could explain why these materials are very active catalysts:

- the oxides are of an intermediate $\text{Mn}^{\text{III}} < x < \text{Mn}^{\text{IV}}$ oxidation state as thermodynamically required for water oxidation by the Pourbaix diagram (and like the OEC!¹⁶).
- defects of the layer structure can act as *coordination sites* for water to Mn.
- some manganese centres have an incomplete coordination sphere of oxido/hydroxide-ligands, making the formation of additional μ -O linkages possible. This would result in charge compensation and redox potential levelling. Highly ordered materials such as the oxides shown in Fig. 7 do not possess this *structural flexibility* which might explain their low catalytic activity.
- similar to the OEC, there are *clearly different Mn sites*. Most suggested mechanisms for water oxidation by the OEC involve some manganese centres to act merely as charge accumulators while O–O bond formation takes place at other sites.^{13,15–17}
- and last, but not least, the most active oxides contain *calcium* ions, which are essential for the activity of PSII even though there precise role in the bioinorganic catalytic cycle is currently not known.

The use of layered (calcium) manganese oxides is thus a very promising approach in the field of water-oxidation chemistry, as efficient, robust and non-toxic catalysts can be synthesised from abundant elements along facile routes. This makes manganese oxides attractive for a potential large-scale use in artificial photosynthesis. Additionally, the materials resemble a number of important aspects of the OEC (Mn oxidation state, flexibility of the structure, Ca in the vicinity of Mn) so that the oxide particles might be considered as “biomimetic rocks”, *i.e.* functional solid-state models for the natural water-oxidation catalyst of PSII.

Interestingly, there have been additional reports on the catalytic activity of layered oxide structures, so the phenomenon seems to be a rather common one. Active birnessite water-oxidation catalysts could be prepared embedded in a Nafion membrane on

a glassy carbon electrode⁹⁵ or as thin films on FTO electrodes for electrocatalysis.⁹⁶ Manganese oxide particles on silica⁹⁷ which very efficiently catalyse reaction (2) were characterised by XAS to be of an intermediate Mn^{III/IV} oxidation state and could thus very well be birnessite-like, too. And also other non-precious metal oxides forming catalytic materials are apparently build-up from layers of MO₆ octahedra, as has been shown for thin-film electrocatalysts consisting of Co- or Ni-oxides.^{98,99} The three-dimensional arrangement of the oxido-bridged metal centres in layered oxides thus seems to be generally advantageous for water-oxidation catalysis.

Conclusions and outlook

The development of manganese-based catalysts for water oxidation has clearly made great advances in the last decades. Inspired by an ever clearer picture concerning both the structure and the function of the OEC, the natural paragon, synthetic chemists have been able to prepare molecular and solid-state model compounds of the active site for water oxidation in Photosystem II.

Investigations of Mn₂-complexes have provided us with a great pool of excellent model chemistry concerning the processes taking place while the OEC is oxidised stepwise from one S-state to the next. The importance of the Mn^{III} and Mn^{IV} oxidation states, the formation of μ -oxido ligands and proton-coupled electron-transfer for water oxidation by Mn has been clearly demonstrated in the studies of these OEC models.

However, it has so far not been possible to synthesise an active homogeneous water-oxidation catalyst in the form of an Mn₂-complex. We have outlined above why we think this approach might not succeed and would thus see a major challenge for this research field in the synthesis of tetranuclear Mn complexes with an oxidation-stable ligand sets. Such species could well be able to manage the high-potential, four-electron chemistry of water-oxidation catalysis. As a key advantage over heterogeneous systems, the investigation of Mn₂-complexes in solution might make a understanding of the catalytic mechanism possible, because spectroscopy and electrochemistry can be used in detail.

For the research areas of manganese oxides and manganese clusters on surfaces any understanding of the catalytic processes is currently still in its infancy. We stated above that a number of important structural similarities exist between the catalytically active compounds and the OEC, but how these might translate into reactivity is so far unknown. Fortunately, the very flexible synthetic routes to catalytically active manganese oxides will allow the preparation of a large amount of different materials so that there are many ways to both broaden mechanistic understanding and to improve catalyst activity.

If manganese-based catalysts are to be used in artificial photosynthesis, water-oxidation catalysis has to be coupled to other electron acceptor reactions than the test systems of today using Ce^{IV} or [Ru(bipy)₃]²⁺. The to us most likely first steps here will be extensive studies of electrocatalytic water oxidation with manganese-oxide anodes and the combination of heterogeneous manganese catalysts with inexpensive (non-ruthenium) dyes to achieve photochemical water oxidation. Clearly, there are many topics to explore for bioinorganic manganese chemists inspired by the amazing machinery of Photosystem II.

Notes and references

- J. M. Berg, J. L. Tymoczko and L. Stryer, *Biochemistry*, W. H. Freeman & Co, New York, 2011.
- P. Atkins, T. Overton, J. Rourke, M. Weller and F. A. Armstrong, *Inorganic Chemistry*, Oxford University Press, Oxford, 2010.
- L. Taiz and E. Zeiger, *Plant Physiology*, Sinauer Ass., Sunderland, 2010.
- N. Armaroli and V. Balzani, *Energy for a Sustainable World*, Wiley-VCH, Weinheim, 2011.
- Energy Production and Storage*, ed. R. H. Crabtree, John Wiley & Sons, Chichester, 2010.
- N. Cox, L. Rapatskiy, J. H. Su, D. A. Pantazis, M. Sugiura, L. Kulik, P. Dorlet, A. W. Rutherford, F. Neese, A. Boussac, W. Lubitz and J. Messinger, *J. Am. Chem. Soc.*, 2011, **133**, 3635–3648.
- H. Dau and M. Haumann, *Coord. Chem. Rev.*, 2008, **252**, 273–295.
- J. Yano, J. Kern, K. Sauer, M. J. Latimer, Y. Pushkar, J. Biesiadka, B. Loll, W. Saenger, J. Messinger, A. Zouni and V. K. Yachandra, *Science*, 2006, **314**, 821–825.
- J. Barber, *Inorg. Chem.*, 2008, **47**, 1700–1710.
- B. Loll, J. Kern, W. Saenger, A. Zouni and J. Biesiadka, *Nature*, 2005, **438**, 1040–1044.
- Y. Umena, K. Kawakami, J.-R. Shen and N. Kamiya, *Nature*, 2011, **473**, 55–60.
- D. A. Pantazis, M. Orio, T. Petrenko, S. Zein, W. Lubitz, J. Messinger and F. Neese, *Phys. Chem. Chem. Phys.*, 2009, **11**, 6788–6798.
- P. E. Siegbahn, *Acc. Chem. Res.*, 2009, **42**, 1871–1880.
- E. M. Sproviero, J. A. Gascon, J. P. McEvoy, G. W. Brudvig and V. S. Batista, *J. Am. Chem. Soc.*, 2008, **130**, 6728–6730.
- C. W. Cady, R. H. Crabtree and G. W. Brudvig, *Coord. Chem. Rev.*, 2008, **252**, 444–455.
- H. Dau, C. Limberg, T. Reier, M. Risch, S. Roggan and P. Strasser, *ChemCatChem*, 2010, **2**, 724–761.
- W. Lubitz, E. J. Reijerse and J. Messinger, *Energy Environ. Sci.*, 2008, **1**, 15–31.
- M. Kirch, J. M. Lehn and J. P. Sauvage, *Helv. Chim. Acta*, 1979, **62**, 1345–1384.
- H. B. Gray, *Nat. Chem.*, 2009, **1**, 7.
- N. S. Lewis and D. G. Nocera, *Proc. Natl. Acad. Sci. U. S. A.*, 2006, **103**, 15729–15735.
- A. Magnuson, M. Anderlund, O. Johansson, P. Lindblad, R. Lomoth, T. Polivka, S. Ott, K. Stensjö, S. Styring, V. Sundstrom and L. Hammarström, *Acc. Chem. Res.*, 2009, **42**, 1899–1909.
- V. Balzani, A. Credi and M. Venturi, *ChemSusChem*, 2008, **1**, 26–58.
- C. Federsel, R. Jackstell and M. Beller, *Angew. Chem., Int. Ed.*, 2010, **49**, 6254–6257.
- A. W. Hofmann, *Introduction to Modern Chemistry*, Walton and Maberly, London, 1866.
- I. C. Man, H. Y. Su, F. Calle-Vallejo, H. A. Hansen, J. I. Martinez, N. G. Inoglu, J. Kitchin, T. F. Jaramillo, J. K. Nørskov and J. Rossmeisl, *ChemCatChem*, 2011, **3**, 1159–1165.
- J. J. Concepcion, M. K. Tsai, J. T. Muckerman and T. J. Meyer, *J. Am. Chem. Soc.*, 2010, **132**, 1545–1557.
- J. K. Hurst, *Coord. Chem. Rev.*, 2005, **249**, 313–328.
- S. Romain, L. Vigara and A. Llobet, *Acc. Chem. Res.*, 2009, **42**, 1944–1953.
- A. Sartorel, P. Miro, E. Salvadori, S. Romain, M. Carraro, G. Scorrano, M. Di Valentin, A. Llobet, C. Bo and M. Bonchio, *J. Am. Chem. Soc.*, 2009, **131**, 16051–16053.
- Q. Yin, J. M. Tan, C. Besson, Y. V. Geletii, D. G. Musaev, A. E. Kuznetsov, Z. Luo, K. I. Hardcastle and C. L. Hill, *Science*, 2010, **328**, 342–345.
- Y. Gorlin and T. F. Jaramillo, *J. Am. Chem. Soc.*, 2010, **132**, 13612–13614.
- A. Harriman, I. J. Pickering, J. M. Thomas and P. A. Christensen, *J. Chem. Soc., Faraday Trans. 1*, 1988, **84**, 2795–2806.
- F. Jiao and H. Frei, *Energy Environ. Sci.*, 2010, **3**, 1018–1027.
- M. W. Kanan and D. G. Nocera, *Science*, 2008, **321**, 1072–1075.
- J. Kiwi and M. Grätzel, *Angew. Chem., Int. Ed. Engl.*, 1978, **17**, 860–861.
- N. D. Morris and T. E. Mallouk, *J. Am. Chem. Soc.*, 2002, **124**, 11114–11121.
- M. M. Najafpour, T. Ehrenberg, M. Wiechen and P. Kurz, *Angew. Chem., Int. Ed.*, 2010, **49**, 2233–2237.

- 38 N. D. McDaniel, F. J. Coughlin, L. L. Tinker and S. Bernhard, *J. Am. Chem. Soc.*, 2008, **130**, 210–217.
- 39 W. C. Ellis, N. D. McDaniel, S. Bernhard and T. J. Collins, *J. Am. Chem. Soc.*, 2010, **132**, 10990–10991.
- 40 *Concepts and Models in Bioinorganic Chemistry*, ed. H.-B. Kraatz and N. Metzler-Nolte, Wiley-VCH, Weinheim, 2006.
- 41 M. N. Collomb and A. Deronzier, *Eur. J. Inorg. Chem.*, 2009, 2025–2046.
- 42 S. Mukhopadhyay, S. K. Mandal, S. Bhaduri and W. H. Armstrong, *Chem. Rev.*, 2004, **104**, 3981–4026.
- 43 C. S. Mullins and V. L. Pecoraro, *Coord. Chem. Rev.*, 2008, **252**, 416–443.
- 44 M. Yagi and M. Kaneko, *Chem. Rev.*, 2001, **101**, 21–35.
- 45 H. Y. Chen, R. Tagore, S. Das, C. Incarvito, J. W. Faller, R. H. Crabtree and G. W. Brudvig, *Inorg. Chem.*, 2005, **44**, 7661–7670.
- 46 V. V. Barynin, M. M. Whittaker, S. V. Antonyuk, V. S. Lamzin, P. M. Harrison, P. J. Artymiuk and J. W. Whittaker, *Structure*, 2001, **9**, 725–738.
- 47 M. Anderlund, PhD Thesis, Stockholm University, 2005.
- 48 P. Huang, J. Höglblom, M. F. Anderlund, L. C. Sun, A. Magnuson and S. Styring, *J. Inorg. Biochem.*, 2004, **98**, 733–745.
- 49 P. Kurz, M. F. Anderlund, N. Shaikh, S. Styring and P. Huang, *Eur. J. Inorg. Chem.*, 2008, 762–770.
- 50 M. F. Anderlund, J. Höglblom, W. Shi, P. Huang, L. Eriksson, H. Weihe, S. Styring, B. Åkermark, R. Lomoth and A. Magnuson, *Eur. J. Inorg. Chem.*, 2006, 5033–5047.
- 51 G. Eilers, C. Zettersten, L. Nyholm, L. Hammarström and R. Lomoth, *Dalton Trans.*, 2005, 1033–1041.
- 52 C. Hureau, G. Blondin, M. F. Charlot, C. Philouze, M. Nierlich, M. Cesario and E. Anxolabehere-Mallart, *Inorg. Chem.*, 2005, **44**, 3669–3683.
- 53 P. Huang, P. Kurz and S. Styring, *Appl. Magn. Reson.*, 2007, **31**, 301–320.
- 54 C. Hureau, L. Sabater, E. Anxolabehere-Mallart, M. Nierlich, M. F. Charlot, F. Gonnert, E. Riviere and G. Blondin, *Chem.–Eur. J.*, 2004, **10**, 1998–2010.
- 55 K. O. Schäfer, R. Bittl, F. Lenzian, V. Barynin, T. Weyhermüller, K. Wieghardt and W. Lubitz, *J. Phys. Chem. B*, 2003, **107**, 1242–1250.
- 56 T. K. Lal and R. Mukherjee, *Inorg. Chem.*, 1998, **37**, 2373–2382.
- 57 S. El Ghachtouli, B. Lassalle-Kaiser, P. Dorlet, R. Guillot, E. Anxolabehere-Mallart, C. Costentin and A. Aukauloo, *Energy Environ. Sci.*, 2011, **4**, 2041–2044.
- 58 H.-M. Berends, T. Homburg, I. Kunz and P. Kurz, *Appl. Clay Sci.*, 2011, **53**, 174–180.
- 59 H. Y. Chen, R. Tagore, G. Olack, J. S. Vrettos, T. C. Weng, J. Penner-Hahn, R. H. Crabtree and G. W. Brudvig, *Inorg. Chem.*, 2007, **46**, 34–43.
- 60 P. Kurz, *Dalton Trans.*, 2009, 6103–6108.
- 61 P. Kurz, G. Berggren, M. F. Anderlund and S. Styring, *Dalton Trans.*, 2007, 4258–4261.
- 62 A. K. Poulsen, A. Rempel and C. J. McKenzie, *Angew. Chem., Int. Ed.*, 2005, **44**, 6916–6920.
- 63 H.-M. Berends, A.-M. Manke, C. Näther, F. Tuzek and P. Kurz, *Molecular Science for Solar Fuel*, Sigtuna, 2009.
- 64 K. Beckmann, H. Uchtenhagen, G. Berggren, M. F. Anderlund, A. Thapper, J. Messinger, S. Styring and P. Kurz, *Energy Environ. Sci.*, 2008, **1**, 668–676.
- 65 D. Shevela, S. Koroidov, M. M. Najafpour, J. Messinger and P. Kurz, *Chem.–Eur. J.*, 2011, **17**, 5415–5423.
- 66 Y. Xu, A. Fischer, L. Duan, L. Tong, E. Gabrielson, B. Åkermark and L. Sun, *Angew. Chem., Int. Ed.*, 2010, **49**, 8934–8937.
- 67 J. Limburg, J. S. Vrettos, L. M. Liable-Sands, A. L. Rheingold, R. H. Crabtree and G. W. Brudvig, *Science*, 1999, **283**, 1524–1527.
- 68 S. Nayak, H. P. Nayek, S. Dehnen, A. K. Powell and J. Reedijk, *Dalton Trans.*, 2011, **40**, 2699–2702.
- 69 R. K. Seidler-Egdal, A. Nielsen, A. D. Bond, M. J. Bjerrum and C. J. McKenzie, *Dalton Trans.*, 2011, **40**, 3849–3858.
- 70 S. W. Kohl, L. Weiner, L. Schwartsburd, L. Konstantinovski, L. J. Shimon, Y. Ben-David, M. A. Iron and D. Milstein, *Science*, 2009, **324**, 74–77.
- 71 G. C. Dismukes, R. Brimblecombe, G. A. N. Felton, R. S. Pryadun, J. E. Sheats, L. Spiccia and G. F. Swiegers, *Acc. Chem. Res.*, 2009, **42**, 1935–1943.
- 72 J. S. Kanady, E. Y. Tsui, M. W. Day and T. Agapie, *Science*, 2011, **333**, 733–736.
- 73 R. Ramaraj, A. Kira and M. Kaneko, *Chem. Lett.*, 1987, 261–264.
- 74 M. Yagi and K. Narita, *J. Am. Chem. Soc.*, 2004, **126**, 8084–8085.
- 75 M. Yagi, K. Narita, S. Maruyama, K. Sone, T. Kuwabara and K. Shimizu, *Biochim. Biophys. Acta, Bioenerg.*, 2007, **1767**, 660–665.
- 76 M. Yagi, M. Toda, S. Yamada and H. Yamazaki, *Chem. Commun.*, 2010, **46**, 8594–8596.
- 77 F. Bergaya, B. K. G. Theng and G. Lagaly, *Handbook of Clay Science 1*, Elsevier, Oxford, Amsterdam, 2006.
- 78 C. Baffert, S. Romain, A. Richardot, J. C. Lepretre, B. Lefebvre, A. Deronzier and M. N. Collomb, *J. Am. Chem. Soc.*, 2005, **127**, 13694–13704.
- 79 H. Y. Chen, M. N. Collomb, C. Duboc, G. Blondin, E. Riviere, J. W. Faller, G. W. Brudvig and R. H. Crabtree, *Inorg. Chem.*, 2005, **44**, 9567–9573.
- 80 G. Li, E. M. Sproviero, R. C. Snoeberger III, N. Iguchi, J. D. Blakemore, R. Crabtree, G. Brudvig and V. S. Batista, *Energy Environ. Sci.*, 2009, **2**, 230–238.
- 81 H. Chen, J. W. Faller, R. H. Crabtree and G. W. Brudvig, *J. Am. Chem. Soc.*, 2004, **126**, 7345–7349.
- 82 D. G. Brookings, *Eh-pH Diagrams for Geochemistry*, Springer, Berlin, Heidelberg, 1988.
- 83 N. Takeno, Atlas of Eh-pH Diagrams, Geological Survey of Japan, published online, 2005.
- 84 M. Morita, C. Iwakura and H. Tamura, *Electrochim. Acta*, 1977, **22**, 325–328.
- 85 S. Trasatti, *J. Electroanal. Chem.*, 1980, **111**, 125–131.
- 86 Y. Matsumoto and E. Sato, *Mater. Chem. Phys.*, 1986, **14**, 397–426.
- 87 V. Y. Shafirovich, N. K. Khannanov and A. E. Shilov, *J. Inorg. Biochem.*, 1981, **15**, 113–129.
- 88 Y. Surendranath, M. Dinca and D. G. Nocera, *J. Am. Chem. Soc.*, 2009, **131**, 2615–2620.
- 89 J. Luo, Q. H. Zhang, A. M. Huang, O. Giraldo and S. L. Suib, *Inorg. Chem.*, 1999, **38**, 6106–6113.
- 90 J. E. Post, *Proc. Natl. Acad. Sci. U. S. A.*, 1999, **96**, 3447–3454.
- 91 T. G. Spiro, J. R. Bargar, G. Sposito and B. M. Tebo, *Acc. Chem. Res.*, 2010, **43**, 2–9.
- 92 B. D. White, C. A. M. dos Santos, J. A. Souza, K. J. McClellan and J. J. Neumeier, *J. Cryst. Growth*, 2008, **310**, 3325–3330.
- 93 C. Gaudefroy, G. Jouravsky and F. Permingeat, *Bull. Soc. Fr. Miner. Crist.*, 1965, **86**, 359–367.
- 94 I. Zaharieva, M. M. Najafpour, M. Wiechen, M. Haumann, P. Kurz and H. Dau, *Energy Environ. Sci.*, 2011, **4**, 2400–2408.
- 95 R. K. Hocking, R. Brimblecombe, L. Y. Chang, A. Singh, M. H. Cheah, C. Glover, W. H. Casey and L. Spiccia, *Nat. Chem.*, 2011, **3**, 461–466.
- 96 B. A. Pinaud, Z. B. Chen, D. N. Abram and T. F. Jaramillo, *J. Phys. Chem. C*, 2011, **115**, 11830–11838.
- 97 F. Jiao and H. Frei, *Chem. Commun.*, 2010, **46**, 2920–2922.
- 98 D. K. Bediako and D. G. Nocera, *Challenges in Renewable Energy (ISACS 4)*, Boston, MA, 2011.
- 99 M. Risch, V. Khare, I. Zaharieva, L. Gerencser, P. Chernev and H. Dau, *J. Am. Chem. Soc.*, 2009, **131**, 6936–6937.

Danksagung

Viele Personen haben zu der Entstehung dieser Arbeit beigetragen. Insbesondere möchte ich mich bedanken bei

- Prof. Dr. Felix Tuczek für die sehr gute Betreuung und vielen Anregungen
- Dr. Philipp Kurz für die zahlreichen Anregungen und Fachgespräche, die immense Hilfsbereitschaft und das jederzeit offene Ohr
- Anne Westphal für viele Gespräche nicht nur über das Thema Spektroskopie
- Mathias Wiechen für die Einführung in und die Unterstützung bei der Verwendung von POV-Ray und PyMOL
- Thomas Homburg und Igor Kunz, die im Rahmen ihrer Abschlussarbeiten einen wichtigen Beitrag zum Applied Clay Science-Paper geleistet haben
- meinen F-Praktikanten Kai-Arne Behrendt, Anne-Marie Manke, Anna Ciuk, Gernot Heitmann, Nele Hermer und Friederike Schulz für ihre Mitarbeit bei den einzelnen Projekten
- dem Rest der Arbeitsgruppen Tuczek und Kurz für die nette und unkomplizierte Arbeitsatmosphäre. Insbesondere möchte ich mich auch bei Ursula Cornelissen, Stefanie Pehlke, Dr. Gerhard Peters und Marianne Karbstein für die analytische Unterstützung bedanken.
- Prof. Dr. Christian Näther und Inke Jeß für die Lösung der Kristallstruktur
- Prof. Dr. Holger Dau und Dr. Ivelina Zaharieva für die XAS-Messungen
- Ralf Suren und dem Werkstatt-Team für die Unterstützung bei technischen Problemen bezüglich des EPR-Spektrometers.
- den Arbeitsgruppen Bensch und Stock für die tatkräftige Unterstützung bei der Analyse der Ton-Hybride.
- meiner Schwägerin Claudia Wenzel für die nun schon neunjährige Leihgabe von zahlreichen Chemiebüchern.
- Wiebke, Ole und Sophia, für ihr Verständnis vor allem in den letzten zehn Monaten.

Curriculum Vitae

Details

name	Hans-Martin Berends
address	Kleiststr. 1, 24105 Kiel, Germany
marital status	married, two children
citizenship	German
date of birth	August 15 th , 1982
place of birth	Aurich
e-mail	hm.berends@gmx.de

Education

09/2007 – 12/2011	Graduate studies with Dr. P. Kurz and Prof. Dr. F. Tuczek, Institute of Inorganic Chemistry, Kiel University, Germany
01/2007 – 07/2007	Diploma thesis under the supervision of Prof. Dr. F. Tuczek, Institute of Inorganic Chemistry, Kiel University: <i>Synthese und spektroskopische Untersuchung von zweikernigen Mangankomplexen mit Relevanz zum Photosystem II</i>
10/2002 – 07/2007	Undergraduate studies in chemistry, Kiel University
07/2001 – 04/2002	Alternative service in lieu of military service at the Europahaus Aurich, Germany
1994–2001	Abitur , Gymnasium Ulricianum Aurich

Conference distributions

2011	Poster presenter at the <i>GDCh-Wissenschaftsforum 2011</i> , Bremen.
2010	Speaker at the <i>13. Norddeutsches Doktorandenkolloquium</i> , Greifswald.
2009	Poster presenter at the <i>International Conference Molecular Science for Solar Fuel</i> in Sigtuna, Sweden.
2008	Poster presenter at the <i>14. Vortragstagung der Wähler-Vereinigung</i> , München.

Eidesstattliche Erklärung

Hiermit erkläre ich, Hans-Martin Berends, an Eides statt, dass die vorliegende Abhandlung - abgesehen von der Beratung durch meine Betreuer Dr. Philipp Kurz und Prof. Dr. Felix Tuzek - nach Inhalt und Form meine eigene Arbeit ist.

Diese Arbeit hat weder in Auszügen noch in ganzer Form einer anderen Stelle im Rahmen eines Prüfungsverfahrens vorgelegen. Sie wurde in ihrer Gesamtheit nicht veröffentlicht und auch nicht zur Veröffentlichung eingereicht. Die Arbeit ist unter Einhaltung der Regeln guter wissenschaftlicher Praxis der Deutschen Forschungsgemeinschaft entstanden.

Kiel, den 26.10.2011

Unterschrift